Newcastle University

What is the function of the ANKH protein in the kidney?

Shabbir Hatim Moochhala

Thesis submitted in partial fulfilment of the requirements
for the degree of Doctor of Philosophy

Newcastle University
Faculty of Medical Sciences
Institute of Cell and Molecular Biosciences
June 2010

ABSTRACT

Pyrophosphate (PPi) has been known since the 1960s as an inhibitor of calcium renal stone formation. Naturally occurring mutations in a putative PPi transporter, ANK, causes renal calcification in mice. We hypothesised that the human homologue, ANKH, plays a role in PPi transport in the human kidney.

Immunocytochemical localisation of ANKH in human kidney showed greater abundance in the cortical collecting duct than elsewhere in the nephron.

The transport function of ANKH was investigated by heterologous expression of ANKH in *Xenopus* oocytes. Despite confirmation of ANKH expression at the oocyte plasma membrane, neither ANKH-mediated PPi efflux (the physiological mode of operation) nor influx was detectable compared to water-injected oocytes. Pyrophosphatase activity was detected at the surface of oocytes, suggesting hydrolysis of PPi to inorganic phosphate.

Screening using a yeast two-hybrid method of the N-terminal of ANKH against a mouse renal library identified a possible protein-protein interaction with the fatty acid transporter SLC27A2, whose acyl-CoA synthetase activity yields PPi as an end product. This suggests that ANKH and protein partners such as SLC27A2 may form a biochemical couple whereby PPi is sequestered by transmembrane transport rather than by hydrolysis. Since there is no pyrophosphatase activity in peroxisomes, we suggest that the ANKH/SLC27A2 complex is a candidate protein for the peroxisomal membrane PPi transporter.

AVP mediates increased expression and localisation of ANK to the apical membrane of a collecting duct model (mpkCCD$_{cl4}$) *in vitro*, suggesting physiologically appropriate regulation, analogous to that of aquaporin-2.

These findings offer insights into the cellular homeostasis of PPi. Instead of cytosolic hydrolysis, coupling of PPi generation and ANKH-mediated transport as part of a protein complex may allow PPi to be compartmentalised, preserving it for use within vesicular structures elsewhere in the cell or allowing export to the extracellular medium to assist in the regulation of apatite deposition.

بِسْمِ اللهِ الرَّحْمٰنِ الرَّحِيْمِ

To my beautiful daughter

Zahabia

who gave me immense joy, love and inspiration

during her wonderful life

ACKNOWLEDGEMENTS

Firstly, I would like to thank my supervisors, Professor Nicholas Simmons and Dr John Sayer - a “dream team” who combine vast experience, enthusiasm, wisdom and encouragement. It has been a true pleasure to work closely with them.

Many thanks are due to Dr Georgina Carr, ‘Queen of the Confocal’, whose scientific expertise, good humour and resilience kept me going during the long, late hours in the lab.

I am very grateful to the following:

- Alison Howard for molecular biology and qPCR advice, Andi Werner for oocyte advice, Dan Swan for help with microarray analysis, Max, Cat, Amy, Emily and all the members of the friendly Epithelial lab at Newcastle University
- Wendy Robson, the patients and urological surgeons at the Freeman Hospital, Newcastle upon Tyne
- Noel, Mark and BBC Radio 2 - for good chat and company in the oocyte room
- and especially to the Northern Counties Kidney Research Fund and the Wellcome Trust for generously funding me.

Special thanks go to Rani, my beautiful wife whom I met and married during my PhD studies, and who never once complained during the long hours spent in the lab and writing this thesis.

And final thanks go to my parents, who have always supported and encouraged me and continue to do so. Their hard work and dedication have made me what I am today.

PUBLICATIONS

Abstracts

Moochhala SH, Carr G, Sayer JA, Simmons NL (2007). The pyrophosphate transporter, ANK, is expressed in mouse and human kidney and co-localises with aquaporin-2 in renal collecting ducts (poster). *J Am Soc Nephrol* **18,** 595A.

Sayer JA, Korkmaz C, Moochhala SH, Carr G (2008). ANKH polymorphisms, ankylosing spondylitis and renal stone disease *J Am Soc Nephrol* Abstracts Issue **19,** 935A.

Moochhala SH, Carr G, Sayer JA, Simmons NL (2009). The Pyrophosphate Transporter, ANK, Traffics with Aquaporin-2 to the Apical Membrane after Arginine Vasopressin Stimulation in the Mouse Renal Collecting Duct Cell Line, mpkCCDCl4. *J Am Soc Nephrol* Abstracts Issue **20,** 761A.

Papers

Moochhala SH, Sayer JA, Carr G, Simmons NL (2008). Renal calcium stones: insights from the control of bone mineralization. *Exp Physiol* **93,** 43-49.

Carr G, Moochhala SH, Eley L, Vandewalle A, Simmons NL, Sayer JA (2009). The pyrophosphate transporter ANKH is expressed in kidney and bone cells and colocalises to the primary cilium / basal body complex. *Cell Physiol Biochem* **24,** 595-604.

Sayer JA, Moochhala SH, Thomas DJ (2010). The medical management of urolithiasis. *Br J Med Surg Urol* **3,** 87-95.

Book chapter

Sayer JA, Carr G, Moochhala SH, Simmons NL (2008). Pyrophosphate Transport and Stones. In: Proc 2nd Intl Urolithiasis Res Symp, Eds. Evan AP, Lingeman JE, McAteer JA, Williams JC. Pub. by Amer. Institute of Physics, Melville, NY, pp. 71-80.

TABLE OF CONTENTS

LIST OF FIGURES

LIST OF TABLES

ABBREVIATIONS

ADH	anti-diuretic hormone (=AVP)
AMP	adenosine monophosphate
ANK	progressive ankylosis protein *(italics denotes gene name)**
AQP2	aquaporin-2
ARCA	anti-reverse cap analogue
ATP	adenosine triphosphate
AVP	arginine vasopressin
BSA	bovine serum albumin
CaPPi	calcium pyrophosphate
CAPS	N-cyclohexyl-3-aminopropanesulfonic acid buffer
CCAL2	chondrocalcinosis type 2
CCD	cortical collecting duct
cDNA	complementary deoxyribose nucleic acid
CDS	coding sequence
CMD	craniometaphyseal dysplasia
CPPD	calcium pyrophosphate deposition disease
CRE	cAMP response element (DNA sequence)
CREB	cAMP response element-binding protein (transcription factor)
cRNA	capped ribose nucleic acid
dNTP	deoxyribonucleotide triphosphate
dpm	disintegrations per minute
EGTA	ethylene glycol tetraacetic acid (chelating agent)
ePPi	extracellular pyrophosphate
FITC	fluorescein isothiocyanate
GAPDH	glyceraldehyde-3-phosphate dehydrogenase
GITC	guanidine isothiocyanate
HEK	(HEK 293) Human Embryonic Kidney cells
HPLC	High performance liquid chromatography
IMAGE	Integrated Molecular Analysis of Genomes and their Expression
IMCD	inner medullary collecting duct
$mpkCCD_{cl4}$	murine cortical collecting duct clone 4 cell line
mRNA	messenger ribose nucleic acid
NAD	nicotinamide adenine dinucleotide (NADH is the reduced form)
NIV	normalised intensity value
NPP	nucleotide pyrophosphatase phosphodiesterase
NTPDase	nucleoside triphosphate diphosphohydrolase
OCT	“optimum cutting temperature” embedding compound
PDE	phosphodiesterase
Pi	phosphate
PPase	pyrophosphatase
PPi	pyrophosphate
PVDF	polyvinylidene fluoride
qPCR	quantitative polymerase chain reaction
RT	reverse transcriptase
RT-PCR	reverse transcriptase – polymerase chain reaction

SNP	single nucleotide polymorphism
TBE	tris-borate ethylenediaminetetraacetic acid buffer
TNAP	tissue-nonspecific alkaline phosphatase
TRITC	tetramethyl rhodamine isothiocyanate
UDPG	uridine diphosphoglucose
UTP	uridine triphosphate
UTR	untranslated region
UV	ultraviolet

* ANK denotes either mouse ANK or ANK generically; whereas ANKH specifically denotes human ANK protein, although both terms are increasingly used interchangeably in the literature.

1 Introduction

1.1 Kidneys and pyrophosphate

1.1.1 Requirement for inhibitors of calcification in the kidney

The kidneys maintain salt and water balance in the body by filtering, secreting and reabsorbing solutes, and by reabsorbing water from the resulting urine, such that less than 1% of the total glomerular filtrate is lost. Net solute loss and water reabsorption causes the concentration of calcium and phosphate salts in the filtrate to exceed their normal limit of solubility resulting in a state of metastable supersaturation especially in the renal distal tubule and collecting ducts. Similarly, solutes may accumulate in the renal medullary interstitium due to tubular transport and recycling. Calcium stone formation may be initiated in the interstitium from a nidus (initiating crystal deposit) of calcium phosphate (hydroxyapatite) (Evan *et al.*, 2003), even in the case of idiopathic calcium oxalate stones. As metastable saturation of calcium salts increases, the risk of crystallisation increases logarithmically. Yet calcification of the tubule lumen or interstitial matrix ultimately leading to formation of urinary stones occurs in only a small percentage of individuals. This calcification is prevented by inhibitory substances in urine such as citrate, magnesium, and urinary proteins together with cellular processes that limit crystal retention and subsequent agglomeration (Sayer *et al.*, 2004; Costa-Bauza *et al.*, 2005; Verkoelen & Verhulst, 2007). One of the most potent of these crystal inhibitors is pyrophosphate (PPi) (Fleisch & Bisaz, 1962; Sidhu *et al.*, 1986). PPi binds to the surface of hydroxyapatite (calcium phosphate) crystals, directly inhibiting their growth (Jung *et al.*, 1973).

1.2 Chemistry of PPi

1.2.1 Role as crystallisation inhibitor

It has been known for many years that pyrophosphate (PPi) is a potent inhibitor of hydroxyapatite crystallisation in the skeleton (Fleisch & Bisaz, 1962; Russell, 1976). Excess extracellular PPi inhibits this mineralisation, whereas a higher inorganic phosphate (Pi) : PPi ratio leads to increased mineralisation. Too high an extracellular PPi concentration can however lead to deposition of crystals of calcium pyrophosphate (CPPD disease, a form of chondrocalcinosis). A balance must therefore exist between these opposing effects of PPi, and mechanisms must operate both intracellularly (where most PPi is produced) and

extracellularly (where most of its crystal inhibitory effects occur) to prevent aberrant crystallisation. Mechanisms may include compartmentalisation in membranes or hydrolysis of PPi by PPases. Decreased extracellular PPi is now being suggested as an aetiological factor in the pathophysiology of uraemic vascular calcification (Lomashvili *et al.*, 2005; O'Neill *et al.*, 2010).

1.2.2 Reactions which generate PPi

PPi is involved in many aspects of eukaryotic cellular physiology. It is generated as part of numerous reactions that synthesise and modify nucleotides, coenzymes and non-essential amino acids. Many of these reactions have been known about since the 1950s (listed in Chapter 1 of (Heinonen, 2001), and the source of PPi is often a nucleotide triphosphate (such as ATP) (Rachow & Ryan, 1988). Accordingly, *in vivo* PPi turnover studies suggest that most PPi metabolism is intracellular (Jung *et al.*, 1970), yet its crystal inhibitory effects are mainly extracellular (Harmey *et al.*, 2004). For example, the PPi concentration in rat liver is relatively high at 130 μM, as measured by Davidson & Halestrap (1988; concentration calculated in Heinonen, 2001, p. 61), with over 90% of PPi being located in mitochondria. This is much higher than in extracellular body fluids such as human urine (15-32 μM; Baykov & Avaeva, 1982) and human plasma (1.8-3.5 μM; (Silcox & McCarty, 1973; Russell *et al.*, 1971); 1-6 μM (Russell, 1976)), and the large difference may account for some of the variability in PPi concentrations measured in extracellular fluids. These data suggest that PPi is highly segregated into cellular compartments, which necessitates movement of the highly charged PPi ion across membranes. Unnecessary hydrolysis of PPi would waste energy as heat unless coupled to other processes, suggesting that PPi transport must occur either as the free ion, as a complex with another ion (for example calcium), or possibly as ATP itself. Although PPi can be generated extracellularly by the action of the NPP enzymes, this would not account for PPi movement between compartments. However, the precise mechanism of PPi transport across membranes remains unknown.

1.2.3 Measurement of PPi in biological systems

PPi has until recently always been measured by indirect assays. The first step was typically to separate PPi from other phosphate-containing compounds by ion-exchange chromatography (Russell *et al.*, 1971), sometimes coupled with boiling to inactivate PPases (Russell & Hodgkinson, 1966). The PPi was then either acid hydrolysed and measured as phosphate or measured enzymatically by PPi consumption during the formation of UTP

from UDPG (Flodgaard & Fleron, 1974). More recently, a zinc-containing organic PPi sensor molecule has been developed, which fluoresces in direct proportion to the PPi concentration (Dong Hoon *et al.*, 2004). No published reports exist of re-measurement of PPi in tissues using such technology, which is a one-step process that is highly selective for PPi over other anions also commonly found such as inorganic phosphate and ATP.

1.3 Molecular biology of ANKH

1.3.1 ANKH is evolutionarily highly conserved

The *ANKH* gene on chromosome 5p encodes a 492-amino acid 54.3 kDa (Ho *et al.*, 2000) multipass transmembrane protein. In mice, a truncating mutation in *ANK* causes basic calcium phosphate deposition, leading to progressive ankylosis (fusion) of joints, giving the gene its name. There is significant conservation of this gene across many vertebrate species and the human homologue *ANKH* is virtually identical to *ANK* in the mouse (Figure 3.2). The protein is called ANKH in humans and ANK in mice, although, perhaps because of their similarity, these terms are now often used interchangeably (as on NCBI Entrez Gene ID 11732).

1.3.2 ANKH is implicated in altering PPi levels locally

Mutations affecting the *ANK* gene in both mouse and humans can cause a range of diseases, with most published work in the early 2000s concentrating on bone and joint diseases. The phenotypes are either calcium PPi deposition disease (CPPD) or progressive ankylosis depending on whether the *ANK* mutation is activating or inactivating, respectively.

Ho *et al.* (2000) were the first to show that ANK has a role in PPi transport. Fibroblasts cultured from mutant $ANK^{ank/ank}$ mice showed increased intracellular PPi but decreased extracellular PPi levels compared to control fibroblasts from wild-type mice. Transfection of the mutant fibroblasts to allow expression of normal ANK protein rescued these changes, consistent with ANK-mediated PPi transport from cell to medium. This transport could be blocked by probenecid at 2.5 mM, a non-specific anion transport inhibitor. More recently, expression of ANK in *Xenopus* oocytes has confirmed ^{32}PPi influx into the oocytes which showed saturation by external PPi with an apparent K_m of ~2 μM (Gurley *et al.*, 2006b). ANK is therefore unlikely to be simply an anion channel but little else is known about ANK function (whether facilitated transporter, symporter or antiporter) and its specificity with respect to anions such as phosphate or even ATP (suggested by (Ryan, 2001).

1.3.3 *ANKH* single gene disorders in humans cause clinical effects via altered PPi levels

Since the role of PPi as a crystal inhibitor had been known for many years, the findings of Ho *et al.* (2000) implicated *ANK (ANKH* in humans) as a candidate gene in disorders of crystallisation. This was enhanced by the observation that the mutations for two disorders of calcification, the familial CPPD subtype CCAL2 (OMIM 118600) and craniometaphyseal dysplasia (OMIM 123000), were both located on chromosome 5p, the same region as the *ANKH* gene (Nurnberg *et al.*, 1997; Ho *et al.*, 2000). Polymorphisms in the *ANKH* gene are now known that can cause an increase or decrease in gene function, and are found in these calcification disorders (Table 1.1). Genetic studies for CCAL2 had identified three mutations, M48T, E490del and -11CT, in different families. Pendleton *et al.* (2002) reconstructed these mutations in a full-length ANK expression construct followed by transfection into COS-7 cells. This showed a significant increase in measured PPi transport extracellularly *in vitro* when compared to a known inactivating mouse mutant. Although this finding suggested increased *ANKH* gene activity for each mutation, it was found to be non-significant with respect to wild type *ANKH*, and an unchanged subcellular distribution of a similar transfected construct for the M48T mutation was recently confirmed by Carr *et al.* (2007). Similarly, three inactivating mutations (two in-frame single amino acid deletions and one insertion) were identified by Reichenberger *et al.* (2001) by direct sequencing in families with CMD, although they did not measure PPi levels to confirm the mechanism. Interestingly, in all cases these mutations occur in the cytosolic domains of the ANKH protein.

Mutations in the *ANKH* gene may thus be associated with gain or loss of ANKH function. These single gene disorders suggest that ANKH is an important component of PPi metabolism in human bone and joints. However, they do not shed light on the mechanism of ANKH function. It is unclear whether PPi transport occurs by transport via ANKH itself or whether ANKH is associated with a separate PPi transporter. Other transporters of PPi may also exist. ANK function in bone is known to be modulated by intracellular and extracellular factors (Harmey *et al.*, 2004) but regulation of its function in the kidney is unknown.

ANK gene activity	Human	Mouse
Increased (hence increased ePPi)	**1. Chondrocalcinosis type 2 (CCAL2)** Deposition of calcium pyrophosphate dihydrate crystals causing acute attacks of pseudogout in large joints. Mild, late onset. *Autosomal dominant CCAL2:* M48T (gain), E490del (gain) and -11CT (gain) (Pendleton *et al.*, 2002) *Sporadic CCAL2:* -4-bp G-to-A SNP (5'UTR) (Zhang & Brown, 2005). Demonstrated increased ANK expression and extracellular PPi *in vitro*. **2. Seizures** in autosomal dominant CCAL: Members of one such family experienced early childhood seizures : +4 N-terminal amino acids added due to premature initiation codon, causing likely gain of function (McKee *et al.*, 2004).	There is no CCAL2 phenotype in mice. $ANK^{M48T/null}$ mice showed restored joint function over $ANK^{null/null}$ but no increased PPi deposition (Gurley *et al.,* 2006b).
Decreased (hence decreased ePPi)	**1. Craniometaphyseal dysplasia (CMD)** Increased mineralisation causes overgrowth and sclerosis of the craniofacial bones and abnormal modelling of long bone metaphyses, but normal joints. *Autosomal dominant CMD:* (Reichenberger *et al.*, 2001): TCT1127–1129 F376del (loss), CTC1122–1124 S375del (loss), CAG1139–1141 A380ins (loss). (Nurnberg *et al.*, 2001): W292R, C331R, S375del, F377del, P380insA, G389R. *Sporadic CMD:* (Zajac *et al.*, 2010): Complex heterozygous mutation in exon 7 **2. Possible link to spondyloarthritides** Association of non-coding *ANKH* polymorphisms suggested by Canales *et al.* (2006) and Korkmaz *et al.* (2005), but not confirmed by Sayer *et al.* (2008). **3. Possible cause of nephrocalcinosis in humans?** Circumstantial evidence: Hypopyrophosphaturia may be a metabolic risk factor in recurrent calcium renal stone formers (Laminski *et al.*, 1990).	**1. Progressive ankylosis** Two mouse models featuring severe ankylosis, indistinguishable from each other: $ANK^{ank/ank}$ is a naturally occurring nonsense mutation causing a 53 amino acid C-terminal truncation (Ho *et al.*, 2000). $ANK^{null/null}$ had an identical phenotype to $ANK^{ank/ank}$ (Gurley *et al.*, 2006a). But not supported *in vitro* by Carr *et al.* (2007) and Pendleton *et al.* (2002). **2. Craniometaphyseal dysplasia** C331R and G389R mutations (Nurnberg *et al.,* 2001) abolish PPi transport in *Xenopus* and transgenic mice (Gurley *et al.,* 2006b) suggesting a dominant negative effect on *ANK*. F377del homozygous knock-in is a mouse model of CMD (Chen *et al.,* 2009). **3. Nephrocalcinosis** Increased calcification in the kidneys of adult $ANK^{ank/ank}$ mice was reported by Ho *et al.* (2000).

Table 1.1 Summary of human and mouse disorders of calcification linked to *ANK* polymorphisms. Polymorphisms or mutations in the *ANK* gene causing either an increase or decrease in gene function exist in both human and mouse, and may lead to increased extracellular PPi which reduces calcification, or *vice versa*.

1.4 PPi, ANKH and inhibition of renal calcification

1.4.1 Mechanisms of nephrocalcinosis/nephrolithiasis

Nephrocalcinosis describes the effect of a heterogeneous group of diseases which cause an increase in the calcium content of the kidney. Many of these causes have now been defined, involving specific mutations in genes encoding tubular transporters (reviewed in Sayer *et al.*, 2004). The location of the initial calcium deposits may indicate separate pathophysiological entities. Interstitial deposits initially at the renal papilla give rise to Randall's plaques which may eventually rupture through the papillary epithelium to form stones within the renal calyces (Evan *et al.*, 2006). Tubular nephrocalcinosis, in contrast, results in intratubular deposits that may block urine flow directly (Verkoelen & Verhulst, 2007) and can lead to a reduction in renal function and ultimately renal failure.

1.4.2 PPi and other calcification inhibitors in the kidney

Fleisch & Bisaz (1962) first demonstrated PPi as an inhibitor of calcification routinely present in human urine, at concentrations of ~10 μM (range 8-32 μM; March *et al.*, 2001; Baykov & Avaeva, 1982). PPi excreted in urine appears to be relatively stable, with complete recovery from an anion exchange resin being possible (March *et al.*, 2001). Twenty-four hour urinary outputs of PPi are positively correlated with urine volume (Roberts *et al.*, 1992) but PPi is elevated in the most concentrated (low volume) samples (Roberts *et al.*, 1992). Calcium stone formers appear, on balance, to show reduced urinary PPi excretion (Baumann *et al.*, 1977; Wikström *et al.*, 1983; Roberts *et al.*, 1992), and in a group of 107 patients with recurrent calcium stones, 48% had reduced urinary PPi:creatinine ratios compared to control subjects (Laminski *et al.*, 1990).

As already noted, PPi directly inhibits hydroxyapatite crystal growth (Jung *et al.*, 1973). *In vitro,* PPi at concentrations similar to those in normal urine (~30 μM) effectively prevents crystallisation of hydroxyapatite in artificial urines (Grases *et al.*, 2000; March *et al.*, 2001). However PPi is not the only inhibitor of crystallisation. Others include citrate, phytate, magnesium, glycosaminoglycans and polyanionic proteins including uromodulin (Tamm-Horsfall protein) and osteopontin. Osteopontin is synthesised within rat and human kidney cells and is excreted in urine. It is normally present at the apical surface of the distal tubule in normal cells, but its synthesis is further increased following toxic or ischaemic stress (Verstrepen *et al.*, 2001; Verhulst *et al.*, 2002). Some of these crystallisation inhibitors may

also act synergistically, for example, PPi and citrate have been shown to have a synergistic effect in artificial urine in preventing hydroxyapatite formation (Costa-Bauza *et al.*, 2002), and similarly molecular modelling studies suggest that there may be additive effects on control of oxalate crystal growth with more than one inhibitor (Qiu *et al.*, 2004). Taken together, this evidence strongly suggests that urinary PPi is capable of inhibiting urinary calcification at naturally occurring PPi concentrations in the urine, and its effect may be augmented by other crystallisation inhibitors.

1.4.3 Clinical effects of abnormal ANKH function in human kidney

Ho *et al.* (2000) demonstrated in mice that inactivation of ANK not only disrupts skeletal mineralisation, but also causes renal calcification. In contrast, the phenotype of disordered *ANKH* gene function in the human kidney is largely unexplored. If *ANKH* is mutated, might we expect a clinical correlation between kidney stones and apatite deposition? In spondyloarthritides such as ankylosing spondylitis, large amounts of apatite are deposited (Sampson *et al.*, 1991) and the mutant $ANK^{ank/ank}$ mouse has been regarded as a valid model of this (Mahowald *et al.*, 1988). Polymorphisms in two different regions of the *ANKH* gene were found to be associated with ankylosing spondylitis (Tsui *et al.*, 2005) although this linkage remains controversial (Timms *et al.*, 2003). A clinical study (Canales *et al.*, 2006) found that there was a higher incidence of kidney stone formation in patients with spondyloarthritides compared to rheumatoid arthritis patients (who do not experience apatite deposition) as controls, even after correcting for drug use and other stone risk factors. They suggest that this makes spondyloarthropathy an independent risk factor for kidney stones.

1.4.4 Origin of PPi in urine

1.4.4.1 The majority of filtered PPi is hydrolysed in the proximal tubule

The extracellular PPi concentration is limited by enzymes with inorganic pyrophosphatase activity (alkaline and acid phosphatases). Intracellularly, PPi is compartmentalised in organelles (e.g. Davidson & Halestrap, 1988) and requires a channel or specific transporter to cross cell membranes (Terkeltaub, 2001). As a result, there is little PPi present in the cytosol. In bone, chondrocytes are a source of PPi (Ryan *et al.*, 1981), but most PPi present in plasma arises from liver metabolism (Rachow & Ryan, 1988). However, ^{32}PPi injected intravenously into dogs is rapidly hydrolysed in plasma with PPi also being filtered at the glomerulus and subject to further hydrolysis within the kidney, such that less than 5% of

intravenous ^{32}PPi appears in urine (Jung *et al.*, 1970). The kidney expresses alkaline phosphatases which hydrolyse PPi to inorganic phosphate. Both the intestinal form of alkaline phosphatase and the tissue non-specific form of alkaline phosphatase (TNAP) are present in kidney (Nouwen & De Broe, 1994). 'Intestinal' alkaline phosphatase is restricted to the pars recta (S3) of the proximal tubule whilst TNAP is expressed along the proximal tubule in the S1, S2 and S3 segments (Nouwen & De Broe, 1994). The proximal location of these alkaline phosphatase isozymes ensures that the majority of PPi delivered by glomerular filtration will be rapidly hydrolysed. The physiologically important increase in urinary PPi after ingestion of orthophosphate may result from inhibition of PPi hydrolysis (Russell, 1976).

1.4.4.2 Some PPi generation can occur extracellularly within the tubule

Apart from glomerular filtration and intracellular origin routes, PPi in the kidney can also be formed entirely extracellularly. ATP has been detected at various locations along the rat tubule lumen (Vekaria *et al.*, 2006b) where it may be secreted by proximal tubular cells in response to flow stimuli (Jensen *et al.*, 2007). It is then rapidly subjected to enzymatic degradation (Vekaria *et al.*, 2006a) by NTPDase and NPP ectoenzymes present in the tubule. Hydrolysis of nucleotide triphosphates by NPP enzymes generates PPi. Due to the proximal localisation of phosphatases and the relatively small amount of extracellular ATP, the component of ATP-derived PPi is likely to be small and locally generated in the distal nephron segments.

1.4.4.3 Transport of PPi across the tubular membrane is likely to be the source of most extracellular PPi in the lumen and interstitium

By far the largest source of PPi generation is as a product of intracellular reactions. Ho *et al.* (2000) showed that ANK functions in the membrane transport of PPi, and demonstrated using Northern blotting, that *ank* mRNA is expressed in many mouse tissues other than joints including heart, brain, liver, spleen, lung and muscle, but importantly also kidney. The pathological effect of abnormal ANKH function on bones and joints is now accepted (section 1.3.3 above), and we hypothesise a similar role for ANKH in suppressing inappropriate mineralisation within the urinary system. Indeed, mutant $ANK^{ank/ank}$ mice exhibit nephrocalcinosis (Ho *et al.*, 2000). Similarities between kidney and joints in this regard include the fact that both have cells expressing ANK in areas where extracellular PPi is present, and both have an important need to prevent or regulate crystal formation in the

face of a crystal-inducing environment.

1.4.5 Localisation of ANK in the kidney

1.4.5.1 ANK is expressed in the collecting duct in mouse

ANK expression has been confirmed by RT-PCR in mouse kidney and the model collecting duct cell-line, mIMCD-3 (Carr *et al.*, 2007). Immunohistochemistry of mouse kidney sections showed ANK immunofluorescence in cortical collecting ducts when identified by co-staining with aquaporin-2 (Carr *et al.*, 2007). No immunofluorescence was observed in the rest of the nephron, including all segments of the proximal tubule, although there was weak staining of glomeruli. ANK expression is therefore prominent in those segments of the nephron downstream from the alkaline phosphatase-expressing proximal segments.

In the mIMCD-3 cell-line and in mouse kidney sections, immunofluorescence showed ANK to be present at both the apical and basolateral membranes (Carr *et al.*, 2007). Overexpression of an ANK-GFP fusion protein in mIMCD-3 cells demonstrated colocalisation with both the endoplasmic reticulum and mitochondria (Carr *et al.*, 2007). An N-terminal GFP-tagged construct containing the inactivating mutation G440X, of mutant $ANK^{ank/ank}$ mice, resulted in disruption of ANK-GFP trafficking to the cell membrane with retention within the endoplasmic reticulum/Golgi apparatus. Mitochondrial localisation was unaffected (Carr *et al.*, 2007). ANK-mediated PPi transport across both apical and basolateral membranes may therefore occur, allowing locally generated PPi to participate in minimising hydroxyapatite nidus formation in both the interstitium and the tubule lumen.

1.4.5.2 Rationale for co-ordination of ANK and aquaporin-2 regulation

Scanning the ANK protein for potential serine/threonine phosphorylation sites and combining this with transmembrane topology (ten or twelve segments, as suggested by Ho *et al.* (2000) and Nurnberg *et al.* (2001) respectively) indicates multiple potential cytoplasmic sites for PKA-mediated phosphorylation. The sub-cellular distribution of ANK overlaps with that of aquaporin-2 (AQP2) in principal cells (Carr *et al.*, 2007) which suggests that the overall activity and perhaps membrane traffic of both proteins is co-ordinated. In a state of systemic dehydration, arginine vasopressin activates V_2 receptors causing an increase in adenylate cyclase activity. This will not only increase cAMP but also increase intracellular PPi as a substrate for ANK-mediated transport. However evidence for

the acute regulation of ANK is still required.

1.5 Aims of this study

1.5.1 Benefits of understanding ANKH function in the kidney

The notion that extracellular PPi inhibits hydroxyapatite formation within the kidney was first proposed in the 1960s. It is clear that the majority of PPi production is intracellular, and transport of this highly charged species across membranes is essential but its mechanism has still not been elucidated. ANK is now conclusively implicated in the regulation of bone mineralisation in both mouse and humans. However little work has been performed in the kidney despite there being a physiological need for constitutive inhibition of renal calcium crystallisation, the localisation of ANK in the murine nephron segment where this is most likely to occur and the demonstration that $ANK^{ank/ank}$ mice exhibit renal calcification. Clarification of ANK's physiological role in the kidney may enhance our understanding of a key physiological mechanism in the prevention of renal calcium crystallisation.

1.5.2 Experimental strategy

We hypothesise that ANKH has a central role in the transport of PPi across membranes in the renal tubule.

There are no published data on human renal ANKH expression. The first part of this thesis will examine the expression and localisation of ANKH in human kidney, demonstrating its localisation to the distal nephron and collecting duct segments. Using the method of Gurdon *et al.* (1971), ANKH-containing constructs are heterologously expressed in *Xenopus* oocytes enabling a wide range of flux experiments to be performed. This will allow insights into the molecular mechanism of ANK-mediated PPi membrane transport. Finally, given the similarity of localisation of ANK and the water channel aquaporin-2, we will explore the regulation of ANK and whether there may be a similar regulatory mechanism for both proteins which would potentially be of physiological benefit.

2 Materials and Methods

2.1 Human renal tissue

2.1.1 Collection of tissue

Tissue was collected from the normal pole of nephrectomised specimens at the Freeman Hospital, Newcastle upon Tyne. Ethical approval was obtained from the Sunderland Local Research Ethics Committee. Kidney tissue was obtained after informed consent from patients undergoing nephrectomy for renal cell carcinoma subject to the following exclusion criteria: serum creatinine > 140 μmol/l, history of renal stones, nephrocalcinosis or arthritis, currently taking bisphosphonate medication, or any evidence of renal scarring.

Tissue was immediately removed to a renal preservation solution (Ahmad *et al.*, 2006) at 4 °C and transported to the laboratory on ice. The solution was made up as: sucrose 140 mM, Na_2HPO_4 42.3 mM and NaH_2PO_4 26.7 mM in distilled water. This was pH corrected to 7.4, and followed by autoclaving, aliquoting into sterile containers and storage at 4 °C until required for use. This solution has been shown to be superior to other commonly used solutions in the preservation of renal tissue after warm ischaemia (Ahmad *et al.*, 2006).

2.1.2 Preparation of tissue

Tissue was cut on ice in a Class II hood and either stored in RNAlater (Sigma) for future RNA extraction or immediately snap frozen in liquid nitrogen-cooled isopentane (2-methylbutane). This allowed rapid freezing without boiling of liquid nitrogen which could damage tissue morphology. Surplus tissue was disposed of as clinical waste. Cubes of 5 mm edge length from each of cortex and medulla were mounted using OCT onto a cork block and stored at -80 °C until used as described in sections 2.5.6.1.

2.2 RT-PCR of ANKH from whole tissue and cell culture lines

2.2.1 Overview

RT-PCR was used for detection and amplification of ANK(H) mRNA from whole human kidney and the cell lines HEK and mpkCCD_{cl4}, to allow sequencing of ANK(H). cDNA in the form of IMAGE clones could be amplified directly using PCR with gene specific primers.

Total RNA was obtained from human kidney and the cell lines using the RNeasy midi kit

(Qiagen). Extracted RNA was reverse transcribed according to the protocol of the Omniscript RT kit (Qiagen). Negative controls omitted RNA or reverse transcriptase. HotStarTaq DNA polymerase (Qiagen) was used for PCR; negative controls omitted DNA. Direct sequencing (Lark Technologies, Essex, UK and MWG, Germany) was used to confirm the identity of the PCR products.

2.2.2 RNA extraction from tissue and cell lines

The RNeasy midi kit (Qiagen Ltd, West Sussex, UK) was used to extract total RNA. Spin columns contain a silica-gel membrane which adsorbs RNA under high salt conditions, allowing elution of bound RNA with water.

2.2.2.1 Cell layers

Cell layers could be lysed directly in the culture dish after washing with phosphate buffered saline (PBS), by exposure to a highly denaturing guanidine isothiocyanate (GITC) containing lysis buffer. This buffer immediately inactivates RNases to ensure isolation of intact RNA. Following lysis the sample was homogenised by passing through a 20-gauge needle several times. Ethanol was added to provide appropriate binding conditions, and the sample was then applied to the RNeasy column containing the silica-gel membrane which bound the RNA. Following washing with supplied buffers, the RNA was eluted in 150 µl RNase-free water, and quality and quantity determined by UV adsorption at 260 nm and 280 nm with the use of a spectrophotometer (Eppendorf supplied by VWR International Ltd., Dorset, UK).

2.2.2.2 Human kidney tissue

The Qiagen kit contained a protocol to optimise RNA yield and purity from tissue samples. This was important as the total yield of mRNA is only about 2% of total RNA extracted. Fresh tissue transported in media (see section 2.1) on ice was stored immediately upon receipt in RNAlater RNA stabilisation reagent (Sigma) at 4°C overnight then at -20 °C long term. The stabilised tissue was homogenised in the GITC-containing lysis buffer using a rotor-stator homogeniser (Qiagen) for 30-60 seconds, and the mixture then centrifuged for 10 min at 3000x *g*. The pellet was discarded, ethanol added and the protocol above was then followed.

2.2.3 Reverse transcription

An RNA-dependent DNA polymerase (reverse transcriptase) was used to obtain cDNA from a total RNA template, using the Omniscript RT kit (Qiagen). Each 20 µl RT reaction contained a final concentration of 1 X RT buffer (Qiagen, proprietary composition), 2 mM dNTP mix (dATP, dGTP, dCTP and dTTP at a concentration of 0.5 mM each), 1 µM random hexanucleotide (n6NTP) primers (or oligo-dT primer), 10 units of RNase inhibitor (Promega, Southampton, UK), 4 units of Omniscript reverse transcriptase enzyme, and total RNA template (typically 0.5-2 µg total RNA, eluted in water) made up to 20 µl with RNase free water.

RNase free water, RNA and n6NTP primers were incubated for 10 minutes at 65 °C and then placed on ice for 2 minutes to denature the RNA. The remaining reagents were added and incubated at 37 °C for 1 h to allow for synthesis of cDNA, followed by an incubation of 3 minutes at 95 °C to inactivate any remaining enzyme, before proceeding directly to a PCR reaction. Incubations were carried out in a thermal cycler (Hybaid, UK). Negative controls omitted either RNA, or RT enzyme to ensure no genomic DNA contamination. All reactions were performed in 0.2 ml microfuge tubes (Eppendorf, supplied by VWR International Ltd., Dorset, UK).

2.2.4 Polymerase chain reaction

The polymerase chain reaction (PCR) allows rapid and exponential amplification of a specific piece of DNA *in vitro.* The HotStarTaq PCR kits (Qiagen) included a Taq DNA polymerase that has been modified to prevent activity and hence formation of misprimed products and primer dimers at low temperatures. A 25 µl PCR reaction mix was prepared, comprising final concentrations of 1 x PCR reaction buffer, 1.5 mM $MgCl_2$ (contained in PCR buffer), 100 µM of each dNTP, 0.1 - 0.5 µM forward primer, 0.1 - 0.5 µM reverse primer, 2.5 units HotStarTaq DNA polymerase, ≤ 1 µg cDNA template from the RT reaction and molecular biology grade water to the final reaction volume. Negative controls were set up in parallel in which the cDNA template was replaced with either an equal volume of the RT negative controls, or an equal volume of molecular biology grade water (PCR negative control). All reactions were performed in 0.2 ml microfuge tubes (Eppendorf, supplied by VWR International Ltd.).

The reaction tubes were placed in a thermal cycler (Hybaid) and heated to 95 °C for 15 minutes allowing activation of the HotStarTaq polymerase. The three step process of

denaturation, annealing and extension involved in PCR was then initiated. The reaction mix was heated for 30 seconds at 94 °C in order to denature the DNA template strands. The temperature was then lowered to a specific optimum annealing temperate for 30 seconds to allow the pair of oligonucleotide primers to bind to their complementary DNA sequences on the single target strands (annealing). Finally, the temperature was raised to 72 °C for 1 minute to allow the DNA polymerase enzyme to extend the primers, using the target strand as template (extension), producing a new complementary DNA strand of the original strand. This three step process was carried out for 35-40 cycles generating an exponential increase in the number of copies of target sequence. At the end of the reaction, the extension time was lengthened to 10 min.

2.2.5 Primers

Gene-specific oligonucleotide primers were designed to allow PCR amplification of either sections (Figure 2.1) or the full-length of ANK(H). Amplified products were then used for cloning, sequencing and cRNA synthesis. Oligonucleotide primers were either designed or were included with cloning kits. A full list is included in Table 2.1.

Primer pairs were designed using Primer3 software[1] from available database sequences (Ensembl) according to the following guidelines: a similar adenine (A) / thymine (T) to guanine (G) / cytosine (C) ratio, with one or two G or C residues at the 3' end for extension stability; avoidance of internal homology and homology between primer pairs to prevent binding to self or primer dimerisation; and similar melting temperature (T_m) of each member of the pair. Primer sequences were verified for specificity using the Basic Local Alignment Search Tool[2] (BLAST). For example, the primer pair JS 600F and 601R was originally designed for an internal mouse ANK product spanning exon-exon boundaries. BLAST search of the human genome confirmed that this sequence uniquely matched exons 2, 3 and 4 of ANKH. Designed primers were custom made by VHBio Limited (Gateshead, UK) and supplied as a dried pellet. Prior to use, oligonucleotides were resuspended in molecular biology grade water to a concentration of 100 μM, which were diluted further to a working concentration of 10 μM and stored at -20 °C.

[1] http://frodo.wi.mit.edu/primer3
[2] www.ncbi.nlm.nih.gov/blast

Primer set	Primer sequences (forward / reverse, from 5' to 3')	Product size (bp)	Optimum annealing temp (℃)	Purpose
JS 600F JS 601R	CATCACCAACATAGCCATCG CCAGGTGACTGTGAAGCAAA	490	58	Detection of internal product of mouse ANK or human ANKH
β-actin F β-actin R	TCCACGAAACTACCTTCAAC TTTAGGATGGCAAGGGAC	682	52	Detection of β-actin in human tissue and mpkCCD$_{cl4}$ cells
SM 201F SM 202R	AGATGTGTGTGGGGTCAGC CGTCCACATGGTGCAGTTTA	397	58	Primer combination to amplify contiguous sequences from ANKH coding sequence (see Figure 2.1)
SM 210F SM 211R	CTGCCGTCTTTCACACACTG CGAAGGTGAACTTCTTGATGTG	699	57	Primer combination to amplify contiguous sequences from ANKH coding sequence (see Figure 2.1)
SM 212F SM 213R	GTGAGCACGAGCAACACAGT GCCGAAGTGTCATCCTGACT	597	57	Primer combination to amplify contiguous sequences from ANKH coding sequence (see Figure 2.1)
GC 206F GC 207R	ATGGTGAAATTCCCGGCG TTATTCATTCTCCTCTCTCATTTCCAC	1479	60	Cloning using GFP Fusion TOPO TA Expression kit; Attempted amplification of full-length human ANKH
SM 401F GC 207R	CACCATGGACTACAAAGACC TTATTCATTCTCCTCTCTCATTTCCAC	1566	55	FLAG F and ANKH R primers for blunt-ended amplification with proof reading polymerase of full length ANKH-NT-3XFLAG, allowing subcloning into T7-containing vector
GC 208F	CGACATCATCCCTGACAGAAG	-	-	Sequencing primer for full-length ANKH-NT-GFP
T7EEV	AAGGCTAGAGTACTTAATACGA	-	-	T7 forward primer (Promega cat Q6700) designed for sequencing in pTNT vector (used for ligated ANKH-pTNT construct with SM 202R)
T7F BGH R	TAATACGACTCACTATAGGG TAGAAGGCACAGTCGAGG	-	-	For sequencing ANK(H) cloned into pcDNA3.1 expression vector
SM 300F	CACCATGGTGAAATTCCCGGCG	-	-	Amplification of full length ANKH for directional cloning into pcDNA3.1 Dir vector. The initiation codon (underlined) falls within a Kozak sequence for optimum translation

Table 2.1 Oligonucleotide primers. Primer names prefixed with two letter codes were designed; others were bought or included with kits. Primer pairs designed specifically for amplification of contiguous portions of ANKH coding sequence are shown on the map in Figure 2.1.

Figure 2.1 Map of primer combinations designed to amplify contiguous sequences from ANKH coding sequence

(Carr *et al.*, 2007)

(Pendleton *et al.*, 2002; Canales *et al.*, 2006)

(Korkmaz *et al.*, 2005; Sayer *et al.*, 2008)

(Wang *et al.*, 2009)

2.2.6 Agarose gel electrophoresis

PCR products were separated by electrophoresis through an agarose gel. Typically, following PCR amplification, 10 µl of each reaction was removed and mixed with 2 µl 5x gel electrophoresis loading buffer (Promega). The samples were then loaded into the wells of a 1-2% agarose gel in 1x TBE buffer containing a final concentration of 0.5 µg/ml ethidium bromide. PCR products were electrophoresed alongside an appropriate DNA size marker (O'Generuler, Fermentas) at 80 V for up to 60 minutes in 1x TBE buffer. Gels were viewed using a UV transilluminator (Alpha Innotech Corporation), and the digitised image was processed with an AlphaImager 1200 software analysis system.

PCR products required for subsequent cloning and sequence analysis were excised under UV light using a clean scalpel, and DNA extracted and purified using a gel extraction kit (Sigma). Extracted DNA was eluted into 30 µl of molecular biology grade water and quantified by spectrophotometry.

2.3 Molecular constructs and cloning of PCR products

2.3.1 Overview of cloning procedure

Attempts at making a full length ANKH expression clone from human mRNA were unsuccessful (section 3.2.3) so an IMAGE clone (IMAGE: 3927236; MGC: 15102; corresponding RefSeq mRNA: NM_054027.3) containing the full length ANKH coding sequence in a pOTB7 (drosophila) plasmid expression vector in *E. coli* was obtained from Geneservice (Cambridge, UK). The pOTB7 plasmid also contained a gene conferring chloramphenicol resistance. This clone is cDNA and therefore contains no introns. However, previous work on ANK using the *Xenopus* oocyte expression system used amphibian (pOX) and mammalian (pcDNA3) expression vectors (Gurley *et al.*, 2006b), the former containing 5' and 3' UTR sequences from frog β-globin. Subcloning was therefore performed from pOTB7 to other vectors, by amplification of the ANKH coding sequence (ATG to stop codon), gel extraction and recloning into the new vector (supplied linearised) to enable expression of mammalian protein in *Xenopus* oocytes.

2.3.2 Cloning and transformation reactions

2.3.2.1 Cloning reaction

The cloning reaction consisted of 3 µl fresh PCR product, 1 µl of salt solution, 1 µl of pcDNA3.1 vector (±NT-GFP) and 1 µl molecular biology grade water. The reactants were mixed gently, incubated for 10 minutes at room temperature then placed on ice. The product was immediately used to transform chemically competent cells.

2.3.2.2 Transformation protocol

2 µl of the plasmid was added to a vial of either TOP10™ chemically competent *E.coli* (Invitrogen) or to NEB™ 5-alpha F′I^{q} High Efficiency Competent *E. coli* (New England Biosciences, cat C2992), mixed gently and incubated on ice for 30 minutes. The cells were 'heat shocked' for 30 s at 42 °C, without shaking in a heat block. The tubes were immediately transferred to ice and incubated for 5 minutes, then 950 µl of room temperature SOC outgrowth medium (provided in kit) was added and the tube shaken horizontally at 250 rpm in an incubator for 60 minutes at 37 °C. A 50 µl aliquot from the transformation was spread on a pre-warmed Luria-Bertani (LB) agar plate containing ampicillin (125 µg/ml) and incubated overnight at 37 °C.

2.3.2.3 PCR screening of DNA recombinants

Colonies were selected to inoculate a duplicate LB plate containing ampicillin and allowed to grow for a further 12-24 h, to allow expansion of the clone before screening directly using PCR. A standard PCR reaction using internal ANK primers (Table) was set up, with the initial 95 °C incubation step allowing release of bacterial DNA. Colonies wire-looped directly from the duplicate plate provided DNA template. Products were analysed using 2% agarose gel electrophoresis.

2.3.2.4 Preparation of plasmid DNA

Positive recombinant colonies identified by PCR screening were cultured overnight in 1 ml LB broth containing ampicillin 125 µg/ml, in aerobic eppendorf tubes on a benchtop vial shaker (Eppendorf) at 200 rpm at 37 °C. Glycerol stocks were prepared by mixing 200 µl of

cultured broth with 800 µl of 50% sterile glycerol, and stored at -80 °C. This stock could be defrosted and used to inoculate further LB broth. The plasmid DNA was isolated and purified using the QIAprep miniprep protocol with the use of a microcentrifuge (Qiagen Ltd.). Plasmid DNA was quantified by UV spectrophotometry and was stored at -20 °C.

2.3.3 Creation of constructs

2.3.3.1 Cloning ANKH into NT-GFP Fusion TOPO TA Expression vector

The NT-GFP Fusion TOPO™ TA Expression Kit was utilised to allow insertion of the PCR DNA into the vector pcDNA3.1/NT-GFP (Invitrogen), allowing expression of the cloned ANKH product with GFP fused to the N-terminus of ANKH. This vector incorporates a gene conferring ampicillin resistance. This 'TA' cloning method exploits the addition by *Taq* DNA polymerase of a single deoxyadenosine to the 3' ends of the PCR product. These 3' A overhangs are used to insert the PCR product into the expression vector which has complementary T overhangs at the insertion site, so that restriction digestion is not required. Transformation was into TOP10 cells.

The sequenced ANKH-NT-GFP contig (Figure 2.2) was checked for reading frame[3] then BLAST search was performed[4]. This showed 100% identity with the amino acid sequence for ANKH, demonstrating that ANKH was present and in-frame with GFP in this construct.

2.3.3.2 Cloning ANKH into pcDNA3.1 Directional TOPO cloning

The pcDNA™3.1 Directional TOPO® Expression Kit (Invitrogen, cat. no. K4900-01) was used. This vector has the advantage of ensuring cloning of the PCR product in the correct orientation by the addition of four bases (CACC) to the forward primer which are complementary to the overhang in the cloning vector (GTGG). This overhang invades the 5' end of the PCR product, annealing to the CACC of the insert, resulting in correct orientation efficiencies of > 90%. Attempted transformation into TOP10 cells resulted in no colonies (although colonies were obtained with the kit's positive transformation control), necessitating use of NEB 5-alpha F´I^q High Efficiency cells. The protocol was otherwise as described above, and sequencing confirmed correct orientation of the insert into the vector (Figure 2.3).

[3] www.ncbi.nlm.nih.gov/projects/gorf/
[4] http://blast.ncbi.nlm.nih.gov/Blast.cgi

Figure 2.2 Sequencing of ANKH-NT-GFP construct

Figure 2.3 Sequencing of ANKH-pcDNA3.1 construct

2.3.3.3 Subcloning ANKH from pcDNA3.1 to pTNT

The pTNT vector (Promega, aliquot kindly donated by Prof F Karet, Cambridge) has been previously used in *Xenopus* experiments (Edashige *et al.*, 2007; Fronius *et al.*, 2010) and contains a 5' β-globin leader sequence which can enhance gene expression (Falcone & Andrews, 1991).

In two separate reactions, 1 μg of closed pTNT vector and 1 μg of ANKH-pcDNA3.1 were double-digested in order to obtain a linearised vector with "sticky ends" and an insert with appropriate restriction sites, respectively. Reactions consisted of: 5 μl of 10x NEB Buffer 2, 0.5 μl of 100x BSA, 1 μl of each of the restriction enzymes *NotI* and *KpnI*, and 1 μg of DNA, made up to 50 μl with molecular grade water. These were incubated at 37 °C for 90 min, then run on a PCR clean-up column (Qiagen) and eluted in water to concentrate and purify the DNA. The cut DNA was separated from supercoiled DNA on a 1% agarose gel, then cut out from the gel and gel purified to obtain pure linearised DNA; the vector being 5249 bp and the insert 1538 bp.

Vector and insert were ligated at "sticky ends" using T4 DNA ligase (NEB, cat. no. M0202S), as follows: 1 μl of 10x buffer, 0.5 μl of T4 DNA ligase, and 0.5-3 μl of vector and insert such that they were each present in separate reactions as vector:insert molar ratios of 1:1, 3:1 and 1:3. The reaction was made up to 10 μl with molecular grade water, and incubated at room temperature for 40 minutes. Negative controls omitted insert (causing religation of the vector) or omitted both insert and T4 DNA ligase (double digested vector only, giving rise to very few colonies). All five ligation reactions were terminated by heating at 65 °C for 10 min, followed by transformation of each DNA into NEB 5-alpha F′I^{q} High Efficiency Competent *E. coli*. PCR screening of duplicate plates was performed using T7EEV as forward (T7 EEV Promoter primer, Promega cat Q6700) and SM 202R as reverse primers (Table 2.1). Sequencing confirmed β-globin upstream and in-frame with ANKH in the pTNT vector (Figure 2.4).

2.3.3.4 Subcloning of ANKH-FLAG into a T7-containing mammalian expression vector

2.3.3.4.1 The FLAG tag

The FLAG® (Sigma) tag is a hydrophilic antigenic epitope consisting of only eight amino acids (DYKDDDDK), synthetically-designed for minimal size but maximum exposure on the surface of the folded protein (Einhauer & Jungbauer, 2001). The 3XFLAG® tandem

repeat (DYKDHDGDYKDHDIDYKDDDK; ~3 kDa) enhances the sensitivity of FLAG by 10-fold, making it particularly useful for detection of proteins that are low-abundance or difficult to express. The tag is preferably inserted at the 5' end of the gene of interest to promote good initiation of translation (Einhauer & Jungbauer, 2001).

2.3.3.4.2 Method of subcloning

ANKH-NT-3XFLAG in pReceiver-M12 vector was obtained from GeneCopoeia (product Mm01188). This product corresponded to NM_020332.2, but direct sequencing in our laboratory revealed the coding sequence to exactly correspond to human ANKH. In order to make cRNA for injection into oocytes, subcloning into a T7-containing expression vector was necessary.

The strategy was as follows. The original clone was single-digested using *NotI* restriction enzyme and digestion verified on a 1% gel. This band was then cut out and gel purified in order to prevent carryover of old vector in the subsequent PCR reaction. PCR was performed using a proofreading DNA polymerase (Phusion, Finnzymes) as follows: 10 µl of 5xPhusion buffer HF, 1 µl of 10mM dNTP, 2.5 µl each of SM 401F and GC 207R full-length primers, 0.5 µl of Phusion DNA polymerase, and 8 ng of single-digested DNA template. PCR conditions were modified as follows: activation , 98 °C for 30 s; and 35 cycles comprising denaturation, 98 °C for 20 s, annealing, 55 °C for 30 s, extension 72 °C for 30 s. The amplified ANKH-NT-3XFLAG insert was verified for size and a single band on a 1% gel, and was then cloned into pcDNA3.1 TOPO vector and transformed into NEB 5-alpha F´I^{q} High Efficiency cells using the protocols above. Sequencing of plasmid DNA using SM 202R confirmed that T7 was upstream and in-frame with ANKH-NT-3XFLAG (Figure 2.5).

Figure 2.4 Sequencing of ANKH-pTNT construct

Figure 2.5 Sequencing of ANKH-NT-3XFLAG construct subcloned into a T7-containing mammalian expression vector

2.4 Preparation of capped RNA for oocyte micro-injection

2.4.1 Overview

Protein synthesis in the *Xenopus* oocyte expression system is best achieved by micro-injection of capped RNA (cRNA) making the RNA analogous to mRNA. The 7-methylguanosine cap is a modified nucleotide at the 5' end of the molecule allowing it to maintain stability during protein synthesis and acting as the start point for transcription by RNA polymerase. The mMESSAGE mMACHINE T7 Ultra kit (Ambion) modifies this by altering a nearby hydroxyl group in order to ensure transcription initiation by T7 RNA polymerase in the correct orientation. The kit incorporates other ways of maximising cRNA yield such as high nucleotide concentrations and an RNase inhibitor. Linearised plasmid DNA that contains a T7 RNA polymerase promoter site is used as template for *in vitro* transcription. The cloning strategies and preparation techniques described in section 2.3 were designed to ensure high quality, pure plasmid cDNA.

2.4.2 Method

2.4.2.1 Linearisation of plasmid DNA

Plasmid DNA was first linearised using a restriction enzyme as follows. NEBcutter V2.0[5] was used to identify a restriction enzyme that would cleave each vector only once, downstream of the insert, and without cleaving the insert itself (see Table 2.2). The following reaction was assembled on ice: 5 µl of 10x NEB Buffer 2, 0.5 µl of 100x BSA, 1 µl of restriction enzyme and 1 µg of DNA, made up to 50 µl with molecular grade water. This was incubated at 37 °C for 2 h then put on ice to stop the reaction. An aliquot of 1 µl was run on a 1% agarose gel to confirm a single band indicating that cleavage was complete.

2.4.2.2 Ethanol precipitation of linearised DNA

Ethanol precipitation was employed to recover pure DNA as well as increasing its concentration. To the ~50 µl sample, 0.1 volumes of 3 M sodium acetate and 2.5 volumes of 95% ethanol were added, which terminated the digest. The sample was frozen at -80 °C for

[5] http://tools.neb.com/NEBcutter2

10 min, then centrifuged at 14000x *g* for 20 min at 4 °C to pellet the DNA. Supernatant was aspirated using a sterile freshly pulled fine glass pipette, and the pellet rinsed in 100 µl of 70% ethanol at -20 °C, pipetted gently down the opposite side to the pellet. The tube was centrifuged again for 10 min as above, then re-aspirated and left to dry in air at room temperature for a few minutes to remove any traces of ethanol. The DNA was then resuspended in 5 µl of molecular grade water.

2.4.2.3 Synthesis of capped RNA

RNase-free consumables were used, other equipment and benches were decontaminated with RNase AWAY™ (Sigma) and pipettes subjected to UV crosslinking (Stratalinker®, Stratagene). The following were added to the pure linearised DNA in water at room temperature: 10 µl of T7 2x NTP/ARCA, 2 µl of 10x T7 reaction buffer, 2 µl of T7 RNA polymerase enzyme mix, 1 µl of RNaseI inhibitor. The reaction was gently mixed, briefly microfuged and incubated at 37 °C for 2 h. Post-reaction DNase treatment to remove template, and poly(A)-tailing to increase mRNA proportion, are not usually required for oocyte microinjection applications. The cRNA end product was diluted with molecular grade RNase-free water, quantified by spectrophotometry, and stored as single-use aliquots at -80 °C.

2.4.3 cRNA types made

Using these methods, cRNA was made for constructs as shown in Table 2.2. This was complemented by total RNA extracted from mouse cell lines and human renal tissue (Table 2.3).

Insert or Construct	Vector	Species	Abbreviation in text	Origin of construct	Linearisation enzyme	Usage
ANKH	pcDNA3.1	Human	ANKH-pcDNA3.1	Cloned in these experiments	*NotI* or *XbaI*	IF, Flux
NaPi-IIb	pSPORT1	Flounder	NaPi-IIb	Kindly gifted by Dr A Werner (Newcastle)	*NotI*	Flux
ANKH	pTNT	Human	ANKH-pTNT	Cloned in these experiments	*NotI*	IF, Flux
ANKH-NT-GFP	pcDNA3.1-NT-GFP	Human	ANKH-GFP	Cloned in these experiments	*XbaI*	Flux
mANK-NT-GFP	pcDNA3.1-NT-GFP	Mouse	mANK-GFP	Kindly obtained from Dr G Carr (Newcastle)	*XbaI*	IF, Flux
ANKH-NT-3XFLAG	pcDNA3.1	Human	ANKH-FLAG	Subcloned in these experiments	*XbaI*	IF, Flux
SLC27A2-CT-GFP	pcDNA3.1-CT-GFP	Mouse	m27A2	Purchased from Genecopoeia	*NotI*	Flux
SLC27A1	pBluescript	Human	h27A1	Purchased from Genecopoeia	*KpnI*	Flux
CD98	pSPORT1	Human	CD98	Kindly obtained from Prof D Thwaites (Newcastle)	-	IF

Table 2.2 Summary of constructs used for synthesis of cRNA, and their usage in downstream applications. All vectors contained a T7 promoter and were ampicillin-resistant. IF, immunofluorescence.

Total RNA type	Species	Origin of construct	Usage
CCD control	Mouse	Extracted from mpkCCD$_{cl4}$ cells	Flux
CCD forskolin-treated	Mouse	Extracted from forskolin-treated mpkCCD$_{cl4}$ cells	Flux
Human kidney	Human	Extracted from human tissue	Flux

Table 2.3 Total RNA types extracted from cells and tissues for co-injection in flux experiments.

2.5 Immunofluorescence

2.5.1 Overview

Membrane proteins present in human renal tissue sections, in cells grown on permeable filters and in *Xenopus* oocytes were detected by immunofluorescent staining using primary and secondary antibodies, with visualisation of localisation using a confocal microscope.

2.5.2 Fixation

Fixation and permeabilisation was performed using methanol for 15 minutes at -20 °C (4 h at 4 °C for oocytes). Tissue due to be treated with anti-CD98 antibody required fixation using 2% paraformaldehyde in PBS for 1 h (4 h for oocytes) on ice (4 °C), with or without subsequent permeabilisation by 0.1% Triton X100. Similarity of results with and without permeabilisation would only be expected of proteins at the membrane.

2.5.3 Primary antibodies

Specific details of antibody use are given in the Results chapters. General details of the primary antibodies used are given in Table 2.4.

Antibody	Species of epitope	Clonality	Abbrev/ alt names	Fixation	Raised in	Conc	Incubation	Source
C-terminal ANK	Mouse/ human	P	Ab3	Meth	Rabbit	1:250	4°C, overnight	Generous gift from Dr Kingsley, Stanford (Ho *et al.*, 2000)
N-terminal ANKH	Human/ mouse	P		Meth	Rabbit	1:100	4°C, overnight	Santa Cruz sc-67242
CD98	Human	M	CD98	PFA	Mouse	1:50	4°C, overnight	BD Pharmingen 556074
AQP2	Human	P		Meth	Goat	1:250	Room temp, 1 h	Santa Cruz sc-28629
NPP1	Human	P	PC-1	Meth	Goat	1:50	4°C, overnight	Santa Cruz sc-23676
NPP3	Human	P	CD203c	Meth	Goat	1:50	4°C, overnight	Santa Cruz sc-27805
hAE1	Human	M		Meth	Mouse	1:10	4°C, overnight	Generous gift from Dr A Toye, Bristol
GFP	-	M	Conjugated to HRP	Meth	Mouse	1:250	4°C, overnight	Santa Cruz sc-9996 HRP
Tamm Horsfall protein	Human	P		Meth	Sheep		Room temp, 1 h	ABD Serotec 8595-0054
Calbindin D28k	Human	P		Meth	Goat	1:100	Room temp, 1 h	Santa Cruz sc-7691
hFATP2	Human	M		Meth	Mouse		4°C, overnight	R&D Systems MAB4659
FLAG	-	M	Anti-FLAG M2	Meth	Mouse	1:80	4°C, overnight	Sigma F3165
FLAG	-	P		Meth	Rabbit	1:80	4°C, overnight	Sigma F7425

Table 2.4 Primary antibodies used for immunofluorescence studies. P = polyclonal, M = monoclonal, Conc = concentration.

2.5.4 Secondary antibodies

Secondary antibodies appropriate to the primary antibody (Alexa Fluor®, Molecular Probes), corresponding to the wavelengths for either FITC (488) or TRITC (568), were used at 1:100 at room temperature for 1 h.

2.5.5 General method

Non-specific binding sites were blocked by incubating fixed material with 3% normal horse serum (Sigma; diluted in PBS) for 30 – 60 minutes at room temperature on a glass slide. The primary antibody/antibodies was diluted in blocking solution, applied to the specimen on the slide and incubated. The specimen was washed three times with PBS then incubated with secondary block (3% normal goat or donkey serum) at room temperature for 30-60 minutes. Bound primary antibody was detected by incubation with secondary antibody diluted in secondary blocking solution and incubated for 1 h at room temperature. Following rinsing in PBS, slides were prepared by applying a tiny drop of Vectashield fluorescence mounting medium (Vector Laboratories, Peterborough, UK) between a coverslip and the specimen. Control experiments omitted the primary antibody.

2.5.6 Specific methods

2.5.6.1 Human renal tissue

Unfixed tissue blocks (section 2.1.2) were removed from storage at -80 °C and were cut into 10-12 μm sections on a cryotome and immediately transferred onto poly-L-lysine coated glass slides (Histobond). Sections were then fixed, permeabilised, and stained using the protocol above.

Predominantly cortical tissue was used; the area below the capsule consisting of medullary rays (tubules perpendicular to the capsule, extending into the medulla) and cortical labyrinth (containing glomeruli, proximal and distal tubules).

2.5.6.2 Cells

Cells were grown on sterile filters (Transwell cat. no. 3401; 12 mm diameter, 0.4 μm pore size). Six days after seeding, resistance of the cell layers was confirmed before and after any

agonist treatment. Filters were washed in PBS, fixed with ice-cold methanol for 15 min, then removed from the plastic Transwell insert and divided into four portions to enable control experiments to be performed on the same cell layer. Primary block was performed on each filter segment while on an orbital shaker at 100 rpm. Antibody solutions were then applied by inverting individual filter segments onto the appropriate drop of solution.

2.5.6.3 Oocytes

Injected oocytes were incubated for at least 72 h to allow maximum expression (Manoharan *et al.*, 2006) then fixed for 4 h at 4 °C in either methanol (Rungroj *et al.*, 2004) or 2% paraformaldehyde in PBS. They were transferred to 30% w/v sucrose in PBS at 4 °C overnight, then embedded in OCT compound on a block of cork, having first drained all sucrose media by temporarily placing the oocyte on top of another drop of OCT. Such oocytes were fragile, and the least traumatic way of handling them was found to be with a plastic Pasteur pipette. The embedded oocyte was flash frozen in liquid nitrogen and a cryotome used to cut 15-20 μm sections onto poly-L-lysine coated glass slides (Histobond). Blocks could be stored for up to 4 weeks at -80 °C, and sections for up to 24 h at -20 °C. Sections were stained using the protocol in section 2.5.5.

2.5.7 Confocal microscopy

Optical sections of stained tissue were obtained using a confocal laser scanning microscopy (CLSM) system (Leica TCS-NT). Fluorescent antibodies and GFP fusion proteins were excited by focused krypton-argon laser light, allowing very thin (micrometre) sections to be visualised. Filter sets for FITC (excitation 488 nm, emission 519 nm), TRITC (excitation 568 nm, emission 572 nm) and transmitted light were used to image series in *x-y* or *x-z* planes, using x40 (numerical aperture (NA) 0.70) lens, or x63 (NA 1.32) or x100 (NA 1.40) oil immersion lens. Within an experiment, identical imaging, illumination intensity and photo-multiplier settings were maintained.

Pixel quantification (in arbitrary units) of mid-cell *xy* sections was performed using Leica TCS-NT analysis software in order to compare the intensity of two simultaneous stains in one section.

2.6 Western blotting

2.6.1 General outline

Protein samples were analysed by sodium dodecyl sulphate (SDS) polyacrylamide gel electrophoresis (PAGE). The detergent SDS denatures proteins which then become negatively charged and migrate according to size when electrophoresed. Following separation, proteins were transferred to a PVDF membrane to allow probing with a specific antibody. A secondary antibody conjugated to the enzyme horseradish peroxidase (HRP) was used to detect the primary antibody and allow detection of itself by enhanced chemiluminescence.

2.6.2 Preparation of protein lysate

2.6.2.1 Method for human renal tissue

Protein lysate from renal cortex of each of three human subjects (H, J, K) was prepared from tissue previously stored in RNA later. Diced tissue was homogenised using 30 strokes of a glass homogeniser on ice in sucrose/Tris lysis buffer, followed by centrifugation at 10,000x *g* for 10 min at 4 °C to pellet debris. The supernatant protein lysate was quantified by Bradford assay and stored at -80 °C.

2.6.2.2 Method for oocytes

Oocytes microinjected with cRNA or water three days earlier (allowing time for protein expression) were lysed in order to isolate total oocyte membranes. The lysis buffer was freshly made and resembled the composition of ORII (see section 2.8.1): 10 mM HEPES and 83 mM NaCl buffered to pH 7.9 and made up to 100 ml with water before adding a protease inhibitor cocktail tablet ('Complete', Roche). 20-50 oocytes were added to this buffer (20 µl /oocyte), and membranes ruptured in a glass homogeniser using 20 strokes on ice. The mixture was centrifuged initially at 500x *g* for 5 min at 4 °C to remove debris. The surface fat layer was gently skimmed off using a cut P1000 pipette tip and the supernatant gently aspirated from the debris layer at the bottom. The supernatant was ultra-centrifuged at 100 000x *g* for 1 h at 4 °C (Beckman Coulter Optima with TLS55 rotor). The resulting membrane pellet was washed with ice-cold lysis buffer, resuspended in fresh lysis buffer (1 µl /oocyte), quantified by Bradford assay and stored at -80 °C.

2.6.3 Protein electrophoresis

Protein lysate (10-50 μg per lane) was heated for 10 min at 85 °C with sample buffer containing β-mercaptoethanol; these reducing conditions causing protein denaturation. Each sample was loaded and run on a 4% (stacking)-10% (running) SDS-polyacrylamide gel at 30 mA for 1 h with MOPS (3-(N-morpholino) propane sulfonic acid) running buffer to enable size fractionation.

2.6.4 Protein transfer

Separated proteins on the gel were then transferred onto a PVDF membrane (Hybond-P, Pharmacia Biotech, UK). Filter paper was pre-soaked in transfer buffer (10% CAPS [Sigma C2632], 10% methanol, 80% water), and a sandwich assembled (from anode to cathode) of: sponge pad, filter paper x2, PVDF membrane, gel, filter paper x2, sponge pad. Transfer was carried out overnight in a cassette with a current of 50 mA running through the transfer buffer.

2.6.5 Immunodetection of protein

Antibody	Raised in	Conc.	Incubation	Source
Primary antibodies				
C-terminal ANK (Ab3)	Rabbit	1:250	4 °C, overnight	Generous gift from Dr Kingsley, Stanford
N-terminal ANKH	Rabbit	1:200	4 °C, overnight	Santa Cruz sc-67242
CD98	Goat	1:500	4 °C, overnight	Santa Cruz sc-7095
β-actin	Mouse	1:1000	Room temp, 2 h	Abcam ab6276
Pre-immune serum	Rabbit	1:500	4 °C, overnight	Davids Biotechnologie, Germany
Secondary antibodies				
anti-goat IgG-HRP		1:2500	Room temp, 1 h	Dako P0160
anti-rabbit IgG-HRP		1:10,000	Room temp, 1 h	Amersham NA9340
Conjugated antibodies				
anti-FLAG (M2)- HRP (monoclonal)	Mouse	1:200	Room temp, 1 h	Sigma A8592

Table 2.5 Antibodies used in Western blotting experiments. Conc., concentration

PVDF membranes were probed for proteins using antibodies as shown in Table 2.5. Non-specific antibody binding sites were blocked by incubation in 5% w/v skimmed milk powder in TBS/0.1% Tween (20 mM Tris buffer, 137 mM NaCl, 0.1% Tween-20, pH 7.6) for 1 h at room temperature on a rocking table. The membrane was then incubated overnight at 4 °C in primary antibody diluted at the required concentration in milk protein-TBS/Tween using a rotary swirler. Controls omitted primary antibody. The membrane was washed three times with TBS/Tween then incubated with appropriate diluted secondary antibody conjugated to HRP for 1 h at room temperature, followed by another series of washes.

The membrane was incubated for 5 minutes with a chemiluminescent substrate detection kit (ECL Plus, Amersham Biosciences), generating photons in the presence of HRP which were detected with autoradiography film (Kodak) after exposure for 1-10 minutes. If required, the membrane was then stripped (Restore Western Stripping Buffer, Pierce) with confirmation of antibody removal and reprobed with another primary antibody. Finally, the membrane

was stained with copper phthalocyanine to demonstrate adequate and equal protein transfer across the membrane.

2.7 Tissue culture procedures

Tissue culture procedures were performed in class II vertical laminar flow hoods (Jouan MSC12, Jouan Ltd, Herts UK) with sterile handling techniques. Culture media, media supplements and consumables were obtained sterile or sterilised before use by high pressure and temperature autoclave, overnight baking at 162 °C in a hot air oven, or filter sterilisation, as appropriate.

2.7.1 Cell lines

In order to study nephron-specific localisation *in vitro*, oncogene-transfected cell lines have been developed in order to enhance cell proliferation. Advantages over primary culture include the availability of a continuous source of cells, improved phenotypic reproducibility, ability to alter the cellular environment over the medium-term, and often greater purity of the population of cells of a particular type.

2.7.1.1 HEK293

The HEK293 cell-line was established from primary cultures of human embryonic kidney which were transformed by sheared human adenovirus type 5 DNA (Graham *et al.*, 1977) and retain some features of tubular epithelial cells (Simmons, 1990). Cells were grown in Modified Essential Medium Eagle's (MEME), supplemented by glutamine (2 mM), non-essential amino acids 10% v/v, fetal bovine serum and 100 µg / 500 ml penicillin /streptomycin. Passages 71-74 were used.

2.7.1.2 mpkCCD$_{cl4}$

The murine cortical collecting duct clone 4 (mpkCCD$_{cl4}$) cell line is a clonal epithelial cell line known to be sodium transporting and responsive to aldosterone and vasopressin (Robert-Nicoud *et al.*, 2001). The line was microdissected from kidneys of a transgenic mouse carrying the simian virus 40 large T antigen gene under the regulatory control of the L-type pyruvate kinase promoter (SV-PK/Tag; (Bens *et al.*, 1999)). Cells were generously gifted by Professor Alain Vandewalle (INSERM, Paris).

mpkCCD$_{cl4}$ was cultured in Ham's F12/Dulbecco's Modified Eagle's Medium (DMEM) 1:1

v/v with: 60 nM sodium selenate; 5 μg/ml transferrin; 2 mM glutamine; 50 nM dexamethasone; 1 nM triidothyronine; 10 ng/ml epidermal growth factor; 5 μg/ml insulin; 20 mM D-glucose; 2% fetal calf serum; 20 mM HEPES at pH 7.4; 100 U/ml penicillin and 100 μg/ml streptomycin. Passages 38-47 were used.

2.7.2 Cell culture

Cells were incubated at 37 °C, with a humidified atmosphere of 5 % CO_2 in air. Cells were passaged weekly and media replaced as necessary.

Permeable Transwell^{TM} filter supports (12 mm diameter, 0.4 μm pore size; Corning Inc Life Sciences, USA) were employed to grow confluent polarised epithelial layers of mpkCCD$_{cl4}$ cells. Cells were seeded onto the filters at 2 x 10^5 cells / cm^2 and incubated for 6-10 days in supplemented DMEM/F12 medium, with medium replacement every 2 - 3 days. By day 6 a significant transepithelial resistance (2.9 ± 0.3 kΩcm^2, n=140) and spontaneous p.d. (6-13 mV basal solution electropositive) were observed that was associated with transepithelial Na^+ absorption. The basal epithelial surface was incubated with arginine vasopressin (AVP; 10 nM), forskolin (10 μM, Sigma F6886) or control media for 24 h. RNA was then extracted or monolayers were fixed for immunofluorescence by methanol immersion as described in section 2.5.6.2.

2.7.3 Serial passages

Cells were subcultured when confluent as determined by light microscopy. Media was removed and cells washed three times with sterile PBS and incubated with 0.05 % v/v trypsin and 0.02 % ethylenediaminetetraacetic acid (EDTA) in Earle's balanced salt solution at 37 °C until cells were detached (20-30 minutes). The trypsinised cells were then decanted into a universal container and cell culture media was added to deactivate the trypsinisation reaction. Centrifugation of the cell suspension was not performed in order to avoid the possibility of cell damage. Cells were resuspended by passing through a wide bore needle several times and cell number determined using an electronic cell counter (Coulter). Cells were used to seed new flasks (approximately 2.5 x 10^5 cells in 75 cm^2 flask) or coverslips (2 x 10^5 cells per 13 mm-diameter coverslip), culturing with the appropriate media.

2.8 Flux experiments using the *Xenopus* oocyte expression system

2.8.1 Preparation of oocytes

Mature female *Xenopus laevis* frogs (*Xenopus* Express, France) were housed in the Comparative Biology Centre at Newcastle University. The frogs were killed by an approved Schedule 1 method and the ovaries removed. Ovaries were cut into small clumps and digested with collagenase A (2 mg/ml) (Roche Diagnostics GmbH, Manheim, Germany) in ORII solution (82.5 mM NaCl, 2 mM KCl, 1 mM $MgCl_2$, 10 mM HEPES, pH 7.5) for 60-120 min. Collagenase treatment was stopped by washing the oocytes six times, first in ORII solution and then in Barth's solution (88 mM NaCl, 1 mM KCl, 0.82 mM $MgSO_4$, 0.41 mM $CaCl_2$, 0.33 mM $Ca(NO_3)_2$, 2.4 mM $NaHCO_3$, 10 mM HEPES, pH 7.5 plus 0.02 mg/ml gentamicin). Healthy stage V/VI oocytes (those with defined vegetal and animal poles) were incubated overnight at 18 ºC in Barth's solution.

2.8.2 Microinjection of oocytes

A glass cannula was heated and stretched to produce a needle of small diameter for microinjection of oocytes (PUL-1 micropipette puller, World Precision Instruments Ltd., Stevenage, UK). The needle was filled with paraffin oil dyed with Oil Red O (BDH, VWR International) and attached to a micro-injector (Drummond 'nanoject', Drummond Scientific Company, Pennsylvania, USA). Needles were backfilled with either cRNA diluted in RNase-free water or RNase-free water alone. Oocytes were placed on to a plastic mesh and bathed in Barth's solution. Using a light microscope, oocytes were injected in the centre of the vegetal pole (yellow hemisphere) with a volume of 50.6 nl of either cRNA or water. The injected oocytes were maintained at 18 ºC for 3 days in Barth's solution to allow expression of the protein encoded by the injected cRNA (Figure 2.12). To compensate for the death of some oocytes over the incubation period, 150-200% of the required number of oocytes were injected. In experiments involving co-injection of ANKH cRNA and human kidney total RNA, the former was used in excess, as used by Kowalczuk (Kowalczuk *et al.*, 2008). Oocytes were re-injected after 3-day incubation with labelled substrate for efflux experiments.

2.8.3 Radiolabelled substrates

Substrates (listed in Table 2.6) were labelled with the high-energy β-emitting isotope ^{32}P

(Perkin-Elmer, USA). As a result, intra-oocyte activity could be accurately quantified, even if the cell had not been completely lysed. In addition, detection would occur even if the substrate is subsequently metabolised.

Radiolabelled tracer & product code	Lot number	Concentration (mCi/ml)	Specific activity (Ci/mmol)	Specific activity (TBq/mmol = MBq/nmol)
PPi NEX019001MC	05081F8	96.6	88.58	3.28
	05081F8	96.6	88.58	3.28
	08081J7	81.7	88.37	3.27
	10081K7	97.3	107.28	3.97
	01091H7	85.6	84.13	3.11
	07091G5	93.9	84.31	3.12
ATP-[γ-^{32}P] NEG002H	09118/1	5	3000	111
	01229/1	5	3000	111
	05149/1	5	3000	111
ATP-[α-^{32}P] BLU003X	07318/1	10	800	29.6
Pi NEX063001MC	P030508W/1		1	0.037
^{14}C-mannitol ACC0127A	080723	0.1	0.055	0.002

Table 2.6 Radiolabelled substrates. All were obtained from PerkinElmer; catalogue numbers are shown.

2.8.4 Influx of radiolabelled substrate

Radioactivity was dispensed according to the laboratory safety protocol in a dedicated room. 200 µl aliquots of each radiolabelled solution were prepared for each experimental condition, along with a little extra to enable calculation of standards.

Usually ten oocytes per experimental condition were aimed for; this allowed for variation between oocytes and loss of some oocytes through rupture. The oocytes were washed in groups in 2 x 500 ml volumes of wash buffer (100 mM NaCl or choline chloride, 2 mM KCl, 1 mM $CaCl_2$, 1 mM $MgCl_2$, 10 mM HEPES, pH adjusted to 7.4 with Tris base) then transferred to a 5 ml polystyrene tube. Residual wash buffer was removed using a Pasteur pipette (to avoid damage to the oocytes) and replaced at timed intervals with 200 µl of appropriate uptake solution. Uptake solutions comprised the radiolabelled substrate diluted in wash buffer. Experiments were incubated in the climate-controlled oocyte room (18 °C) usually over 40 min.

Following incubation, uptake solution was removed using a pipette and the oocytes were washed by addition of 5 ml ice-cold (to prevent further ion flux) wash buffer to the test tube. The wash buffer was removed by aspiration and the oocytes were washed a further three times. Individual oocytes were then placed into scintillation vials. 2 ml of scintillation cocktail (Optiphase Hisafe 2, Perkin Elmer) was added to each vial, which was then vortexed for a few seconds. 4 x 10µl samples were taken from each radiolabelled uptake solution and counted alongside the oocyte samples to provide a standard reference for each experiment. Uptake of [^{32}P]-substrate was measured by scintillation counting over 5 minutes per sample using standard settings for ^{32}P isotope, and the results expressed as fmol per oocyte per hour.

An influx experiment at zero-time was performed by immersing oocytes into uptake solution then immediately removing, washing and counting the activity in the usual way (Table 5.3, ANKH-FLAG, influx time =0). There was no increase in influx into the ANKH-FLAG-injected oocyte over water-injected at zero time.

2.8.5 Efflux of radiolabelled substrate

2.8.5.1 Overview and preparation

The principle was to pre-inject the radiolabelled substrate into each previously cRNA- or

water-injected oocyte immediately before the start of the efflux experiment. As the functions of relevant transporters were unknown, preloading by incubation (as in (Scott & Karniski, 2000)) was not possible.

Radioactivity was dispensed as above, either undiluted or diluted into either potassium chloride 150 mM or unlabelled PPi as required. 24 oocytes in each cRNA-injected group were aimed for, requiring ~30 healthy oocytes. This included a few standards to calibrate the initial labelled activity and concentration (section 2.8.6.3.3). Oocytes were injected using the micro-injector behind suitable shielding. Substrate-injected oocytes were washed twice by transferring into two beakers of wash buffer at room temperature using a Pasteur pipette, to remove any surface-bound ^{32}P.

2.8.5.2 Method

To start the efflux measurement, oocytes were transferred individually into 1 ml of ordinary wash buffer (time = 0) in separate wells in a 24-well plate. Unlabelled PPi was added to the room temperature wash buffer if needed for trans-stimulation experiments. A cut-off and sanded P1000 filter pipette tip was used to pick up individual oocytes while minimising trauma. A minimal setting on the Gilson pipette meant that a constant extra 50 µl of wash buffer was also transferred with the oocyte, but was necessary in order to keep the membrane intact during transfer. Oocytes were left at 18 °C to efflux for the desired time period (usually 2-4 hours), and the plate was gently shaken periodically to dissipate any gradient surrounding the oocyte (as suggested in Chapter 3 of (Baldwin, 2000)).

After incubation, each oocyte was again individually transferred into a scintillation vial, and the buffer solution for that oocyte was transferred into a separate paired scintillation vial. This allowed calculation of the efflux as a percentage of the total activity in the system (oocyte plus buffer solution), a measure that other groups have used (Jutabha *et al.*, 2003). Standard oocytes (which were injected with labelled substrate but did not participate in efflux) for each cRNA-type were also placed individually into vials, as well as a blank vial (to estimate background) and some 0.5-1 µl samples of the labelled substrate solution. Any damage to oocytes during pipetting was noted prospectively.

2.8.5.3 Alternative method

As a result of technique refinement, an alternative method was used for efflux in later experiments. Six oocytes were used, with injection and surface washing as above. An initial

15-minute "recovery" efflux experiment was performed in a 96-well plate, by placing each oocyte into 200 µl of buffer solution for 15 minutes. After this incubation, 100 µl of this solution was drawn off for counting, and the oocyte was transferred (with ~50 µl of remaining buffer) to a polythene tube. Remaining buffer was carefully removed and replaced with 100 µl of fresh buffer. After the experimental incubation period, an 80 µl buffer aliquot was collected for counting, and the oocyte washed/aspirated three times in ice-cold buffer before activity was counted. This technique had the advantages of: (a) a smaller volume of buffer into which substrate could efflux, allowing a higher concentration for counting, (b) intra-oocyte control measurement of any post-injection leak of labelled substrate in the first 15 minutes, and (c) further surface wash after efflux solution collection, to prevent surface binding of any effluxed substrate being counted with the oocyte.

2.8.5.4 Conditions for efflux

Variations in experimental conditions were made as follows. Unlabelled sodium pyrophosphate (Sigma) was added to the room temperature buffer solution for trans-stimulation experiments. Proton dependence of ^{32}PPi efflux was investigated by varying the buffer pH using MES (4-morpholineethanesulfonic acid) for pH 5.5 buffer, HEPES for pH 7.0 and Tris for pH 8.0. Each additive had a pK_a (or pK_b) of approximately the final desired pH of the buffer.

2.8.5.5 Quality control

Experiments in which oocyte quality was poor, usually manifested as a significant death rate during the three-day incubation, were omitted. Only visibly undamaged oocytes were transferred into scintillation vials. Individual data points were only subsequently removed from the analysis if there was clear evidence of total or partial oocyte rupture (scintillation counts being higher in buffer than intra-oocyte) or non-injection of tracer into an oocyte (counts equivalent to background radiation control samples).

2.8.6 Variables affecting transporter kinetics

2.8.6.1 Substrate concentration

Transport at different substrate concentrations can be resolved into two components: a saturable component reflecting Michaelis-Menten kinetics of an expressed transporter, and a linear component that is directly proportional to the substrate concentration (Figure 2.6).

Water-injected oocytes are used as controls to demonstrate the linear component, which is likely to be a combination of:

- flux occurring due to membrane damage such as trauma caused by oocyte injection (this damage is worsened by poor quality oocytes)
- non-specific binding (mostly removed by washing)
- simple diffusion (< 2% of the total flux)
- minor saturable components resulting from the presence of multiple or endogenous transporters for the substrate (Baldwin, 2000).

When substrate concentration is much higher than the K_m, the transporters are saturated, and the limiting factor is the rate of substrate transport of the transporter-substrate complex. The maximal rate of transport (capacity) can thus be determined under these conditions. However, at very high substrate concentrations, the linear component is proportionately much higher, and non-specific mass effects can result. When substrate concentration is less than the K_m, then binding of the transporter with its substrate is more important, and the substrate concentration itself becomes the limiting factor. Competition with non-labelled substrates can be used to determine inhibition of the transporter.

2.8.6.2 Incubation time

The rate of flux (gradient of the curve) is greatest at substrate concentrations less than the K_m. Due to the large size of oocytes there is relatively slow equilibration of transport, allowing the initial rate of flux to be sustained for long periods (minutes to hours) (Baldwin, 2000)), allowing initial flux rates to be determined by experiments conducted over this time period. On the other hand, excessively long incubation times can introduce inaccuracies due to metabolism/breakdown of substrates over time, inhibitory effects on the transporter, and also intra-experiment oocyte death. It is normally not possible to distinguish these from the transported component, and so they constitute a source of error in the rate of flux calculated from the experiment. In the case of labelled PPi, surface hydrolysis over similar time periods (in influx experiments; section 5.2.4) or intracellular hydrolysis (in efflux experiments) would result in overestimation of flux due to transport via inorganic phosphate transporters.

Figure 2.6 Diagram illustrating effect on flux (rate of radiolabel transport) of increasing substrate concentration.

2.8.6.3 Radioactive decay of the radiolabel

2.8.6.3.1 Problem of cis-inhibition due to decay

The ^{32}P isotope has a decay half life of 14.3 days. The specific activity (activity per unit mass or activity per mole) of the ^{32}P containing isotope therefore decreased markedly over only a few weeks, whereas new batches were available only every three months (see PerkinElmer website for schedule). At low activity:concentration ratio, the radiolabelled tracer molecules are diluted by non-radioactive tracer molecules. This reduces counts per minute for any given amount of tracer, which depending on the K_m, effectively results in a *cis*-inhibition. This might account for misleadingly low flux results, which may be difficult to distinguish from background especially in experiments involving transporters that have low transport capacity (V_{max}).

2.8.6.3.2 Optimum specific activity

The optimum conditions for detection of flux would be high specific activity (SA) of the tracer as well as a high enough PPi concentration to activate the transporter, but not so high as to result in a significant linear component (see diagram above). In fact, the highest usable SA of tracer per oocyte was obtained when the radiolabelled tracer stock was a few weeks old. In contrast, fresh stock had very high activity necessitating dilution in either KCl or unlabelled PPi. In practice, the actual activity and concentration of labelled substrate used in each experiment was variable (see results tables).

2.8.6.3.3 Calculation of tracer activity

The decay corrected specific activity (SA) of the undiluted tracer was obtained using a decay correction chart (Perkin Elmer datasheets). The SA (in Bq/pmol) was adjusted for dilution with wash buffer (influx) or with an excess of either cold PPi or KCl (efflux). The total amount of labelled PPi present in the diluted uptake solution (influx) or in the 50 nl of diluted stock injected into each oocyte (efflux) was then calculated. In the case of influx experiments incorporating experimental conditions aiming to investigate the effect of competitive inhibition of labelled substrate ("knockdown"), only the amount of *radiolabelled* substrate was considered. Multiplying the latter two values gives the total radioactivity in the uptake solution (influx) or injected into each oocyte (column D in Table 5.4 -Table 5.6 for efflux). This activity is representative of the total labelled PPi concentration available for subsequent flux, but values in column D (Bq) were very

variable.

2.8.6.3.4 Estimation of initial substrate concentration

In efflux experiments, the initial substrate concentration was corrected for dilution after injection into the oocyte. Assuming a diameter of 1 mm, oocyte volume is $5x10^{-10}$ m^3, so an injection of 50nl ($5x10^{-11}$ m^3) of PPi substrate represents a dilution of 10-fold assuming it distributes evenly throughout the oocyte. This value is given in column E in Table 5.4 - Table 5.6 for efflux experiments.

2.8.7 Control experiments for efflux protocol

2.8.7.1 Negative efflux control: 14C-mannitol

Mannitol is an osmotic agent that does not pass through cell membranes. Six previously-uninjected oocytes were injected with 50 nl of ^{14}C-mannitol and were then either washed twice in fresh buffer or not washed before transferring into a well on a 96-well plate. Excess buffer was removed and 100 µl of oocyte buffer was added. Oocytes were incubated for varying time periods, following which the activity of an 80 µl aliquot of each incubation buffer was counted. This count was adjusted for 100 µl and the oocyte's activity (after three ice-cold washes) also counted in order to measure the total activity in each single-oocyte system.

Figure 5.7 A shows that only 1-2% of the initially injected labelled substrate was detected in the extracellular buffer solution for time periods up to 2 h, confirming that ^{14}C-mannitol is impermeable to the undamaged oocyte membrane. The lack of increase in time suggests that the oocyte membrane was intact over this time period. There was no clear difference between washed and unwashed oocytes, suggesting that surface binding of ^{14}C-mannitol is unimportant (but see section 2.8.7.4 for results with PPi). However, experiments with ^{32}PPi may differ in that PPi may be metabolised, oocytes were previously injected with water or cRNA, and even a 1% extracellular detection rate may be significant in relation to measured ^{32}PPi efflux. The second graph (Figure 5.7 B) suggests that for injected ^{14}C-mannitol, post-injection leakage of isotope is likely to account for the extracellularly detected tracer, rather than an effect of surface binding of tracer requiring extensive washing.

2.8.7.2 Positive efflux control: active efflux of Lucifer Yellow

Though tested as an intended impermeant intracellular marker, Lucifer Yellow proved to be

a useful control for injection, intra-oocyte equilibration and efflux. Lucifer Yellow is an actively secreted fluorescent organic anion in renal tubules (Masereeuw *et al.*, 1999) allowing it to be used as a positive control of the efflux protocol. Lucifer Yellow (di-lithium salt, Sigma L0259) was diluted in 50% w/w in water to 400 µg /ml final concentration. A 50 nl aliquot was diluted into 100 µl of Barth's solution and subsequent 1:1 serial dilution series made in triplicate. The fluorescence of 50 ul aliquots of each dilution was detected using a Tecan Infinite plate reader (section 2.9.1; excitation 425 nm, emission 520 nm). The mean fluorescence value of the three separate dilution series was used to generate a standard curve (Figure 5.8 A), showing that fluorescence over this range of Lucifer Yellow dilutions is proportional to the concentration.

To measure the time course of Lucifer Yellow exit from oocytes, groups of oocytes were injected two days earlier with water, ANKH-pcDNA3.1 cRNA or not-injected. They were then re-injected in duplicate with 50 nl of Lucifer Yellow diluted in water as above, briefly washed by transfer via Barth's solution, and incubated for varying lengths of time in 100 µl of Barth's, up to 120 min. Following incubation, 50 nl aliquots were removed for fluorescence counting, and the mean value obtained. Lucifer Yellow exit was expressed as the fluorescence of dye detectable extracellularly after each incubation period, as a percentage of that detectable after 120 min incubation. Figure 5.8 shows that there is an increase in extracellular fluorescence over time with all three oocyte types, suggesting that efflux of dye is occurring at constant rate over 100 min. Efflux (or diffusion) is more likely to account for this constant rate of exit than leakage due to membrane puncture. These results are in direct contrast to the radiolabelled mannitol efflux data. There is no difference between water-injected or ANKH-injected oocytes showing that no non-specific action of ANKH protein is evident. It may be concluded that an endogenous transporter is present in oocytes to mediate Lucifer Yellow exit.

2.8.7.3 Post-injection leakage control: 15-minute recovery method

The modified efflux method outlined in section 2.8.5.3 included a count of bathing buffer after 15 minutes, allowing detection of any post-injection leak of labelled substrate prior to the main experiment. This leak tended to be less than 5% of the calculated injected substrate, and was usually closer to 1-2% (Figure 2.7).

Figure 2.7 Effect of prior water-injection on subsequent detection of ^{32}P activity in oocytes.

Figure 2.8 Contamination of non-injected oocytes with activity acquired from surrounding buffer.

(A) Effect of exposure to surrounding buffer on detectable activity. Oocytes were injected 3 days earlier with either water (left pair of bars) or ANKH-pTNT (right pair). In each batch, ~50 oocytes were each re-injected with 23 pmol of labelled sodium pyrophosphate. Six non-injected oocytes were collected from the buffer solution at the end of each injection session, and their mean ^{32}P activity measured (red bars). Mean activity of six oocytes which had not been present during injections was measured as a control (blue bars). Error bars represent SEM for n = 6 oocytes, $p < 0.01$ between pairs of bars.

(B) Effect of washing on detectable activity. Oocytes were injected 3 days earlier with human kidney cRNA. 6-11 oocytes were collected from each buffer solution at the end of injection sessions ("exposed"; left pair of bars) or non-present controls as above ("non-exposed"; right pair of bars). In each group, oocytes were either washed three times with fresh buffer (pink bars) or not washed (red bars). Errors bars represent SEM for n = 2-6 oocytes, * denotes $p = 0.02$.

Fig 2.8 goes here

2.8.7.4 Surface binding of tracer and its removal

It was noted that the radioactive content of the buffer increased during the injection of oocytes with radiolabel, and it was important to determine whether this may result in an increase in surface binding of activity and if so, whether this was adequately removed by the washing protocol. During radiolabel injections of ~50 oocytes bathed in one aliquot of oocyte buffer, the activity of six non-injected oocytes was counted at the end of the procedure. Figure 2.8 A shows that non-injected oocytes in the same dish become contaminated in this way.

Oocytes treated in this way then underwent three washing/aspiration cycles. This procedure significantly reduced ($p = 0.02$) their activity (Figure 2.8 B). In practice, the oocyte buffer was changed frequently during radiolabel injections.

The equivalent experiment for the influx protocol was performed using water-injected oocytes at influx time = 0 (i.e. tracer-labelled buffer added and immediately removed). After three washing cycles, the final count was ~10% of that obtained for water-injected oocytes at time = 80 min.

In summary, surface binding of radiolabel is not an important factor for either influx or efflux measurements.

2.8.7.5 Validity of water-injected controls: comparison with uninjected oocytes

Uninjected control oocytes were used alongside water-injected oocytes as controls, and all were injected three days later with labelled substrate. There was no significant difference in the amount of ^{32}P detected extracellularly between these conditions (Figure 2.7), during both the 15-minute recovery period ($p = 0.57$) or the efflux experiment ($p = 0.08$).

2.8.8 Data quality and statistics

2.8.8.1 Results and data quality

Results were obtained as dpm per oocyte. From this, pmol substrate per oocyte (influx experiments) or % efflux of the total counts in the system (oocyte + bathing buffer)(efflux experiments) were calculated. Obvious instances of partially or totally ruptured oocytes were excluded from analysis, e.g. intra-oocyte count lower or similar to extra-oocyte count, or >5% loss of counts during the 15-minute recovery period post-injection. However, most

exclusions occurred after visually confirming rupture during the experiment. Oocyte quality is a very important factor which is known to vary seasonally, with poorer quality over the summer months (Baldwin, 2000; Weber 1999).

The standard error of the mean was calculated. Significance testing against values obtained using water-injected oocytes in each experiment was performed using one-tailed *t*-tests, on the grounds that the hypothesis predicted that cRNA-injected oocytes were likely to demonstrate more flux than water-injected oocytes.

2.8.8.2 Statistical comparisons between groups

Using Minitab 15® statistical software, tests for variances were performed using Bartlett's (parametric) test rather than an F test, as there were usually more than two levels for each factor. In all cases, *p* was less than 0.05, rejecting the null hypothesis and demonstrating that variances were unlikely to be equal. In addition, datasets were unbalanced due to differing numbers of oocytes not surviving each experimental condition. This precluded use of two-way ANOVA. Since flux was the only response variable, a regression method called the General Linear Model was used, with Tukey's method to examine pairwise comparisons between means. Significance was accepted at 95%.

2.9 Pyrophosphate assay

2.9.1 Background

In order to determine endogenous pyrophosphatase activity on the surface of *Xenopus* oocytes, measurement was made of the reduction in PPi concentration of a known amount of PPi-containing buffer in the presence of oocytes for varying lengths of time. Initial attempts employed a coupled enzyme assay using fructose-6-phosphate kinase to convert fructose-6-phosphate with PPi to fructose-1,6-diphosphate, followed by D-glyceraldehyde-3-phosphate and then dihydroxyacetone phosphate. The resulting oxidation of two moles of NADH to NAD^+ per mole of PPi present are detectable spectrophotometrically (Sigma cat no P7275), but attempts were unsuccessful since no difference in PPi was measurable over time in the detectable range of this assay (1 mM). To allow lower PPi concentrations to be studied, a recently introduced highly sensitive assay kit was used (PhosphoWorks™ Fluorimetric Pyrophosphate Assay Kit, ABD Bioquest, California, USA, cat no 21611) in which the fluorescence of the proprietary PPi 'sensor' compound is proportional to the PPi concentration. 50 µl samples were analysed for PPi by detection of fluorescence (excitation

368 nm, emission 415 nm) using a Tecan Infinite M200 fluorescence plate reader after 30 minutes incubation with the sensor at room temperature in a UV-range 96-well plate (Corning) according to the manufacturer's instructions. Testing by the manufacturers shows no interference even in the presence of up to 20 mM of calcium and/or magnesium (personal communication).

2.9.2 Validation of PPi assay

Buffer solutions based on Barth's solution (section 2.8.1) were made with and without calcium and magnesium. A standard dilution series from the 50 mM PPi kit component was made using these buffers, and 50 µl aliquots were taken from each dilution (in duplicate) to allow generation of a standard curve for PPi assay (Figure 5.5). A further 50 µl aliquot was taken and added to 1 µl of PPase enzyme already present in the 96-well plate, and mixed carefully. Inorganic PPase (cat I1643, Sigma) was previously diluted in molecular grade water to 0.25 units/ µl (equating to formation of ~15 µmol Pi per hour), so that the enzyme was in a large excess compared to PPi. This allowed confirmation of the effect of PPase enzyme activity on PPi of varying concentrations. Analysis with the assay kit confirmed that PPi activity was reduced to zero in the presence of this amount of PPase except at very high PPi concentration (Figure 5.5), confirming specificity of the assay for PPi.

2.9.3 Estimation of oocyte surface PPase activity

Oocyte experiments were performed in the 3.6 µM dilution with normal (calcium and magnesium-containing) buffer, this dilution being in the middle of the detectable range. Storage buffer was carefully aspirated from groups of 7-10 healthy uninjected oocytes in a PPi-free eppendorf tube, to which 70 µl of 3.6 µM PPi-containing buffer was added. Oocytes were incubated at 18 °C for varying time periods, including zero time. At the end of the incubation timer period, 50 µl of experimental buffer was collected, as well as simultaneous collection of 50 µl of unused 3.6 µM PPi buffer. The latter acted as a "no-oocyte" control to investigate any changes in the buffer over time, e.g. precipitation of PPi.

Attempts to estimate intracellular PPase by performing PPi assays in the presence of centrifuged oocyte lysates were unsuccessful, as the mild turbidity present even after lengthy centrifugation caused major interference and failure of the fluorescence assay.

2.10 Identification of proteins interacting with ANK by yeast two-hybrid screening

2.10.1 Choice and overview of yeast two-hybrid screening

Protein complexes, rather than individual proteins, are increasingly recognised as the molecular basis of cellular fluxes (Bruckner *et al.*, 2009). However, standard gel electrophoresis would cause these complexes to denature. Protein complexes can be purified by tagging an epitope, then either immunoprecipitating with a specific antibody or using affinity columns which recognise the tag, followed by analysis of the complex using mass spectrometry. This method is expensive and time consuming, is not suitable for high throughput, and requires detergents to prevent dissociation of membrane protein complexes (such as might be important for ANKH function) when the lipid bilayer is disrupted (Hooker *et al.*, 2007). In contrast, the yeast two-hybrid system, developed by Fields and Song in 1989 (Fields & Song, 1989) allows *in vivo* detection of interacting protein pairs in living yeast cells. Positive interactions activate reporter genes that enable growth on specific media (see Figure 2.10 for method and terminology). Since the identity of potential interactors (prey) with ANK (bait) was unknown, a mouse kidney cDNA library was used. These cDNA fragments aim to cover the entire transcriptome of mouse kidney so increasing the sensitivity of the screen (Bruckner *et al.*, 2009) but at the expense of specificity, causing a false positive rate of up to 50% (Hooker *et al.*, 2007).

2.10.2 Choosing the bait

The mouse ANK clone NP_065065 was used. It is highly likely that the fully folded 492-amino acid ANK protein would not be able to enter the nucleus of the yeast cell, so to reduce false negatives it is standard practice to use a representative fragment of the protein, although there is an inherent risk of misfolding due to a protein fragment being used and its fusion to the DNA-binding domain of the transcription factor. TMHMM[6]/SMART[14] transmembrane domain prediction software predicts eight transmembrane segments in ANK, and the N- and C-terminals are both cytoplasmic (Ho *et al.*, 2000). No part of ANK corresponds to any known motif/domain as predicted by InterPro[7]. To our knowledge, there is no published work which has used ANK in a yeast two-hybrid system. The screening company (see section 2.10.3.1) had neither previously screened ANK nor found it as prey in

[6] www.cbs.dtu.dk/services/TMHMM
[7] www.ebi.ac.uk/interpro/

a screen. For these reasons, there was little guidance on the choice of optimum ANK fragment suitable for a yeast two-hybrid experiment.

The bait was chosen to be intracellular and avoid transmembrane segments. Since we were using a C-terminal anti-ANK antibody (Ab3), we have previously made fusion constructs at the N-terminal (ANKH-NT-GFP and ANKH-NT-3XFLAG). Staining and membrane localisation of both constructs has been confirmed with Ab3 as well as anti-GFP (Carr *et al.*, 2007) and anti-FLAG (Chapter 4) antibodies respectively. C-terminal truncation (Carr *et al.*, 2007) stopped trafficking from the endoplasmic reticulum to the Golgi. Wang *et al.* (2009) showed that the ANK N-terminal M48T mutation abolished interaction between ANK and the basolateral sodium/phosphate transporter PiT-1, suggesting that the N-terminal contained an interacting site. Hence an N-terminal ANK fragment encompassing this residue was used for the screen (Figure 2.9).

2.10.3 Experimental protocol

2.10.3.1 Testing of the bait construct

Yeast two-hybrid screening was performed by Hybrigenics SA, Paris, France (www.hybrigenics-services.com). The coding sequence for amino acids 24-85 of mouse ANK (GenBank accession number gi: 157951667) was PCR-amplified generating a product with amino acid translation NIAIDFGEQALNRGIAAVKEDAVEMLASYGLAYSL MKFFTGPMSDFKNVGLVFVNSKRDRAK. This cDNA fragment was fused to the C-terminal of the DNA-binding domain (BD) of the transcription factor LexA for optimum folding of the bait. This bait construct (N-LexA-Ank(24-85)-C; one of the "hybrids") was cloned into the vector pB27. The construct was checked by sequencing the entire insert and using it as bait to screen a random-primed mouse kidney cDNA library containing 10 million independent fragments constructed into the pP6 vector. Since the library is random, each possible kidney DNA could be represented by one or more unique prey fragments or even multiple identical fragments. Additionally, only about a third of clones will have the correct reading frame, and half of these are likely to be antisense. This initial screen of the bait construct allowed identification of the most appropriate selection medium, and excluded any autoactivating or toxic effect of the bait itself (the latter leading to no positive interacting clones).

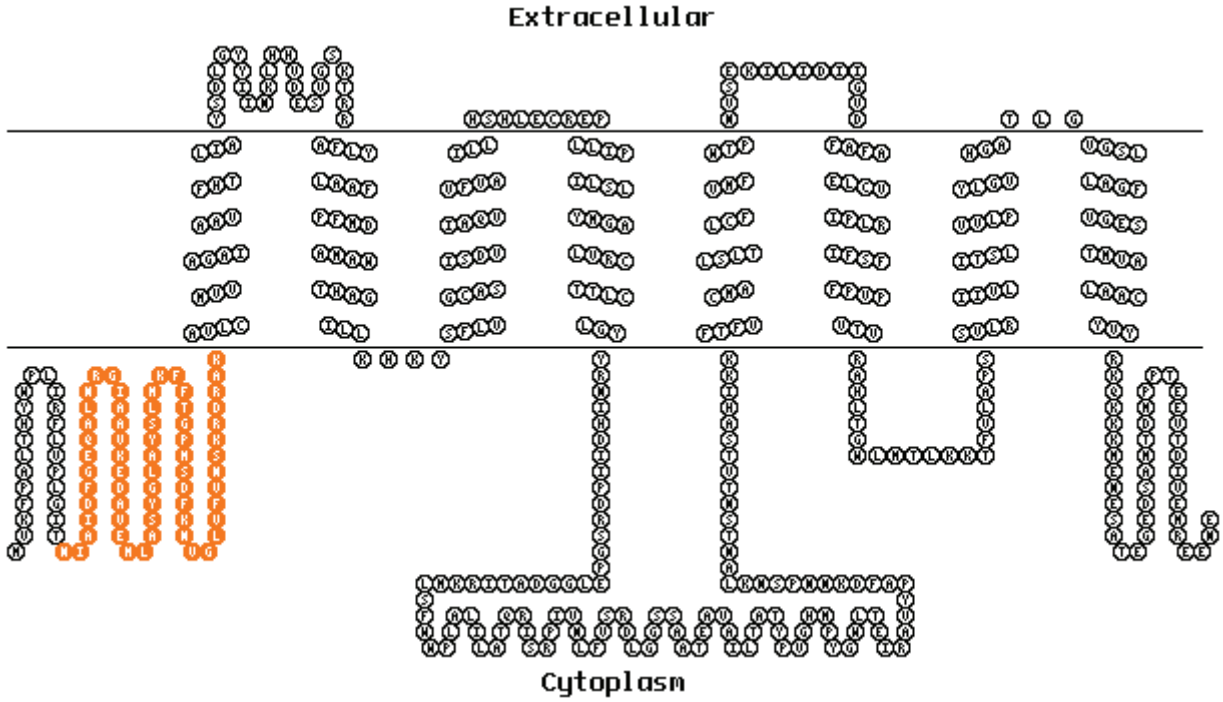

Figure 2.9 Location of the ANK N-terminal fragment (residues 24-85, in orange) used for the bait fusion construct. Transmembrane domain predictions were obtained from SMART and the graphics were created using TOPO2 Transmembrane protein display software (Johns S.J., www.sacs.ucsf.edu/TOPO2/).

Figure 2.10 Classical yeast two-hybrid system with ANK as the protein of interest.
A C-terminal fragment of ANK (green) was fused to a DNA binding domain (BD; light blue) of a transcription factor, forming a construct called the "bait" **(1)**. Plasmid cDNAs coding for potentially interacting proteins P,Q,R,S are each fused to the activation domain (AD; yellow) of the same transcription factor – this forms constructs called "prey" **(2)**. Once translated, the BD protein binds to the upstream activator sequence (dark blue line) of the transcription factor **(3)**. Interaction of the "two hybrids" (i.e. bait with prey) allows the BD and AD to function together as a transcription factor **(4)**. This allows RNA polymerase II to initiate transcription of the reporter gene, in this case His3, within the yeast cell. Its protein product, imidazole glycerol phosphate dehydratase, allows yeast cells to grow on a selective medium lacking histidine **(5)**. In this way, the process selects out only those cells that contained a cDNA plasmid whose protein product directly interacted with ANK.

Fig above

2.10.3.2 Yeast two-hybrid screening procedure

An ULTImate Y2H screen (Hybrigenics) was performed, in which the bait construct was transformed into yeast cells each containing random fragments from the cDNA library. An outline of the experiment is shown in Figure 2.10. This yielded 55.3 million interactions (5.5-fold the complexity of the library). After selection on medium lacking histidine, growing yeasts represented positive interacting clones, these originally containing two hybrid transcription factors which directly interacted, causing activation of the reporter gene. The plasmid DNA in these positive yeast colonies was extracted, and the corresponding prey fragments were amplified by PCR and sequenced.

2.10.3.3 Analysis of interacting prey sequences

The sequences were analysed for reading frame (all F2), submitted as a BLAST query against the mouse genome to identify the interacting prey, and the amino acid sequences aligned using Multalin[8] (Corpet, 1988). The minimum common amino acid domain shared by all prey fragments corresponding to the same protein was deduced to be the interacting domain. As a post-screening check, the bait construct was also extracted from yeast cells and sequenced to verify the integrity of the bait fragment. Bioinformatics software (Hybrigenics) attributed a confidence score to each interaction and screened out known false positives.

2.10.4 Weaknesses of the yeast two-hybrid technique

2.10.4.1 Experimental verification of putative interactions is necessary

The *in vivo* nature of the technique, specifically overexpression of bait, potential post-translational deficiencies in the host yeast cell, and necessity to cross the nuclear membrane, all contribute to the large number of false positives and negatives in the yeast two-hybrid technique. The accuracy of a classic yeast two-hybrid screen such as the present study may be only 10% compared to data sets obtained using other techniques (Bruckner *et al.*, 2009). It is therefore essential to re-interpret any output from a physiological point of view, and then to verify putative interactions experimentally using colocalisation in cell lines or functionally using co-immunoprecipitation or functional overexpression (Chapter 5).

[8] http://multalin.toulouse.inra.fr/multalin/multalin.html

2.10.4.2 Limitation of false positive interactions

False positives, which can be up to 50% of putative interactions (Hooker *et al.*, 2007) can arise from overexpression of bait and prey, especially if they are in a non-physiological subcellular compartment. The possibility of auto-activation of the reporter gene by the bait was excluded. Techniques to limit false positives include: selection for more than one reporter gene in parallel (increases specificity at the cost of sensitivity), and reconfirmation of positive interactions by direct yeast two-hybrid interaction experiments between bait and positive preys. An alternative might be to repeat the experiment after swapping DNA binding domain-Bait and AD-prey constructs, so that each fuses with the other.

2.10.4.3 Causes of false negatives

False negatives may occur when the bait used does not contain the interacting domain of the protein. Other reasons include the inability of yeasts to perform all the post-translational modifications or glycosylation necessary for interaction of mammalian proteins. Expression levels of bait and prey depend on the yeast promoter used. The protein-protein interaction in a yeast two-hybrid experiment occurs in the cytosol, but if the bait-prey membrane protein complex is unable to move into the nucleus, transcription of the reporter gene will not occur.

2.11 Expression profiling

2.11.1 Aims and benefits of expression profiling

2.11.1.1 Principle of the experiment

The transcriptome of a cell or cell type can vary over short periods of time and changes with the cell's function or environment (e.g. response to hormones), as compared to the genome which is stable over time in cells (unless mutations occur). It is a surrogate for the proteome which is more difficult to characterise either by protein microarrays or by Western blotting.

The expression profile of the transcriptome is the pattern of gene expression produced when an ANK-expressing tissue of interest is subjected to a physiological intervention. This allows functional insights, such as potential molecules involved in the regulation of ANK. Since ANK and AQP2 were found to colocalise in human tissue (Chapter 3), mouse tissue and mouse cell lines, with clear evidence of co-ordinated regulation ANK and AQP2 in AVP-stimulated filter layers of mpkCCD$_{cl4}$ cells (Chapter 6), AVP was selected as agonist.

mpkCCD$_{cl4}$ cells have previously been shown to respond to AVP treatment by increased expression of AQP2 (Hasler *et al.*, 2002).

2.11.1.2 Advantages and caveats of the technique

Microarray experiments offer the major advantage of being able to study the effects on many genes of a single intervention at a point in time without knowing in advance which genes might change (Kurella *et al.*, 2001). Negative aspects include: the relatively high cost, only one physiological intervention is possible per experiment, the altered transcriptome does not necessarily reflect equivalent protein expression, and a large and sometimes unwieldy dataset may include false positives. These features render the microarray a screening tool, the results of which require subsequent confirmation by other techniques such as RT-PCR or immunocytochemistry.

2.11.2 Validation of total RNA quality

Total RNA was extracted from mpkCCD$_{Cl4}$ cells grown on filters under control (non-treated) and AVP-treated (10^{-8} M for 24 hours) conditions, using a Qiagen RNeasy Midi kit, and was stored at –80 °C or transported on dry ice. A small portion of the filter was retained for immunofluorescent confirmation of ANK and AQP2. The concentration and quality of the RNA was assessed using spectrophotometry and by cDNA synthesis of an aliquot of each sample using an Agilent Bioanalyzer 2100 (Figure 2.11; Medical Solutions Ltd, Nottingham; www.medical-solutions.co.uk).

2.11.3 Overview of experiment

A DNA oligonucleotide microarray ("gene chip") is a matrix of thousands of cDNA probes bound to a solid support (Kurella *et al.*, 2001). The Affymetrix GeneChip® Mouse Genome 430 2.0 Array (Affymetrix, Santa Clara, CA) is a very high-density array, containing ~12000 synthesized oligonucleotide probes. Each of these probes corresponds to a separate gene (Kurella *et al.*, 2001), but many probes exist per gene. mRNA is extracted and purified from cells (section 2.11.2), reverse-transcribed using nucleotides labelled with a fluorophore and fragmented. Each labelled fragment was allowed to hybridise over 16 hours to its complementary sequence on the array. The array is then washed and stained, and the bound probe detected with a confocal laser. Each RNA (three control, three treated) was hybridised to a separate array.

Figure 2.11 **Validation of total RNA quality**

The raw data produced as a confocal microscope image is transformed into the names of the probes, by correlation to the location of probes on the array, and can be output as a text file. These can then be converted into GenBank gene names. Specialised software analyses the images and text files and performs statistics, resulting in data such as the magnitude of gene expression. More sophisticated downstream analyses can then be performed, such as overlaps with other published datasets, to look for patterns of gene expression and attempts to identify potentially related biological functions.

2.11.4 Data analysis

The large dataset generated by the microarray requires a number of analyses to be performed in sequence. First, the data must be normalised, which is the process used to remove non-biological variation between the samples. This is followed by quality control checks and finally tests for differential expression (*t*-tests, fold changes).

2.11.4.1 Normalisation

The raw data as Affymetrix text (CEL) files were imported into GeneSpring GX 10 (Agilent, Palo Alto, CA, USA), and the six microarrays used were identified to the software as being either "control" or "treated". A "probeset" is a collection of oligonucleotide probes (there are 45101 probesets in total per array), and there are sometimes multiple probesets per gene. Two normalisation methods were used. Initial quality control was achieved by analysis of the hybridisation of groups of probes (MAS5 software, Affymetrix, USA (Liu *et al.*, 2002)), and by the use of Affymetrix control probesets containing deliberate mismatches which should prevent hybridisation of DNA fragments. Probesets that were present or marginal in at least two out of the six samples were deemed to be significant above background. The final quality controlled list of non-treated and treated probesets contained 25343 probesets (Figure 6.7).

The second normalisation method (Robust Multi-Array Average, (Irizarry *et al.*, 2003)) provides a "normalised intensity value" (NIV) for each probeset, which is calculated by subtracting from each probe the median of the log summarized values for each probe across all six samples (both AVP-treated and controls). Positive NIV values occur when the result is above the median for all samples, and negative values occur when the result is below the median for all samples. The NIVs were plotted for each array (Figure 2.12). The "whiskers" on the figure indicate that the spread and distribution of the values from each array were

similar to the other arrays in the experiment, for both control and treated samples.

2.11.4.2 Clustering of quality controlled data

The quality controlled NIV results were grouped hierarchically using the Pearson correlation coefficient with average linkage as a similarity measure. This clustering was performed two-dimensionally in order to gather information about co-regulation. Clustering between arrays determined which arrays were similar to which other arrays (shown in the six columns in Figure 2.13) hence attempting to group arrays into control versus treated conditions. Clustering was also performed between probesets, showing which probesets were similar to which other probesets (shown as many individual rows in Figure 2.13). The colours represent the NIVs of each probeset, with expression values maximally above the median expression for that particular probeset being coloured in red, and values maximally below the median expression in blue. For example, the probeset for AQP2 can be seen (arrowed on Figure 2.13) as either very red or very blue, indicating a large degree of change of each array with respect to the median AQP2 expression for all arrays. These results showed at an early stage that the biological replicates segregated into control and treatment groups. This can be seen more clearly in Figure 6.5 where significance testing has been carried out and the probesets have been rearranged to form two obvious groups.

2.11.4.3 Hybridisation control

A further technical quality control to check for adequate hybridisation was performed on the final quality controlled probe set list (25343 probesets). Four additional RNA transcripts had previously been artificially introduced into the experimental RNA samples. These are known to hybridise and express at varying levels, and are used to check the hybridisation reaction and subsequent washing and staining steps. Figure 2.14 shows the four control probesets on the *x*-axis, each with increasing signal values, followed by sister probesets representing the same four transcripts. The trend line connecting these eight data points therefore gives rise to two ‘spikes’. The resulting “spike” of the chips with respect to controls had similar profiles across all chips in the experiment.

Figure 2.12 Normalisation of raw data

Figure 2.13 Hierarchical clustering of normalised microarray data

Figure 2.14 Hybridisation controls forming a 'spike' plot
(Davidson & Halestrap, 1988)
(Pendleton *et al.*, 2002)
(Reichenberger *et al.*, 2001)

2.11.4.4 *t*-testing and fold change selection of normalised results

The normalised, quality controlled probesets were used to generate a list of genes expressed differentially between control and AVP-treated samples, after removing the 60 control probesets, giving a total of 25283 probesets. Since these two groups were parametric and the hypothesis of the experiment made a difference between means the expected result, significant changes were tested for using an unpaired *t*-test with significance at *p* value <0.05 (Genespring GX 10 software). Since 5% of 25283 samples is 1264, this could represent a relatively large type I error (false positive rate) in the final gene list. This was further reduced by performing a multiple testing correction known as the Benjamini-Hochberg False Discovery Rate (Benjamini & Hochberg, 1995), which ensured that <5% of the genes in the final list were false positives.

The *t*-tested list was then further selected for a fold change in the NIV of each probeset (gene) of greater than 1.18 in the treated condition with respect to the control condition. Although this particular value is arbitrarily chosen, it allows a robust minimum level of detection for changes in an experiment such as this with three replicates per condition.

2.11.4.5 Overlap analysis with list of genes containing CREB

The CREB targets database list (Zhang *et al.*, 2005) consists of 16242 probesets. This list was refined by CRE/TATA box (to ~12000) then sorted by "full site" to ~600. The overlap between this list and our final list of differentially expressed genes in the microarray was computed (see section 6.3.3.4). In order to determine if this overlap was more or less than expected by chance, a representation factor score (defined in (Kim *et al.*, 2001)) can be calculated as follows:

(number of genes in common between both lists)(number of genes in the mouse genome)/(number of differentially expressed genes in microarray)(number of genes in CREB target list)

$$= \frac{256 \times 35661}{364 \times 16242}$$

= 1.5

This indicates more overlap than expected by chance between these two independent groups of genes. Using the same figures, an exact hypergeometric probability of random overlap[9] was calculated to be 7 x 10^{-25}, indicating that the overlap is highly significant, and thus likely to be relevant.

2.12 Quantitative RT-PCR

2.12.1 Outline

Total RNA extracted from mpkCCD$_{cl4}$ cells for use in microarray experiments was reverse transcribed to cDNA and PCR-amplified using gene-specific primers. Amplification products were identified by comparing their melting temperatures to those obtained from previously prepared standards. These standards were specific PCR products of known concentration, from which a standard curve could be obtained to allow interpolation of concentration of amplified samples. The increase in the concentration of cDNAs by gene-specific primers is proportional to the initial expression level of transcripts. These results were normalised by comparison to the expression of the reference gene *GAPDH*.

2.12.2 Method

2.12.2.1 DNase

Using a Promega DNase kit the following were added on ice, for each of the six RNA samples: 1 µg RNA, 4.5 µl DNase, 2 ul START buffer RQ, made up to 20 µl with molecular grade water. The reaction was incubated at 37 °C for 30 min, then terminated using 4 µl of EGTA-containing STOP buffer. The RT reaction was performed after heating at 65 °C for 10 min.

2.12.2.2 RT reaction

RT was performed using random hexamer primers, in order to capture all target sequences. 1 µl of 0.5 µg/µl random hexamer primers were added to each DNase-treated 1 µg RNA aliquot or to water alone (RNA-ve control). Samples were made up to the same volume with molecular grade water, denatured at 65 °C for 5 min then cooled on ice for 2 min. A mix

[9] stattrek.com/tables/hypergeometric.aspx

containing 5x buffer, 2 mM dNTPs, 0.5 µl RT enzyme and 0.25 µl HPRI (RNaseA) per sample was added to each reaction. RT enzyme was omitted in RT negative reactions. Reactions were incubated at 42 °C for 1 h, followed by 70 °C for 3 min to destroy the RT enzyme.

2.12.2.3 Primers

Primers optimised for use with SYBR-green systems were supplied (Tebu-bio) as pre-mixed pairs each at 10 µM. Primers for SLC27A2 were designed using D-LUX^{TM} software[10] and supplied HPLC-purified by VH Bio Ltd (Gateshead, UK). These are summarised in Table 2.7.

Gene symbol	RefSeq Accession number	Sequence or reference positions	T_m (°C)	Exon	Product size
PDE4B	NM_019840.2	4062-4080	60		98
AQP2	NM_009699.3	1271-1291	60		138
ANK	NM_020332.4	1086-1104	60		89
GAPDH	NM_008084	309-329	60		140
SLC27A1	NM_011977.3	507-527	60		136
SLC27A2	NM_011978.2	GTACATTGGTGAACTGCTTCG	57.9	4	74
		CTTTGTGGTCCCGGTCATTTG	59.8	5	

Table 2.7 Primer sequences used in quantitative RT-PCR experiments. Since T_ms for all primers were ~60 ℃, experiments could be run simultaneousl y for all primer sets.

2.12.2.4 Standard curves

Clones were available for ANK (ANK-GFP construct, (Carr *et al.*, 2007)) and SLC27A2 (mouse IMAGE clone 30348317). These were diluted 1:100,000 before further 1:10 serial dilutions. For the other target genes, template DNA from section 2.12.2.2 was amplified using the primer sets above, and 1:10 serial dilutions made of the amplified products. All dilutions were performed in duplicate, with the range covering all likely concentration ranges encountered in the target gene. The first step of the qPCR reaction (below) denatures any coiled DNA present in the clones.

[10] http://escience.invitrogen.com/lux/index.jsp

2.12.2.5 qPCR method

All experiments were performed from the same batch of original cDNA samples (in order to exclude inter-batch RT variations) in a LightCycler® 480 Instrument with a SYBR Green Master Mix kit (Roche Diagnostics, UK). cDNAs were diluted 1:8 to reduce the effects of pipetting errors. 10 µl reactions were set up in a 96-well plate as follows: 5 µl SYBR Green I Master Mix (containing SYBR green I dye, FastStart Taq DNA polymerase, reaction buffer, dNTP mix and $MgCl_2$), 0.5 µl of 20x primer and 4.5 µl of diluted cDNA (the latter replaced by water for no-template controls). The programme was: denaturation for 10 min at 95°C, then amplification through 45 cycles of 95 °C (15 s), 60 °C (60 s), 72 °C (1 s, during which fluorescence was acquired). This was followed by a melt curve programme of 95 °C (5 s), 60 °C (60 s), 97 °C (with continuous acquisition of fluorescence).

2.12.3 Data analysis

2.12.3.1 Construction of standard curves

Results were obtained using Roche LightCycler 480 Software. The "crossing point" (Cp) is the amplification cycle number at which a sample's fluorescence first rises above background fluorescence. This is calculated as the point at which the rate of increase of the already increasing fluorescence (hence "second derivative") is maximal. Samples with less initial DNA thus require more amplification cycles to become visible above background noise, resulting in a higher Cp. Standard curves are plotted as the Cp for each dilution (*y* axis) against the logarithm of the sample's initial DNA concentration (*x* axis), from which a linear regression is calculated (Figure 6.8). The slope of each standard curve indicates the rate at which amplification of the initial DNA template proceeds. This can also be expressed as efficiency, where efficiency = $10^{(-1/slope)}$. The perfect amplification would result in a doubling of the initial DNA, giving an efficiency of 2 (corresponding to a slope of -3.3). The mean squared error of each data point's fit to the regression line was < 0.03 in all cases (acceptable < 0.2).

2.12.3.2 Relative quantification

Determination of expression of each gene transcript was carried out on three sample pairs of untreated and AVP-treated samples. Since only the change in levels between untreated and treated samples was desired, quantification of expression was performed relative to the reference gene glyceraldehyde-3-phosphate dehydrogenase (*GAPDH*) which did not

change recognisably between experimental conditions. Results were expressed relative to the expression of *GAPDH* in the *same* sample, enabling normalisation of differences between individual samples.

Evidence for the validity of using *GAPDH* as a reference gene included: the efficiencies of the *GAPDH* standards and the test samples were all 2.00 – 2.01 (to 2 decimal places); test samples were all extracted and reverse transcribed under the same conditions; and *GAPDH* expression has previously been used as a control in qPCR experiments involving forskolin in human renal epithelial cells (Rubis *et al.*, 2006) and found not to vary.

2.12.3.3 Calculation of fold change in expression

Fold changes in expression were calculated using the method of Pfaffl (Pfaffl, 2001). This method accounts for efficiency and allows normalisation to a reference gene. Results are expressed as a proportion of the reference gene to normalise for inter-experimental variations. The fold change for each target gene is calculated thus:

$$\text{change in expression} = \text{efficiency}^{\text{Cp (untreated) - Cp (treated)}}$$

Calculation of errors in this analysis is not usually undertaken. Here, experiments were performed on multiple occasions and the mean Cp calculated. A standard error could be calculated from this but may not be meaningful as the total number of repeats was quite small in the present experiments.

3 Results (I): Expression and localisation of ANKH in human kidney

3.1 Introduction

Using Northern analysis of ANK transcripts, Ho *et al.* (2000) found that ANK mRNA is expressed in many mouse tissues including brain, liver, spleen, lung, muscle and kidney. Two transcripts of ~3500 bp and ~4000 bp were detected in each tissue, suggesting usage of different polyadenylation sites. Carr *et al.* (2007) have confirmed expression of *ANK* at mRNA level using RT-PCR in native murine kidney and in the mouse inner medullary collecting duct cell-line mIMCD-3.

3.1.1 Anti-ANK antibodies

An anti-ANK antibody (Ab3) has been raised against residues 477-492 of the protein sequence at the intracellular C-terminal (Ho *et al.*, 2000), and was kindly gifted to us by the Kingsley laboratory. This C-terminal peptide sequence (PTEEVTDIVEMREENE) is identical in both mouse and humans (Figure 3.1). Work in our own laboratory has shown that immunofluorescent detection of ANK by Ab3 has been shown to parallel that of an ANK-NT-GFP fusion protein when expressed in fixed and permeabilised IMCD-3 cells (Carr *et al.*, 2007), and Ab3 fails to recognise a C-terminal deletion mutant R480X ANK-NT-GFP fusion protein expressed in these cells. Although Ab3 (Ho *et al.*, 2000) has previously been shown in mouse cell lines, mouse tissue and monkey cell lines to detect ANK on Western blotting and immunofluorescence, it has never so far been used to detect ANK in human kidney tissue. A commercially available anti-ANK antibody raised against residues 1-300 of the N-terminal human protein sequence was also available (Table 2.4). Both antibodies are polyclonal and raised in rabbit.

3.1.2 Aims of this section

The main aim of this section was to clarify whether ANKH mRNA is expressed in human kidney. The specific expression of ANKH protein in human kidney tissue could then be investigated. In order to implicate ANKH in a crystal inhibitory role, localisation of expression to the more distal nephron segments and collecting duct would be expected. The specificity of the two available anti-ANK antibodies, each directed against different peptide sequences, was tested using Western blotting and immunofluorescence studies in human renal tissue in order to validate their use in protein expression studies.

Figure 3.1 Evolutionary conservation of ANK (amino acid sequences)

Figure 3.2 Evolutionary conservation of ANK (nucleotide sequences)

3.2 Results

3.2.1 Comparison of human ANKH sequence with other species

Ho *et al.* (2000) found that there is significant conservation of the ANK gene across vertebrates and the human homologue *ANKH* is virtually identical to that in mouse. Figure 3.2 shows a remarkable conservation of ANK at the nucleotide level in four vertebrate species.

For protein sequences (Figure 3.1) there is 83% amino acid identity of the human sequence with the zebrafish ANK homologue, and 98% identity with the mouse homologue. Differences between substitutions are often conservative e.g. residue 21 (alanine/glycine) and residue 130 (arginine/lysine). Although bacterial species do have some small conserved domains, these are unlikely to code for the whole functional protein. A search of the NCBI Protein database revealed only four bacterial species in which hypothetical proteins with similarity to ANKH exist. One such occurs in *Desulfuromonas acetoxidans* (ZP_01311818) which has 84/428 identities with ANKH (19%). A prediction of the transmembrane segments of the peptide sequence is shown in Figure 3.3.

3.2.2 ANK mRNA is expressed in human kidney, and in human and mouse cell lines

Total RNA from human kidney, human embryonic kidney (HEK) cells and mpkCCD$_{cl4}$ cells was extracted (section 2.2.2.1), reverse transcribed and amplified using internal ANK primers. ANK human IMAGE clone (3927236; Geneservice) was used as a positive control. Results obtained with the mouse collecting duct cell line mpkCCD$_{Cl4}$ and with mouse kidney tissue are also shown as further positive controls (Carr *et al.*, 2009). Direct sequencing of gel-extracted PCR products confirmed the identity of the 490 bp products as ANK in all positive samples (Figure 3.4).

Figure 3.3 Putative domains of the ANKH protein

Figure 3.4 Expression of an ANK amplification product in human kidney cell line and tissue

3.2.3 *ANKH* full-length coding sequence is confirmed in 6 human subjects

In order to investigate the expressed nucleotide sequence of ANKH mRNA in human kidney, including the possible existence of polymorphisms and splice variants, it was necessary to verify the expression in kidney from normal human subjects of full length ANKH mRNA representing the coding sequence.

Attempts to use long-range PCR with primers designed for full-length ANKH coding sequence were unsuccessful, so primers were instead designed to amplify overlapping regions of the ANKH gene. It was not possible to amplify products greater than about 800 base pairs. Three primer pairs (see section 2.2.5) were successfully used to amplify overlapping products (Figure 3.5). β-actin controls showed product only in RT positive samples, excluding genomic DNA contamination. Contigs of the complete nucleotide sequence were then assembled (Figure 3.6) after gel extraction and direct sequencing of products (see section 2.2.6).

3.2.3.1 SNP found in three out of six human subjects

Contiguous sequences showed that ANKH residue 294 was determined as either a cytosine, thymine or heterozygous ('N') by the sequencing reaction (corresponding to position 317 in Figure 3.6). The sequencing chromatograms (Figure 3.7) confirmed that three subjects had a cytosine in this position, one had a thymine, and two were heterozygous for both C and T. Both possible codons, GCC and GCT, are synonymous for alanine at amino acid position 97. The SNP in ANKH at this position is annotated as RS17251667 in exon 2 (SNP database on NCBI), and has a quoted heterozygosity index across all populations of 0.111 ± 0.208.

Figure 3.5 RT-PCR of ANKH products from human renal cortex.

Total RNA extracted from the renal cortex of three normal human subjects (H, J, K) was reverse transcribed. ANKH mRNA expression was observed by separation on a 2% agarose gel of amplified overlapping products using three different ANKH-specific primer pairs. The first (201F/202R) produced a 397 bp product, the second (210F/211R) a 699 bp product, and the third (212F/213R) a 597 bp product. No alternative splice variants were detected. Results from β-actin primer pairs are shown in the lower figure. RT negative controls are shown for each human subject (lanes h, j, k). Negative controls for 210F/211R were run over two gels. The no-RNA control is in lane c; PCR negative control is in lane x. Similar results were obtained in three further human subjects.

Fig 3.5 goes here

Figure 3.6 Example of full length ANKH sequence from a human subject.

Contiguous sequences were obtained by amplification of RT products from patient E using three primer combinations: 201F/202R (E1), 210F/211R (E2), 212F/213R (E3). These were aligned using Multalin software (Corpet, 1988). The coding sequence (CDS) obtained from NCBI (NM_054027) is shown in red. Similar results were obtained in five other human subjects. In three subjects, an SNP was detected at position 317 (highlighted in green).

Fig 3.6 goes here

Figure 3.7 Detection of a single nucleotide polymorphism in ANKH coding sequence in six human subjects

3.2.4 Western analysis of ANKH protein expression in human kidney

Probing a protein lysate obtained from human kidney cortex using the N-terminal ANK antibody revealed two prominent bands at 50 kDa and ~60 kDa with a less distinct band at ~55 kDa (Figure 3.8). In contrast, using the C-terminal ANK antibody (Ab3), a single band was obtained at 50 kDa. The Kingsley group had previously found that a single protein band of ~50 kDa is recognised by Ab3 when ANK was transfected into COS-7 monkey kidney cells (Ho *et al.*, 2000) and when heterologously expressed in *Xenopus* oocytes (Figure 4.3E). The question of antibody specificity under the latter conditions is investigated further in Chapter 4. Copper phthalocyanine staining of the membranes as controls for protein loading and transfer were satisfactory.

Control experiments included a no-primary antibody control which yielded no bands (Figure 3.9A), with detection of actin protein at 42 kDa in each lane after stripping (Figure 3.9B). Separately, rabbit pre-immune serum revealed only a faint band at ~40 kDa (Figure 3.9D) despite adequate protein loading and transfer (Figure 3.9E), and no band was observed at 50 kDa.

These data suggest that Ab3 is capable of recognising a single polypeptide of the correct predicted size in human kidney, and therefore provides a more specific reagent for immunolocalisation of ANKH in this tissue than the N-terminal ANK antibody.

Figure 3.8 Western blot analysis of human renal cortex, probed with ANK N- and C-terminal antibodies.

Protein lysate (50 µg per lane for N-terminal ANK staining, 10 µg per lane for C-terminal) from three human subjects (H, J, K) was size fractionated on a 4-10% SDS-polyacrylamide gel and transferred to a PVDF membrane. The membrane was stained with anti-N-terminal-ANK antibody (Santa Cruz) at 1:100 at room temperature for 2 hours (A; n=3) or Ab3 1:500 overnight at 4℃ (B). Detection was by anti-rabbit IgG-HRP and visualisation was with a chemiluminescent substrate detection kit.

Fig 3.8 goes here

Figure 3.9 Western blot controls for ANK detection in human renal tissue.

Protein lysate (50 µg per lane) from three human subjects (H, J, K) was size fractionated on a 4-10% SDS-polyacrylamide gel and transferred to a PVDF membrane. The membrane was incubated for two hours or overnight (in separate experiments) with milk protein-TBS/Tween without any primary antibody (A; n=2), followed by anti-rabbit IgG-HRP (1:10,000) after washing. The membrane was then stripped and reprobed with mouse anti-actin antibody at 1:1000 for 2 hours at room temperature (B). Copper phthalocyanine membrane staining is shown (C).

15µg of protein lysate per lane was treated in the same way, and the membrane incubated with rabbit pre-immune serum at 1:500 overnight at 4℃ (D), followed by secondary antibody and detection as above. Copper phthalocyanine membrane staining is shown (E).

Western blot data from mouse kidney cell lines and tissue, probed with anti-ANK antibodies. Protein lysates (50 µg per lane) from mouse cell lines mpkCCD_{cl4} (CCD), M1 (M1), and whole mouse kidney (MK) were probed with anti-N-terminal-ANKH antibody (Santa Cruz) at 1:100 at room temperature for 2 hours (F; n=4) or Ab3 at 1:500 overnight at 4ºC (G) (experiment performed by Dr Georgina Carr (Carr *et al.*, 2009)).

Fig 3.9 goes here

3.2.5 Specificity of Ab3 staining in human renal cortex

Ab3 immunofluorescence is strongest in a small subset of renal tubules, which are identified morphologically from their location and cobblestone appearance as cortical collecting ducts (Figure 3.10). A weaker, more generalised, immunofluorescent signal is observed in other renal tubules. Using a rabbit pre-immune serum as the primary antibody under the same conditions revealed much lower staining intensity (Figure 3.10 C). No staining was observed using secondary antibody alone (Figure 3.10 D). Preadsorption of Ab3 antibody by its immunising peptide showed decreasing staining as the peptide concentration increased, confirming that staining in this tissue is specific to Ab3 (Figure 3.11).

3.2.6 ANKH localises to the collecting duct in human kidney

Aquaporin-2 is a marker of the principal cells of the collecting duct (Nielsen *et al.*, 2002) and traffics to the apical membrane allowing regulated water reabsorption from the tubule lumen. ANK reliably co-localised with AQP2 in four experiments, each using kidney tissue obtained from separate normal human subjects. Similar findings were observed in both cortical and medullary sections. Cortical sections often contained prominent medullary rays adjacent to the glomerulus-containing cortical labyrinth (Figure 3.12 B), and medullary sections were characterised by medullary collecting ducts and loops of Henle, as seen in cross-section in Figure 3.12 A. AQP2 staining was always observed to be concentrated at the apical (luminal) pole of the cells (Figure 3.12). ANK staining is seen to outline the tubular cells, suggesting plasma membrane staining at both apical and basolateral membranes. In addition, all cells within the collecting duct stain positively for ANK. This was further investigated by staining with a primary antibody against human AE1 (kindly provided by Dr A Toye, University of Bristol); this basolateral Cl^-/HCO_3^- exchanger occurs only in α-intercalated cells. Basolateral AE1 staining was found to colocalise with Ab3 staining (Figure 3.13).

3.2.7 ANKH expression elsewhere in the human nephron

On morphological grounds, proximal tubules were found to stain only faintly with Ab3, by comparison to distal segments (Figure 3.14 A). This was confirmed by using an antibody to CD98, a marker of the proximal tubule (Rossier *et al.*, 1999) (discussed further in section 4.3.1). Tubules that were CD98-positive did not stain brightly for ANK. The single tubule in Figure 3.14 C that stains brightest with ANK antibody is neither CD98 positive nor a proximal tubule on the basis of morphology. Staining with CD98 required PFA fixation and

Triton X100 permeabilisation. Ab3 clearly detects ANK in collecting ducts of PFA-fixed mouse tissue (Dr G Carr, unpublished results).

Some tubules were noted to stain moderately brightly with Ab3 but were AQP2-negative despite being similar in appearance. These segments could be either early distal tubule or Loop of Henle. Tamm Horsfall protein (Phillips *et al.*, 2004) is a marker of both apical and basolateral membranes of the thick ascending limb of the Loop of Henle and also the early distal convoluted tubule (Chakraborty *et al.*, 2004); (Ronco *et al.*, 1987). Figure 3.15 (A) shows two large tubules staining with Ab3, but only the left one shows obvious co-staining with anti-Tamm Horsfall antibody, giving a slightly yellow colour in the overlay image. In (B) many tubules stain moderately brightly with Ab3, and all but the largest, brightest tubule colocalise with anti-Tamm Horsfall antibody staining.

3.2.8 Localisation of NPP enzymes in human kidney

The ectoenzymes nucleotide pyrophosphatase phosphodiesterase-1 and -3 (NPP1, NPP3) generate PPi from ATP or other nucleotide triphosphates (Vekaria *et al.*, 2006a). NPP1 is expressed basolaterally in murine distal tubule (Harahap & Goding, 1988). Our results show NPP1 expression basolaterally in AQP2-positive cells in human kidney (Figure 3.16 B). NPP1 staining alone (Figure 3.16 C) and co-staining with Ab3 (Figure 3.16 A) confirmed some interstitial staining.

NPP3 was found to localise to the apical membrane of proximal tubules (identified morphologically; Figure 3.17 A), as was seen in mouse kidney (Vekaria *et al.*, 2006a); (Goding *et al.*, 2003). Staining was present but more limited in distal segments (Figure 3.17 B).

Figure 3.10 ANK immunofluorescence using the Ab3 antibody in human kidney

.

Figure 3.11 Preadsorption of Ab3 antibody by its immunising peptide.

Figure 3.12 Colocalisation of ANK with AQP2 in human kidney.

Figure 3.13 Colocalisation of ANK with AE1 in human kidney.

Figure 3.14 ANK is minimally expressed in human proximal tubule.

CLSM images showing:

(A) x20 image of human renal cortex. Parallel medullary rays are seen in the centre, top and top-right, and stain brightly with anti-C-terminal ANK antibody, Ab3. Proximal tubules are seen to the left and bottom of the image, and stain very poorly with Ab3. Scale bar = 40 μm.

(B) No-primary antibody control from the same experiment.

(C) Human renal cortex fixed with PFA and permeabilised with Triton X100 0.1%. Staining was with Ab3 (green channel), anti-CD98 antibody (red channel) and overlay image. Scale bar = 20 μm.

Fig 3.14 here

Figure 3.15 ANK is expressed to a limited extent in Loop of Henle/distal convoluted tubule.

Figure 3.16 Expression of NPP1 in the collecting duct of human kidney.

CLSM images showing immunofluorescence in human renal cortex. Scale bar = 20 μm for all images.

(A) Anti-C-terminal ANK antibody (Ab3; green channel), anti-NPP1 antibody (red channel), and overlay of images

(B) Anti-AQP2 antibody (green channel), anti-NPP1 antibody (red channel), and overlay of images

(C) No-primary control and anti-NPP1 antibody staining alone.

Fig 3.16 here

Figure 3.17 Expression of NPP3 in the proximal tubule of human kidney.

3.3 Discussion

3.3.1 Expression of ANKH mRNA in human subjects

ANK is highly conserved throughout evolution. This applies to some other membrane transporters such as AE1 (Jarolim *et al.*, 1998) and the vacuolar H^+-ATPase (Gogarten *et al.*, 1989), but the ANKH domain is unique in the human and mouse genomes (Figure 3.18). Prediction of transmembrane domains using 11 different programs showed that between 7 and 12 domains are likely (Williams *et al.*, 2002); (Wang *et al.*, 2009). Although no further structural experiments are available in the literature, Ho *et al.* (2000) demonstrated that the C-terminal, to which Ab3 is raised, is likely to be intracellular.

Results of the RT-PCR of internal ANK products show that ANK is endogenously expressed in a human renal cell line (HEK) and, importantly, in human kidney. The primers detected the identical product in mouse collecting duct cell line and mouse kidney tissue, since mouse and human sequences are almost identical in the region between these primers. However attempts using RT-PCR to amplify the entire 1479 bp ANK coding sequence using two separate primer pairs each flanking the whole sequence were unsuccessful. Using three contiguous sequences, we have sequenced for the first time the full length ANKH coding sequence from the kidneys of six normal human subjects (not known to have chondrocalcinosis or CMD). Sequence analysis revealed a synonymously coding SNP, which has an average heterozygosity frequency of 11 ± 21% [11], suggesting that it occurs in up to ~30% of subjects.

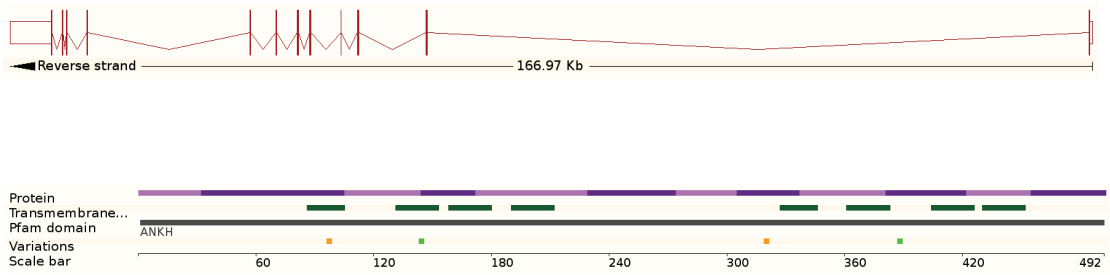

Figure 3.18 ANKH transcript and protein summaries from Ensembl.

Upper: There is only one known ANKH transcript (number ENST00000284268), which is encoded on the reverse strand. Vertical lines are exons (coding sequence) and horizontal lines are introns. Unfilled boxes are UTR (untranslated region) exons. *Lower:* Parts of the ANKH protein coded for by the 12 ANKH exons are shown in alternating pink and purple colours, followed by the predicted transmembrane segments in green. The Pfam database of protein domains shows ANKH as a single unique domain (pfam07260; grey line). The positions of four known SNPs are marked (coloured dots); the first is rs17251667 which was detected in three of the six human subjects in this study. Figures were downloaded from www.ensembl.org

[11] www.ncbi.nlm.nih.gov/SNP

3.3.2 Detection of ANKH in human kidney tissue using Western blotting

Detection of endogenous ANKH protein on Western blot in human kidney tissue has been confirmed. Findings using a C-terminal antibody (Ab3) are consistent with those of the Kingsley group (Ho *et al.*, 2000) who obtained a major band at 50 kDa in ANK-pCMV-transfected monkey kidney cells, although no data are given for any minor bands they obtained. Yet the Kingsley group were never able to detect endogenous ANK in tissues using Ab3 (Dr KA Gurley, personal communication). This band compares favourably with the predicted protein size of 54.3 kDa based on the coding sequence for ANKH. We have also confirmed that Ab3 detects ANK-FLAG overexpressed in *Xenopus* oocytes (section 4.2.6) at 50 kDa, in agreement with Kingsley *et al* (Figure 4.3E), as well as Ab3's detection of both endogenous and overexpressed ANK in HEK293 cells (Carr *et al.*, 2009) and CCD cells (Figure 6.1).

In human tissue, the N-terminal antibody (Santa Cruz; Table 2.4) consistently gave a band at ~50 kDa but also a further band at ~60 kDa. This additional band is unlikely to represent the formation of a hetero-oligomer as experiments were performed under reducing conditions. N-terminal anti-ANK antibody detection was reconfirmed in ANK-overexpressing *Xenopus* oocytes (Figure 4.7), in the endogenously ANKH mRNA-expressing mouse cell lines mpkCCD$_{Cl4}$ (Figure 3.4 A) and M1 (Carr *et al.*, 2009), and in mouse kidney tissue. In *Xenopus* oocyte expression studies using FLAG-tagged ANK, the N-terminal antibody failed to detect it. In addition a 60-65 kDa band was observed in both water and ANKH-injected oocytes (Figure 4.3 A). In mouse cell lines and tissue a single band of ~60 kDa is seen with N-terminal ANK antibody, compared to a band size of 50 kDa with Ab3 in cell lines together with additional bands of smaller size seen in the mouse tissue sample (Figure 3.9 F&G). Santa Cruz's datasheet[12] shows product sizes of either ~50 kDa or ~60 kDa with N-terminal ANK antibody in separate experiments in transfected HEK293 cells. This antibody is raised against amino acids 1-300 of human ANKH, a very large epitope which contains two amino acid differences from the mouse sequence. These discrepancies in expected band size in our experiments and the company's own data, as well as the very large epitope, suggest that the Santa Cruz N-terminal antibody is less specific than Ab3 and does not recognise ANKH specifically.

[12] www.scbt.com

Rabbit pre-immune serum was used since both N- and C-terminal antibodies were raised in rabbit. This together with the no-primary antibody control demonstrated that bands arising with Ab3 after detection by the secondary antibody are specifically due to binding of Ab3.

Taken together, these results confirm that human kidney tissue expresses the ANKH protein. The weight of evidence from the present study as well as published data, and the calculated protein size, favours a band size of ~50 kDa. Given the inconsistency of results obtained in human tissue between N- and C-terminal anti-ANK antibodies, all tissue immunofluorescence was performed using the C-terminal antibody (Ab3).

3.3.3 Detection of ANKH in human kidney tissue using immunofluorescence with Ab3

Previous results (Carr *et al.*, 2007) have shown that ANK is expressed in the cortical collecting ducts of mouse kidney tissue. The present study confirms expression of ANKH in the human kidney with localisation to the collecting ducts. It offers some evidence of limited expression in the preceding nephron segments (thick ascending limb of the Loop of Henle or early distal convoluted tubule). This is the first time that ANKH has been localised in human renal tissue. The data also suggest that there is very little expression in the proximal tubule.

All sections show that ANK staining occurs on both membranes of human collecting duct cells *in situ*. This is similar to findings in non-polarised cell lines such as HEK293 and in polarised cell lines such as mIMCD-3 (Carr *et al.*, 2007) and mpkCCD$_{cl4}$ cells (Chapter 6). In many cases, staining was noted to be particularly marked on the apical aspect (Figure 3.10 A). Given its predominant expression in the collecting duct, this places ANK in the same physiological location as AQP2. This suggests that there may be a functional relationship between these two proteins, supporting the hypothesis that transport of PPi to the tubule lumen may be involved in the inhibition of calcium crystal formation. This is investigated further in Chapter 6. The AE1 antibody studies show that ANK also localises to the basolateral membrane. This suggests a possible role in the inhibition of interstitial calcification, perhaps complementing the role of the ectoenzyme NPP1.

Validation of the Ab3 antibody using appropriate controls for immunofluorescent staining in human tissue is important, particularly since the pattern of staining may be different to that observed for Ab3 in Western blotting. The reduction of immunofluorescence by pre-adsorption with the C-terminal peptide to which Ab3 is raised provides support for its specificity in human renal tissue. Ab3 has been previously validated for

immunofluorescence in mouse tissue and cells using a Glu440X C-terminal deletion mutant (Carr *et al.*, 2007). Unfortunately human patients with ANKH C-terminal deletions have not been described, and tissue from the mutant $ANK^{ank/ank}$ mouse (Jackson Laboratory, Maine, USA) was not available to us. Results in Chapter 4 using a FLAG-tagged ANK construct and CD98 membrane marker show that human ANKH expressed after cRNA was injected into *Xenopus* oocytes is indeed localised to the plasma membrane, and that Ab3 can detect plasma membrane-expressed ANKH.

3.3.4 Implications

Since active calcium regulation occurs in the distal tubule (Bindels, 1993), and the final urinary concentration is regulated via AQP2 in the collecting duct, the localisation of ANKH to these nephron segments places it in the most useful anatomical position to function in the limitation of calcium crystal formation. This is supported by the finding that the PPi-producing ectoenzyme NPP1 is localised to the distal nephron in human kidney. ANKH expression was particularly marked on the apical membrane, which would be structurally consistent with PPi transport into the lumen in support of this theory. However ANKH was expressed on both membranes and is also present in the medullary collecting ducts. There may also be a role for basolateral ANKH transport into the medullary interstitium, this area also being recognised in the pathogenesis of renal stones (Sayer *et al.*, 2004).

4 Results (II): Intracellular and plasma membrane expression of ANKH overexpressed in *Xenopus* oocytes

4.1 Introduction

4.1.1 Confirmation of heterologous overexpression in oocytes

Having confirmed ANKH expression and membrane localisation in human renal collecting ducts, ANKH function may now be investigated by overexpressing heterologous ANKH constructs in *Xenopus* oocytes.

Unlike epithelial cell lines, oocytes do not exhibit tight junctions and membrane polarity, and hence act as a single membrane separating cytosol and extracellular compartments. The major advantage of oocytes is that rather than transfecting with DNA as in cell lines, the vast protein manufacturing ability and quality-control mechanisms of the oocyte can be utilised to produce huge numbers of expressed protein molecules from a few ng of heterologous cRNA. Since overexpression in this way results in 10^{10}-10^{11} transporters in the membrane per oocyte, etc (Zampighi *et al.*, 1995), and very few endogenous oocyte membrane transporters exist (Weber, 1999), it should in theory be easy to determine positive membrane expression by immunofluorescent staining (IF) or Western blotting. In reality, these techniques presented many technical problems; for IF these included: method of fixation, preservation of morphology, delineation of the membrane itself and autofluorescence of the oocyte. As a result, there are numerous different protocols for oocyte IF available in the literature, and although oocyte IF is sometimes performed e.g. (Kohl *et al.*, 1998), it is often omitted if the flux results are convincing (e.g. (Bröer *et al.*, 1998); (Wagner *et al.*, 2000).

4.1.2 Aim of this section

The aim of this section is to confirm expression of the heterologous ANKH-constructs in the oocyte and localisation to the plasma membrane. These constructs would thus be validated for use in functional experiments. Experiments were performed on oocytes from a batch which was then used in subsequent functional experiments. In tissue, a discrepancy was observed between results obtained with the N- and C-terminal anti-ANK antibodies, with the latter found to be most consistent. To avoid any doubt in oocytes, a FLAG-tagged ANKH construct was made and staining results checked with both anti-ANK antibodies. Localisation to the plasma membrane was confirmed using the specific marker CD98.

4.2 Expression of ANKH protein in *Xenopus* oocytes

4.2.1 Confirmation of purity of oocyte membrane fraction preparation

Oocytes were injected with human CD98 cRNA. The anti-CD98 antibody used detects the extracellular C-terminal of the dimer at ~120 kDa [13] (Rossier *et al.*, 1999). A band was seen at ~120 kDa in the membrane fraction only of CD98-injected oocytes (Figure 4.1 A). The lack of a band in water-injected oocytes showed that CD98 does not occur endogenously in oocytes. No bands were seen in the cytoplasmic protein fraction. Bands of approximately the same size were obtained from the protein lysate of kidney from three normal human subjects (Figure 4.1 B).

4.2.2 Expression of the ANKH-FLAG construct in oocytes

To verify detection of ANK by the anti-ANK antibodies, an ANKH-NT-3XFLAG fusion construct was obtained and cRNA made. Oocytes were injected with ANKH-FLAG and membrane fractions were prepared in the same way as for CD98. A very strong band was seen at ~50 kDa in the membrane fractions, consistent with detection of the construct (Figure 4.2 A). The copper stained membrane confirms that increased transfer of ANKH-FLAG protein compared to water-injected protein was not the cause (Figure 4.2 B). A lighter band of the same size was seen in the cytoplasmic fraction of experiment '2' only. Non specific bands were seen at 37 kDa.

Using 0.6 μg of protein also resulted in a strong band at 50 kDa, showing that detection of FLAG is highly sensitive using this technique (Figure 4.2 C). Boiling in SDS did not affect the results, confirming the efficacy of the protocol used (section 2.6.2.2). Protein from CD98-injected oocytes was used as a negative control, demonstrating specificity of FLAG detection.

4.2.3 Results with Ab3 agree with results of anti-FLAG in detection of ANKH-FLAG in oocyte membrane

The same fractions as those used in experiment 1 in Figure 4.2 A were used to investigate detection of anti-ANK antibodies. Anti-N-terminal ANK antibody was unable to detect the ANKH-FLAG protein at the expected size in the membrane fraction, giving only non-specific bands (Figure 4.3 A). This confirms the lack of detection observed with this antibody in human tissue. The anti-C-terminal Ab3 antibody gave a convincing band at 50

[13] http://datasheets.scbt.com/sc-7095.pdf

kDa in the ANKH-FLAG membrane fraction only (Figure 4.3 B), agreeing with the result of anti-FLAG immunodetection. Non-specific bands were seen at ~40-42 kDa in all lanes. Omission of primary antibody resulted in no bands (Figure 4.3 D).

Ab3 was then used to confirm expression of ANKH-pcDNA3.1 construct, i.e. without the FLAG tag. Although the protein lysate was not fractionated, clear bands at ~50 kDa are seen in lanes from ANKH-injected oocytes, with no difference between the bands for 85 ng and 175 ng of initially injected cRNA (Figure 4.4). The slight reduction in band size may be due to omission of the ~3 kDa FLAG tag.

4.2.4 Attempts to localise ANKH to the plasma membrane on immunofluorescence

The mouse ANK-NT-GFP construct has been shown to localise to plasma membrane, endoplasmic reticulum, acidic endosomes and mitochondria in IMCD-3 cells (Carr *et al.*, 2007). Attempts to detect mouse and human ANK-GFP constructs in oocytes by visualising GFP fluorescence were unsuccessful partly due to autofluorescence of the oocytes, and use of anti-GFP antibodies was also unsuccessful. Since Ab3 was found to stain ANK on Western blotting, localisation was attempted with Ab3 in injected oocytes. Representative images in Figure 4.5 show that ANKH-pcDNA3.1, mouse ANK-GFP and ANKH-pTNT constructs gave an outer rim of positive staining compared to water, which was brightest in the image for mouse ANK-GFP. There was marked intracellular staining, seen also on water-injected oocytes but not on the no-primary control, which may indicate either non-specific staining due to Ab3 or the presence of endogenous ANK.

4.2.5 Ab3, but not anti-N-terminal ANK antibody, colocalises with FLAG

Anti-FLAG staining in both Figure 4.6 and Figure 4.7 showed a bright outer rim of staining in ANKH-FLAG sections compared to much dimmer or no staining of water controls. Appearances of positive and control oocytes are the same as those shown in Figure 5 of (Wagner *et al.*, 2000). This pattern was mirrored by Ab3 staining (Figure 4.6) but there was very little staining with anti-N-terminal ANK antibody (Figure 4.7). Overlay images confirmed colocalisation of staining due to Ab3 and anti-FLAG.

As seen above, diffuse intracellular staining was noted on both water-injected and ANKH-FLAG-injected sections, but not on the no-primary control. However the sub-membrane area was noticeably brighter on Ab3 and anti-FLAG staining of the ANKH-FLAG injected

sections compared to water-injected sections. All results were consistent over experiments performed on separate batches of oocytes on two separate occasions. In a parallel experiment, anti-FLAG antibody raised in rabbit rather than mouse was used separately as primary antibody, and was detected with anti-rabbit FITC. This produced similar results to those in Figure 4.6 and Figure 4.7 from the mouse anti-FLAG (images not shown).

4.2.6 ANKH-FLAG expression in oocytes occurs at the plasma membrane

Having established CD98 overexpressed in oocytes as only detectable in the membrane fraction, these oocytes were sectioned and stained with anti-CD98. Staining was observed along the outer rim of the oocyte (Figure 4.8). No staining was seen in water-injected controls, or no-primary controls with either injected type. This confirms that the outer rim of the oocyte is the plasma membrane.

Oocytes were injected with either water, ANKH-FLAG or co-injected with both ANKH-FLAG and CD98. Anti-FLAG antibody detected ANKH-FLAG at the membrane in oocyte sections that contained this construct (Figure 4.9 rows 3 and 4), giving rise to the green spikes on the profile plot of pixel intensity. Similarly, anti-CD98 antibody detected CD98 at the membrane in CD98-injected oocyte sections. This is different to the background fluorescence seen with water-injected controls. Colocalisation of ANKH-FLAG and CD98 at the plasma membrane is confirmed, indicated by a yellow colour on the overlay image and an arrow showing the merging red and green peaks on the pixel quantification (Figure 4.9 row 4). Experiments were performed on separate batches of ANKH-FLAG-injected oocytes on four separate occasions, and on two occasions with CD98 co-injection.

Figure 4.1 Detection of CD98 expressed in oocyte membrane by probing with anti-CD98 antibody

Western blot analysis of oocytes injected three days earlier with water (W) or CD98 (CD) cRNA fractionated into membrane (m) and cytosolic (c) components, and whole human kidney cortex lysate.

(A) Protein lysate (40 µg/lane for membrane fraction, 10 µg/lane for cytoplasmic fraction) was loaded with sample buffer containing β-mercaptoethanol at room temperature (as Halestrap protocol), size fractionated on a SDS-polyacrylamide gel and transferred to a PVDF membrane before probing with polyclonal goat anti-human CD98 antibody (Santa Cruz sc-7095) at 1:500 (3 hours, room temp), with HRP-anti-goat at 1:2500 as secondary.

(B) Protein lysate (40 µg/lane) from whole renal cortex of three normal human subjects (H, J, K) was loaded, run and probed as above.

Fig 4.1 here

Figure 4.2 Expression of ANKH-FLAG construct in oocytes, detected by anti-FLAG antibody

Western blot analysis of oocytes injected three days earlier with water (W), CD98 (CD) cRNA or ANKH-FLAG (AF) cRNA, fractionated into membrane (m) and cytosolic (c) components.

(A) Protein lysate (10 µg/lane) was loaded with sample buffer containing β-mercaptoethanol at room temperature (as Halestrap protocol), size fractionated on a SDS-polyacrylamide gel and transferred to a PVDF membrane before probing with anti-FLAG M2-HRP conjugated antibody at 1:200 (1 hour, room temp). Two separate experiments are shown (labelled 1 and 2); total n=3.

(B) The PVDF membrane from experiment 2 was stained with copper phthalocyanine for 30 min, then washed for 30 min with 12 mM hydrochloric acid.

(C) Protein lysate (0.6 µg/lane) was loaded with sample buffer containing β-mercaptoethanol, then either boiled for 10 min at 95℃ (left three lanes) or kept for 10 min at room temperature (right three lanes). They were then run and probed as above. The results are similar regardless of whether samples were first boiled or not.

Fig 4.2 here

Figure 4.3 Confirmation of ANKH-FLAG expression in oocytes by detection with Ab3 antibody

Western blot analysis of oocytes injected three days earlier with water (W) or ANKH-FLAG (AF) cRNA, fractionated into membrane (m) and cytosolic (c) components.

(A) Protein lysate (40 µg/lane for membrane fraction, 10 µg/lane for cytoplasmic fraction) as used in experiment 1 in Figure 4.2 A was loaded and run as above. The membrane was probed with anti-N-terminal-ANKH antibody at 1:200 (Santa Cruz) overnight at 4℃, with detection by anti-rabbit IgG -HRP (1:10,000) as secondary.

(B) Protein lysate (50 µg/lane for membrane fraction, 25 µg/lane for cytoplasmic fraction) as used in experiment 1 in Figure 4.2 A was loaded and run as above. The membrane was probed with anti-C-terminal-ANKH antibody (Ab3) at 1:500 overnight at 4℃, with detection by anti-rabbit HRP as above (n=2).

(C) The membrane from (B) was stripped for 8 minutes according to manufacturer's protocol and lack of detection of bands was confirmed after incubation with a chemiluminescent substrate detection kit (data not shown). The membrane was washed in TBS/Tween and reprobed with anti-alpha tubulin 1:1000 overnight at 4℃. Bands of expected size of 50 kDa can be seen m uch more prominently in the cytosolic fractions (c) than in the membrane fractions (m).

(D) Protein lysate (50 µg/lane for membrane fraction, 25 µg/lane for cytoplasmic fraction) as used in Figure 4.2 A was loaded and run as above. The membrane was incubated overnight with milk protein-TBS/Tween without any primary antibody, followed by anti-rabbit HRP after washing, and visualisation with a chemiluminescent substrate detection kit. No bands are visible despite adequate protein loading and transfer as confirmed on the adjacent copper phthalocyanine membrane staining.

(E) Data from the Kingsley group, confirming detection of a band at 50 kDa using Ab3 in frog oocytes injected with ANK (left lane). This band was not seen in oocytes injected with an ANK mutant missing the C-terminal epitope against which Ab3 was raised (right lane). Non-specific bands are seen in both lanes, notably at ~35 kDa. Data kindly provided by Dr Kyle Gurley, Kingsley lab, Stanford, USA.

Fig 4.3 here

Figure 4.4 Detection of ANKH-pcDNA3.1 expression in oocytes using Ab3 antibody

Figure 4.5 ANK constructs localise to the oocyte plasma membrane

CLSM images of oocyte sections (10-15 μm thickness) fixed with methanol 5 d after injection with either water (row 1) or cRNA of ANKH-pcDNA3.1 (row 2), mouse ANK-GFP (row 3), ANKH-pTNT (row 4).

Overnight staining at 4℃ with Ab3 is shown (column 1), except where primary antibody was omitted as stated. Secondary staining in all sections was with anti-rabbit FITC. Transmitted light appearances are shown in column 2, and an overlay of Ab3 staining onto transmitted light (column 3). Scale bar = 50 μm (applies to all images).

Fig 4.5 here

Figure 4.6 Identical and enhanced staining in ANKH-FLAG-injected oocytes using both Ab3 and anti-FLAG antibodies

CLSM images of oocyte sections (10-15 μm thickness) fixed for 4 h with methanol 3 d after injection with either water (upper row) or ANKH-NT-3XFLAG cRNA (lower row).

Overnight staining at 4℃ was simultaneously perfor med with Ab3 (second column), mouse anti-FLAG (third column), or primary antibody was omitted (first column). Secondary staining in all sections was with anti-rabbit FITC and anti-mouse TRITC. Overlay of staining with both antibodies onto a transmitted light image is shown in the fourth column. Scale bars = 50 μm, n = 2 separate experiments.

Fig 4.6 here

Figure 4.7 Non-identical staining of ANKH-FLAG-injected oocytes using anti-N-terminal ANK and anti-FLAG antibodies

CLSM images of oocyte sections (10-15 µm thickness) fixed for 4 h with methanol 3 d after injection with either water (upper row) or ANKH-NT-3XFLAG cRNA (lower row).

Overnight staining at 4℃ was simultaneously perfor med with rabbit anti-N-terminal ANK (second column), mouse anti-FLAG (third column), or primary antibody was omitted (first column). Secondary staining in all sections was with anti-rabbit FITC and anti-mouse TRITC. Overlay of staining with both antibodies onto a transmitted light image is shown in the fourth column. Scale bars = 50 µm, n = 2 separate experiments.

Fig 4.7 here

Figure 4.8 CD98 marks the plasma membrane of *Xenopus* oocytes

CLSM images of oocyte sections (10-13 µm thickness) fixed with 2% PFA 3 d after injection with either water (top row) or human CD98 cRNA (other rows). Staining was performed with mouse anti-human CD98, with primary antibody omitted as a control (example in bottom row). Secondary staining was with anti-mouse TRITC in all sections. Overlay onto a transmitted light image is shown opposite each corresponding section. Anti-rabbit FITC was used separately as a further secondary antibody control, but no staining was observed. In all sections, results were the same regardless of whether (second row) or not (third row) permeabilisation with 0.1% Triton X100 had been performed.

Fig 4.8 here

Figure 4.9 Confirmation of ANKH-FLAG localisation to the oocyte plasma membrane

CLSM images of oocyte sections (10-15 µm thickness) 2% PFA-fixed 3 d after injection with either water (row 2), ANKH-NT-3XFLAG (row 3) or ANKH-NT-3XFLAG with CD98 (rows 1 and 4).

Staining was simultaneously performed with rabbit anti-FLAG (green; column 1) and mouse anti-CD98 (red; column 2) as primary antibodies. Overlay of anti-FLAG and anti-CD98 images (column 3), and transmitted light views (column 4) are shown. No-primary antibody controls (row 1) were similar for all injected oocyte types. Secondary staining was with donkey anti-rabbit FITC and donkey anti-mouse TRITC in all sections. All sections were stained with and without 0.1% Triton X100 permeabilisation for 15 min after fixation; results were indistinguishable from each other. Scale bars represent 50 µm and apply to all images.

Pixel intensity quantification for each channel using Leica software along a transect (marked with blue line; arbitrary units) for each overlay image is shown in column 5. Plasma membrane staining is marked by the asterisk.

Fig 4.9 here

4.3 Discussion

4.3.1 Purity of oocyte membrane fractions and definition of the plasma membrane outline

Endogenous oocyte membrane proteins may not be present in sufficient quantities to allow robust detection, so the specific membrane protein CD98 was overexpressed. CD98 (also known as 4F2) is composed of two subunits; a heavy chain membrane glycoprotein (SLC3A2) and a non-glycosylated light chain (SLC7A5), which dimerise to form a functional amino acid transporter as demonstrated by overexpression in *Xenopus* oocytes (Rossier *et al.*, 1999). CD98 is expressed in many cell types but only on plasma membranes (Kanai *et al.*, 2000). In kidney CD98 is a subunit of the LAT2 amino acid transporter which localises to the basolateral membrane of the renal proximal tubule (Rossier *et al.*, 1999). Our results confirm expression and detection of the endogenous CD98-light chain complex in human kidney. Since CD98 is only expressed on the plasma membrane, it can be concluded that membrane and cytosol extracts are each reasonably pure. A pure membrane fraction will contain minimal cytoskeleton, and the much reduced alpha tubulin detection in the membrane fraction of oocytes also confirms this (Figure 4.3 C).

CD98 staining experiments were performed on the *same* batch of oocytes as was used for CD98 detection by Western blotting. The results of staining (Figure 4.8) indicate that the red outer band seen on staining must be the membrane of the oocytes and not the vitelline layer. The similarity of appearances regardless of permeabilisation with detergent also confirms membrane staining.

4.3.2 Confirmation of ANKH expression in oocytes

The results confirm that ANKH-FLAG is expressed in the oocyte membrane. The lighter band seen on only one of the cytoplasmic fractions indicates the presence of cytoplasmic ANKH-FLAG, or more likely that there is contamination of the cytoplasmic preparation. Although immunofluorescence showed staining of intracellular membranes with all antibodies except anti-CD98, some of this may be non-specific given that it also occurs in water-injected oocytes. There is a brighter sub-membrane band in Ab3 and FLAG-stained ANKH-FLAG-injected oocytes (Figure 4.6) which may be due to massive overexpression of the protein resulting from injection of ~50 ng cRNA. Membrane proteins are transported in vesicles from the endoplasmic reticulum to the membrane, causing excess protein to simply collect below the membrane (Hirsch *et al.*, 1996); (Forster *et al.*, 1999). Cytoplasmic

staining was much reduced when only 5 ng of cRNA was used (Fernandes *et al.*, 2007). Figure 4.4 confirms ANKH expression with injection of the non-FLAG tagged construct, which is probably maximal given the large amount of cRNA injected.

Ab3 paralleled anti-FLAG's immunodetection, hence validating Ab3 and supporting results obtained in Chapter 3 with this antibody in human tissue. It also agrees with results obtained by the Kingsley group (Figure 4.3 E), who also showed loss of the band when a C-terminal epitope deletion mutant (E440X) was probed with Ab3 (Figure 1a in (Gurley *et al.*, 2006b)).

None of the additional bands with either anti-FLAG or Ab3 immunodetection were consistent, suggesting that these are non-specific rather than representing detection of interacting partners in a complex within the oocyte.

4.3.3 ANKH-FLAG localises to the plasma membrane when overexpressed in oocytes

Staining of the outer rim of oocytes injected with ANKH-containing constructs was observed using Ab3. This appearance was confirmed with anti-FLAG staining, which exactly reflected staining with Ab3 in ANKH-FLAG-expressing oocytes. Finally, CD98 was established as a precise marker of the oocyte membrane, seen in our experiments at the outer rim. Colocalisation of ANKH-FLAG and CD98 was seen in oocytes expressing both these constructs, confirming that ANKH-FLAG is localised to the oocyte plasma membrane.

4.3.4 The pattern of oocyte immunofluorescence is consistent with previously published studies

Cytosolic staining was noted on immunofluorescence using all antibodies. Massive protein overexpression can lead to insertion into heterotopic membranes, which could include intracellular membranes (Wagner *et al.*, 2000), and localisation of ANK in intracellular organelles is known (Carr *et al.*, 2007). No immunodetection was observed in the cytoplasmic fraction of oocyte protein lysates, suggesting that the cytosolic staining may be artefactual. Oocyte autofluorescence (Manoharan *et al.*, 2006) is unlikely to be a cause given the negative results of no-primary antibody controls.

The outer rim of staining was more pronounced with methanol-fixed (Figure 4.6 and Figure 4.7) compared to PFA-fixed sections (Figure 4.8). Methanol is a coagulating protein fixative causing dehydration which results in up to 50% shrinkage of cell volume (Bacallao *et al.*,

2006). But staining of the outer rim was consistent with membrane localisation even in PFA-fixed oocytes (Kunchaparty *et al.*, 1999). The apparent gap is likely due to a layer of dark sub-membranous cortical granules (Figure 4.10; and (Dumont, 1972)), as seen in transmitted light images (Figure 4.6 to Figure 4.8).

4.4 Conclusions

Expression of heterologous ANKH-constructs in the *Xenopus* oocyte has now been confirmed, with definite localisation to the plasma membrane. The purity of the membrane fraction of protein lysate, and definition of the oocyte plasma membrane were verified. Ab3 was validated using a FLAG-tagged construct as suitable for confirming expression and detecting localisation of ANK(H) in oocytes using both immunofluorescence and Western blotting. On the other hand, the commercially available anti-N-terminal ANK antibody was found not to reliably detect ANK on either Western blot or immunofluorescence.

ANKH-FLAG was constructed in the pcDNA3.1 mammalian expression vector. These results demonstrate that ANKH cloned into the pcDNA3.1 vector, as used in many of the functional experiments, is capable of expression of a membrane protein in oocytes, without modification or addition to the vector such as the β-globin gene, as previously suggested by Gurley *et al.* (2006b).

Figure 4.10 Schematic diagram of ultrastructure of the vegetal pole of a Stage VI *Xenopus* oocyte

5 Results (III): Functional studies of ANKH in *Xenopus* oocytes

5.1 Introduction

5.1.1 Rationale for transport measurements in *Xenopus* oocytes

The original paper by the Kingsley group (Ho *et al.*, 2000) identified *ank* as the defective gene causing hereditary ankylosis in mice. Evidence relating to the physiological function of ANK was derived from experiments using primary fibroblast cultures from wild type and mutant $ANK^{ank/ank}$ mice, where no increase in extracellular PPi concentration was observed in the latter, and from the observed abolition of abnormalities in mutant $ANK^{ank/ank}$ mice when transfected with pCMV-*ANK*. They concluded that ANK functioned directly in PPi export. A second paper from this group (Gurley *et al.*, 2006b) overexpressed the mouse ANK protein in *Xenopus* oocytes, using the isotope ^{33}PPi to measure uptake of PPi, specificity being gauged by increased uptake of PPi relative to water injected oocytes. This technique, pioneered by Gurdon *et al.* (1971), has been widely used, as the oocytes can efficiently translate RNA for many membrane transporters and membrane receptor systems (Wagner *et al.*, 2000). Many effects of disease-causing mutations are similar between oocytes and mammalian cells (Kamsteeg & Deen, 2001) even though oocytes are non-polar cells. Gurley *et al.* (2006b) demonstrated apparent specificity for their data regarding ANK-mediated ^{33}PPi uptake by demonstrating that expression of the E440X truncation mutation effectively eliminated ^{33}PPi uptake.

Gurley *et al.* (2006b) also showed saturation by external pyrophosphate (PPi) of ^{33}PPi influx into ANK-expressing oocytes with an apparent K_m of ~1.3 μM, suggesting that ANK shows transporter rather than channel characteristics. This low K_m for influx suggests high affinity but low capacity for extracellular PPi. As noted by these authors, the physiological direction of PPi transport is export rather than import, however, they were unable to perform this key experiment for unspecified "technical reasons".

The data presented in Chapters 3 and 4 have shown that transcription of ANKH cRNA can occur from various template constructs, and is efficiently translated to protein which traffics to the plasma membrane of oocytes. It is now possible to address the physiological mode of action of ANKH with radiolabelled tracer studies. The isotope ^{32}PPi is readily available from PerkinElmer for studies of biosynthetic pathways and is of a high enough specific activity for flux determinations. The main advantage of ^{33}PPi is its radio-stability compared

to the short half-life of ^{32}PPi (14.7 days).

5.1.2 Aims of this section

The objectives of this section are firstly to validate the experiments of Gurley *et al.* (2006b), then to investigate PPi transport in the physiologically relevant efflux mode. Given the data that emerged, it was considered important to revisit several aspects of the original work performed by Gurley, namely in control experiments for the stability of PPi against external phosphatase activity (so potentially releasing radiolabelled Pi) and the specificity of endogenous or overexpressed transport by NaPi (SLC34) for both Pi and PPi. Since ANKH-mediated PPi transport (either in influx or efflux modes) could not be convincingly demonstrated, alternative possibilities concerning the nature of ANKH function were hypothesised and tested. Some transporters require assembly of a protein complex for function, such as CD98 (see section 4.3.1) which requires oligomeric association of light and heavy chains. In order to identify binary protein interactions, the N-terminal of ANK was used as bait using a high-quality mouse kidney cDNA library to perform a genome-wide screen using the yeast two-hybrid method.

5.2 Results

5.2.1 Demonstration of an endogenous sodium-dependent phosphate influx in oocytes, and confirmation of phosphate influx into NaPi-injected oocytes

An endogenous sodium-dependent influx of inorganic phosphate (Pi) was clearly discerned in water-injected oocytes (Figure 5.1 A), with a median value of 1.5 pmol/oocyte/hour (Figure 5.1 A and Table 5.1). This endogenous transporter is likely to represent either a *Xenopus* type II Na^+/P_i cotransporter (SLC34) which preferentially transports divalent HPO_4^{2-} or a type III Na^+/P_i cotransporter (SLC20; e.g. PiT-1) which transports monovalent $H_2PO_4^-$ (Virkki *et al.*, 2007). In oocytes injected three days earlier with flounder NaPi-IIb cRNA there is a marked increase in the sodium-dependent component of Pi influx compared to that obtained with endogenous transporters (Figure 5.1 B). Calculated fold changes of this influx with respect to endogenous (water-injected) influx was 4, 11 and 110 in three separate experiments (Table 5.1), illustrating the inherent variability in expression levels achieved between batches of oocytes from different frogs. In the absence of sodium, Pi influx was negligible (Figure 5.1 B).

Table 5.1 Influx of ^{32}P activity as sodium phosphate into *Xenopus* oocytes.

Figure 5.1 Mean influx of ^{32}P as 20 μM NaH_2PO_4 into *Xenopus* oocytes over 40 minutes.

5.2.2 Investigation of the substrate specificity of NaPi-IIb for Pi and PPi

5.2.2.1 NaPi-IIb-injected oocytes can be *cis*-inhibited by unlabelled Pi

A key issue that arises in these experiments is the possibility that PPi transport may be mediated by Pi (or other anion) transporting systems independently of ANKH, especially given the finding above that an endogenous Pi transport is present in oocytes. Additionally the presence of extracellular pyrophosphatase activity will release Pi from PPi. In order to determine whether either possibility exists, Pi or PPi were used at 1.25 mM in the extracellular medium as competitive inhibitors of ^{32}Pi uptake. The flounder NaPi-IIb used in this experiment has a K_m for Pi of ~40 μM and mouse kidney NaPi-IIa has a K_m for Pi of ~70 μM (Nalbant *et al.*, 1999), indicating that saturation and hence knock-down of ^{32}Pi transport would be expected at an extracellular [Pi] of 1.25 mM, as was observed (Figure 5.2: A *vs* C; hatched bars; p=0.0001). A similar *cis*-inhibition of the endogenous NaPi transporter is also seen (Figure 5.2: A *vs* C; black bars).

5.2.2.2 Excess unlabelled PPi can cause a degree of *cis*-inhibition of ^{32}Pi uptake

When extracellular PPi was present at 1.25 mM, ^{32}Pi influx via flounder NaPi transporters was non-significantly inhibited by 43% (p = 0.26, Figure 5.2: A *vs* B; hatched bars). Thus there may be a component of either competition of PPi with Pi for uptake via the same transporter, or extracellular hydrolysis of PPi enabling generation of sufficient non-labelled Pi to dilute out the effect of ^{32}Pi and cause competitive inhibition of NaPi-mediated ^{32}Pi uptake. Further experiments to determine the level of surface pyrophosphatase activity present in oocytes are presented in section 5.2.4, and experiments to investigate possible PPi transport via NaPi are presented in section 5.2.3.3.

5.2.2.3 Removal of divalent cations from buffer causes non-specific effects

Both Ca^{2+} and Mg^{2+} can give rise to complexes with both Pi and PPi which could reduce free substrate availability, so the effect of removing these cations from the extracellular buffer was tested. ^{32}Pi transport into NaPi-injected oocytes was reduced but non-significantly (p = 0.14) in the absence of extracellular calcium and magnesium (Figure 5.2: A *vs* D; hatched bars), but this also applies to the corresponding result with water-injected oocytes. This non-specific effect may indicate an increased membrane permeability occurring in the absence of Ca^{2+}/Mg^{2+} (Orlov *et al.*, 2005) followed by increased loss of

intracellular label in the wash phases. A significant *cis*-inhibition of Pi uptake by 1.25 mM Pi was still observed with excess unlabelled Pi (Figure 5.2: D *vs* F; hatched bars; $p < 0.001$), and there was also reduction of ^{32}Pi uptake with excess PPi but again this was not significant (D *vs* E, $p = 0.93$).

5.2.3 ANKH-mediated influx of ^{32}PPi into oocytes

5.2.3.1 Uptake of ^{32}PPi into ANKH-injected oocytes was not consistent

^{32}PPi influx was tested in ANKH cRNA-injected oocytes, three or six days post-injection so that a direct comparison could be made with data obtained by Gurley *et al.* (2006b). Using an extracellular ^{32}PPi concentration of ~10 μM, the level of ^{32}PPi uptake in ANKH-injected oocytes was 176 ± 41 fmol/oocyte/hour; Table 5.1), compared to uptake (or surface binding) of 40 ± 8 fmol/oocyte/hour in water-injected oocytes, giving a 4.4-fold increase that was statistically significant (($p = 0.002$), Table 5.1 and Table 5.3). In a similar influx experiment with a separate oocyte preparation (Figure 5.3) but using a 1 μM PPi external solution, only a 1.7-fold increase of ANKH- versus water-injected conditions was observed.

These values compare favourably with the ~180 fmol/oocyte/hour reported by Gurley for ANKH-expressing oocytes at 7 μM external PPi (Figure 1 in Gurley *et al.* (2006b)). However, this represents an increase of at least 20-fold over the rate for water-injected oocytes, since Gurley obtained values of just ~5 fmol/oocyte/hour for influx into water-injected oocytes. Corresponding values in our experiments were much higher even at equivalent substrate concentrations (Table 5.3; section 5.2.3.2).

The effect of omission of divalent cations (Ca^{2+} and Mg^{2+}) on ^{32}PPi influx was also tested (Figure 5.3). This gave similar suppression of radiolabel uptake as was seen with ^{32}P influx (section 5.2.2.3), ruling out complex formation as a reason for the low signal relative to water-injected oocytes.

5.2.3.2 Unexpectedly large variability in flux occurred in the water-injected oocytes

In subsequent experiments using cRNA prepared from the ANKH-pcDNA3.1 construct, a significant and reproducible increment in ^{32}PPi uptake over water-injected oocytes was not observed (Table 5.3). The level of ^{32}PPi uptake in water injected oocytes was in the range 8 - 4530 fmol/oocyte/hour (over a 0.5 - 109 μM external ^{32}PPi range), yielding a fold change of ANKH cRNA-injected over water-injected oocytes in the present data of less than two

(except for the single measurement at 4.4-fold). Such small fold changes are likely to be too small to provide reliable evidence of an effect.

Figure 5.4 shows an experiment where the difficulties associated with such a low fold change of increased flux due to ANKH are evident. Here the ability of unlabelled PPi or Pi to *cis*-inhibit ^{32}PPi uptake was tested. The increment in ^{32}PPi uptake was only 1.6-fold compared to water-injected oocytes, and whereas 0.25 mM PPi reduced ^{32}PPi uptake to similar values compared to water-injected, 0.25 mM Pi also reduced ^{32}PPi uptake to similar values. The variability is evident in the values for water-injected oocytes.

5.2.3.3 Substrate specificity of NaPi and ANKH for both PPi and Pi

Given the ability of unlabelled PPi to suppress a component of ^{32}Pi uptake via the flounder NaPi-IIb and the endogenous oocyte NaPi transporter (section 5.2.2.2), the ability of 32PPi to act as a substrate in NaPi-IIb-injected oocytes was directly tested (Table 5.1). The level of ^{32}PPi uptake (from 10 μM external ^{32}PPi) into NaPi-IIb-injected oocytes was 615 ± 83 fmol/oocyte/hour, which was significantly enhanced compared to water-injected controls ($p<0.001$); indeed it was also above the level of 32PPi uptake into ANKH-injected oocytes ($p < 0.001$; Table 5.1, see also Table 5.3). With ^{32}PPi at 100 μM (i.e. much higher than the K_m of PPi for ANKH reported by (Gurley *et al.*, 2006b)), the fold change of ANKH- over water-injected was 1.4 compared to 2.7 for NaPi-IIb:water. It may be concluded that PPi is a substrate for NaPi-IIb and/or that ^{32}P is created from ^{32}PPi during the experiment (see section 5.2.4).

	Activity of tracer available (Bq/μl)	Final tracer conc (μM)	**NaPi-injected**	SEM	n	**ANKH-pcDNA3.1-injected**	SEM	n	**Water-injected**	SEM	n
^{32}PPi influx	3140	10	**615**	83	8	**176**	41	10	**40**	8	10
(fmol/oocyte /h) n=2	3924	109	**12166**	612	14	**6513**	597	14	**4530**	275	14
^{32}Pi influx (fmol/oocyte /h)	270	21	**112484**	16002	8	**5831**	2399	6	**1022**	162	10

Table 5.2 Direct comparison of influx of ^{32}PPi and ^{32}P into variously cRNA-injected oocytes. Oocytes were injected three days earlier with either ANKH-pcDNA3.1 cRNA, flounder NaPi-IIb or water, and influx experiments were performed using ^{32}PPi or ^{32}P as substrate. Each horizontal line represents a set of experiments performed simultaneously. Statistical analysis was with Tukey's test enabling pairwise comparisons (results in text).

Figure 5.2 Effect of varying external conditions on the influx of labelled Pi into NaPi-IIb and water-injected oocytes.

Figure 5.3 Influx of labelled PPi into ANKH-pcDNA3.1 injected oocytes.

Table 5.3 Influx of ^{32}P activity as sodium pyrophosphate into *Xenopus* oocytes

Figure 5.4 Influx of labelled PPi into ANKH-pcDNA3.1-injected oocytes under conditions of excess unlabelled substrate.

5.2.3.4 Strategies to augment detection of PPi flux into ANK(H)-injected oocytes

Table 5.3 summarises several strategies that were attempted to improve the functional expression of ANK(H). Of greatest concern was the stability and integrity of the cRNA that was injected for translation in oocytes. All constructs were fully sequenced (Figure 2.2 to Figure 2.5) with no coding sequence errors. Data are shown for the various constructs used including mouse ANK-GFP (N-terminal), ANKH-GFP (N-terminal) and ANKH-FLAG (N-terminal). Variation of constructs, oocyte incubation over 2-6 days, influx time period, concentration and activity of the tracer (Table 5.3) were all attempted, but none allowed consistent improvement of the fold change for ^{32}P influx with construct- over water-injected. It should be noted that the amounts of cRNA that were injected allowed robust detection of ANK protein expression and plasma membrane location (see Chapter 4). The median fold-increase above water for all 22 experiments was 1.24, but in the majority of these experiments this increase was not significant.

5.2.4 Hydrolysis of PPi

Surface hydrolysis of PPi was determined by incubation of oocytes in a PPi-containing standard influx buffer solution under standard conditions. PPi concentration was determined directly used a novel fluorescent chemical sensor for PPi (see section 2.9). A typical standard curve for PPi concentration in the buffer used for oocytes is shown in Figure 5.5. The linear part of the standard curve confirmed that the useful range of the sensor was 0.3 to ~10 μM PPi. Furthermore, addition of an excess of PPase showed that the sensor was sensitive for PPi over Pi.

Figure 5.6 shows that in the absence of oocytes PPi concentration is well maintained in the oocyte influx buffer. In the presence of oocytes there is a time-dependent decrease in PPi, with a loss over 60 minutes of 18% of initial PPi. The *y*-intercepts confirm that the initial PPi concentrations were the same (3.6 μM). Using the slope of the line, the amount of PPi in the 70 μl aliquot lost due to oocytes at 60 minutes can be calculated, and adjusted for the doubling of molar amount of Pi formed (PPi→2 Pi), giving a rate of Pi formation of ~13 pmol/oocyte/h. This is within the range of many of the results obtained for PPi influx (Table 5.3). These data provide direct evidence that PPi may be hydrolysed to form Pi in the presence of oocytes, and show that substrate hydrolysis followed by alternative transport is a very important issue in influx experiments.

Figure 5.5 Standard curves for PPi assays using a chemical PPi sensor.

Figure 5.6 Determination of pyrophosphatase activity on the surface of *Xenopus* oocytes.

5.2.5 ANKH-mediated efflux of ^{32}PPi from oocytes

5.2.5.1 Control experiments established the validity of substrate-injected oocytes

In order to measure the efflux of ^{32}PPi from ANKH- or water-injected oocytes it was first necessary to establish a protocol that allowed injection, sealing and subsequent maintenance of oocyte integrity during the efflux measurements. The inert sugar mannitol was used as a non-transported marker of the intracellular space (Figure 5.7). [^{14}C]-mannitol was injected into oocytes, followed by washing and transfer into unlabelled oocyte incubation buffer using the efflux protocol (section 2.8.5.2). Loss of intracellular [^{14}C]-mannitol activity was minimal (1-2%, Figure 5.7 A) when expressed as a proportion of the total activity (extracellular medium plus oocyte activity). Post-injection washing of oocytes does not substantially alter extracellular activity suggesting that surface activity and leakage after injection are minimal. In addition, there was no change in detected extracellular activity up to 120 minutes of incubation. The small but constant difference between calculated and measured mannitol in the system supports expression of efflux as a percentage of the total, rather than as an absolute number (Figure 5.7 B).

The fluorescent organic anion Lucifer Yellow is actively secreted by isolated killifish proximal tubules (Masereeuw *et al.*, 1999). Water-injected, ANKH-injected and uninjected oocytes re-injected with Lucifer Yellow resulted in the loss of ~70% of the injected amount at one hour (Figure 5.8). This shows that an endogenous "active" efflux mechanism for this substrate exists in *Xenopus* oocytes and that the efflux protocol is capable of detecting it.

5.2.5.2 Efflux of ^{32}PPi from ANK-injected oocytes under varying conditions

A significant increase in efflux of labelled PPi in ANK-injected over water-injected oocytes was detected in only five out of 19 experiments with a maximum fold change of 5.3. Since mannitol leakage of up to 2.5% was seen, % ^{32}PPi efflux values of greater than 2.5% would give additional experimental confidence that an ANK(H)-mediated efflux was occurring. Applying this, six of the 19 experiments are positive. Table 5.4 summarises the use of differing vectors, post-injection incubation periods, times over which efflux was measured, and the concentration and activity of intracellular radiolabelled tracer. There is no apparent correlation with any of these factors. Attempts at varying the injected cRNA concentration over the range 1-8 μg/μl resulted in premature oocyte death by two days' incubation for cRNA concentrations greater than 3 μg/μl.

Figure 5.7 Estimation of ^{14}C-mannitol leakage after micro-injection into *Xenopus* oocytes

(A) Post-injection extracellular detectability of ^{14}C-mannitol. Previously uninjected oocytes at 4 days after harvesting were injected with 50.6 nl of ^{14}C-mannitol and incubated individually for varying time periods in 100 µl of oocyte buffer. Oocytes were either washed twice in fresh buffer between injection and start of incubation (red), or not washed (blue). After the required incubation time, 80 µl of buffer was drawn off for counting of ^{14}C activity. Oocytes were resuspended in fresh buffer, then washed three times in ice-cold buffer before counting ^{14}C activity. Results are expressed as the percentage of total activity (oocyte + buffer) left remaining in the buffer after the incubation period. Error bars represent SEM for n=6 oocytes.

(B) Comparison of measured versus calculated total ^{14}C activity in system. The mean measured total activity in each individual oocyte/buffer system at end of each incubation was calculated as the sum of the activity in oocyte and in the buffer after the incubation period, for both washed (red) and unwashed (blue) oocytes. The calculated total amount of substrate injected per 50.6 nl aliquot is shown in green. Error bars represent SEM for n=6 oocytes.

(Fig 5.7 goes here)

Figure 5.8 Active efflux from *Xenopus* oocytes re-injected with Lucifer Yellow

(A) Standard curve of fluorescence due to Lucifer Yellow in oocyte buffer solution. Lucifer Yellow (dilithium salt) was diluted into oocyte buffer solution, and 1:1 serial dilutions were made in this buffer, to a total volume of 100 µl each on a 96-well plate. The mean values from three separate dilution series were used. Fluorescence was measured at 520 nm, after excitation at 425 nm. The trend line shows a linear fit when fluorescence is plotted as a function of the Lucifer Yellow dilution (log scale shown here), showing that fluorescence over this range of Lucifer Yellow dilutions in oocyte buffer is proportional to the concentration.

(B) Time course of Lucifer Yellow efflux/leakage from *Xenopus* oocytes. Groups of oocytes, injected two days earlier with either water (light blue) or ANKH-pcDNA3.1 cRNA (red), or not injected (dark blue) were re-injected with 50 nl of Lucifer Yellow diluted in water. Each oocyte was immediately incubated in 100 µl of oocyte buffer for the required length of time, with a further oocyte in 100 µl buffer for 2 h. After incubation, 50 µl of buffer was removed to a separate 96 well plate and fluorescence at λ = 520 nm (excitation at 425 nm) was measured. Mean values from two oocytes per time-point were used. Data are expressed as fluorescence in the buffer at the end of the incubation period as a percentage of the total fluorescence of the single oocyte system at 2 h incubation.

Fig 5.8 here

Table 5.4 Efflux of ^{32}P activity as sodium pyrophosphate from *Xenopus* oocytes.

5.2.5.3 Further investigation of the lack of observed ^{32}PPi efflux

Intracellular PPi hydrolysis may partially account for the lack of observed efflux. However, there was no correlation between the estimated intra-oocyte PPi concentration attained and the resulting flux (Table 5.4), suggesting that PPi hydrolysis is not the sole reason. Attempts to measure PPi stability within the cytosol using the fluorescent PPi assay (section 5.2.4) were unsuccessful due to interference of oocyte homogenate with the assay (not shown).

Facilitated transport displays an acceleration of unidirectional (*cis* to *trans*) flux when the *trans*-concentration of unlabelled substrate accelerates re-orientation of the carrier, this phenomenon being known as "*trans*-stimulation". Its potential effect on detection of mediated ^{32}PPi exit was tested by raising the extracellular concentration of unlabelled PPi to 1 mM (Table 5.5). A significant increase in % efflux over water-injected oocytes was observed in only two out of five experiments, with only one of these giving rise to an efflux above 2.5%, with a maximum fold change of 3.4 (Table 5.5).

These data show that either "technical reasons", such as intra-oocyte PPi hydrolysis, prevent detection of ANKH-mediated efflux of PPi, or that the results are consistent with PPi not being the substrate for ANKH.

5.2.5.4 ATP as a substrate for ANKH

Rather than direct transport of PPi, it is possible that ATP may act as the original substrate. ANKH might then be an "active" carrier, allowing ATP binding and subsequent hydrolysis to release PPi followed by export of PPi to the external medium. Therefore efflux experiments using [^{32}P]ATP labelled at either α or γ-phosphate positions were undertaken. Since PPi release would be expected to occur after hydrolysis between the α and β-phosphates of ATP (forming AMP + PPi, (Heinonen, 2001)), the [α-^{32}P]ATP acted as a negative control. Sufficient [^{32}P]ATP was injected to give an estimated intracellular concentration over the range 9-167 μM, ensuring that a significant proportion of the whole intracellular ATP pool (normally ~1 mM) would be labelled. A significant increase in the % of ^{32}P efflux that also exceeded the 2.5% criterion (described in section 5.2.5.2) was recorded in only one of nine experiments (Table 5.6). Flounder NaPi-IIb is included as another negative control. On balance, these results do not provide compelling evidence that ANKH uses ATP directly in order to generate PPi export.

Table 5.5 Efflux of ^{32}P activity as sodium pyrophosphate from *Xenopus* oocytes under trans-stimulation conditions.

Table 5.6 Efflux of ^{32}P activity as ATPγ/α from *Xenopus* oocytes.

5.2.5.5 Possible environmental influences on ^{32}PPi efflux via ANKH

The pH of urine can alter markedly even over a few hours, but calcium phosphate stones form only at high pH (Sayer *et al.*, 2010), implying a potential role for increased PPi export under these conditions. Proton dependence of ANKH in two vectors was investigated by altering pH of the buffer (Figure 5.9). Statistical analysis with Tukey's test showed a difference only between pH 7.0 and 8.0 ($p=0.02$) with efflux from ANKH-pcDNA3.1-injected oocytes being significantly increased compared to water controls ($p<0.001$).

The effect of acute stimulation of ANKH activity was investigated using the cAMP activator forskolin and the intracellular free calcium augmenter thapsigargin. No increase in ^{32}PPi efflux was observed with either forskolin ($p=0.61$) or thapsigargin ($p=0.49$) above the non-stimulated condition (Figure 5.10).

5.2.5.6 Possible requirement for a partner protein

The transport function of some membrane proteins requires the formation of dimers or oligomers at the plasma membrane (e.g.(Rossier *et al.*, 1999)), without which a protein subunit is non-functional. To investigate the effect on efflux of potential partner proteins, ANKH-pcDNA3.1 cRNA was co-injected with total RNA extracted from whole human kidney (Table 5.7 and Figure 5.11). All pairwise comparisons between all groups in all three experiments were non-significant, except for one significant comparison as shown in Figure 5.11 which occurred at much higher tracer activity (Table 5.7; see section 2.8.6.3 for an explanation of the relevance of activity). Although suggestive, these data can only be regarded as preliminary at present.

Figure 5.9 Effect of pH on efflux of ^{32}P as sodium pyrophosphate from *Xenopus* oocytes.

Figure 5.10 Effect of acute stimulation of ANKH activity on efflux of ^{32}P as sodium pyrophosphate from *Xenopus* oocytes.

Table 5.7 and Figure 5.11 Efflux of ^{32}P activity as sodium pyrophosphate from *Xenopus* oocytes co-injected with ANKH-pcDNA3.1 cRNA and human kidney total RNA.

5.2.6 Yeast two-hybrid screen

In order to screen for potential interacting partner proteins for ANKH, a commercial yeast two-hybrid screen was conducted using an N-terminal ANK fragment (residues 24-85) of mouse ANK as bait against a mouse kidney library (section 2.10.2; Figure 2.9). The output of the yeast two-hybrid screen is a list of positively interacting cDNA clones (prey fragments) many of which are fragments of actual mouse genes (Table 5.8). The interacting domain is deduced after aligning the fragments, and is defined as the minimum common domain shared by all the prey fragments corresponding to the same protein (Figure 5.12). However, the extent of the true interaction may actually be only about 20 amino acids.

Overall, 33% of all interactions were deemed "high" or "very high" confidence as scored by Hybrigenics' bioinformatics software; this corresponded to six genes. The remainder were all of either "good" or "moderate" confidence, and corresponded to 12 genes. No post-scored interactions were deemed to be low confidence or due to known artefacts. Due to the heterogeneity of the mouse kidney cDNA library, many fragments may correspond to the same gene, which serves to increase the confidence in the result, provided that the interacting domain is the same in all the fragments, e.g. as with the Slc27a2 result (Figure 5.12). However two putative interacting domains were identified within the 26 positive fragments for Aldh6a1 (aldehyde dehydrogenase; Figure 5.13). Two such domains very close together but not overlapping on the same protein suggests that this may be a false positive. In contrast, clones positive for Eef1a1 showed tight alignment.

Table 5.8 Positive interacting clones obtained from a yeast two-hybrid screen of an N-terminal ANK fragment.

```
                77
       1.  PHKPFLLFRD ETLTYAQVDR RSNQVARALH DQLGLRQGDC VALFMGNEPA
       2.  PHKPFLLFRD ETLTYAQVDR RSNQVARALH DQLGLRQGDC VALFMGNEPA
       3.  ..KPFLLFRD ETLTYAQVDR RSNQVARALH DQLGLRQGDC VALFMGNEPA
       4.  ......LFRD ETLTYAQVDR RSNQVARALH DQLGLRQGDC VALFMGNEPA
       5.  ......LFRD ETLTYAQVDR RSNQVARALH DQLGLRQGDC VALFMGNEPA
       6.  .......... ETLTYAQVDR RSNQVARALH DQLGLRQGDC VALFMGNEPA
Consensus  ......lfrd ETLTYAQVDR RSNQVARALH DQLGLRQGDC VALFMGNEPA

           117
       1.  YVWIWLGLLK LGCPMACLNY NIRAKSLLHC FQCCGAKVLL ASPDLQEAVE
       2.  YVWIWLGLLK LGCPMACLNY NIRAKSLLHC FQCCGAKVLL ASPDLQEAVE
       3.  YVWIWLGLLK LGCPMACLNY NIRAKSLLHC FQCCGAKVLL ASPDLQEAVE
       4.  YVWIWLGLLK LGCPMACLNY NIRAKSLLHC FQCCGAKVLL ASPDLQEAVE
       5.  YVWIWLGLLK LGCPMACLNY NIRAKSLLHC FQCCGAKVLL ASPDLQEAVE
       6.  YVWIWLGLLK LGCPMACLNY NIRAKSLLHC FQCCGAKVLL ASPDLQEAVE
Consensus  YVWIWLGLLK LGCPMACLNY NIRAKSLLHC FQCCGAKVLL ASPDLQEAVE

           167
       1.  EVLPTLKKDA VSVFYVSRTS NTNGVDTILD KVDGVSAEPT PESWRSEVTF
       2.  EVLPTLKKDA VSVFYVSRTS NTNGVDTILD KVDGVSAEPT PESWRSEVTF
       3.  EVLPTLKKDA VSVFYVSRTS NTNGVDTILD KVDGVSAEPT PESWRSEVTF
       4.  EVLPTLKKDA VSVFYVSRTS NTNGVDTILD KVDGVSAEPT PESWRSEVTF
       5.  EVLPTLKKDA VSVFYVSRTS NTNGVDTILD KVDGVSAEPT PESWRSEVTF
       6.  EVLPTLKKDA VSVFYVSRTS NTNGVDTILD KVDGVSAEPT PESWRSEVTF
Consensus  EVLPTLKKDA VSVFYVSRTS NTNGVDTILD KVDGVSAEPT PESWRSEVTF

           217
       1.  TTPAVYIYTS GG......
       2.  TTPAVYIYTS GTTGLPK.
       3.  TTPAVYIYTS GTTGLPK.
       4.  TTPAVYIYTS GTTGLPKA
       5.  TTPAVYIYTS GTTGLPKA
       6.  TTPAVYIYTS ........
Consensus  TTPAVYIYTS gttglpk.
```

```
ETLTYAQVDRRSNQVARALHDQLGLRQGDCVALFMGNEPAYVWIWLGLLKLGCPMACLNYNIRAKSLLHCFQCCGAKVLLASPDLQEAVEEV
LPTLKKDAVSVFYVSRTSNTNGVDTILDKVDGVSAEPTPESWRSEVTFTTPAVYIYTS
```

Figure 5.12 Alignment of amino acid sequences for Slc27a2 clone fragments that interacted with N-terminal ANK bait in a yeast two-hybrid screen. Nucleotide sequences for six individual Slc27a2 cDNA prey hits that interacted with ANK were obtained from the raw data (Hybrigenics). These were translated to amino acid sequences (SHOWORF), which were then aligned (Multalin). The conserved domain (green) is likely to contain the interaction domain. The numbers indicate the residues from the start of the coding sequence. The transmembrane domains (calculated from SMART) are at positions 5-27 and 266-288, both of which are outside the interaction domain, although TMPRED suggests a possible further transmembrane domain at 118-134.

Figure 5.13 Mapping of consensus sequences of interacting Aldh6a1 clones to the coding sequence. Nucleotide sequences for the 26 individual Aldh6a1 cDNA prey clones that interacted with C-terminal ANK bait in a yeast two-hybrid screen were obtained from the raw data (Hybrigenics). These were translated to amino acid sequences (SHOWORF), which were then aligned (Multalin). The sequences were found to segregate into two categories; shown as consensus sequences *x* and *y*, with mapping to the Aldh6a1 coding sequence. 21 clones mapped to one section (consensus sequence *x*; purple). The other five clones mapped to a separate section (consensus sequence *y*; green).

```
           1                                                  50
  Aldh6a1  .......... .......... .......... .......... ..........
         x  QVSSKVNATW YPASSFSSSS VPTVKLFIDG KFVESKSDKW IDIHNPATNE
         y  .......... .......... .......... .......... ..........
Consensus  .......... .......... .......... .......... ..........

           51                                                 100
  Aldh6a1  .......... ..MDAAVESC KRAFPAWADT SILSRQQVLL RYQQLIKENL
         x  VVGRVPQSTK AEMDAAVESC KRAFPAWADT SILSRQQVLL RYQQLIKENL
         y  .......... .......... .......... .......... ..........
Consensus  .......... ..mdaavesc krafpawadt silsrqqvll ryqqlikenl

           101                                                150
  Aldh6a1  KEIARLITLE QGKTLADAEG DVFRGLQVVE HACSVTSLML GETMPSITKD
         x  KEIARLITLE QGKTLADAEG DVFRGLQVVE HACSVTSLML GETMPSITKD
         y  .......... .......... .......... .......... ..........
Consensus  keiarlitle qgktladaeg dvfrglqvve hacsvtslml getmpsitkd

           151                                                200
  Aldh6a1  MDLYSYRLPL GVCAGIAPFN FPAMIPLWMF PMAMVCGNTF LMKPSERVPG
         x  MDLYSYRLPL GVCAGIAPFN FPAMIPLWMF PMAMVCGNTF LMKPSERVPG
         y  .......... .......... .......... .......... ..........
Consensus  mdlysyrlpl gvcagiapfn fpamiplwmf pmamvcgntf lmkpservpg

           201                                                250
  Aldh6a1  ATMLLAKLLQ DSGAPDGTLN IIHGQHDAVN FICDHPDIKA ISFVGSNQAG
         x  ATMLLAKLLQ DSGAPDGTLN IIHGQHDAVN FICDHPDIKA ISFVGSNQAG
         y  .......... .......... .......... .......... ..........
Consensus  atmllakllq dsgapdgtln iihgqhdavn ficdhpdika isfvgsnqag

           251                                                300
  Aldh6a1  EYIFERGSRN GKRVQANMGA KNHGVVMPDA NKENTLNQLV GAAFGAAGQR
         x  EYIFERGSRN GKRVQANM.. .......... .......... ..........
         y  .......... .......... .......... .......... ..........
Consensus  eyifergsrn gkrvqanm.. .......... .......... ..........

           301                                                350
  Aldh6a1  CMALSTAILV GEAKKWLPEL VDRAKNLRVN AGDQPGADLG PLITPQAKER
         x  .......... .......... .......... .......... ..........
         y  .......... .......... .......... .......... .LITPQAKER
Consensus  .......... .......... .......... .......... .litpqaker

           351                                                400
  Aldh6a1  VCNLIDSGTK EGASILLDGR RIKVKGYENG NFVGPTIISN VKPSMTCYKE
         x  .......... .......... .......... .......... ..........
         y  VCNLIDSGTK EGASILLDGR RIKVKGYENG NFVGPTIISN VKPSMTCYKE
Consensus  vcnlidsgtk egasilldgr rikvkgyeng nfvgptiisn vkpsmtcyke

           401                                                450
  Aldh6a1  EIFGPVLVVL ETETLDEAIK IVNDNPYGNG TAIFTTNGAT ARKYAHMVDV
         x  .......... .......... .......... .......... ..........
         y  EIFGPVLVVL ETETLDEAIK IVNDNPYGNG TAIFTTNGAT ARKYAHMVDV
Consensus  eifgpvlvvl etetldeaik ivndnpygng taifttngat arkyahmvdv

           451                                                500
  Aldh6a1  GQVGVNVPIP VPLPMFSFTG SRSSFRGDTN FYGKQGIQFY TQLKTITSQW
         x  .......... .......... .......... .......... ..........
         y  GQVGVNVPIP VPL....... .......... .......... ..........
Consensus  gqvgvnvpip vpl....... .......... .......... ..........

           501              519
  Aldh6a1  KEEDATLSSP AVVMPTMGR
         x  .......... .........
         y  .......... .........
Consensus  .......... .........
```

5.3 Discussion

5.3.1 Meaningful PPi influx across membranes is not proven

The mechanism of PPi transport is unknown. PPi is a polar molecule and would be unable to cross a lipid bilayer at a significant rate (Visser *et al.*, 2005). Gurley *et al.* (2006b) quantified ANK functional activity by influx since efflux determinations were limited by "technical considerations". Since the presumed role of ANK is the export of PPi to the extracellular medium (Ho *et al.*, 2000) and since the majority of PPi production is intracellular (Heinonen, 2001), it is unclear what physiological role influx of PPi would serve. Even if influx occurred, PPi ($P_2O_7^{4-}$) would move against its electrochemical gradient (resting intracellular potential in oocytes is -40 to -80 mV (Dascal *et al.*, 1984)).

The present data replicate those of Gurley *et al.* (2006b) in the overall magnitude of PPi influx, but differ in both the consistency and nature of PPi influx in water-injected control oocytes. One unusual feature of the data of Gurley is that the high variability in oocyte fluxes caused the authors to omit both the highest and lowest influxes in replicate data sets. Although obvious contamination or bursting of oocytes would cause exclusion from data analysis, the systematic removal of such data suggests an actual variability not accounted for by the indicated variances. Since we have demonstrated (for the first time) membrane expression of ANKH due to translation from injected cRNAs in various vectors, our data therefore do not support the idea that meaningful PPi influx is mediated by ANKH.

5.3.2 Endogenous phosphate transporters in oocytes

Two families of phosphate transporters are known: type II Na^+/P_i cotransporters (SLC34) which preferentially transport divalent HPO_4^{2-} and type III Na^+/P_i cotransporters (SLC20; e.g. PiT-1) which transport monovalent $H_2PO_4^-$ (Virkki *et al.*, 2007). Only the type II transporters have been shown to exist endogenously in oocytes (Weber, 1999), and transport has been previously well characterised (Bröer *et al.*, 1998). We confirmed that endogenous sodium-dependent phosphate flux exists, using flounder NaPi-IIb-injected oocytes as a positive control.

Flounder NaPi-IIb has a K_m for Pi of 40 μM and mouse kidney NaPi-IIa has a K_m for Pi of 70±30 μM (Nalbant *et al.*, 1999). We showed that *cis*-inhibition of ^{32}Pi transport occurs at an extracellular non-labelled Pi concentration much higher than the K_m, consistent with saturation of ^{32}Pi transport. We found that excess extracellular PPi tended to inhibit ^{32}Pi influx (by 43%). Possible explanations that were tested further include extracellular

hydrolysis of PPi giving rise to generation of non-labelled Pi and subsequent competition, and PPi itself being a substrate for NaPi.

The magnitude of ^{32}Pi influx was reduced (but not always significantly) where divalent cations were absent including endogenous Pi transport. The NaPi transporter is not known to require divalent cations, but the absence of divalent cations can increase membrane permeability (Orlov *et al.*, 2005), allowing increased loss of intracellular label in the wash phases. Alternatively, phosphatase activity is much reduced under Mg-free conditions since many triphosphatases use Mg-ATP as substrate (see section 5.3.4).

5.3.3 Is the recorded influx due to PPi or Pi?

Apparent ^{32}PPi influx into ANKH-injected oocytes was even smaller than that using ^{32}PPi into NaPi-injected oocytes. Again a possible explanation is that extracellular hydrolysis to labelled phosphate allowed subsequent influx of Pi via NaPi. Tracer influx of ^{32}Pi via ANKH was greater than endogenous (water-injected) ^{32}Pi transport, and of a similar magnitude to tracer influx of ^{32}PPi via ANKH, suggesting that ANKH may transport both Pi and PPi. Recently, (Wang *et al.*, 2009) suggested that ANK may interact directly with the Na-Pi transporter PiT-1, supporting the idea of a physiological relationship between Pi and PPi transport. The strategy of blocking endogenous Pi transport by using NaPi inhibitors such as foscarnet (Wang *et al.*, 2005) and/or phosphatases (e.g. fluoride (Kocinsky *et al.*, 2007) or levamisole (Lomashvili *et al.*, 2008)) was rejected as the effect on ANKH function is unknown.

5.3.4 PPi in buffer is ionised and available for measurement using a sensitive bioassay

An enzymatic assay for PPi (Sigma reagent, section 2.9.1) was unable to accurately detect PPi at concentrations lower than 100 μM. The fluorescent sensor system developed by (Dong Hoon *et al.*, 2004) uses two oxygen atoms on the PPi ion ($P_2O_7^{4-}$) to form a bridge between two Zn^{2+} ions in the sensor molecule. It shows high selectivity for PPi over Pi and ATP. Our results confirm that the sensor is useful over a suitably low PPi concentration range, and that PPi is removed from solution by PPase except when divalent cations are absent and PPi concentration is high. PPase enzymes require a divalent metal ion, usually Mg, for function (Miro *et al.*, 1989). Indeed Fleisch (Russell *et al.*, 1971) detected slow hydrolysis of PPi in blood over >20 hrs, which was almost abolished by adding the divalent cation chelator EDTA. The K_m of PPase ranges from 0.5 μM (Miro *et al.*, 1989) to 18.8 μM

(ocean Thermococcus (Lee *et al.*, 2009)) showing relatively high affinity for PPi.

Surprisingly, the presence or absence of divalent cations in the incubation buffers made no difference to measured PPi detection over the linear part of the standard curve. Since the sensor recognises free PPi ions, our results suggest that PPi must be biologically available in ionised form over the detectable range at pH 7.4, regardless of the formation of insoluble complexes with divalents or dissociation of PPi. No chelator was used so low divalent cation concentrations (e.g. ~1 μM) would have been present even in the Ca/Mg-free buffer. Pyrophosphoric acid is a polybasic acid, therefore PPi solutions are always partially dissociated depending on the pH of the solution and the dissociation constants (McGilvery & Crowther, 1954). The third acid dissociation constant (pK_3) is 7 (p. 424 in (Cotton, 1999)), hence PPi is mostly ionised at physiological pH and unlikely to spontaneously hydrolyse over the experimental time period. These facts support the conclusion that PPi exists in the buffer in mostly ionised form, with good bioavailability to the sensor over the range 1-10 μM even in the presence of divalent cations.

5.3.5 PPase activity is present on the surface of oocytes

The reduction in PPi concentration over time strongly suggests surface PPase activity on oocytes. This is sizeable compared to the small measured flux of ^{32}PPi and means that the interpretation that PPi influx occurs solely via ANKH is implausible. It is also consistent with the results showing apparently increased influx using ^{32}PPi in NaPi-injected oocytes compared to ANKH- or water-injected oocytes. The oocyte follicular layer has high Ca^{2+}/Mg^{2+}-dependent ATPase activity (Ziganshin *et al.*, 1995) but since all oocytes used were defolliculated, the molecular nature of the extracellular pyrophosphatase in oocytes remains unknown.

Our results strongly conflict with those of Gurley *et al.* (2006b), who used thin-layer chromatography to claim that "no detectable hydrolysis of PPi to Pi occurred in transport buffer incubated with oocytes during the time periods used for PPi assays", but provided no data in their paper. Numerous attempts to examine intracellular PPase activity using centrifuged oocyte (cytosolic) homogenates were unsuccessful due to turbidity affecting the fluorescence of the sensor.

5.3.6 Significant efflux from ANKH-injected oocytes was not detected under a wide variety of experimental conditions

Using control experiments with mannitol and Lucifer yellow, we defined a protocol to measure efflux of possible substrates from ANKH-injected oocytes. Gurley *et al.* (2006b) failed in a similar attempt due to "technical limitations" despite acknowledging that the predicted direction of transport via ANK (Ho *et al.*, 2000) required measurement of efflux rather than influx. They generalised the results of influx on the basis of likely bidirectionality of transport, although there is no evidence to support this and indeed it conflicts with the presumed physiological mode of transport and the prevailing electrochemical gradient.

Our results show that a consistently significant efflux ratio compared to water-injected oocytes was not detectable despite testing different combinations of vectors, substrates, substrate activities and concentrations, incubation times, buffer pH, two possible acute regulators and two different experimental techniques. As already demonstrated in Chapter 4, cRNA transcribed from various constructs has been shown to be generate ANKH protein which is expressed in the oocyte membrane. Therefore either ANK does not transport PPi, or appropriate conditions for efflux have not yet been fulfilled; notably any intracellular hydrolysis of PPi may rapidly deplete the substrate at the plasma membrane.

This conclusion was supported by considering various technical issues. Enough free PPi must be available for export. We used intra-oocyte ^{32}PPi concentrations of between 1 and 100 μM. At very high concentrations, non-specific transport effects may be observed, but the availability of PPi would still be maintained even if PPase activities are saturated (their K_ms are likely to be low; see section 5.3.4), yet significant export of hydrolysed or non-hydrolysed radiolabel was often not observed. Leakage via membrane damage from re-injection was found not to be significant using the technique of retention of labelled mannitol (section 5.2.5.1). Finally, the possibility that ATP may directly interact with ANKH, with membrane protein-associated binding and hydrolysis of ATP releasing PPi for transport to the external medium was considered. Efflux experiments using injections of both α and γ-labelled [^{32}P]ATP failed to show a robust increase in radiolabel of ANKH-injected oocytes compared to water-injected oocytes.

5.3.7 Yeast two-hybrid screen

Domain analysis of the mouse ANK protein (Ensembl reference ENSMUSP00000022875) using SMART[14] reveals eight transmembrane segments, giving N- and C-terminals that are intracellular (Figure 2.9), but otherwise there are no recognised domains. Therefore ANK is unusual in consisting of a single, unique domain. A yeast two-hybrid screen using an N-terminal ANK bait with a mouse cDNA kidney library was used to identify possible interacting proteins. Of the several possible interacting proteins identified, notably no phosphate transporters are identified despite their relatively high abundance within the kidney and possible co-operative behaviour between ANK and phosphate transporters (Wang *et al.*, 2009). The N-terminal bait peptide used would have incorporated the site of the known M48T mutation that interrupts the ANKH interaction with PiT-1 (Wang *et al.*, 2009).

The possible biological significance of each of the interactions identified is now considered.

5.3.7.1 Aldh6a1

Aldh6a1 is the only CoA-dependent aldehyde dehydrogenase (Kedishvili *et al.*, 2000); it localises to the mitochondrial matrix where it catalyses acetyl CoA production from malonate. ANK localises to the mitochondria in the mouse collecting duct cell-line mIMCD-3 (Carr *et al.*, 2007), but is not present in mitochondrial DNA. It is conceivable that ANK therefore requires a chaperone such as Aldh6a1 to allow mitochondrial localisation. On the other hand, the present screen revealed apparently two consensus interacting domains of Aldh6a1, which map to different amino acid sequences (Figure 5.13). Although these two domains are very close together, they do not overlap on the same protein sequence. Notably, sequence 'x' (Figure 5.13) maps partially to an area before the start of the Aldh6a1 coding sequence (5' UTR). These factors may suggest a spurious interaction which has caused a false positive. In addition, reactions involving Aldh6a1 do not generate PPi (Kedishvili *et al.*, 1992).

5.3.7.2 Eef1a1

The ubiquitously expressed and highly conserved protein Eef1a1 (eukaryotic translation elongation factor 1 alpha 1) allows the delivery of aminoacyl tRNAs to ribosomes in the process of protein translation and elongation. PPi is a product of the overall reaction catalysed by aminoacyl-tRNA synthetase (amino acid + ATP + tRNA→ aminoacyl-tRNA +

[14] http://smart.embl-heidelberg.de/

AMP + PPi). As components of this process, the cellular localisation of aminoacyl-tRNA synthetase, elongation factors and ribosomes is likely to be co-ordinated. Oocytes contain many ribosomes, and intra-oocyte ANKH staining was noted in confocal sections where ANKH protein was expressed (Figure 4.6 and Figure 4.7). Removal of PPi is necessary to maintain the equilibrium for aminoacyl-tRNA formation (Heinonen, 2001) in membrane-bound ribosomal complexes. Enzymatic hydrolysis of PPi may account for its removal, but this may also occur by PPi transport to the endoplasmic reticulum lumen.

However it should be noted that Eef1a1 has many other important functions relating to the cytoskeleton (Mansilla *et al.*, 2008), such as directing mRNA translation (Condeelis, 1995), and regulation of transcript selection (Zhang *et al.*, 2009). In fact Eef1a1 is the second most abundant protein after actin in most cells (Condeelis, 1995) and the ubiquitous nature of this protein means that this putative interaction may represent a false positive in yeast two-hybrid experiments. Elongation factors are a known cause of false positives[15].

5.3.7.3 Physiological relevance of Slc27a2 as an interacting protein

Slc27a2 (also known as FATP2) which has 2-3 predicted transmembrane domains (SMART[14]/TMpred[16]) mediates transport of long chain fatty acids into cells (some diffuse through the lipid bilayer). Localisation is confined to kidney cortex and liver (Hirsch *et al.*, 1998). There is high homology between FATP2 and other family members. Richards (Richards *et al.*, 2003) showed that FATP1 (Slc27a1) forms dimers and possibly larger complexes, most likely through interactions between amino acids 191 and 475, as deduced by co-immunoprecipitation of truncated FATP1 constructs tagged with different markers. The present screen showed that a convincing interaction domain with N-terminal ANK was highly conserved among six clones (Figure 5.12), and occurred between residues 77 and 227.

All FATPs have a highly conserved AMP-binding region at around position 250 (Hirsch *et al.*, 1998), which mediates ATP binding, enabling metabolism of long chain fatty acids to occur. FATPs mediate both fatty acid transport and acyl CoA-synthetase activity, the latter catalysing the hydrolysis of ATP to AMP and PPi (shown in Figure 5.14). Since this reaction is reversible (p. 191 in (Ernster, 1992)), PPi must be rapidly removed to favour production of long-chain acyl CoA for beta-oxidation, and this must occur immediately at the site of PPi production. ANK is present in membranes of many cell compartments (Carr

[15] www.fccc.edu/research/labs/golemis/InteractionTrapInWork.html
[16] www.ch.embnet.org/software/TMPRED_form.html

et al., 2007). A direct interaction between FATP and ANK would be energetically favourable in maintaining the forward reaction, and would allow a physiological role for PPi on the *trans* side of the membrane without wasting energy by uncoupled hydrolysis of PPi by a pyrophosphatase.

FATP2 is found on the membranes of renal peroxisomes, allowing entry of fatty acids from the cytosol. Visser *et al.* (2005) demonstrated a renal peroxisomal membrane transporter that facilitates "phosphate and possibly pyrophosphate" export. They were able to distinguish phosphate transport activity from that in mitochondria by using specific inhibitors, and demonstrated inhibition of phosphate transport by unlabelled PPi. They found no detectable PPase activity in the renal peroxisome fractions; similar findings have been shown in rat liver cells (Shatton *et al.*, 1981). Given the findings of intracellular localisation, kidney expression, interaction data and lack of membrane-associated PPase, we suggest that ANK is a candidate peroxisomal membrane PPi transporter.

5.4 Conclusions

5.4.1 Possible reasons for apparent lack of transmembrane PPi flux mediated by ANK

Since (a) ANKH has been implicated in PPi export, (b) ANKH protein can be expressed in the oocyte membrane, and finally (c) PPi transport across a plasma membrane almost certainly requires the presence of a transporter, the possibility of PPi transport across this membrane in both directions was directly investigated. Previous studies have not considered in detail factors such as stability and bioavailability of PPi, the possibility of other substrates, and substrate specificity for ANKH or phosphate transporters. Even accounting for these, our studies showed no convincing influx or efflux due to ANKH even with various combinations of these experimental variables. Apparent lack of transport could be due to:

1. Substrate non-availability – Substrate microinjected into oocytes may become sequestered inside the oocyte e.g. by ANKH present in intracellular membranes; hydrolysed by intracellular pyrophosphatases; unable to diffuse through the large cell volume of the oocyte to the surface; or complexed with free calcium inside the cell. In addition, the specific activity/concentration ratio of the substrate may not have been high enough after accounting for these factors.

2. Hydrolysis at cell surface – this may reduce PPi availability for ANK-mediated influx, especially at low initial PPi concentration, although intracellular PPase activity could not be assayed.

3. Incorrect hypothesis – PPi may not be transported by ANKH itself but by another unknown protein with ANKH acting as a co-factor or regulator. The oocyte system would not replicate a multi-component system as found in the intact cell or kidney tissue.

4. Requirement for binding partner – Slc27a2 (FATP2) was the only positive interacting clone on the yeast two-hybrid screen that is directly involved in PPi generation. It localises to the peroxisome in kidney, where a physiological role exists for PPi transport out of the peroxisome. However this may not reflect the situation at the apical membrane of collecting duct cells, as FATP2 is not known to localise to the plasma membrane. Conversely FATP1 is present at the plasma membrane but is expressed at low levels in kidney and was not a positive interacting clone in the yeast two-hybrid screen.

5.4.2 An alternative strategy for investigating ANK function

The localisation of ANKH expression to the cortical collecting duct of human kidney was shown in Chapter 3, and supports previous data obtained in mouse kidney collecting duct cells (Carr *et al.*, 2007). An alternative way of investigating ANK function would be to study a model epithelial cell line which retains specific differentiation appropriate to this tubule segment, such as AVP (ADH) responsiveness. Reconstituted epithelial layers grown on filters are polar in nature, allowing aspects of vectorial transport to be determined. The mouse cell-line, mpkCCD$_{cl4}$, meets these requirements and was therefore chosen for further investigation (Chapter 6).

Figure 5.14 Possible interaction between FATP and ANKH.

(Singh & Poulos, 1988); (Steinberg *et al.*, 1999)).

6 Results (IV): Regulation of ANK using a mouse collecting duct cell line, mpkCCD$_{Cl4}$

6.1 Introduction

6.1.1 Introduction and hypothesis

The principal cells of the cortical collecting duct (CCD) are AVP-sensitive, allowing AQP2 to be expressed in the apical membrane under appropriate conditions (Nielsen *et al.*, 2002). We have shown that ANK and AQP2 proteins are both expressed in the collecting duct in human kidney, with previously similar findings in mouse (Carr *et al.*, 2007). Water reabsorption via AQP2 causes increased calcium concentration in the lumen, which creates a physiological requirement for the co-ordinated inhibition of crystallisation. Export of PPi into the lumen via ANK would serve this role. We therefore hypothesise that the surface membrane expression of ANK is regulated by AVP in a similar manner to that of AQP2.

Screening using the yeast two-hybrid method identified SLC27A2 as a potential interacting partner with ANK that may form a biochemical couple. SLC27A2 is expressed only in liver and kidney (Hirsch *et al.*, 1998). It localises to rat liver peroxisomes and microsomes but not to mitochondria (e.g. Singh & Poulos (1988); Steinberg *et al.* (1999)). The plasma membrane of liver cells was not examined in this study and no published studies have defined subcellular localisation in particular nephron segments[17]. Whether or not SLC27A2 is expressed in the plasma membrane of CCD cells, and is therefore available for potential interaction with ANK, is consequently unknown.

6.1.2 Justification for using mpkCCD$_{cl4}$ cells to investigate regulation

Obtaining pure mRNA specific to collecting duct cells is a key requirement in these experiments. Extraction of mRNA from principal cells isolated directly from microdissected CCDs would give rise to only small amounts of mRNA (Robert-Nicoud *et al.*, 2001). Bulk isolation would risk contamination with other cell types as well as requiring the maintenance of animals in dehydrated, euvolaemic and overhydrated water states. Establishing primary cultures of cells from the normal pole of resected human kidney would present similar isolation problems and would require extensive testing. Human cell lines originating from renal carcinomas invariably lose key phenotypic features (Charlton, 1993).

[17] http://locate.imb.uq.edu.au

A well characterised clonal cell line, mpkCCD$_{cl4}$, was used instead. This cell line is derived from CCD segments isolated from the kidney of a one month old SV-PK/Tag transgenic mouse (Bens *et al.*, 1999). ANK expression in mpkCCD$_{cl4}$ murine cortical collecting duct cells and in whole mouse kidney was confirmed by RT-PCR (Figure 3.4), and endogenous protein expression has previously been confirmed at the expected size (~50 kDa) using Ab3 antibody (Carr *et al.*, 2009). mpkCCD$_{cl4}$ cells display a polarised epithelial phenotype with steroid-sensitive sodium transport (Bens *et al.*, 1999). Importantly, they have also been shown to respond to AVP treatment by increased expression of AQP2 (Hasler *et al.*, 2002). They have also been studied in microarray analyses (see section 6.3.3.3), and the mouse ANK protein is virtually identical to the human homologue (Figure 3.1).

6.1.3 Likelihood of ANK being regulated

Short-term regulation of membrane proteins occurs via interactions with other proteins or subunits and by phosphorylation (Van Winkle, 1993). ANK contains multiple serine/threonine and tyrosine phosphorylation sites within its cytoplasmic loops (NetPhos2 prediction[18]) indicating such potential. Regulation over the longer term by growth factors and phorbol esters has been reported, which up-regulate ANK mRNA and protein expression (Guo *et al.*, 2001).

6.1.4 Aim of this section

The aim of this section is to investigate whether the regulation of ANK is linked to that of AQP2, and whether SLC27A2 or other partner proteins are expressed and involved in this process. Elucidating control of ANK regulation may provide clues to its molecular physiology and the identity of alternative partner proteins. The objectives were to examine the effects of AVP stimulation of a collecting duct cell line on expression of ANK and AQP2 proteins by immunofluorescence and on the pattern of gene expression, with confirmation of results using quantitative PCR.

6.2 Effect of AVP stimulation on expression of ANK protein

6.2.1 Results

6.2.1.1 Upregulation of ANK and AQP2

Cell monolayers were grown on filters allowing measurements of resistance and transepithelial potential difference to be made to confirm the integrity and differentiation of

[18] www.cbs.dtu.dk/services/NetPhos/

the CCD layers. Under non-stimulated conditions, there was no AQP2-specific immunofluorescence. Using Ab3 antibody, ANK immunofluorescence of cilia was seen at the apical surface (top row in Figure 6.1 A), with subsequent confocal sections in a more basolateral direction showing plasma membrane outlines of ANK immunofluorescence in all cells (top row in Figure 6.1 B). This positive immunofluorescence in both apical and basolateral membrane areas was confirmed by co-staining using anti-ZO1 secondary immunofluorescence to identify tight junctions (Dr G Carr, unpublished results).

After incubation with AVP in the basal bathing media for 24 h, an average of 6.6% of cells in random fields of view across four separate experiments showed marked upregulation of AQP2, with strong secondary immunofluorescence now present at the apical membrane. In similar analysis 1.8% of cells showed upregulation and apical secondary immunofluorescence for ANK (Figure 6.1). Surprisingly, after AVP exposure, the AQP2-positive cell population was quite distinct from the ANK-positive population, with only very isolated instances of colocalisation of upregulated ANK and AQP2 at the apical membrane (not shown). Similar data were obtained after 24 h treatment with 10 μM forskolin applied to the basal bathing solution.

6.2.1.2 Upregulation and apical colocalisation of ANK and calbindin-D$_{28K}$

The unexpected results obtained in section 6.2.1.1 above, showing heterogeneity between cells in their response, suggests that the clonal nature of the cell line had not been maintained. An alternative possibility is that several phenotypes arising from the cortical collecting duct are represented. Since active calcium reabsorption occurs only in the adjacent distal tubule and connecting tubule segments (Hoenderop *et al.*, 2002), the possibility that an unexpected calcium-transporting phenotype was represented was tested by investigating expression of calbindin-D$_{28K}$. No anti-calbindin secondary immunofluorescence was seen in any section under non-stimulated conditions (Figure 6.2). In contrast, AVP treatment resulted in upregulation of both ANK and calbindin staining, with co-localisation in all positive cells to the apical plasma membrane. Unlike AQP2 immunofluorescence above, only one population of positively stained cells was revealed. Three-channel confocal microscopy was not available, but similar immunofluorescence was seen when anti-calbindin antibody was used alone. A cytofluorogram of pixel intensity over the whole field showed that fluorescence of green (ANK) and red (calbindin) channels overlapped considerably producing a yellow colour, with evidence of separate green and red pixels, though green predominated in the peripheries.

Figure 6.1 (next two pages) CLSM images of methanol-fixed mpkCCD$_{cl4}$ epithelial layers, under control conditions and after incubation for 24 h with either arginine vasopressin (AVP; 10^{-8}M) or forskolin (10^{-5}M). Immunofluorescence was simultaneously performed with Ab3 (green; column 1) and goat anti-AQP2 (red; column 2) as primary antibodies. Overlay of Ab3 and anti-AQP2 images is shown in column 3. Secondary staining was with donkey anti-rabbit FITC and donkey anti-goat TRITC in all sections. Scale bars represent 20 µm and apply to all images. Representative images from four separate experiments each are shown.

Figure A:

Top row: *xy* sections under resting (untreated) conditions

Middle row: *xy* sections after incubation with AVP

Lower row: *xz* sections after incubation with AVP (apical surface uppermost)

Figure B:

Top row: *xy* sections under resting (untreated) conditions

Middle row: *xy* sections after incubation with forskolin

Lower row: *xz* sections after incubation with forskolin

(Data for figure B from Dr G Carr, unpublished results)

Fig 6.1 A goes here

Fig 6.1 B goes here

Figure 6.2 CLSM images of methanol-fixed mpkCCD$_{cl4}$ epithelial layers, under control conditions and after incubation for 24 h with arginine vasopressin (AVP; 10^{-8}M), using anti-calbindin antibody.

Immunofluorescence was simultaneously performed with Ab3 (green; column 1) and goat anti-calbindin-D$_{28K}$ (red; column 2) as primary antibodies. Overlay of Ab3 and anti-calbindin-D$_{28K}$ images is shown in column 3. Secondary antibodies were donkey anti-rabbit FITC and donkey anti-goat TRITC respectively in all sections. Scale bars represent 20 µm and apply to all images. Representative images from three separate experiments each are shown.

First row: *xy* sections under control (untreated) conditions

Second row: *xy* sections after incubation with AVP

Third row: *xz* sections after incubation with AVP (apical surface uppermost)

Fourth row: Cytofluorogram for Ab3 immunofluorescence (*x*-axis) and anti-calbindin-D$_{28K}$ immunofluorescence (*y*-axis)

Fig 6.2 here

(Davidson & Halestrap, 1988)

These results are consistent with colocalisation of ANK and calbindin-D$_{28K}$ at the apical membrane, and with ANK immunofluorescence alone in intracellular and lateral membrane locations. The absence of any sequence similarity between the C-terminal epitope of ANK (to which Ab3 is raised) and calbindin-D$_{28K}$, recognition by different secondary antibodies and the antibody controls preclude non-specific recognition of the ANK-positive cells by calbindin.

6.2.2 Discussion

6.2.2.1 ANK is upregulated by AVP, but heterogeneity exists in the mpkCCD$_{cl4}$ cell line

The results show that ANK is capable of being upregulated by AVP, and the similar results obtained with forskolin confirm that this is via a cAMP-dependent mechanism. Given the localisation of ANK in the CCD, we had predicted that ANK would be upregulated by AVP in cells that stained positively for AQP2, i.e. principal cells, with ANK-positive AQP2-negative cells (representing intercalated cells) being in the minority. Instead, immunofluorescence of ANK and AQP2 in AVP-treated sections resulted in the identification of multiple cellular phenotypes. In contrast, the results of calbindin immunofluorescence showed identical colocalisation with ANK at the apical membrane after AVP treatment. Over 90% of the cells did not stain positively for AQP2, demonstrating that the mpkCCD$_{cl4}$ cell line used in the experiments may not consist of normally functioning principal cells and is therefore not truly clonal. The same anti-AQP2 antibody was able to identify principal cells in human (Chapter 3) and mouse tissue (Carr *et al.*, 2007) which correlated with tissue morphology, and colocalisation with ANK was demonstrated in both species. ANK is present in α-intercalated cells (section 3.2.6), and this may account for a small proportion of the ANK-positive AQP2-negative immunofluorescent cells. This unexpected cellular heterogeneity with very low overall immunofluorescence means that attempts to measure PPi transport to apical and basal solutions under AVP-stimulated conditions in this cell line would be very likely to yield a false negative result. Recloning of the cell line with expansion of the ANK-positive phenotype would allow AVP-induced PPi transport to be investigated.

6.2.2.2 ANK function may not be restricted to the collecting duct

The distribution of upregulated cells in this cell line may suggest that functional ANK expression is not solely limited to the principal cells of the collecting duct. AQP2

expression is found uniquely and precisely in the apical membranes of cortical, medullary and papillary collecting ducts in kidneys of human, rat (Marples *et al.*, 1995) and horse (Floyd *et al.*, 2007). In contrast, active renal calcium transport occurs in both the DCT and connecting tubule (Hoenderop *et al.*, 2005); (Hoenderop *et al.*, 2002). Additionally, calbindin-D$_{28K}$ is also found in CCD of rabbit and in the medullary collecting duct of certain rat and monkey species (Moutairou *et al.*, 1996). Since calbindin-D$_{28K}$ is unique to calcium-transporting epithelia (Schlatter, 2006), this again suggests that the mpkCCD$_{cl4}$ cell line is not a true clone of collecting duct cells. During transcellular calcium transport, calbindin-D$_{28K}$ traffics from the cytosol towards the apical membrane, where it buffers calcium entering the cell via the apical calcium transporter TRPV5 with which it colocalises and is coexpressed (Lambers *et al.*, 2006). Subsequent facilitated exchange diffusion of calcium via calbindin is thought to deliver calcium to the basal sodium/calcium exchanger or calcium-ATPase for export to the blood whilst maintaining a low intracellular calcium.

We have shown at least limited ANK expression in the thick ascending limb of human kidney (section 3.2.7), and the colocalisation with calbindin-D$_{28K}$ demonstrated here suggests some ANK expression in the distal tubule. Our results may therefore reflect the wider distribution of ANK in various nephron segments, such as thick ascending limb or distal tubule. Since these segments are not primarily AVP responsive, ANK expressed in each segment may require regulation in different ways. The crystallisation tendency of high luminal calcium concentrations in any of these segments would be reduced by allowing increased calcium buffering via TRPV5/calbindin at the same time as promoting PPi export into the lumen via ANK. Given that most calcium transport occurs in the distal tubule rather than the CCD, ANK expression in these areas would be consistent with the overall hypothesis.

6.2.2.3 Summary of immunofluorescence findings

Immunofluorescence studies in the mpkCCD$_{cl4}$ cell line have shown that ANK is upregulated by AVP treatment, but biochemical confirmation of function is limited by very low overall detectable expression in this system and possibly by heterogeneity of the clonal cell line. ANK may also be expressed in calcium-transporting nephron segments, which is consistent with localisation data obtained in Chapter 3. Confirmation of AVP regulation of the *ANK* gene is now required. This would also allow clarification of the transcriptional regulation of *ANK* under AVP-stimulated conditions. It may also help to identify interacting or co-regulated proteins.

6.3 Effect of AVP on the expression profile of mpkCCD$_{cl4}$ cells

6.3.1 Aims of expression profile analysis

Investigation of the effects on the pattern of gene expression in mpkCCD$_{cl4}$ cells in response to AVP stimulation allows confirmation of transcriptional regulation by AVP. The experimental aim was to identify the genes expressed when mpkCCD$_{cl4}$ cells are stimulated by AVP under the same conditions as in the immunofluorescence experiment, and to determine if ANK is among them. The secondary aim was to quantify any up- or down-regulation. The expression profile thus generated is a surrogate for the resulting proteome. Even though the percentage of positively immunofluorescent cells with AVP was low in the immunofluorescence experiment, this is not necessarily proportional to mRNA copy number present.

6.3.2 Results

6.3.2.1 Criteria used to create a list of genes differentially expressed due to AVP

Normalised, quality controlled probesets were used to generate a list of genes expressed differentially between control and AVP-treated samples. The threshold of significance was set at $p = 0.05$, with these results further selected for an up- or down-regulation with fold change of at least 1.18 compared to controls. This resulted in a list of 364 genes which were differentially expressed due to AVP (Figure 6.3 and Figure 6.4). Multiple probesets may map to a single gene, but the selection criteria resulted in only one of the two probesets for the highly AVP-upregulated PDE4b gene being included in the final analysis (Figure 6.4 and Figure 6.6).

The effect of this selection was checked by rearranging the 364 probesets, coloured according to their NIVs, by control versus treated (columns in Figure 6.5) and by those probesets with higher expression (redder; rows in Figure 6.5) versus those with lower expression (bluer; rows in Figure 6.5). These corresponded to genes upregulated by AVP and genes downregulated by AVP, respectively. The pattern of colours confirms that there are only two visible groups, indicating that the only significant differences were between the AVP-treated and untreated conditions.

6.3.2.2 Important genes which were shown to be up/down regulated

The full list of probesets representing genes which were up- or down-regulated, with fold changes, is given in Appendix 1. Specific genes of interest are shown in Table 6.1 and as an expression profile plot (Figure 6.6). Upregulation was confirmed of *PDE4b, AQP2* and *ANK* (in descending order of fold change), but not of *SLC27A1* or *SLC27A2*.

6.3.3 Discussion

6.3.3.1 *ANK* gene expression is upregulated by AVP stimulation

The probeset with the highest fold change in the array was one of those for PDE4b. PDEs are enzymes that hydrolyse cyclic nucleotides, and are a major determinant of intracellular cyclic nucleotide concentration (Cheng & Grande, 2007). In tubular epithelia (cell line LLC-PK1) catabolism of the AVP-dependent cAMP pool occurs by PDE1 and PDE4 (Cheng & Grande, 2007), but PDE4 is the most highly expressed isoenzyme in rat renal cortex (Matousovic *et al.*, 1997). An increase in cAMP induces *PDE4* gene expression (Manganiello, 2002). *PDE4b* together with *AQP2* represented positive controls for AVP treatment. Despite only 6% of cells being positive for immunofluorescence of AQP2, a 3.4-fold change in corresponding mRNA availability was found after significance testing. Under these circumstances the 1.4-fold increase in *ANK* gene expression demonstrates clear upregulation of *ANK* in mpkCCD$_{cl4}$ cells with AVP treatment, and suggests that the actual amount of gene expression in individual cells that express *ANK* might in fact be very high indeed, causing a large underestimation of the true fold change in the present experiment.

6.3.3.2 *SLC27A2* gene expression was not confirmed in the mpkCCD$_{cl4}$ cell line

The gene for the potentially interacting protein SLC27A2 (section 5.3.7.3) was not identified here above background in any of the six arrays, this being confirmed subsequently by PCR (section 6.4.2.2.6). Only one *SLC27A2* probeset, consisting of ten oligonucleotide probes, was available but the sequences of all ten probes were found to map as expected to the consensus NC_000068.6 sequence of *SLC27A2*. Of note, SLC27A2 is localised to proximal tubule of rat kidney (Thukral *et al.*, 2005) whereas the mpkCCD$_{cl4}$ cells used here are a collecting duct cell line. In addition, it is located intracellularly in peroxisomes and ER of liver cells (Steinberg *et al.*, 1999). Transfection of SLC27A2 into mpkCCD$_{cl4}$ cells in our laboratory gave intracellular rather than membrane staining, consistent with published findings (Dr G Carr, unpublished results). This is unlike SLC27A1 which is also expressed

in kidney but located in the plasma membrane (Schaffer & Lodish, 1994), and is shown to be present but not upregulated by AVP in this experiment. The yeast two-hybrid screen answered a different question to the microarray experiment: it suggested SLC27A2 as a potential binding partner, which could be true even if its expression is minimal.

Figure 6.3 Change in expression of each probeset (gene) according to array.

Figure 6.4 Change in probeset (gene) expression due to AVP treatment, for normalised and quality-controlled microarray data.

Figure 6.5 Hierarchical clustering of quality controlled probesets (genes), selected for p<0.05 and fold change >1.18.

Table 6.1 Some of the genes differentially expressed on AVP-stimulation of mpkCCD$_{cl4}$ cells.

Figure 6.6 Change in expression of five genes with AVP treatment.

6.3.3.3 Comparison with published mpkCCD$_{cl4}$ transcriptome datasets

A search of the ArrayExpress database[19] for published microarray experiments involving ANK in mouse tissue or cell lines yielded only six experiments, all involving mouse kidney tissue, and showed very low basal expression with respect to other tissues. Robert Nicoud *et al* (Robert-Nicoud *et al.*, 2001) treated mpkCCD$_{cl4}$ cells with 10^{-8} M vasopressin for 4 hours and looked at the resulting transcriptome to try and identify new AVP-dependent signalling pathways. mRNA was collected, and sequence tags were analysed by attempting to match them against known mouse genes in a process called "serial analysis of gene expression" (SAGE). SAGE gives a list of many short sequence tags and the number of times each of these transcripts is observed. It therefore differs from a microarray screen in which only sequences to which a probe already exists can be detected, and even then there is potential for mis-hybridisation. If the genes to be investigated are already known, SAGE can allow more accurate quantification of gene expression than a DNA microarray study. Unfortunately, this database, as given in their paper, can no longer be located.

Another earlier study, also by the Knepper group (Legato *et al.*, 2003) also used results from both SAGE and microarray techniques in the mpkCCD$_{cl4}$ cell line to collate a list of the major collecting duct proteins under resting conditions (data at http://cddb.nhlbi.nih.gov/cddb/). This was an early, basic list of genes involved in transport and cellular regulation in this cell line, which has since been superseded by the results available from analysis of microarray data by software such as GeneSpring. More recently, the Knepper group (Yu *et al.*, 2009) used Affymetrix GeneChip® Mouse Genome 430 2.0 Arrays to analyse gene expression in the mpkCCD$_{cl4}$ cell line, looking for regulators of *AQP2* gene expression. They found that AQP2 immunofluorescence of cells in confluent mpkCCD$_{cl4}$ monolayers was variable, just as we noted (section 6.2.1.1). In order to avoid this heterogeneity they subcloned the original mpkCCD$_{c14}$ cell line on the basis of naturally varying aquaporin-2 (AQP2) protein expression levels after incubation with 10^{-10} M AVP basolaterally for five days. Microarray screens were carried out on five different clones and the original cell line. Results also included a post-normalisation ratio of gene expression of the clone with the highest *AQP2* expression (clone 11 in their database) to the clone which lacked *AQP2* expression (clone 2), even though both were stimulated with 10^{-10} M AVP.

[19] www.ebi.ac.uk/arrayexpress using gene ID ENSMUSG00000022265

For *AQP2*, there was a 42-fold increase with treatment. Details of their published searchable database are given below[20].

6.3.3.4 Substantial overlap with the Knepper dataset, but *ANK* was not upregulated

The Knepper study was similar to ours apart from their use of 100-fold lower AVP concentration and the lack of non-AVP treated mpkCCD$_{cl4}$ clones, although their 'clone 2' had almost no AQP2 gene or protein expression (Yu *et al.*, 2009). We used GeneSpring GX 10 to re-analyse the raw Knepper dataset under our normalisation and quality-control criteria to determine any differences in relative ANK expression using this lower AVP concentration (Figure 6.7). Only 30 (0.4% of the total) probesets in the Knepper list were not present in our quality-controlled list (QC in Figure 6.7), indicating a very high degree of overlap. All Knepper probesets were included within our pre-quality-controlled list (T in Figure 6.7). Of our final t-tested list of 364 differentially expressed genes, about half appeared in the Knepper list, and *ANK* was among these (Figure 6.7 B).

Knepper probesets were further selected for a fold change of at least 2.0 from the clone expressing highest *AQP2* (clone 11) to the lowest (clone 2), and compared to our final differentially expressed list of 364 genes. 75 probesets were shared, including *AQP2* and *ANK*, but *PDE4b* was not, and *ANK* was *downregulated* by 3.8-fold in the clone with highest AQP2 expression compared to that with the lowest. It is possible that *ANK* requires a higher AVP concentration to promote expression or that *ANK* is downregulated over the five days of 10^{-10} M AVP stimulation. The lack of PDE expression supports the idea that AVP may cause upregulation over shorter time periods. It is known that some AVP-stimulated gene transcription can be maximal at around 30 minutes (Mayr & Montminy, 2001); see below for further discussion on this) and greater than 24 hours of exposure to AVP can result in marked morphological changes in the principal cell, which can affect gene transcription independently of AVP (Robert-Nicoud *et al.*, 2001).

Despite Knepper's comparison of AQP2-sensitive and -insensitive clones, the difference compared to our results suggests that ANK may require a higher level of AVP to enable expression, and/or there is a difference between acute and chronic regulation. Further investigation of this result in comparison with studies into the mechanism of action of AVP is performed below. Such a scenario is consistent with the overall hypothesis that *ANK* is

[20] Database is available at http://dir.nhlbi.nih.gov/papers/lkem/mpkccdtr/default.aspx. Raw data is available from Gene Expression Omnibus (http://www.ncbi.nlm.nih.gov/geo; GSE13672; Yu *et al*., 2009).

acutely upregulated in conditions of dehydration and hence acutely increased basolateral AVP concentration.

6.3.3.5 Assessment of the likelihood of *ANK* being an AVP-responsive gene

AVP binding to the V_2 receptor activates the cAMP system. cAMP activates the cAMP-response element binding protein (CREB) by phosphorylating its Ser-133 residue (Mayr & Montminy, 2001). Activated CREB binds to genes which contain a cAMP-responsive element (CRE) motif causing gene transcription, peaking at about 30 minutes after cAMP stimulation, although not all genes containing CRE are activated by cAMP. CREs are most functional when located within 100 base pairs of the "TATA" box transcription promoter, and hence this can be used to predict which genes contain CRE, and might therefore be cAMP responsive (Table 6.2). Zhang *et al.* (2005) performed modified microarray analysis on various cell lines to differentiate tissue-specific functions of CREB, resulting in an expression profile unique to each tissue in response to cAMP activation. These data are published online at http://natural.salk.edu/CREB.

We hypothesised that genes in our QC list (Figure 6.7) that do not contain CRE motifs are unlikely to be functionally significant. The overlap between the list of genes containing CREB (~600 genes) and our QC list (364 genes) was computed using Ingenuity software (www.ingenuity.com). 256 of the 364 differentially expressed genes overlapped with the CREB database list, including ANK and AQP2.

Conserved CRE sites, whether full or half sites, are the most likely functional CREs, and they usually occur within 100 base pairs of the "TATA" box transcription promoter (Mayr & Montminy, 2001). These data show that ANK has a non-conserved half site between 3743 and 3030 base pairs prior to the start of the coding sequence, which suggests that it may not be entirely regulated by cAMP in this way. Forskolin stimulation of tissues was performed on HEK293 cells, followed by chromatin immunoprecipitation and microarray hybridisation in arrays of various cell lines. This genome-wide location analysis allowed functional determination of CRE activation, although the results are not directly comparable to ours as we used AVP rather than forskolin. Again, this gave similar results to the table above (Table S4 at http://natural.salk.edu/CREB). On the other hand, ANK does not appear in the list of cAMP responsive genes (as observed after forskolin treatment) in the non-polarised non-collecting duct cell line HEK293T generated by an Affymetrix array experiment (Table S5 at http://natural.salk.edu/CREB), but this simply reflects the tissue-

specificity of responses.

There is little evidence in terms of appropriate CRE sites on the *ANK* gene promoter available for regulation by cAMP. This suggests that AVP may not be the only acute transcriptional regulator of ANK, and supports the findings of increased *ANK* expression at 24 hours, but not at 5 days, after stimulation with higher AVP concentration.

Figure 6.7 Summary of rationalisation of microarray data and overlap with Knepper dataset.

Table 6.2 Prediction of functional CREs on promoters of mouse genes.

6.4 Confirmation of upregulated genes by quantitative RT-PCR

6.4.1 Aim

The expression profile resulting from stimulation of mpkCCD$_{cl4}$ cells with AVP for 24 h appeared to support the findings of upregulation of AQP2 and ANK seen on immunofluorescence. However, the fold increase of ANK mRNA was relatively small, and differences from previously published datasets were noted. Confirmation by actual detection of transcriptional regulation in the same mRNA as used above was now performed by quantitative PCR using gene-specific primers. The aim was to quantify the expression levels of target genes in the experimental samples with respect to a non-changing reference gene.

6.4.2 Results

6.4.2.1 Determination of reaction efficiency

Standard curves were obtained by amplification of either pre-sequenced clones or RT products, in order to estimate the efficiency of DNA amplification of known dilutions of DNA from six genes (Figure 6.8). All data points touched the regression line, indicating that dilutional errors were minimal. Amplification curves were parallel and equally separated in all cases (Figure 6.9).

All standard curves gave efficiencies very close to the optimum of 2.0, corresponding to a slope of -3.2. The curve for ANK did not encompass the very low range of ANK crossing points obtained in the experiment, and so extrapolation of the curve was required. Although not desirable, this is probably a reasonable estimate given that errors were very low.

Analysis of the T_ms showed that a single identical product was formed in all dilutions of a standard, with the exception of SLC27A1, where two products were found (see section 6.4.2.2.5 below).

Figure 6.8 Standard curves showing efficiency of DNA amplification of known dilutions of DNA from six genes.

The "crossing point" (Cp) is the amplification cycle number at which a sample's fluorescence first rises above background fluorescence. More dilute samples (less initial DNA in the sample) thus require more cycles to become visible above background noise, resulting in a higher crossing point. Standard curves comprise the crossing point for each dilution (green dots) plotted against the logarithm of the sample's initial DNA concentration (*x* axis), and a linear regression is calculated (blue line). The slope of each standard curve indicates the rate at which amplification of the initial DNA template proceeds. This can also be expressed as efficiency, where efficiency = $10^{(-1/\text{slope})}$. The perfect amplification would result in a doubling of the initial DNA, giving an efficiency of 2 (corresponding to a slope of -3.3). The mean squared error of fitting to the regression line was < 0.03 in all cases (acceptable < 0.2).

Fig 6.8 here

Figure 6.9 Examples of amplification curves.

The fluorescence (arbitrary units) of each amplification reaction is shown as a function of the cycle number. Each curve commences as a near-horizontal line until fluorescence from the PCR product rises above background. This is followed by an exponential phase and concludes with a plateau as one or more ingredients in the reaction is used up. (**A**) Amplification of seven 1:10 serial dilutions of a plasmid DNA containing the coding sequence of *ANK* using specific primers (this was used to generate the standard curve in the previous figure). Amplification of the most concentrated ANK sample (left-most curve) commenced earlier and finished sooner than those for successive dilutions. Each dilution was performed in duplicate. (**B**) Amplification of experimental cDNA samples using the same *ANK*-specific oligonucleotide primers. The exponential phase commences beyond cycle 30, indicating relatively small amounts of ANK cDNA template in the samples. This can be compared to amplification curves of experimental cDNA samples obtained using *AQP2*-specific oligonucleotide primers (**C**) and *GAPDH* oligonucleotide primers (**D**), where the exponential phase commences earlier than for *ANK*.

fig 6.9 here

6.4.2.2 Analysis of amplified products

6.4.2.2.1 PDE4b

Only one (C2) out of the three untreated samples generated a product of correct T_m (highlighted in red in Table 6.3), as defined by the T_m of the standards. The others led only to a product with lower T_m, most likely primer dimer, resulting in either a higher Cp or undefined Cp. In contrast, AVP treatment led to the correct product in all three RT positive samples, with Cp around 30-32. All control samples (RT negative samples, no RNA, no template) were satisfactory, and yielded primer dimer, non-specific products, or no product. Similar results were obtained in two separate experiments using the same samples. As a result of this lack of consistent product from untreated samples in multiple experiments, fold change for *PDE4b* can not be calculated.

6.4.2.2.2 AQP2

Results were similar to those of *PDE4b*. Only one of the untreated samples, but all three AVP-treated samples, generated a product of the correct T_m (highlighted in red in Table 6.3; see also Figure 6.10). Other untreated samples and all negative controls yielded either primer dimer (~78 °C) or non-specific product. Accordingly, a valid fold change result for *AQP2* can not be calculated.

6.4.2.2.3 ANK

Primers optimised to yield a single product of T_m of ~86.6 °C from the cloned *ANK* coding sequence were obtained (section 2.12.2.3). This was confirmed by obtaining a high quality ANK standard curve (Figure 6.8). Despite this, multiple products were obtained in the experimental samples using these primers (Table 6.3 and Figure 6.10). These can be grouped as shown in Table 6.4.

One RT negative sample (AVP1) contained a product of correct T_m, although analysis of Cp shows that it had 64-fold (26) lower yield with respect to the corresponding RT positive, and that another non-specific product was also formed. This indicates slight contamination of the RT negative in this case. Other negative controls yielded primer dimer (blue in Table 6.4) or non-specific product (green in Table 6.4).

Table 6.3 Results of real time RT-PCR amplification of mpkCCD$_{cl4}$ samples with and without AVP treatment.

	RT positive		RT negative	
	1st product	2nd product	1st product	2nd product
C1	77.0	86.3	83.1	
C2	86.7		77.6	
C3	86.6		83.0	77.0
AVP1	86.9		86.8	79.7
AVP2	86.5	79.2	77.3	
AVP3	86.4	79.2	82.7	76.7
No RNA	83.4	77.4	n/a	n/a

Table 6.4 Melting temperatures (℃) for amplificati on products of experimental samples using ANK-specific optimised primers. Results are given for the most abundant (1st product) and lesser product (2nd product) for RT positive and negative samples for each of three untreated (C) and three AVP-treated (AVP) samples, together with the no-RNA control. A second product was not obtained in every case (left blank on table). The results segregated into three groups (Figure 6.10), labelled here as red (corresponding to the single product obtained from standards), green and blue. The PCR negative (water) control gave one product at 74.9℃. Similar results were obtained in a separate repeat experiment using the same experimental samples.

6.4.2.2.4 GAPDH

GAPDH was used as the reference gene for the reasons given in section 2.12.3.2. As with ANK, the correct product was also formed in two of the RT negatives (C3- and AVP1-), but the difference in Cps was at least 12 cycles, giving a fold difference of at least 4000. This indicates a very small amount of genomic DNA contamination in two of the six untreated samples, despite DNAse treatment. Otherwise, a single product of the expected T_m was obtained in all six RT positive samples.

6.4.2.2.5 SLC27A1

No clone was available for *SLC27A1* so the standards were obtained by amplification and re-dilution of experimental RT products using the commercially available optimised primers. Unusually, the resulting standard curve yielded two products, the product with T_m of ~84 °C showing 50% of the fluorescence of the product at 89 °C. RT positive samples

yielded a product with AVP1 at 12.7 fluorescence units (arbitrary scale) at 89 °C, and another with C2 at 7.5 units at 84.7 °C. All other RT positives yielded either no product or non-specific products of <0.5 units. Similarly, all controls yielded either no product or non-specific products.

6.4.2.2.6 SLC27A2

Amplification of the SLC27A2 IMAGE clone yielded a single well-defined product with T_m over a narrow range of 82.2-82.5 °C. However, no such product was obtained with any of the experimental samples, and hence Pfaffl analysis was not possible. This failure to amplify using *SLC27A2* oligonucleotide primers was confirmed by performing an end-point PCR, the products of which were run on a 2.5% gel and also yielded no products (Figure 6.10). End-point PCR using primers designed to amplify calbindin-D_{28K} similarly showed no bands.

	GAPDH	***ANK***
Untreated	28.30	33.47
AVP treated	26.46	31.84
Untreated - AVP treated (ΔCp)	1.84	1.64
Efficiency	1.967	1.992
Change (efficiency$^{\Delta Cp}$)	3.47	3.09
Change normalised to *GAPDH*	**1.0**	**0.9**

Table 6.5 Cp values and fold change calculations for RT-PCR amplification.
Average Cp values (number of cycles; see text) are given for amplification of samples either untreated or treated with AVP, for pairs of *GAPDH* and *ANK* gene-specific primers. The difference in cycles (ΔCp) is calculated. Efficiency of gene amplification was calculated from standard curves (Figure 6.8). Fold change between untreated and AVP treated conditions is calculated as efficiency$^{\Delta Cp}$. Fold changes in target gene expression are normalised against the change in reference gene (GAPDH) expression. Values for *PDE4b* and *AQP2* could not be calculated (see text).

Figure 6.10 Identification of amplification products by determination of melting peaks.

Top row: Melting peaks for products generated by amplification of clones or RT products in a standard dilution series (as shown in figure 6.8). For each gene, identity of a single correctly-sized product from each dilution is confirmed by melting temperatures (T_m) occurring over a very narrow range.

Middle row: Melting peaks for products generated by amplification of experimental cDNA samples segregate into multiple groups (red indicates one peak per sample, green indicates two peaks per sample). Using AQP2 and ANK primer pairs, some products resulted in overlapping peaks each at the correct T_m as identified by the standards (blue dotted lines). RT negative, RNA negative and cDNA template negative controls usually produced products of lower T_m (other peaks). In the case of SLC27A2, no product of correct T_m was amplified. This was confirmed by end-point PCR analysis (***lower figure***) of products obtained with this primer pair which was designed to give products of 74 bp. Lanes: low range DNA ladder (L), one AVP-treated RNA sample with (A+) and without (A-) RT, one untreated RNA sample with (C+) and without RT (C-), and PCR negative control (X).

Fig 6.10 here

(Kowalczuk *et al.*, 2008)

6.4.3 Discussion

6.4.3.1 Validity of the experiment

The RNA samples used in these experiments were identical to those used in the microarray experiment. They had been quality controlled and tested as described in section 2.11.2. The melting temperature (T_m) is characteristic of each amplified product. Analysis of the melting curves formed when the fluorescence of each product is plotted against temperature was used to identify correct products, as defined by those obtained using the same primers against standards obtained either from a clone or amplified and re-diluted from RT products. Melting peaks tended to segregate into those indicating the expected product (mostly found in RT positive test samples), and those indicating secondary and tertiary products, primer dimer or no product at all.

RT positive samples sometimes yielded more than one product despite optimisation of primers, and RT negative sample controls yielded primer dimer or non-specific products. Since the extracted RNA was DNase treated before RT, these extra products are unlikely to consist of genomic DNA. Any trace RT activity of the DNA polymerase on any RNA that was carried over would have been little or nil, because RNaseH was used to destroy RNA at the end of the RT. Products obtained in the no-RNA control were of lower T_m, excluding contamination of the RT reagents with the exception of that for *GAPDH*. In the latter case, the lack of product with RT negatives, or the very large cycle differences between RT positive and negative pairs, together with the very precise overlapping of all T_m curves for *GAPDH* suggests that this contamination can be dismissed. Contamination from the PCR was excluded in all cases as the no-template (water) control always gave either a different product of lower T_m or no product.

6.4.3.2 *PDE4b* differential expression is not proven but likely to occur

Expression profiling demonstrated 10-fold differential expression of *PDE4b* in response to AVP (Figure 6.4). Confirmation of this using real-time PCR, a highly sensitive technique, was expected but did not occur. Calculation of fold change was not possible since untreated samples gave rise to either no defined Cp or no appropriate product. Since cAMP induces *PDE* gene expression (see section 2.12.3.2), a lack of detectable gene expression in untreated samples might be expected; in two of the untreated samples the primers simply dimerised giving a product of lower T_m. This might explain why only one of the two *PDE4b* probesets was significant on expression profiling (Figure 6.4). It would have been useful to

verify the specificity of the primers, but these facts make it highly likely that *PDE4b* is differentially expressed, even though the fold change with respect to the untreated state can not be quantified here.

6.4.3.3 AQP2 results correlate with those of immunofluorescence

Using AQP2 oligonucleotide primers, only one of the three untreated samples resulted in a product of correct T_m, yet all three AVP-treated samples formed that product. This correlates with the immunofluorescence results (section 6.2.1.1), where no AQP2 immunofluorescence was observed in the resting state, with very marked immunofluorescence after AVP treatment. For similar reasons to those given for *PDE4b* analysis above, calculation of fold change was not possible in order to confirm the 3.4-fold upregulation seen in the microarray experiment.

6.4.3.4 *ANK* gene expression does not change with AVP stimulation

Products coloured in blue in Table 6.4 are most likely primer dimers. In the case of C1, primer dimer was more abundant (fluorescent) than expected product, suggesting low starting levels of ANK cDNA in the sample. Since SYBR green detects the total fluorescence of any and all products, the presence of a significant amount of secondary non-specific product could artefactually increase the apparent Cp for the correct product. In fact, the non-specific peaks (Figure 6.10) are more intensely fluorescent than the true peaks, and may result in an overestimation of its true expression. Pfaffl analysis shows a normalised fold change of ~1 with AVP treatment.

Taken together, these results illustrate the importance of examining T_m first, but suggest that there is no detectable change in *ANK* expression due to AVP treatment. In contrast, microarray analysis showed a relatively small AVP-induced fold increase of 1.4.

Although fold changes do not relect the absolute amount of expression, it is possible that *ANK* is expressed at very low average levels in the template. Immunofluorescent staining of similarly treated cells was clearly seen in only ~2% of cells in the field of view. The apparent clumping of positive cells on the immunofluorescence suggests that RNA sampling could change markedly over a very small area, accounting for the large variability in quantification between samples. Both of these could potentially be improved by cell sorting to enrich the AVP-stimulated ANK-positive cell population.

6.4.3.5 *GAPDH* is a valid reference gene in this analysis

Results of RT positive samples with *GAPDH* confirmed the validity of *GAPDH* as the reference gene. The mean ΔCp value between treated and untreated conditions was 1.8 and Cps were in the range 23-30. Since *GAPDH* has previously been shown to be unaltered in experiments involving AVP (see section 2.12.3.2), this change likely represents higher initial RNA content of the AVP-treated samples, despite attempting to load equal amounts. It illustrates why normalisation to expression of a non-changing standard gene (as was calculated using the Pfaffl method) is essential in these experiments. It would be desirable to normalise against more than one standard gene, such as β-actin, especially when considering very low calculated fold changes such as those obtained for *ANK*.

6.4.3.6 *SLC27A1* and *SLC27A2* are present in negligible amounts or not at all

A good quality standard curve (Figure 6.8) was obtained for *SLC27A1* despite amplification of two products (Table 6.3). Either the bought-in primers were not optimal, or there was very little initial SLC27A1 cDNA, causing amplification to be slower and possibly inaccurate. The latter is supported by sample Cp values that were far higher than those for other primer sets, although detailed comparison of these values with those from other primers would require absolute quantification techniques rather than the methods used here. An SLC27A1-positive control tissue or clone would have been desirable. Since there were no instances of the same products resulting in both untreated and treated categories, it was not possible to include SLC27A1 in the Pfaffl analysis.

The SLC27A2 experiment was the only one in which a non-optimised primer set was used. However, it was designed to span exon-exon boundaries (details in section 2.12.2.3) and using an annealing T_m of 60 °C was proven to be highly efficacious in amplifying the cloned SLC27A2 cDNA on the standard curve. The T_ms of experimental samples from real-time PCR (Table 6.5), and the appearance of the lower end of the end-point PCR gel (Figure 6.10), are consistent with the formation of primer dimer only. Thus *SLC27A2* was not amplified at all, strongly suggesting that it is not present in any of these samples. Although a different primer pair could be used for reconfirmation, this is not necessary since these data confirm the results of the microarray analysis. However, a useful positive control might be to use RNA extracted from a proximal tubular cell line.

6.5 Conclusion

mpkCCD$_{cl4}$ cells stimulated for 24 h with AVP caused significant upregulation of *PDE4b* and *AQP2*. Expression profiling confirmed that *ANK* was upregulated to a much lower extent under these conditions, but this finding was not supported by quantitative PCR using the same mRNA samples. Immunofluorescence showed that only a small proportion of cells showed upregulation of ANK and AQP2, as well as displaying cellular heterogeneity, which may have contributed to underestimation of *ANK* transcriptional upregulation. Similarly, co-localisation of calbindin-D$_{28K}$ with ANK was observed, yet calbindin-D$_{28K}$ mRNA was not detected using gene-specific primers on end-point PCR (data not shown). An alternative explanation is that protein translation and post-translational events such as altered trafficking to the apical cell surface are the main regulators of apical ANK expression.

A previous study performed on subcloned mpkCCD$_{cl4}$ populations at 100-fold lower AVP concentration over a much longer time period did not confirm *PDE* expression and suggested *ANK* downregulation. Mouse *ANK* possesses two half CRE sites but these are well upstream from the start codon, and they are not conserved between mouse and human genomes. Taken together, these data suggest that if transcriptional activation of *ANK* occurs, it is in an agonist, chronicity and species-dependent manner.

The yeast two-hybrid experiment yielding SLC27A2 as a potential interacting protein was performed on a whole mouse kidney cDNA library, but gene expression of *SLC27A2* was not confirmed in this collecting duct cell line. Its tissue and subcellular localisation may explain why it is unlikely to be present in this nephron segment. Although this does not exclude interaction in other segments, it is less likely that SLC27A2 is the interacting partner protein for ANK within the mouse collecting duct.

7 Concluding discussion

7.1 Existing knowledge and unanswered questions

7.1.1 The role of ANKH in the renal collecting duct

The published literature on ANK has focused on calcification abnormalities in bones and joints due to mutations affecting the gene encoding ANK. Since over-expression of *ANK* in fibroblasts increases extracellular PPi whilst reducing intracellular PPi (Ho *et al.*, 2000) it is likely that ANK is either a membrane transporter of PPi or closely involved in its regulation. This effect is reversed in fibroblasts cultured from $ANK^{ank/ank}$ animals (Ho *et al.*, 2000). In addition, extracellular probenecid inhibits ANK function in ANK-expressing cells, suggesting that ANK is likely to be the PPi transporter itself (Ho *et al.*, 2000). Ho *et al.*'s observation that calcification of the kidneys occurred in the $ANK^{ank/ank}$ mouse knockout prompted our hypothesis of ANK expression and function in the kidney.

The origin of urinary PPi is still unknown. PPi in the bloodstream is filtered by the glomerulus and mostly hydrolysed in the proximal tubule. The majority of PPi-generating reactions are intracellular, and there is a need in many of these reactions to immediately remove PPi in order to enable the reaction to proceed without inhibition by end-products (see below). These facts together suggest that much urinary PPi is locally generated within the kidney. However, the proportion of locally generated and effluxed PPi versus filtered or luminally produced PPi is unknown.

Although Gurley *et al.* (2006b) claimed to be the first to demonstrate actual membrane transport of PPi by ANK, they were unable to measure PPi efflux from oocytes. They postulated, but did not prove, that the membrane localisation and the transporter structure of ANK allowed it to function either as a PPi transporter itself, or as a regulator of a PPi transporter already present in oocyte membranes. Although the present work was also unable to show efflux from oocytes, the data from the yeast two-hybrid protein interactions and whole-genome regulation experiments are now able to throw some light on possible functions of ANK in the collecting duct.

7.1.2 Drawbacks of using the oocyte expression system for PPi flux experiments

A major part of this thesis was the use of the oocyte expression system of Gurdon *et al.* (1971) for heterologous overexpression of ANK. This robust functional model allows expression of almost any protein, but no significant influx/efflux was found despite

confirmation of membrane localisation. Flux experiments in oocytes (Chapter 5) were complicated by significant technical problems when using PPi as a substrate. Oocytes are large cells, so the initial influx rate could be subsequently limited by intracellular diffusion. ANK may be present on the intracellular membranes of the numerous yolk platelets of the oocyte, causing compartmentalisation of injected PPi and inhibition of efflux. The size of these cells may mean that they are able to rapidly buffer or metabolise injected PPi, reducing apparent efflux. Finally, oocyte systems are less suitable when the transporter K_m is below the minimum substrate concentration needed to achieve robustly detectable specific activity when using radiolabelled substrates.

7.1.3 Production of PPi and the importance of membrane transport

PPi is a small, highly charged molecule that is produced by about 190 biochemical reactions (Heinonen, 2001), including the synthesis of DNA, RNA, amino acids, proteins and lipids, and participates in the regulation of several metabolic reactions. The reaction ATP → AMP + PPi liberates 20 kJ/mol more energy than ATP → ADP + Pi (Heinonen, 2001). Therefore synthetic reactions progress more favourably when coupled to the formation of PPi from ATP (or other nucleotide triphosphates). For this process to continue, the PPi end-product must be rapidly removed from the reaction, shifting the equilibrium in favour of the reaction products rendering the reaction irreversible. PPi removal is likely to occur in more than one way, such as by pyrophosphatases, spontaneous hydrolysis or membrane transport. Until recent work on the peroxisome was published (Visser *et al.*, 2005), studies have overlooked the possibility that PPi could be removed by transport across membranes. This is particularly surprising because PPi transport between compartments has been implicitly assumed in cellular work since the 1960s, but no mechanism was put forward until the discovery of the ANK protein by Ho *et al.* (2000).

ANK mRNA is ubiquitous in tissues and evolutionarily highly conserved in vertebrates, strongly suggesting that it has an important role in cell function that is not restricted to calcified tissues. It is present on intracellular and extracellular membranes (see below). Most published work has concentrated on the role of ANK in bone metabolism, supported by good evidence of the clinical effects on bones and joints occurring in the ANK null (Gurley *et al.*, 2006a) and homozygous Phe377del (Chen *et al.*, 2009) mouse models. The present hypothesis, based on work performed in mouse kidney (Carr *et al.*, 2007) and outlined in Moochhala *et al.* (Moochhala *et al.*, 2008) investigates for the first time the role of ANK in the kidney, another system in which the regulation of crystallisation is crucial.

However it is important to consider that the role of ANK in pyrophosphate transport/metabolism may be equally important in other systems and especially in the intracellular environment. Finally, no data exist on the regulation of ANK, acutely or in the longer term. Information about regulation can help to elucidate protein function under different physiological conditions.

7.2 Function of ANKH in the distal nephron

7.2.1 Role of ANK at the plasma membrane of collecting ducts

Plasma membrane expression of ANKH in human kidney has been confirmed by Western blot and immunofluorescence. Our experiments confirmed that ANK was present at both apical and basal membranes of collecting duct cells, and a mouse cell model revealed increased traffic of ANK to the apical membrane in response to stimulation with AVP. PPi influx via ANKH is neither physiologically relevant nor supported by our data in any meaningful way, especially since a relatively large oocyte-surface PPase activity was detected. However, no consistent and significant increase in efflux of labelled PPi in ANK-injected over water-injected oocytes was detected, despite positive localisation by immunofluorescence.

Very little free PPi is likely to exist in the cytosol under normal conditions since most intracellular PPi is compartmentalised into organelles (Davidson & Halestrap, 1988) and highly active pyrophosphatases exist (Shatton *et al.*, 1981). Since relatively large amounts of PPi were injected into oocytes, the lack of detectable efflux or leak is an important finding. Apart from technique limitations, possible mechanistic explanations include a requirement for: activation by one or more proteins; multiple subunits forming a functional channel (for example, as in the case of the epithelial sodium transporter ENaC); activation by an agonist; or ANK being a regulator for an adjacent transporter or channel.

7.2.2 Evidence for an interacting partner protein

The presence of a required partner protein can lead to a large increase in function. For example, Kowalczuk *et al.* (2008) demonstrated a 10-fold augmentation of amino acid flux due to the transporter hBAT1 in oocytes, in the presence of a relatively smaller amount of partner protein (25 ng BAT1 transporter + 10 ng ACE2, after optimisation). Wang *et al.* (2009) suggest that the dominant nature of ANK mutations in both CMD and familial CPPDD (Table 1.1) suggests an interaction with another component. ANK is present in many tissues (section 1.4.4.3) and might therefore have more than one interactor.

The distal tubular sodium/phosphate transporter PiT-1 (SLC20A1) has been shown to co-immunoprecipitate ANKH (Wang *et al.*, 2009), but we did not detect this interaction using the N-terminal ANK fragment as bait in a yeast two-hybrid screen. Since the location of the interacting domain is unclear, this interaction is not excluded by our findings, although Wang *et al.* did show that the M48T (likely N-terminal) mutation in ANK prevented its co-immunoprecipitation with PiT-1. Indeed, given that the N-terminal has been successfully used for GFP (Carr *et al.*, 2007) and FLAG (section 2.3.3.4) tags, it is possible that a C-terminal interaction site could have resulted in further physiologically relevant interactions. In addition, yeast two-hybrid interactions occur within the cytosol and may possibly exclude membrane proteins.

Evidence of protein-protein interaction is not the same as proof of coupled function. Thus Wang *et al.*'s findings are unlikely to suggest that PiT-1 is the actual PPi transporter with ANK acting as a regulator or cofactor, since they did not prove that ANK binds directly to PiT-1 (Wang *et al.*, 2009) and the highly charged nature of PPi makes it improbable that it could share a common membrane transporter with Pi. In contrast, the interaction of SLC27A2 with ANK (section 5.3.7.3), together with its intracellular localisation, kidney expression and lack of membrane-associated PPase, suggests that ANK is a candidate peroxisomal membrane PPi transporter. PPi export to the cytosol rather than enzyme-mediated PPi hydrolysis has physiological utility in this location, but this PPi flux from vesicle to cytosol would not be detectable by radiolabelled PPi injected into the cytosol. We have so far found no evidence that a similar metabolic construct occurs at the plasma membrane to give rise to extracellular PPi export.

7.2.3 Regulatory mechanisms and possible linkage of PPi and calcium membrane transport

Our results and those of others (section 6.3.3.4) suggest that regulation by AVP occurs acutely (over minutes) rather than chronically. Although our collecting duct model was limited by cellular heterogeneity, clear apical trafficking of ANK was demonstrated in response to AVP. Despite this, the results of the expression profile and quantitative PCR were more equivocal, suggesting that regulation by AVP may not occur via transcriptional regulation. Alternatives could include movement of vesicles, similar to that of AQP2 regulation, phosphorylation, other compartmentalisation in the cell, or the effect of extracellular nucleotides, which are capable of downregulating AQP2 in this cell line (Wildman *et al.*, 2009).

These alternative possibilities may be linked to other transport mechanisms. Davidson & Halestrap (1988) found that intra-mitochondrial PPi concentration in hepatocytes was increased by stimulation with gluconeogenic hormones such as glucagon and AVP. AVP produced a much larger increase in intracellular PPi concentration than glucagon. Interestingly, AVP's effect was abolished in the absence of extracellular calcium ions, despite the fact that AVP is capable of releasing intracellular calcium stores by itself. These facts raise the possibility that membrane transport of calcium and PPi may be linked in these cells.

In rat renal collecting duct cells, Goel *et al.* (Goel *et al.*, 2007) showed that the apically located calcium channel TRPC3 colocalised with AQP2 in intracellular vesicles and trafficked to the apical membrane in response to AVP. They also demonstrated transepithelial calcium flux due to TRPC3 at the apical membrane. Not only is this an example of co-ordinated regulation of AQP2 with another apical membrane transporter, but by allowing a reduction of luminal calcium concentration at times of increased water reabsorption, it may contribute to the prevention of luminal calcium crystallisation. In contrast, the apical calcium receptor (CaR) in rat IMCD contributes to a reduction in AVP effect, limiting apical water permeability when luminal calcium rises (Sands *et al.*, 1997). Similarly, our evidence for co-ordinated acute regulation of ANK and AQP2 (see section 6.2.1.1) would have physiological utility by increasing luminal PPi concentration. Combining these mechanisms links aspects of calcium, PPi and water transport at the apical membrane of the collecting duct, via regulation by AVP.

7.2.4 Source of PPi in the collecting duct

The origin of PPi available for efflux into the collecting duct lumen remains unclear. Evidence obtained from other tissues suggests that the cytosolic PPi concentration is likely to be low. Since most PPi in liver is produced in the mitochondria (Davidson & Halestrap, 1988), it is likely that PPi would be exported from the mitochondria to the cytosol. Here, PPi may be hydrolysed (PPi survived for less than 0.5 s in bacteria (p. 23 in (Heinonen, 2001)) by cytosolic PPases. On the other hand, enough PPi-generating reactions may occur in the cytosol at the apical aspect of the cell to allow adequate substrate for PPi efflux. PPi may also locally buffer calcium ions, for example in the primary cilium (as suggested in (Carr *et al.*, 2009)), although too high concentrations of calcium or PPi would cause precipitation of insoluble CaPPi. Cytosolic PPi could also be transported across membranes into other cellular compartments, or out of the cell into the tubular lumen, these processes

requiring a membrane PPi transporter acting intracellularly as well as on the plasma membrane. Carr *et al.* (2007) showed in mIMCD-3 cells using a GFP-tagged ANK construct that ANK is present in intracellular membranes such as endoplasmic reticulum, Golgi, acidic endosomes and especially in mitochondria. ANK in these locations could allow movement of PPi across these membranes. Thus PPi may have roles in calcium binding and hence compartmentalisation of both calcium and itself. Our finding of an association between ANK and calbindin-D_{28K} under AVP-stimulation is consistent with this, although the mechanism is unclear.

7.3 Summary of ANKH function in the collecting duct

7.3.1 Summary of main findings of this thesis

1. ANKH mRNA is expressed in humans, and ANKH protein is present in human kidney, where it localises to the collecting duct and is present in both principal and α-intercalated cells. ANKH is present at both apical and basolateral membranes in these locations. Expression in other nephron locations is less evident. This places ANKH in the most useful location for its proposed function in the limitation of calcium crystal formation.

2. An ANKH-NT-3XFLAG fusion construct was overexpressed in the membrane of *Xenopus* oocytes, with little or no expression occurring in the cytoplasm. Purity of oocyte membrane fractions using Western blotting, and exact localisation of the plasma membrane using immunofluorescence, were confirmed by detection of overexpression of the membrane protein CD98. Colocalisation of the ANKH-FLAG construct with CD98 confirmed that the ANKH construct was localised to the oocyte plasma membrane. This finding verified that ANKH, cloned into the pcDNA3.1 vector used in these experiments, was expressed in the oocyte membrane without the need for a β-globin gene, as previously suggested by Gurley *et al.* (2006b), and could therefore be used in functional experiments.

3. The Kingsley group (Gurley *et al.*, 2006b) had apparently demonstrated influx of PPi into ANKH-overexpressing *Xenopus* oocytes, but meaningful and reproducible PPi influx was not confirmed here. In contrast to Gurley's results, hydrolysis of PPi at the oocyte surface was confirmed using a highly sensitive PPi assay at a rate of ~13 pmol/oocyte/h. Similarly, no significant or consistent PPi efflux was observed

from ANKH-expressing oocytes pre-injected with radiolabelled PPi, despite a satisfactory positive efflux control experiment using the transported organic dye Lucifer yellow. A genome-wide screen was performed using the yeast two-hybrid method, in which an N-terminal ANK fragment was bait and a mouse kidney cDNA library was prey. This suggested potential interacting proteins, of which SLC27A2 was most likely to be a genuine result and which catalyses a reaction that generates PPi.

These results for PPi influx and hydrolysis conflict strongly with those of Gurley *et al.* The lack of any detectable PPi transmembrane flux in this system may be explained by pyrophosphatase activity (hydrolysis) or by the necessity for a binding partner. Since pyrophosphatase activity is not known in peroxisomes, the ANKH/SLC27A2 complex may be a candidate protein for the putative peroxisomal membrane PPi transporter.

4. AVP stimulation of mpkCCD$_{cl4}$ cell monolayers showed marked apical localisation of AQP2 in 6.6% of cells, with apical localisation of ANK in 1.8% of a different population of cells in the same monolayer. AVP stimulation resulted in colocalisation between ANK and calbindin-D$_{28K}$ also at the apical membrane. The change in pattern of gene expression after AVP treatment in these monolayers was determined using expression profiling. This showed a 3.4-fold increase in *AQP2* expression and a 1.4-fold increase in *ANK* expression. Attempted verification of these results using quantitative RT-PCR revealed a normalised fold change of 0.9 for *ANK*, with a lack of detectable AQP2 in untreated cells preventing fold change calculation for *AQP2*.

   Despite the obvious heterogeneity in the mpkCCD$_{cl4}$ cell line, apical trafficking of ANK occurs in response to AVP, in support of the hypothesis. Similar results obtained with calbindin suggest that ANK function may not be restricted to the collecting duct. Although the expression of *ANK* was increased on the microarray in response to AVP, this was not observed using quantitative RT-PCR. This may imply that changes in expression occur more transiently than in these experiments, or that altered trafficking is a more important regulator in this situation than transcriptional upregulation.

7.3.2 A model of ANKH function

Using the data obtained from this thesis as well as published data allows a model to be suggested for ANKH function in the collecting duct cell (Figure 7.1). Four possible roles for ANKH are outlined.

Intracellularly, ANKH and SLC27A2 form a functional couple that moves PPi produced in peroxisomes into the cytosol as described in section 5.3.7.3. Mitochondria produce PPi in synthetic reactions (Davidson & Halestrap, 1988); p. 61 in Heinonen (2001)) and ANK is detectable on the mitochondrial membrane in inner medullary collecting duct cells (Carr *et al.*, 2007). ANKH may function in this location to rapidly remove PPi from the mitochondria to allow reactions to proceed. Once in the cytosol, PPi can be hydrolysed by cytosolic pyrophosphatases. Similar processes may occur in other organelles, and indeed ANK is detectable in the membranes of acidic endosomes in mouse collecting duct cells (Carr *et al.*, 2007). Another possibility is that ANKH may act in reverse to store PPi from the cytosol in intracellular vesicles, which are then trafficked apically, fusing with the membrane. In this way, ANKH would eventually arrive at the apical membrane and the PPi load would be discharged luminally.

In the collecting duct cell, AVP activates the basal V_2 receptor. During the resulting production of cAMP, a contribution to cytosolic PPi is made. ANKH, as well as AQP2, is acutely regulated by AVP. AQP2 channels in vesicles migrate and fuse with the apical membrane (Nielsen *et al.*, 2002). ANKH may be transported to the membrane by a similar mechanism, either in the same vesicles as AQP2 (as is the case with the apical calcium transporter TRPC3 in these cells), in different vesicles or via a chaperone molecule. However, the former possibility is less likely given that ANK was not present in the AQP2 vesicle proteome (Barile *et al.*, 2005). Calbindin-D28K, also present in the collecting duct (Roth *et al.*, 1982), may be involved in this process, perhaps as a chaperone when it is recycled to the apical membrane. ANK requires a partner protein (possibly itself a channel) at the apical membrane in order to function and allow exit of PPi, but its identity is unknown.

The interaction of ANKH with PiT-1 (Wang *et al.*, 2009) has been demonstrated in murine chondrocytes. A proposed mechanism is outlined by (Wang *et al.*, 2005), and allows the re-entry of Pi arising from breakdown of PPi previously exported by ANKH. This is directed at the stimulation of TNAP activity at the cell surface which reduces the PPi concentration of the matrix to promote bone formation. This is less relevant in the kidney as TNAP is more

prevalent in proximal segments. Although PiT-1 is likely to be located basolaterally (Collins *et al.*, 2004), basolateral PPi export would reduce calcification in the renal interstitium which is a known mechanism of stone formation (Sayer *et al.*, 2004). Of note, PiT-1 is inhibited by alkaline pH (Collins *et al.*, 2004), which would limit influx of TNAP-produced Pi via PiT-1 under conditions favouring calcium phosphate stone formation.

In parallel studies in our laboratory (Carr *et al.*, 2009), ANK was found to localise to cilia and basal body in mouse kidney tissue and two collecting duct cell lines. Cilia are chemosensors and ciliated collecting duct epithelia demonstrate large increases in intracellular calcium in response to mechanical deformation (Praetorius & Spring, 2003). There is a need for rapid buffering of calcium activity, and this interesting intracellular location suggests a role for PPi delivered locally via ANKH.

7.3.3 Final conclusions

At a molecular level, these findings offer the first insight into how PPi might be transported across membranes in humans, and suggest that ANKH is likely to function as a PPi transporter in an obligatory manner as part of a protein complex. In this way, intact PPi can be compartmentalised, preserving it for use within vesicular structures elsewhere in the cell or in the extracellular medium in a more energy-efficient way than by first hydrolysing it to orthophosphate. More generally, the lack of data on PPi in mammalian cellular energetics may arise from the existence of PPi only transiently as an intermediate in tightly spatially coupled biochemical reactions.

7.4 Future work

The observations can be taken forward in several important directions. PPi transport could be accurately measured using the highly-sensitive fluorescence assay in cell layers of collecting duct cell lines under various conditions. Flux experiments using techniques such as HPLC or mass spectrometry would improve upon radioactive tracer studies by specifically identifying intact PPi. Regulation by alteration of gene transcription over longer periods of time needs to be investigated, and may result in an increase in the amount of ANKH protein rather than trafficking of existing protein. Since gene regulation occurs in response to Pi or PPi levels (Harmey *et al.*, 2004; Wang *et al.*, 2009), it is possible that high levels of injected PPi may actually reduce gene transcription. Co-immunoprecipitation of ANK might help to confirm interacting proteins.

Clinical studies of the urine of calcium stone formers would need to be preceded by studies of urinary PPi using the highly-sensitive fluorescence assay. Initial attempts at this have been limited by interference due to urochrome (urobilin), and ion exchange methods may be useful in purifying PPi in urine samples. A key question is whether hypopyrophosphaturia is a metabolic risk factor for calcium stone formation, or merely an effect of depletion of PPi levels in patients who form stones. Such a study might include proteomic measurement of ANKH present in urinary exosomes of stone forming patients and normal controls, to determine a positive (cause) or negative (effect) correlation between urinary PPi and ANKH levels. If hypopyrophosphaturia persists even when hypercalciuria is treated, it may be a risk factor for calcium stone formation. This risk factor may be potentially modifiable by therapy with bisphosphonates, a commonly used stable analogue of PPi.

Figure 7.1 Potential roles of ANK in the principal cell of the renal collecting duct

(A) Intracellular: PPi is produced in the cytosol as a result of biochemical reaction inside organelles, coupled to ANK in the organelle membrane. Most PPi is rapidly degraded by intracellular PPases, but potentially PPi could be also compartmentalised into vesicles that could discharge PPi apically.

(B) Apical membrane: AVP activates the basolateral V_2 receptor, generating PPi and stimulating the movement of vesicles containing AQP2 to the apical surface. These vesicles may also contain ANK along with calcium channels such as TRPC3, for eventual fusion with the apical membrane. Alternatively, ANK may exist inside its own vesicles, or be chaperoned to the membrane by the calcium-transporting protein calbindin-D_{28K}. At the apical surface, calbindin binds to calcium ions entering the cell via TRPV6 and is recycled. At the apical surface, ANK associates with its partner protein to enable PPi export into the lumen. This PPi is either cytosolic or arises as a reaction product of the partner protein.

(C) Basolateral membrane: ANK interacts with the sodium phosphate transporter PiT-1 (Type III NaPi, SLC20A1) allowing basal PPi export into the renal interstitium, with possible recycling of hydrolysed products. The ectoenzyme NPP1 allows local generation of PPi.

(D) Primary cilium: ANK present in the cilium and basal body allows release of PPi from vesicles to provide rapid local buffering of large calcium fluxes induced by cilial deformation.

Fig 7.1 here

(Gurdon *et al.*, 1971)

References

Ahmad N, Pratt JR, Potts DJ & Lodge JP (2006). Comparative efficacy of renal preservation solutions to limit functional impairment after warm ischemic injury. *Kidney Int* **69,** 884-893.

Bacallao RL, Sohrab S & Phillips CL (2006). Guiding Principles of Specimen Preservation for Confocal Fluorescence Microscopy. In *Handbook of biological confocal microscopy*. ed. Pawley JB, pp. 368-380. Springer Science and Business Media, New York.

Baldwin SA (2000). *Membrane transport*. Oxford University Press, Oxford ; New York.

Barile M, Pisitkun T, Yu MJ, Chou CL, Verbalis MJ, Shen RF & Knepper MA (2005). Large scale protein identification in intracellular aquaporin-2 vesicles from renal inner medullary collecting duct. *Mol Cell Proteomics* **4,** 1095-1106.

Baumann JM, Bisaz S, Felix R, Fleisch H, Ganz U & Russell RG (1977). The role of inhibitors and other factors in the pathogenesis of recurrent calcium-containing renal stones. *Clin Sci Mol Med* **53,** 141-148.

Baykov AA & Avaeva SM (1982). A sensitive method for measuring pyrophosphate in the presence of a 10,000-fold excess of orthophosphate using inorganic pyrophosphatase. *Anal Biochem* **119,** 211-213.

Benjamini Y & Hochberg Y (1995). Controlling the False Discovery Rate: A Practical and Powerful Approach to Multiple Testing. *Journal of the Royal Statistical Society. Series B (Methodological)* **57,** 289-300.

Bens M, Vallet V, Cluzeaud F, Pascual-Letallec L, Kahn A, Rafestin-Oblin ME, Rossier BC & Vandewalle A (1999). Corticosteroid-Dependent Sodium Transport in a Novel Immortalized Mouse Collecting Duct Principal Cell Line. *J Am Soc Nephrol* **10,** 923-934.

Bindels RJ (1993). Calcium handling by the mammalian kidney. *J Exp Biol* **184,** 89-104.

Bröer S, Schuster A, Wagner CA, Bröer A, Forster I, Biber J, Murer H, Werner A, Lang F & Busch AE (1998). Chloride Conductance and P i Transport are Separate Functions Induced by the Expression of NaPi-1 in Xenopus Oocytes. *Journal of Membrane Biology* **164,** 71-77.

Bruckner A, Polge C, Lentze N, Auerbach D & Schlattner U (2009). Yeast two-hybrid, a powerful tool for systems biology. *Int J Mol Sci* **10,** 2763-2788.

Canales BK, Leonard SM, Singh JA, Orzano IM, Zimmermann B, Weiland D, Monga M & Krug HE (2006). Spondyloarthropathy: an independent risk factor for kidney stones. *J Endourol* **20,** 542-546.

Carr G, Moochhala SH, Eley L, Vandewalle A, Simmons NL & Sayer JA (2009). The Pyrophosphate Transporter ANKH is Expressed in Kidney and Bone Cells and Colocalises to the Primary Cilium/Basal Body Complex. *Cellular Physiology and Biochemistry* **24,** 595-604.

Carr G, Sayer JA & Simmons NL (2007). Expression and localisation of the pyrophosphate transporter, ANK, in murine kidney cells. *Cell Physiology and Biochemistry* **20,** 507-516.

Chakraborty J, Below A & Solaiman D (2004). Tamm-Horsfall protein in patients with kidney damage and diabetes. *Urological Research* **32,** 79-83.

Charlton JAS, N.L. (1993). Established human renal cell lines: Phenotypic characteristics define suitability for use in in vitro models for predictive toxicology. *Toxicology in vitro* **7,** 129-136.

Chen IP, Wang CJ, Strecker S, Koczon-Jaremko B, Boskey A & Reichenberger EJ (2009). Introduction of a Phe377del mutation in ANK creates a mouse model for craniometaphyseal dysplasia. *J Bone Miner Res* **24,** 1206-1215.

Cheng J & Grande JP (2007). Cyclic Nucleotide Phosphodiesterase (PDE) Inhibitors: Novel Therapeutic Agents for Progressive Renal Disease. *Experimental Biology and Medicine* **232,** 38-51.

Collins JF, Bai L & Ghishan FK (2004). The SLC20 family of proteins: dual functions as sodium-phosphate cotransporters and viral receptors. *Pflugers Arch* **447,** 647-652.

Condeelis J (1995). Elongation factor 1 alpha, translation and the cytoskeleton. *Trends Biochem Sci* **20,** 169-170.

Corpet F (1988). Multiple sequence alignment with hierarchical clustering. *Nucleic Acids Res* **16,** 10881-10890.

Costa-Bauza A, Barcelo C, Perello J & Grases F (2002). Synergism between the brushite and hydroxyapatite urinary crystallization inhibitors. *Int Urol Nephrol* **34,** 447-451.

Costa-Bauza A, Isern B, Perello J, Sanchis P & Grases F (2005). Factors affecting the regrowth of renal stones in vitro: a contribution to the understanding of renal stone development. *Scand J Urol Nephrol* **39,** 194-199.

Cotton FA (1999). *Advanced inorganic chemistry*. Wiley, New York ; Chichester.

Dascal N, Landau EM & Lass Y (1984). Xenopus oocyte resting potential, muscarinic responses and the role of calcium and guanosine 3',5'-cyclic monophosphate. *The Journal of Physiology* **352,** 551-574.

Davidson AM & Halestrap AP (1988). Inorganic pyrophosphate is located primarily in the mitochondria of the hepatocyte and increases in parallel with the decrease in light-scattering induced by gluconeogenic hormones, butyrate and ionophore A23187. *Biochem J* **254,** 379-384.

Dong Hoon L, Soon Young K & Jong-In H (2004). A Fluorescent Pyrophosphate Sensor with High Selectivity over ATP in Water. *Angewandte Chemie* **116,** 4881-4884.

Dumont JN (1972). Oogenesis in Xenopus laevis (Daudin). I. Stages of oocyte development in laboratory maintained animals. *Journal of Morphology* **136,** 153-179.

Edashige K, Ohta S, Tanaka M, Kuwano T, Valdez DM, Hara T, Jin B, Takahashi S-i, Seki S, Koshimoto C & Kasai M (2007). The Role of Aquaporin 3 in the Movement of Water and Cryoprotectants in Mouse Morulae. *Biology of Reproduction* **77,** 365-375.

Einhauer A & Jungbauer A (2001). The FLAG(TM) peptide, a versatile fusion tag for the purification of recombinant proteins. *Journal of Biochemical and Biophysical Methods* **49,** 455-465.

Ernster L (1992). *Molecular mechanisms in bioenergetics*. Elsevier, Amsterdam ; New York.

Evan A, Lingeman J, Coe FL & Worcester E (2006). Randall's plaque: pathogenesis and role in calcium oxalate nephrolithiasis. *Kidney Int* **69,** 1313-1318.

Evan AP, Lingeman JE, Coe FL, Parks JH, Bledsoe SB, Shao Y, Sommer AJ, Paterson RF, Kuo RL & Grynpas M (2003). Randall's plaque of patients with nephrolithiasis begins in basement membranes of thin loops of Henle. *J Clin Invest* **111,** 607-616.

Falcone D & Andrews DW (1991). Both the 5' untranslated region and the sequences surrounding the start site contribute to efficient initiation of translation in vitro. *Mol. Cell. Biol.* **11,** 2656-2664.

Fernandes CF, Godoy JR, Doring B, Cavalcanti MC, Bergmann M, Petzinger E & Geyer J (2007). The novel putative bile acid transporter SLC10A5 is highly expressed in liver and kidney. *Biochem Biophys Res Commun* **361,** 26-32.

Fields S & Song O (1989). A novel genetic system to detect protein-protein interactions. *Nature* **340,** 245-246.

Fleisch H & Bisaz S (1962). Isolation from urine of pyrophosphate, a calcification inhibitor. *Am J Physiol* **203,** 671-675.

Flodgaard H & Fleron P (1974). Thermodynamic parameters for the hydrolysis of inorganic pyrophosphate at pH 7.4 as a function of (Mg2+), (K+), and ionic strength determined from equilibrium studies of the reaction. *J Biol Chem* **249,** 3465-3474.

Floyd RV, Mason SL, Proudman CJ, German AJ, Marples D & Mobasheri A (2007). Expression and nephron segment-specific distribution of major renal aquaporins (AQP1-4) in Equus caballus, the domestic horse. *Am J Physiol Regul Integr Comp Physiol* **293,** R492-503.

Forster IC, Traebert M, Jankowski M, Stange G, Biber Jr & Murer H (1999). Protein kinase C activators induce membrane retrieval of type II Na+-phosphate cotransporters expressed in Xenopus oocytes. *The Journal of Physiology* **517,** 327-340.

Fronius M, Bogdan R, Althaus M, Morty RE & Clauss WG (2010). Epithelial Na+ channels derived from human lung are activated by shear force. *Respiratory Physiology & Neurobiology* **170,** 113-119.

Goding JW, Grobben B & Slegers H (2003). Physiological and pathophysiological functions of the ecto-nucleotide pyrophosphatase/phosphodiesterase family. *Biochim Biophys Acta* **1638,** 1-19.

Goel M, Sinkins WG, Zuo C-D, Hopfer U & Schilling WP (2007). Vasopressin-induced membrane trafficking of TRPC3 and AQP2 channels in cells of the rat renal collecting duct. *Am J Physiol Renal Physiol* **293,** F1476-1488.

Gogarten JP, Kibak H, Dittrich P, Taiz L, Bowman EJ, Bowman BJ, Manolson MF, Poole RJ, Date T, Oshima T & et al. (1989). Evolution of the vacuolar H+-ATPase: implications for the origin of eukaryotes. *Proc Natl Acad Sci U S A* **86,** 6661-6665.

Graham FL, Smiley J, Russell WC & Nairn R (1977). Characteristics of a human cell line transformed by DNA from human adenovirus type 5. *J Gen Virol* **36,** 59-74.

Grases F, Ramis M & Costa-Bauza A (2000). Effects of phytate and pyrophosphate on brushite and hydroxyapatite crystallization. Comparison with the action of other polyphosphates. *Urol Res* **28,** 136-140.

Guo Y, Hsu DK, Feng SL, Richards CM & Winkles JA (2001). Polypeptide growth factors and phorbol ester induce progressive ankylosis (ank) gene expression in murine and human fibroblasts. *J Cell Biochem* **84,** 27-38.

Gurdon JB, Lane CD, Woodland HR & Marbaix G (1971). Use of frog eggs and oocytes for the study of messenger RNA and its translation in living cells. *Nature* **233,** 177-182.

Gurley KA, Chen H, Guenther C, Nguyen ET, Rountree RB, Schoor M & Kingsley DM (2006a). Mineral formation in joints caused by complete or joint-specific loss of ANK function. *J Bone Miner Res* **21,** 1238-1247.

Gurley KA, Reimer RJ & Kingsley DM (2006b). Biochemical and genetic analysis of ANK in arthritis and bone disease. *Am J Hum Genet* **79,** 1017-1029.

Harahap AR & Goding JW (1988). Distribution of the murine plasma cell antigen PC-1 in non-lymphoid tissues. *J Immunol* **141,** 2317-2320.

Harmey D, Hessle L, Narisawa S, Johnson KA, Terkeltaub R & Millan JL (2004). Concerted regulation of inorganic pyrophosphate and osteopontin by akp2, enpp1, and ank: an integrated model of the pathogenesis of mineralization disorders. *Am J Pathol* **164,** 1199-1209.

Hasler U, Mordasini D, Bens M, Bianchi M, Cluzeaud F, Rousselot M, Vandewalle A, Feraille E & Martin P-Y (2002). Long Term Regulation of Aquaporin-2 Expression in Vasopressin-responsive Renal Collecting Duct Principal Cells. *J. Biol. Chem.* **277,** 10379-10386.

Heinonen JK (2001). *Biological role of inorganic pyrophosphate*. Kluwer Academic, Boston ; London.

Hirsch D, Stahl A & Lodish HF (1998). A family of fatty acid transporters conserved from mycobacterium to man. *Proceedings of the National Academy of Sciences of the United States of America* **95,** 8625-8629.

Hirsch JR, Loo DDF & Wright EM (1996). Regulation of Na+/Glucose Cotransporter Expression by Protein Kinases in Xenopus laevis Oocytes. *Journal of Biological Chemistry* **271,** 14740-14746.

Ho AM, Johnson MD & Kingsley DM (2000). Role of the mouse ank gene in control of tissue calcification and arthritis. *Science* **289,** 265-270.

Hoenderop JG, Nilius B & Bindels RJ (2005). Calcium absorption across epithelia. *Physiol Rev* **85,** 373-422.

Hoenderop JGJ, Nilius B & Bindels RJM (2002). Molecular mechanism of active Ca^{2+} reabsorption in the distal nephron. *Annual Review of Physiology* **64,** 529-549.

Hooker BS, Bigelow DJ & Lin CT (2007). Methods for mapping of interaction networks involving membrane proteins. *Biochem Biophys Res Commun* **363,** 457-461.

Irizarry RA, Hobbs B, Collin F, Beazer-Barclay YD, Antonellis KJ, Scherf U & Speed TP (2003). Exploration, normalization, and summaries of high density oligonucleotide array probe level data. *Biostat* **4,** 249-264.

Jarolim P, Rubin HL, Zakova D, Storry J & Reid ME (1998). Characterization of seven low incidence blood group antigens carried by erythrocyte band 3 protein. *Blood* **92,** 4836-4843.

Jensen ME, Odgaard E, Christensen MH, Praetorius HA & Leipziger J (2007). Flow-Induced $[Ca^{2+}]i$ Increase Depends on Nucleotide Release and Subsequent Purinergic Signaling in the Intact Nephron. *J Am Soc Nephrol* **18,** 2062-2070.

Jung A, Bisaz S & Fleisch H (1973). The binding of pyrophosphate and two diphosphonates by hydroxyapatite crystals. *Calcif Tissue Res* **11,** 269-280.

Jung A, Russel RG, Bisaz S, Morgan DB & Fleisch H (1970). Fate of intravenously injected pyrophosphate-^{32}P in dogs. *Am J Physiol* **218,** 1757-1764.

Jutabha P, Kanai Y, Hosoyamada M, Chairoungdua A, Kim DK, Iribe Y, Babu E, Kim JY, Anzai N, Chatsudthipong V & Endou H (2003). Identification of a novel voltage-driven organic anion transporter present at apical membrane of renal proximal tubule. *J Biol Chem* **278,** 27930-27938.

Kamsteeg EJ & Deen PM (2001). Detection of aquaporin-2 in the plasma membranes of oocytes: a novel isolation method with improved yield and purity. *Biochem Biophys Res Commun* **282,** 683-690.

Kanai Y, Segawa H, Chairoungdua A, Kim JY, Kim DK, Matsuo H, Cha SH & Endou H (2000). Amino acid transporters: molecular structure and physiological roles. *Nephrol. Dial. Transplant.* **15,** 9-10.

Kedishvili NY, Goodwin GW, Popov KM & Harris RA (2000). Mammalian methylmalonate-semialdehyde dehydrogenase. *Methods Enzymol* **324,** 207-218.

Kedishvili NY, Popov KM, Rougraff PM, Zhao Y, Crabb DW & Harris RA (1992). CoA-dependent methylmalonate-semialdehyde dehydrogenase, a unique member of the aldehyde dehydrogenase superfamily. cDNA cloning, evolutionary relationships, and tissue distribution. *J Biol Chem* **267,** 19724-19729.

Kim SK, Lund J, Kiraly M, Duke K, Jiang M, Stuart JM, Eizinger A, Wylie BN & Davidson GS (2001). A gene expression map for Caenorhabditis elegans. *Science* **293,** 2087-2092.

Kocinsky HS, Dynia DW, Wang T & Aronson PS (2007). NHE3 phosphorylation at serines 552 and 605 does not directly affect NHE3 activity. *Am J Physiol Renal Physiol* **293,** F212-218.

Kohl B, Wagner CA, Huelseweh B, Busch AE & Werner A (1998). The Na+-phosphate cotransport system (NaPi-II) with a cleaved protein backbone: implications on function and membrane insertion. *The Journal of Physiology* **508,** 341-350.

Korkmaz C, Ozcan A & Akcar N (2005). Increased frequency of ultrasonographic findings suggestive of renal stones in patients with ankylosing spondylitis. *Clin Exp Rheumatol* **23,** 389-392.

Kowalczuk S, Broer A, Tietze N, Vanslambrouck JM, Rasko JEJ & Broer S (2008). A protein complex in the brush-border membrane explains a Hartnup disorder allele. *FASEB J.* **22,** 2880-2887.

Kunchaparty S, Palcso M, Berkman J, Velazquez H, Desir GV, Bernstein P, Reilly RF & Ellison DH (1999). Defective processing and expression of thiazide-sensitive Na-Cl cotransporter as a cause of Gitelman's syndrome. *Am J Physiol* **277,** F643-649.

Kurella M, Hsiao L-L, Yoshida T, Randall JD, Chow G, Sarang SS, Jensen RV & Gullans SR (2001). DNA Microarray Analysis of Complex Biologic Processes. *J Am Soc Nephrol* **12,** 1072-1078.

Lambers TT, Mahieu F, Oancea E, Hoofd L, de Lange F, Mensenkamp AR, Voets T, Nilius B, Clapham DE, Hoenderop JG & Bindels RJ (2006). Calbindin-D28K dynamically controls TRPV5-mediated Ca2+ transport. *Embo J* **25,** 2978-2988.

Laminski NA, Meyers AM, Sonnekus MI & Smyth AE (1990). Prevalence of hypocitraturia and hypopyrophosphaturia in recurrent calcium stone formers: as isolated defects or associated with other metabolic abnormalities. *Nephron* **56,** 379-386.

Lee HS, Kim YJ, Lee J-H & Kang SG (2009). Identification and Characterization of Inorganic Pyrophosphatase and PAP Phosphatase from Thermococcus onnurineus NA1. *J. Bacteriol.* **191,** 3415-3419.

Legato J, Knepper MA, Star RA & Mejia R (2003). Database for renal collecting duct regulatory and transporter proteins. In *Physiol. Genomics*, vol. 13, pp. 179-181.

Liu WM, Mei R, Di X, Ryder TB, Hubbell E, Dee S, Webster TA, Harrington CA, Ho MH, Baid J & Smeekens SP (2002). Analysis of high density expression microarrays with signed-rank call algorithms. *Bioinformatics* **18,** 1593-1599.

Lomashvili KA, Garg P, Narisawa S, Millan JL & O'Neill WC (2008). Upregulation of alkaline phosphatase and pyrophosphate hydrolysis: Potential mechanism for uremic vascular calcification. *Kidney Int* **73,** 1024-1030.

Lomashvili KA, Khawandi W & O'Neill WC (2005). Reduced plasma pyrophosphate levels in hemodialysis patients. *J Am Soc Nephrol* **16,** 2495-2500.

Mahowald ML, Krug H & Taurog J (1988). Progressive ankylosis in mice. An animal model of spondylarthropathy. I. Clinical and radiographic findings. *Arthritis Rheum* **31,** 1390-1399.

Manganiello V (2002). Short-term regulation of PDE4 activity. *Br J Pharmacol* **136,** 339-340.

Manoharan C, Wilson MC, Sessions RB & Halestrap AP (2006). The role of charged residues in the transmembrane helices of monocarboxylate transporter 1 and its ancillary protein basigin in determining plasma membrane expression and catalytic activity. *Mol Membr Biol* **23,** 486-498.

Mansilla F, Dominguez CAG, Yeadon JE, Corydon TJ, Burden SJ & Knudsen CR (2008). Translation elongation factor eEF1A binds to a novel myosin binding protein-C-like protein. *Journal of Cellular Biochemistry* **105,** 847-858.

March JG, Simonet BM & Grases F (2001). Determination of pyrophosphate in renal calculi and urine by means of an enzymatic method. *Clin Chim Acta* **314,** 187-194.

Marples D, Knepper MA, Christensen EI & Nielsen S (1995). Redistribution of aquaporin-2 water channels induced by vasopressin in rat kidney inner medullary collecting duct. *Am J Physiol Cell Physiol* **269,** C655-664.

Masereeuw R, Moons MM, Toomey BH, Russel FGM & Miller DS (1999). Active Lucifer Yellow Secretion in Renal Proximal Tubule: Evidence for Organic Anion Transport System Crossover. *Journal of Pharmacology and Experimental Therapeutics* **289,** 1104-1111.

Matousovic K, Tsuboi Y, Walker H, Grande JP & Dousa TP (1997). Inhibitors of cyclic nucleotide phosphodiesterase isozymes block renal tubular cell proliferation induced by folic acid. *Journal of Laboratory and Clinical Medicine* **130,** 487-495.

Mayr B & Montminy M (2001). Transcriptional regulation by the phosphorylation-dependent factor CREB. *Nat Rev Mol Cell Biol* **2,** 599-609.

McGilvery JD & Crowther JP (1954). The hydrolysis of the condensed phosphates. *Canadian Journal of Chemistry* **32,** 174–185.

McKee S, Pendleton A, Dixey J, Doherty M & Hughes A (2004). Autosomal dominant early childhood seizures associated with chondrocalcinosis and a mutation in the ANKH Gene. *Epilepsia* **45,** 1258-1260.

Miro A, Costas MJ, Garcia-Diaz M, Hernandez MT & Cameselle JC (1989). A specific, low Km ADP-ribose pyrophosphatase from rat liver. *FEBS Lett* **244,** 123-126.

Moochhala SH, Sayer JA, Carr G & Simmons NL (2008). Renal calcium stones: insights from the control of bone mineralization. *Exp Physiol* **93,** 43-49.

Moutairou K, Hayez N, Pohl V, Pattyn G & Pochet R (1996). Calbindin localization in African giant rat kidney (Cricetomys gambianus). *Biochim Biophys Acta* **1313,** 187-193.

Nalbant P, Boehmer C, Dehmelt L, Wehner F & Werner A (1999). Functional characterization of a Na+-phosphate cotransporter (NaPi-II) from zebrafish and identification of related transcripts. *J Physiol* **520 Pt 1,** 79-89.

Nielsen S, Frokiaer J, Marples D, Kwon TH, Agre P & Knepper MA (2002). Aquaporins in the kidney: from molecules to medicine. *Physiol Rev* **82,** 205-244.

Nouwen EJ & De Broe ME (1994). Human intestinal versus tissue-nonspecific alkaline phosphatase as complementary urinary markers for the proximal tubule. *Kidney Int Suppl* **47,** S43-51.

Nurnberg P, Thiele H, Chandler D, Hohne W, Cunningham ML, Ritter H, Leschik G, Uhlmann K, Mischung C, Harrop K, Goldblatt J, Borochowitz ZU, Kotzot D, Westermann F, Mundlos S, Braun HS, Laing N & Tinschert S (2001). Heterozygous mutations in ANKH, the human ortholog of the mouse progressive ankylosis gene, result in craniometaphyseal dysplasia. *Nat Genet* **28,** 37-41.

Nurnberg P, Tinschert S, Mrug M, Hampe J, Muller CR, Fuhrmann E, Braun HS & Reis A (1997). The gene for autosomal dominant craniometaphyseal dysplasia maps to chromosome 5p and is distinct from the growth hormone-receptor gene. *Am J Hum Genet* **61,** 918-923.

O'Neill WC, Sigrist MK & McIntyre CW (2010). Plasma pyrophosphate and vascular calcification in chronic kidney disease. *Nephrol Dial Transplant* **25,** 187-191.

Orlov SN, Aksentsev SL & Kotelevtsev SV (2005). Extracellular calcium is required for the maintenance of plasma membrane integrity in nucleated cells. *Cell Calcium* **38,** 53-57.

Pendleton A, Johnson MD, Hughes A, Gurley KA, Ho AM, Doherty M, Dixey J, Gillet P, Loeuille D, McGrath R, Reginato A, Shiang R, Wright G, Netter P, Williams C & Kingsley DM (2002). Mutations in ANKH cause chondrocalcinosis. *Am J Hum Genet* **71,** 933-940.

Pfaffl MW (2001). A new mathematical model for relative quantification in real-time RT-PCR. *Nucleic Acids Res* **29,** e45.

Phillips CL, Miller KJ, Filson AJ, Nurnberger J, Clendenon JL, Cook GW, Dunn KW, Overbeek PA, Gattone VH, 2nd & Bacallao RL (2004). Renal cysts of inv/inv mice

resemble early infantile nephronophthisis. *J Am Soc Nephrol* **15,** 1744-1755.

Praetorius HA & Spring KR (2003). The renal cell primary cilium functions as a flow sensor. *Curr Opin Nephrol Hypertens* **12,** 517-520.

Qiu SR, Wierzbicki A, Orme CA, Cody AM, Hoyer JR, Nancollas GH, Zepeda S & De Yoreo JJ (2004). Molecular modulation of calcium oxalate crystallization by osteopontin and citrate. *Proc Natl Acad Sci U S A* **101,** 1811-1815.

Rachow JW & Ryan LM (1988). Inorganic pyrophosphate metabolism in arthritis. *Rheum Dis Clin North Am* **14,** 289-302.

Reichenberger E, Tiziani V, Watanabe S, Park L, Ueki Y, Santanna C, Baur ST, Shiang R, Grange DK, Beighton P, Gardner J, Hamersma H, Sellars S, Ramesar R, Lidral AC, Sommer A, Raposo do Amaral CM, Gorlin RJ, Mulliken JB & Olsen BR (2001). Autosomal dominant craniometaphyseal dysplasia is caused by mutations in the transmembrane protein ANK. *Am J Hum Genet* **68,** 1321-1326.

Richards MR, Listenberger LL, Kelly AA, Lewis SE, Ory DS & Schaffer JE (2003). Oligomerization of the murine fatty acid transport protein 1. *J Biol Chem* **278,** 10477-10483.

Robert-Nicoud M, Flahaut M, Elalouf J-M, Nicod M, Salinas M, Bens M, Doucet A, Wincker P, Artiguenave Fo, Horisberger J-D, Vandewalle A, Rossier BC & Firsov D (2001). Transcriptome of a mouse kidney cortical collecting duct cell line: Effects of aldosterone and vasopressin. *Proceedings of the National Academy of Sciences of the United States of America* **98,** 2712-2716.

Roberts NB, Dutton J, Helliwell T, Rothwell PJ & Kavanagh JP (1992). Pyrophosphate in synovial fluid and urine and its relationship to urinary risk factors for stone disease. *Ann Clin Biochem* **29 (Pt 5),** 529-534.

Ronco P, Brunisholz M, Geniteau-Legendre M, Chatelet F, Verroust P & Richet G (1987). Physiopathologic aspects of Tamm-Horsfall protein: a phylogenetically conserved marker of the thick ascending limb of Henle's loop. *Adv Nephrol Necker Hosp* **16,** 231-249.

Rossier G, Meier C, Bauch C, Summa V, Sordat B, Verrey F & Kuehn LC (1999). LAT2, a New Basolateral 4F2hc/CD98-associated Amino Acid Transporter of Kidney and Intestine. *Journal of Biological Chemistry* **274,** 34948-34954.

Roth J, Brown D, Norman AW & Orci L (1982). Localization of the vitamin D-dependent calcium-binding protein in mammalian kidney. *Am J Physiol* **243,** F243-252.

Rubis B, Krozowski Z & Trzeciak WH (2006). Arginine vasopressin stimulates 11beta-hydroxysteroid dehydrogenase type 2 expression in the mineralocorticosteroid target

cells. *Molecular and Cellular Endocrinology* **256,** 17-22.

Rungroj N, Devonald MAJ, Cuthbert AW, Reimann F, Akkarapatumwong V, Yenchitsomanus P-t, Bennett WM & Karet FE (2004). A Novel Missense Mutation in AE1 Causing Autosomal Dominant Distal Renal Tubular Acidosis Retains Normal Transport Function but Is Mistargeted in Polarized Epithelial Cells. *Journal of Biological Chemistry* **279,** 13833-13838.

Russell RG (1976). Metabolism of inorganic pyrophosphate (PPi). *Arthritis Rheum* **19 Suppl 3,** 465-478.

Russell RG, Bisaz S, Donath A, Morgan DB & Fleisch H (1971). Inorganic pyrophosphate in plasma in normal persons and in patients with hypophosphatasia, osteogenesis imperfecta, and other disorders of bone. *J Clin Invest* **50,** 961-969.

Russell RG & Hodgkinson A (1966). The urinary excretion of inorganic pyrophosphate by normal subjects and patients with renal calculus. *Clin Sci* **31,** 51-62.

Ryan LM (2001). The ank gene story. *Arthritis Res* **3,** 77-79.

Ryan LM, Cheung HS & McCarty DJ (1981). Release of pyrophosphate by normal mammalian articular hyaline and fibrocartilage in organ culture. *Arthritis Rheum* **24,** 1522-1527.

Sampson HW, Davis RW & Dufner DC (1991). Spondyloarthropathy in progressive ankylosis mice: ultrastructural features of the intervertebral disk. *Acta Anat (Basel)* **141,** 36-41.

Sands JM, Naruse M, Baum M, Jo I, Hebert SC, Brown EM & Harris HW (1997). Apical extracellular calcium/polyvalent cation-sensing receptor regulates vasopressin-elicited water permeability in rat kidney inner medullary collecting duct. *J Clin Invest* **99,** 1399-1405.

Sayer JA, Carr G & Simmons NL (2004). Nephrocalcinosis: molecular insights into calcium precipitation within the kidney. *Clin Sci (Lond)* **106,** 549-561.

Sayer JA, Korkmaz C, Moochhala SH & Carr G (2008). ANKH polymorphisms, ankylosing spondylitis and renal stone disease (abstract). *J Am Soc Nephrol* **19,** 935A.

Sayer JA, Moochhala SH & Thomas DJ (2010). The medical management of urolithiasis. *Br J Med Surg Urol* **3,** 87-95.

Schaffer JE & Lodish HF (1994). Expression cloning and characterization of a novel adipocyte long chain fatty acid transport protein. *Cell* **79,** 427-436.

Schlatter E (2006). Who Wins the Competition: TRPV5 or Calbindin-D28K? *J Am Soc*

Nephrol **17,** 2954-2956.

Scott DA & Karniski LP (2000). Human pendrin expressed in Xenopus laevis oocytes mediates chloride/formate exchange. *Am J Physiol Cell Physiol* **278,** C207-211.

Shatton JB, Shah H, Williams A, Morris HP & Weinhouse S (1981). Activities and properties of inorganic pyrophosphate in normal tissues and hepatic tumors of the rat. *Cancer Res* **41,** 1866-1872.

Sidhu H, Gupta R, Thind SK & Nath R (1986). Inhibition of calcium oxalate monohydrate (COM) crystal growth by pyrophosphate, citrate and rat urine. *Urol Res* **14,** 299-303.

Silcox DC & McCarty DJ (1973). Measurement of inorganic pyrophosphate in biological fluids. Elevated levels in some patients with osteoarthritis, pseudogout, acromegaly, and uremia. *J Clin Invest* **52,** 1863-1870.

Simmons NL (1990). A cultured human renal epithelioid cell line responsive to vasoactive intestinal peptide. *Exp Physiol* **75,** 309-319.

Singh H & Poulos A (1988). Distinct long chain and very long chain fatty acyl CoA synthetases in rat liver peroxisomes and microsomes. *Arch Biochem Biophys* **266,** 486-495.

Steinberg SJ, Wang SJ, Kim DG, Mihalik SJ & Watkins PA (1999). Human Very-Long-Chain Acyl-CoA Synthetase: Cloning, Topography, and Relevance to Branched-Chain Fatty Acid Metabolism. *Biochemical and Biophysical Research Communications* **257,** 615-621.

Terkeltaub RA (2001). Inorganic pyrophosphate generation and disposition in pathophysiology. *Am J Physiol Cell Physiol* **281,** C1-C11.

Thukral SK, Nordone PJ, Hu R, Sullivan L, Galambos E, Fitzpatrick VD, Healy L, Bass MB, Cosenza ME & Afshari CA (2005). Prediction of Nephrotoxicant Action and Identification of Candidate Toxicity-Related Biomarkers. *Toxicol Pathol* **33,** 343-355.

Timms AE, Zhang Y, Bradbury L, Wordsworth BP & Brown MA (2003). Investigation of the role of ANKH in ankylosing spondylitis. *Arthritis Rheum* **48,** 2898-2902.

Tsui HW, Inman RD, Paterson AD, Reveille JD & Tsui FW (2005). ANKH variants associated with ankylosing spondylitis: gender differences. *Arthritis Res Ther* **7,** R513-525.

Van Winkle LJ (1993). Endogenous amino acid transport systems and expression of mammalian amino acid transport proteins in Xenopus oocytes. *Biochimica et Biophysica Acta (BBA) - Reviews on Biomembranes* **1154,** 157-172.

Vekaria RM, Shirley DG, Sevigny J & Unwin RJ (2006a). Immunolocalization of ectonucleotidases along the rat nephron. *Am J Physiol Renal Physiol* **290,** F550-560.

Vekaria RM, Unwin RJ & Shirley DG (2006b). Intraluminal ATP concentrations in rat renal tubules. *J Am Soc Nephrol* **17,** 1841-1847.

Verhulst A, Persy VP, Van Rompay AR, Verstrepen WA, Helbert MF & De Broe ME (2002). Osteopontin synthesis and localization along the human nephron. *J Am Soc Nephrol* **13,** 1210-1218.

Verkoelen CF & Verhulst A (2007). Proposed mechanisms in renal tubular crystal retention. *Kidney Int* **72,** 13-18.

Verstrepen WA, Persy VP, Verhulst A, Dauwe S & De Broe ME (2001). Renal osteopontin protein and mRNA upregulation during acute nephrotoxicity in the rat. *Nephrol Dial Transplant* **16,** 712-724.

Virkki LV, Biber J, Murer H & Forster IC (2007). Phosphate transporters: a tale of two solute carrier families. *Am J Physiol Renal Physiol* **293,** F643-654.

Visser WF, Van Roermund CW, Ijlst L, Hellingwerf KJ, Wanders RJA & Waterham HR (2005). Demonstration and characterization of phosphate transport in mammalian peroxisomes. *Biochem. J.* **389,** 717-722.

Wagner CA, Friedrich B, Setiawan I, Lang F & BrÃ¶er S (2000). The Use of Xenopus laevis Oocytes for the Functional Characterization of Heterologously Expressed Membrane Proteins. *Cellular Physiology and Biochemistry* **10,** 1-12.

Wang J, Tsui HW, Beier F & Tsui FWL (2009). The CPPDD-Associated ANKH M48T Mutation Interrupts the Interaction of ANKH with the Sodium/Phosphate Cotransporter PiT-1. *The Journal of Rheumatology* **36,** 1265-1272.

Wang W, Xu J, Du B & Kirsch T (2005). Role of the progressive ankylosis gene (ank) in cartilage mineralization. *Mol Cell Biol* **25,** 312-323.

Weber WM (1999). Endogenous Ion Channels in Oocytes of Xenopus laevis: Recent Developments. *Journal of Membrane Biology* **170,** 1-12.

Wikström B, Danielson BG, Ljunghall S, McGuire M & Russell RGG (1983). Urinary pyrophosphate excretion in renal stone formers with normal and impaired renal acidification *World Journal of Urology* **1,** 150-154.

Wildman SS, Boone M, Peppiatt-Wildman CM, Contreras-Sanz A, King BF, Shirley DG, Deen PM & Unwin RJ (2009). Nucleotides downregulate aquaporin 2 via activation of apical P2 receptors. *J Am Soc Nephrol* **20,** 1480-1490.

Williams CJ, Zhang Y, Timms A, Bonavita G, Caeiro F, Broxholme J, Cuthbertson J, Jones Y, Marchegiani R, Reginato A, Russell RG, Wordsworth BP, Carr AJ & Brown MA (2002). Autosomal dominant familial calcium pyrophosphate dihydrate deposition disease is caused by mutation in the transmembrane protein ANKH. *Am J Hum Genet* **71,** 985-991.

Yu M-J, Miller RL, Uawithya P, Rinschen MM, Khositseth S, Braucht DWW, Chou C-L, Pisitkun T, Nelson RD & Knepper MA (2009). Systems-level analysis of cell-specific AQP2 gene expression in renal collecting duct. *Proceedings of the National Academy of Sciences* **106,** 2441-2446.

Zajac A, Baek SH, Salhab I, Radecki MA, Kim S, Hakonarson H & Nah HD (2010). Novel ANKH mutation in a patient with sporadic craniometaphyseal dysplasia. *Am J Med Genet Part A* **152A,** 770-776.

Zampighi GA, Kreman M, Boorer KJ, Loo DD, Bezanilla F, Chandy G, Hall JE & Wright EM (1995). A method for determining the unitary functional capacity of cloned channels and transporters expressed in Xenopus laevis oocytes. *J Membr Biol* **148,** 65-78.

Zhang J, Guo H, Mi Z, Gao C, Bhattacharya S, Li J & Kuo PC (2009). EF1A1-actin interactions alter mRNA stability to determine differential osteopontin expression in HepG2 and Hep3B cells. *Exp Cell Res* **315,** 304-312.

Zhang X, Odom DT, Koo S-H, Conkright MD, Canettieri G, Best J, Chen H, Jenner R, Herbolsheimer E, Jacobsen E, Kadam S, Ecker JR, Emerson B, Hogenesch JB, Unterman T, Young RA & Montminy M (2005). Genome-wide analysis of cAMP-response element binding protein occupancy, phosphorylation, and target gene activation in human tissues. *Proceedings of the National Academy of Sciences of the United States of America* **102,** 4459-4464.

Zhang Y & Brown MA (2005). Genetic studies of chondrocalcinosis. *Curr Opin Rheumatol* **17,** 330-335.

Ziganshin AU, Ziganshina LE, King BE & Burnstock G (1995). Characteristics of ecto-ATPase of Xenopus oocytes and the inhibitory actions of suramin on ATP breakdown. *Pflugers Arch* **429,** 412-418.

Appendix

Appendix 1 (following pages): Full list of genes differentially expressed on AVP-stimulation of mpkCCD$_{cl4}$ cells.
The list was generated by performing unpaired t-testing (accepting significance at $p < 0.05$) and selecting for fold change (FC) > 1.18, ordering by increasing fold change. The direction of gene regulation under AVP-stimulated conditions relative to control is given. Each line represents a probeset that meets these criteria.

Appendix 1 goes here

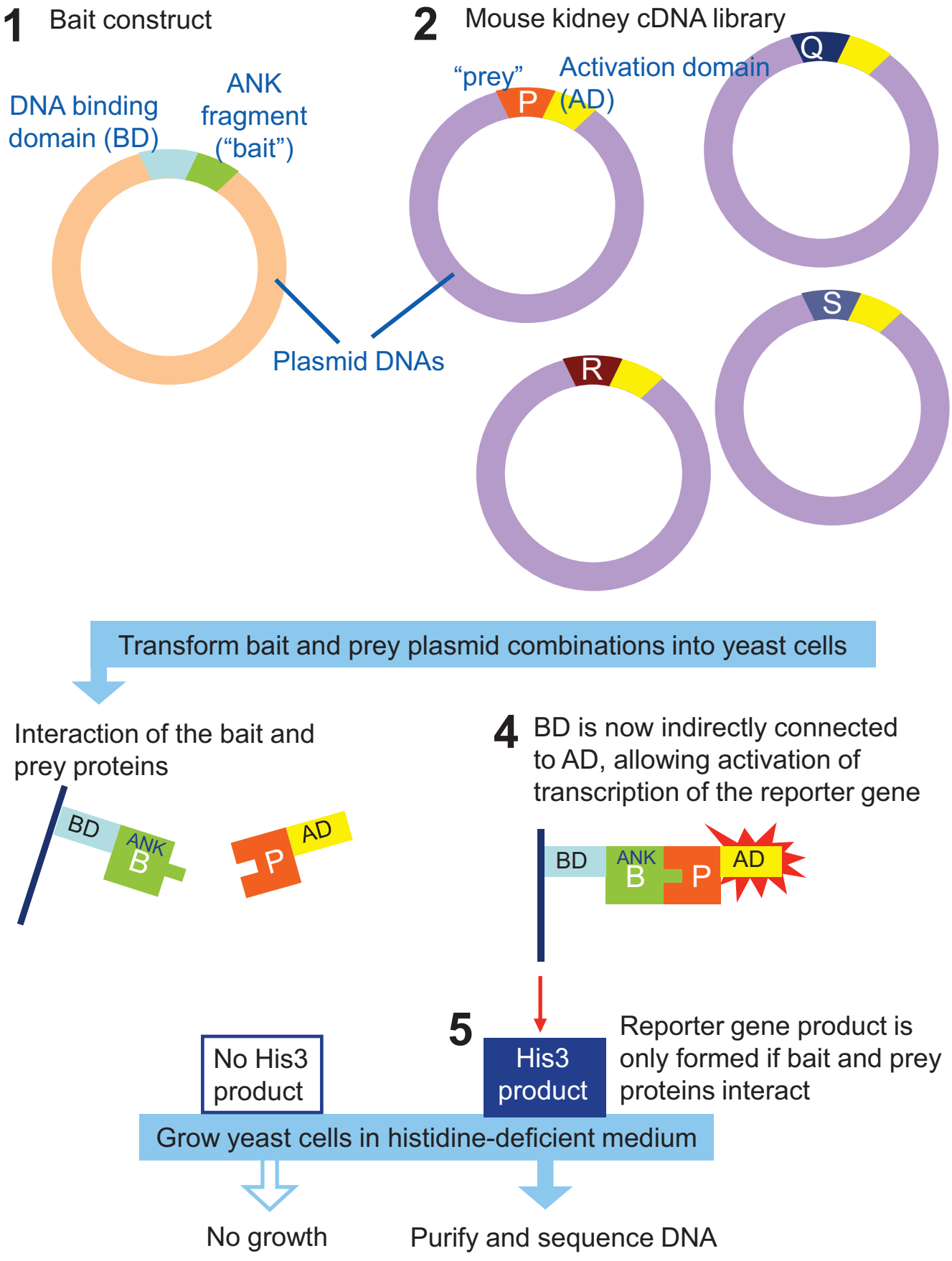
1
Bait construct
DNA binding domain (BD)
ANK fragment ("bait")
2
Mouse kidney cDNA library
"prey"
Activation domain (AD)
P
Q
S
R
Plasmid DNAs
Transform bait and prey plasmid combinations into yeast cells
3
Interaction of the bait and prey proteins
BD
ANK
B
P
AD
4
BD is now indirectly connected to AD, allowing activation of transcription of the reporter gene
5
No His3 product
His3 product
Reporter gene product is only formed if bait and prey proteins interact
Grow yeast cells in histidine-deficient medium
No growth
Purify and sequence DNA

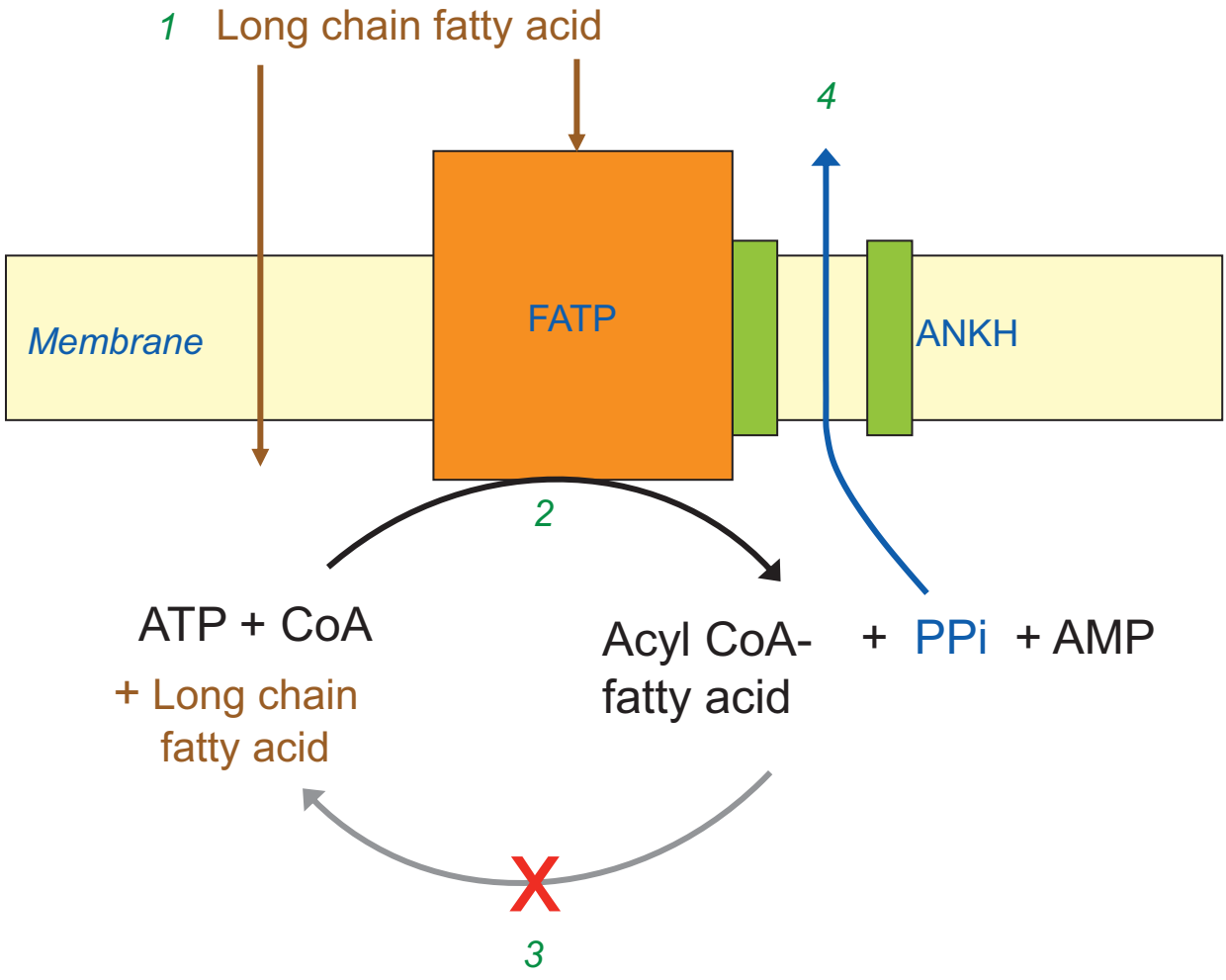

Figure 5.14 Possible interaction between FATP and ANKH. Long chain fatty acids diffuse or are transported across the membrane by FATP (**1**). An associated acyl CoA synthetase catalyses the esterification of the fatty acid (**2**). Energy comes from ATP, and produces PPi. To prevent reversal of this reaction (**3**), PPi must be immediately removed, possibly by compartmentalisation across the membrane via ANKH (**4**).

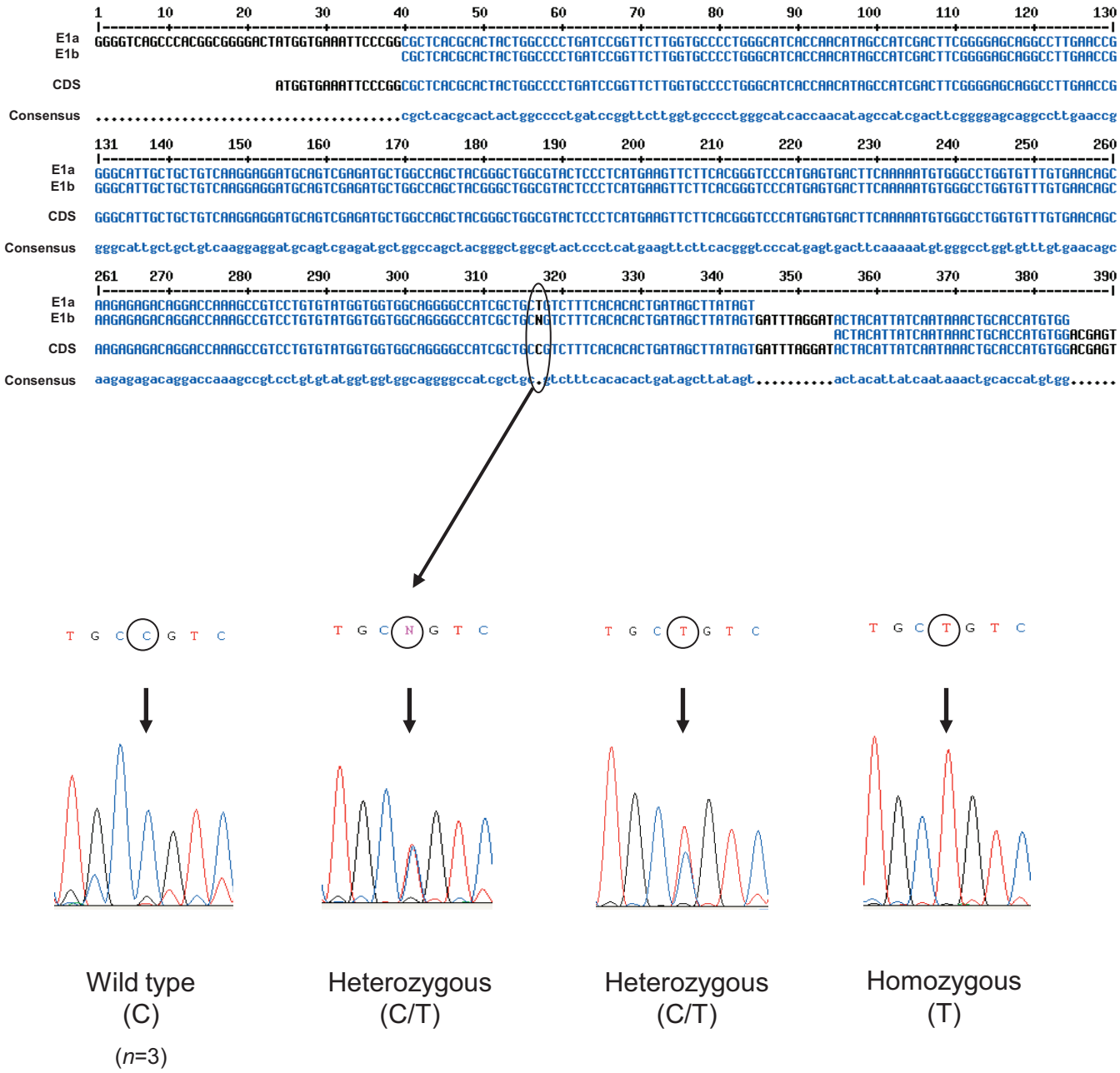

Figure 3.7 Detection of a single nucleotide polymorphism in ANKH coding sequence in six human subjects. Part of the contiguous nucleotide sequence for one of the subjects is shown (above). This fragment was sequenced twice (E1a, E1b) using different primer sets, and is aligned with the ANKH coding sequence NM054027. Extracts from sequencing chromatograms (below) show that the nucleotide at position 294 (317 on sequence above) was either a cytosine (C) or thymine (T), or both alleles were present. The resulting codons GCC or GCT are synonymous for alanine at residue position 97. This SNP is annotated as RS17251667.

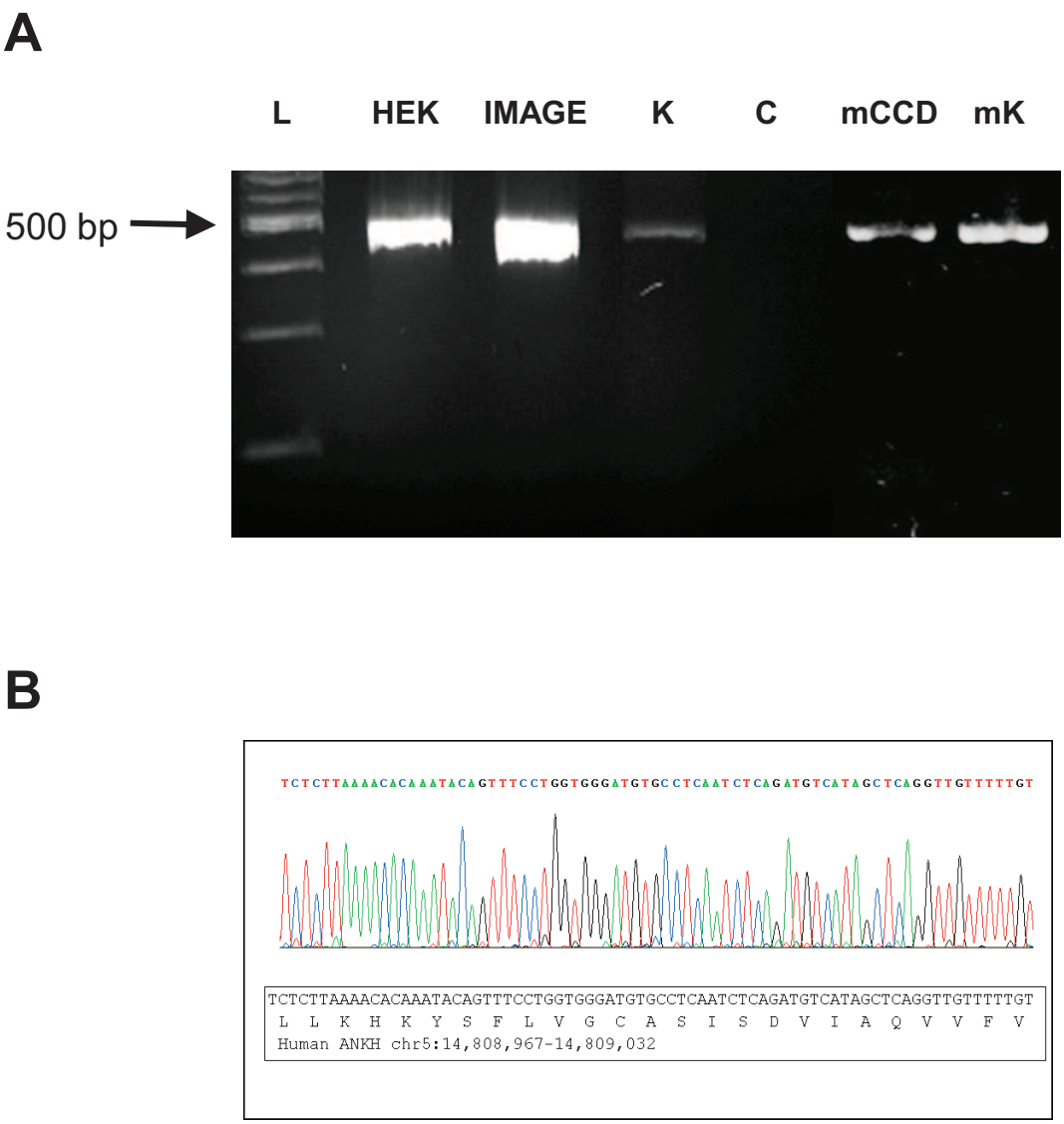

Figure 3.4 Expression of an ANK amplification product in human kidney cell line and tissue

(**A**) RT-PCR of an internal (490bp) ANK product. mRNA expression is observed in human embryonic kidney (HEK293) cells (**HEK**) and human renal cortex (**K**). IMAGE clone 3927236 cDNA (Geneservice) containing human full length ANK coding sequence (**IMAGE**) is the positive control. The water control (**C**) and ladder (**L**) in 100bp steps are also shown. Comparison with results for the mouse collecting duct cell line mpkCCD$_{cl4}$ (**mCCD**) and mouse kidney tissue (**mK**) (run on a separate gel) are shown. RT negative and RNA negative controls have been omitted.

(**B**) Example of sequencing chromatogram for product from HEK293 cells. Identity of PCR products was confirmed by direct sequencing. Identical sequencing was observed for human renal cortex and IMAGE clone.

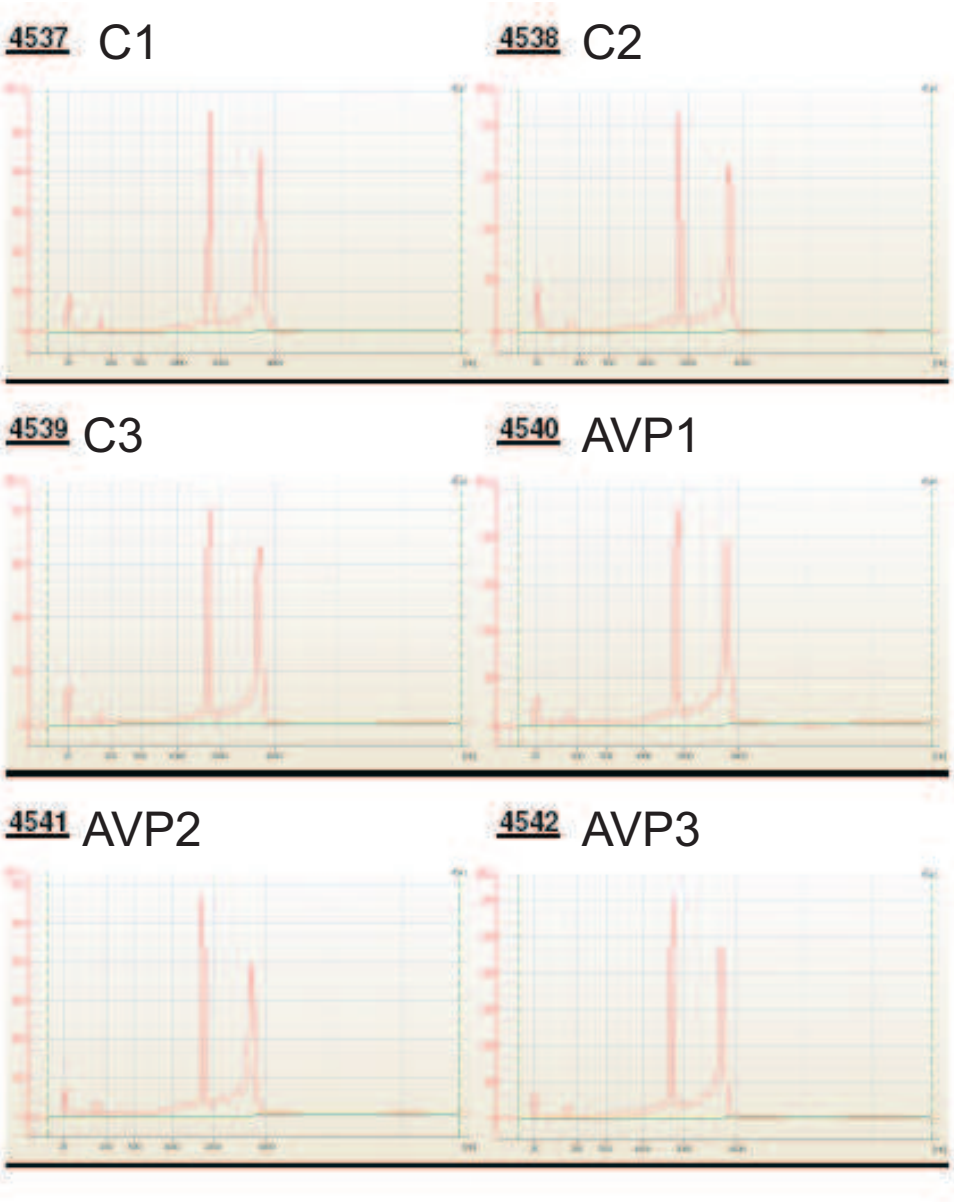

Sample ID	λ(260/280)	Concentration (ng/μl)	Yield (μg)
C1	2.03	399.6	3.2
C2	2.04	400.4	3.2
C3	2.04	431.8	3.5
AVP1	2.03	397.1	3.2
AVP2	2.04	505.0	4.0
AVP3	2.04	461.2	3.7

Figure 2.11 Validation of total RNA quality. Three control (C) and three AVP-treated (AVP) RNA samples were run on an Agilent bioanalyzer 2100. All results show two high and well-defined ribosomal peaks (28S, 18S). The small additional peaks below the ribosomal bands indicate a tiny amount of RNA degradation. The lack of peaks after the 28S ribosomal peak indicates a lack of genomic contamination. The table shows results of spectrophotometric analysis.

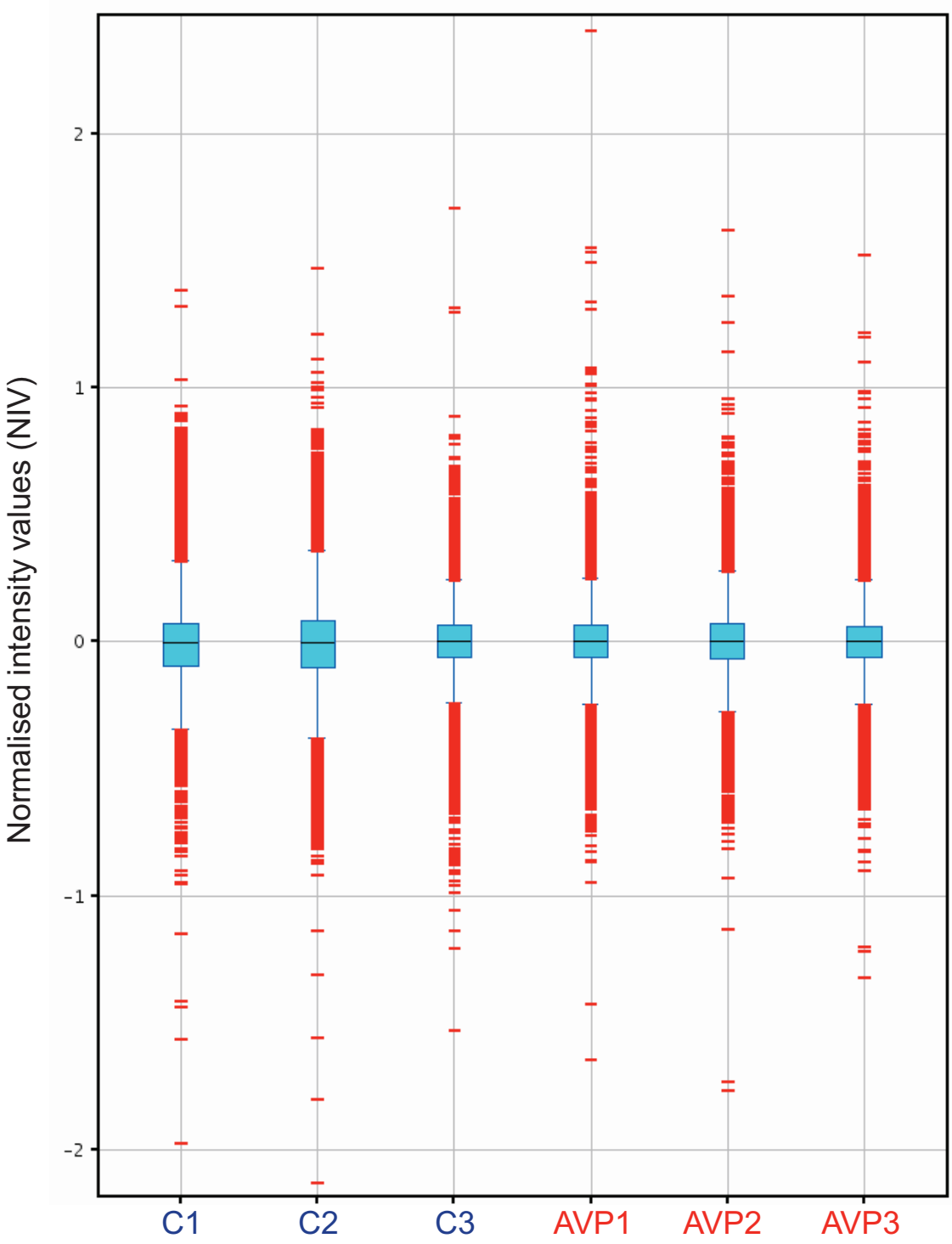

Figure 2.12 Normalisation of raw data. The log summarised values for each probe across all six samples is subtracted from each probe at each sample, hence reducing background 'noise' in the data. The resulting normalised intensity values (NIV) allow description of the position of each probe above the median (positive NIVs) or below it (negative NIVs). The data are seen here to distribute evenly across the experiment for all six samples, whether control (C) or treated (AVP).

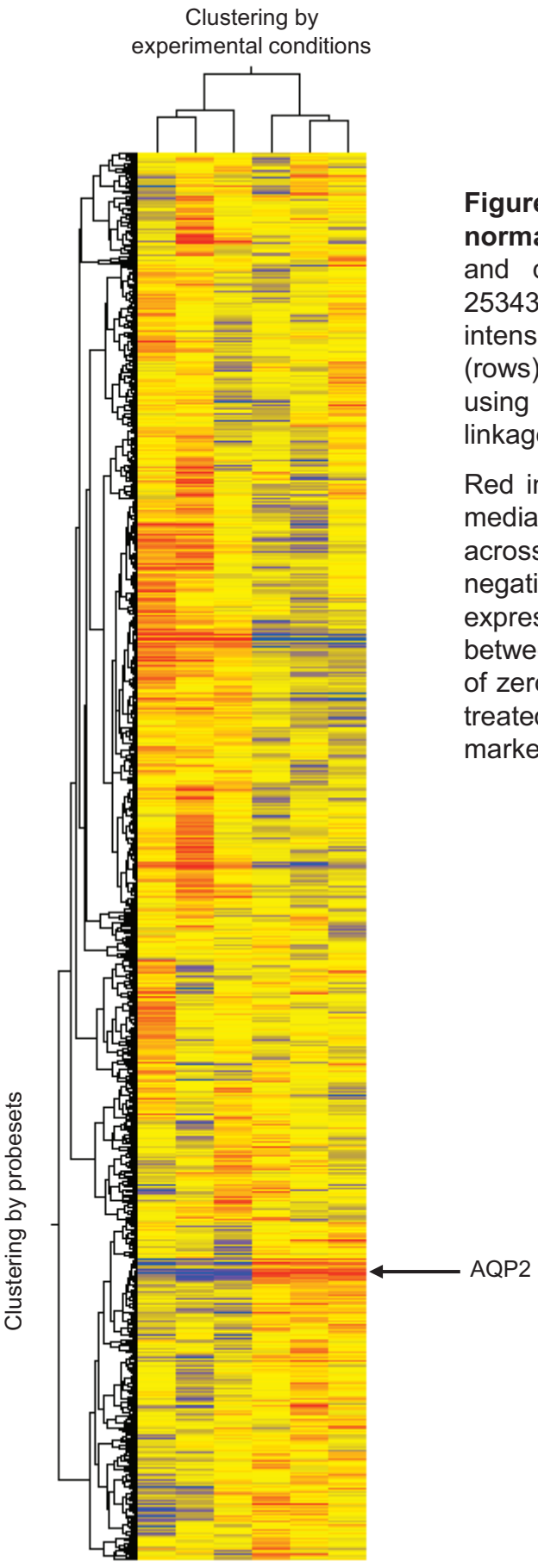

Figure 2.13 Hierarchical clustering of normalised microarray data. The full normalised and quality-controlled probeset list (containing 25343 probesets) was clustered by normalised intensity value (NIV) according to both probesets (rows) and control versus treatment (columns), using a Pearson centred correlation with average linkage.

Red indicates positive NIVs maximally above the median expression for that particular probeset across all six arrays, blue similarly indicates negative NIVs maximally below median expression. Shades of colour reflect NIVs between these extremes. Yellow denotes an NIV of zero, indicating no change between control and treated conditions. A probeset for aquaporin-2 is marked.

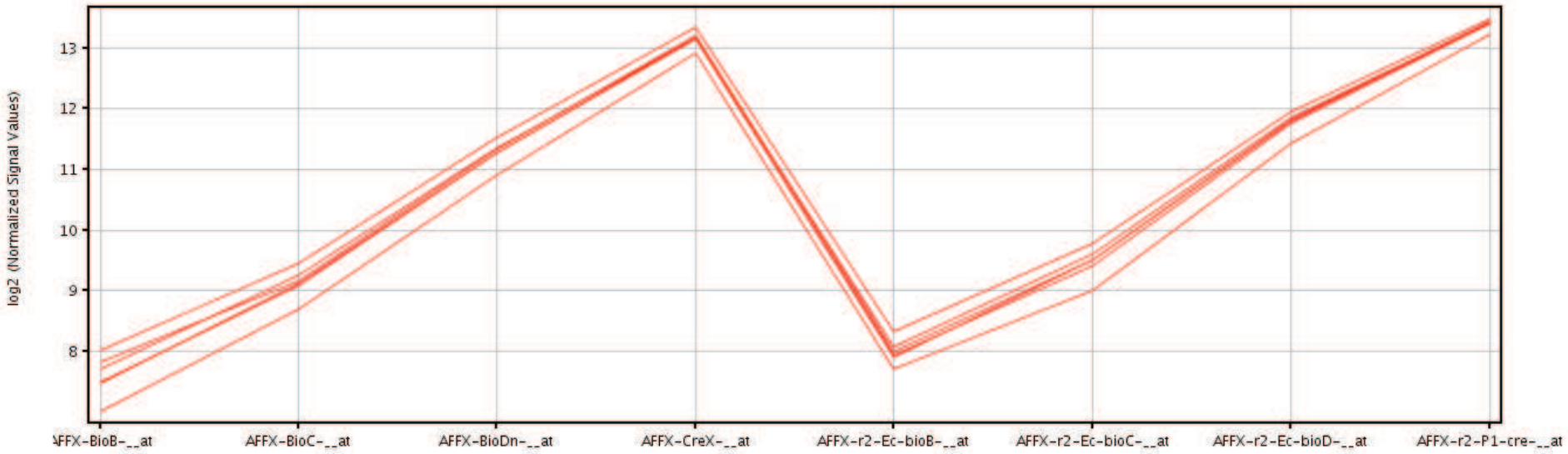

Figure 2.14 Hybridisation controls forming a 'spike' plot. Four additional RNA transcripts were added to the hybridisation mixture at known and increasing concentrations. The first transcript, bioB, is at the lower limit of detection of the arrays and has a 70% chance of being detected by the probesets (two for each transcript, causing the right-hand spike to look similar to the left-hand spike). The other controls (bioC, bioD, and cre) are well above the threshold for detection and should give rise to increasing normalised signal (expression) values (shown log transformed on the y-axis), as is the case here. Non-detection or values lower than expected would suggest a failure of the hybridisation reaction or subsequent washing and staining procedure.

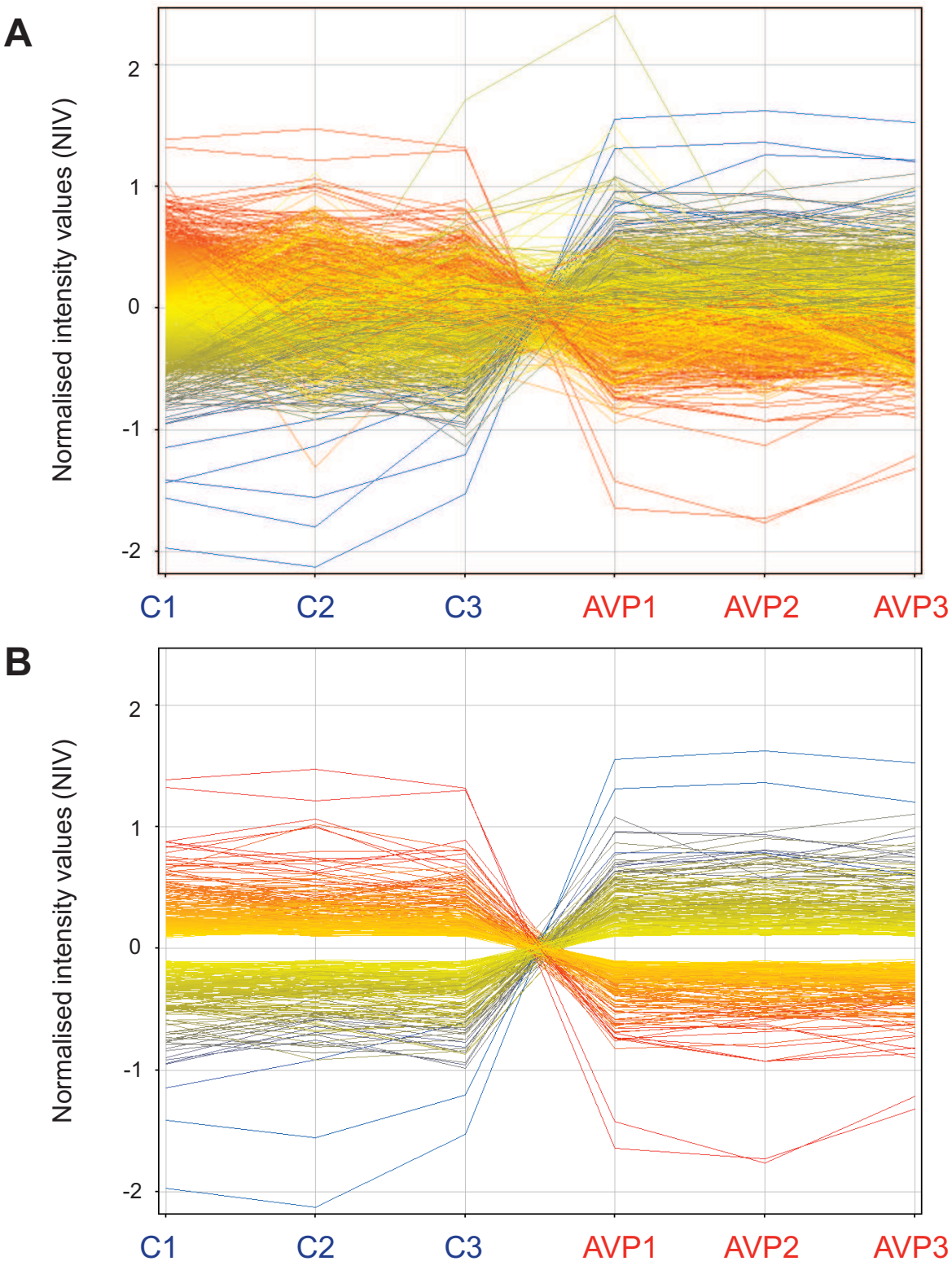

Figure 6.3 Change in expression of each probeset (gene) according to array. Each trend line connects a particular probeset at its normalised intensity value (NIV) in each of the six arrays (C1-3 control, AVP1-3 treated), with the crossover in NIV between conditions, if any, seen in the middle. An NIV of zero indicates the median value of the gene across all six arrays. (**A**) shows the raw data; (**B**) shows the final data (quality-controlled and t-tested). This comprises only the 364 probesets that changed by greater than 1.18-fold in either direction between the two conditions of the experiment, causing the central area of graph (**B**) to be blank. Detail of changes in specific genes are shown in Figure 6.6.

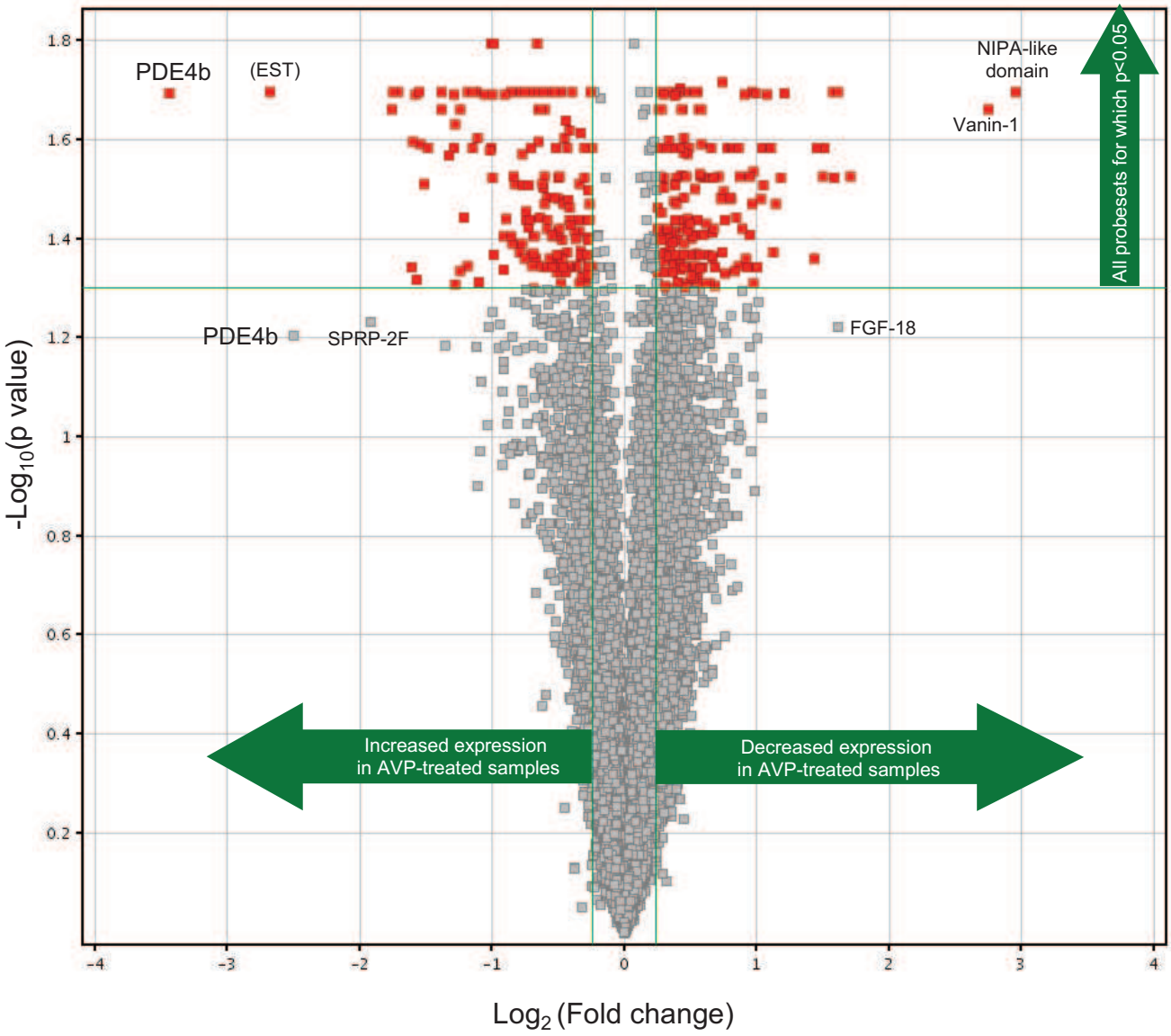

Figure 6.4 Change in probeset (gene) expression due to AVP treatment, for normalised and quality-controlled microarray data. All normalised quality-controlled data points are arranged by fold change of each gene in *control arrays with respect to AVP-treated arrays* (x-axis) and by p value (both expressed as log transformed values). Values above the horizontal green line represent those with $p<0.05$, and values lateral to the vertical green lines represent fold changes of >1.18 in each direction. The combination of these two cut-offs is represented by the red values, which number 364 in total. Notable probesets with large fold changes are labelled. There were two probesets for PDE4b, only one of which was significant.

SPRP-2F: small proline-rich protein 2F; FGF-18: fibroblast-growth factor-18.

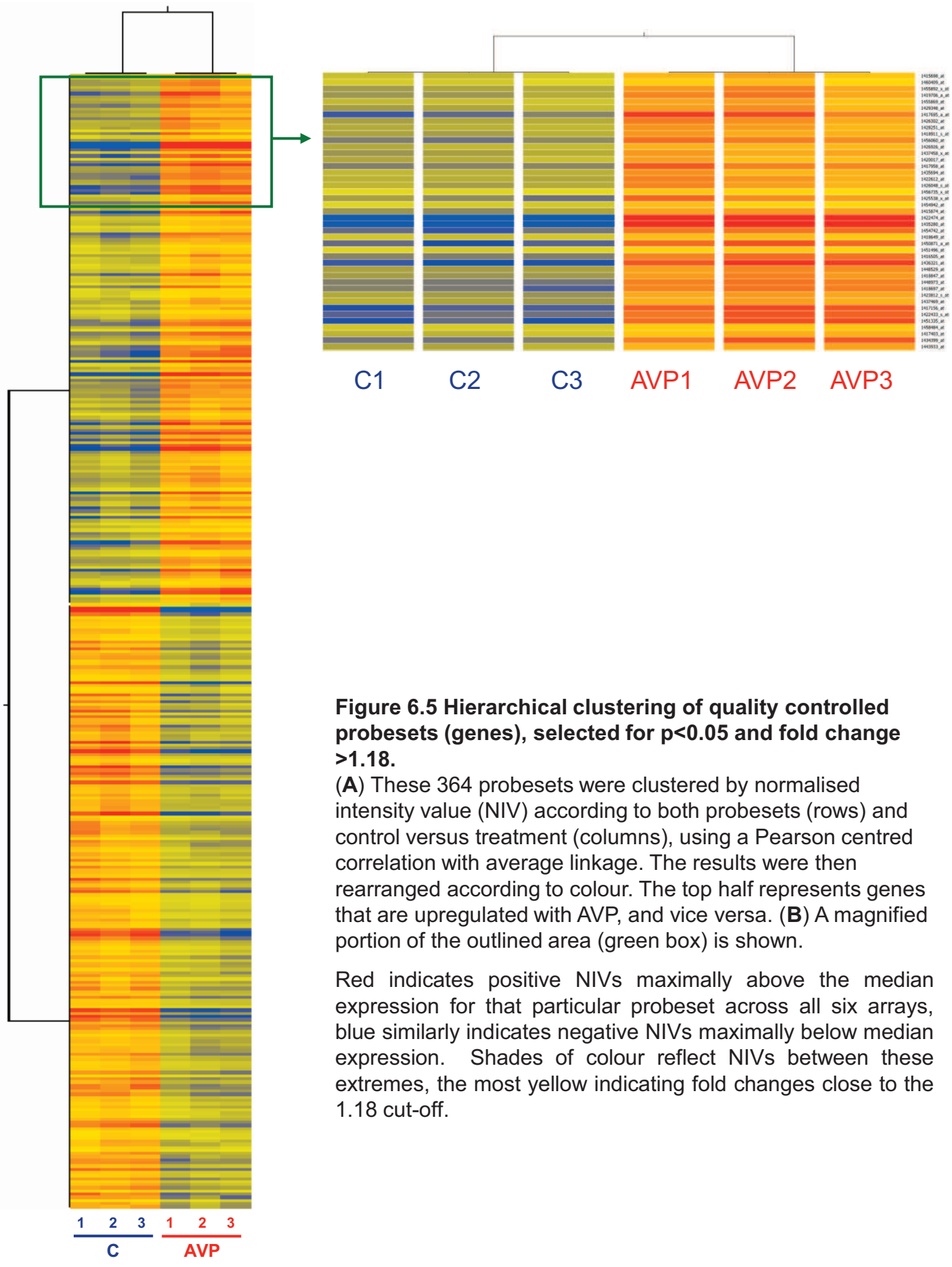

Figure 6.5 Hierarchical clustering of quality controlled probesets (genes), selected for p<0.05 and fold change >1.18.
(**A**) These 364 probesets were clustered by normalised intensity value (NIV) according to both probesets (rows) and control versus treatment (columns), using a Pearson centred correlation with average linkage. The results were then rearranged according to colour. The top half represents genes that are upregulated with AVP, and vice versa. (**B**) A magnified portion of the outlined area (green box) is shown.

Red indicates positive NIVs maximally above the median expression for that particular probeset across all six arrays, blue similarly indicates negative NIVs maximally below median expression. Shades of colour reflect NIVs between these extremes, the most yellow indicating fold changes close to the 1.18 cut-off.

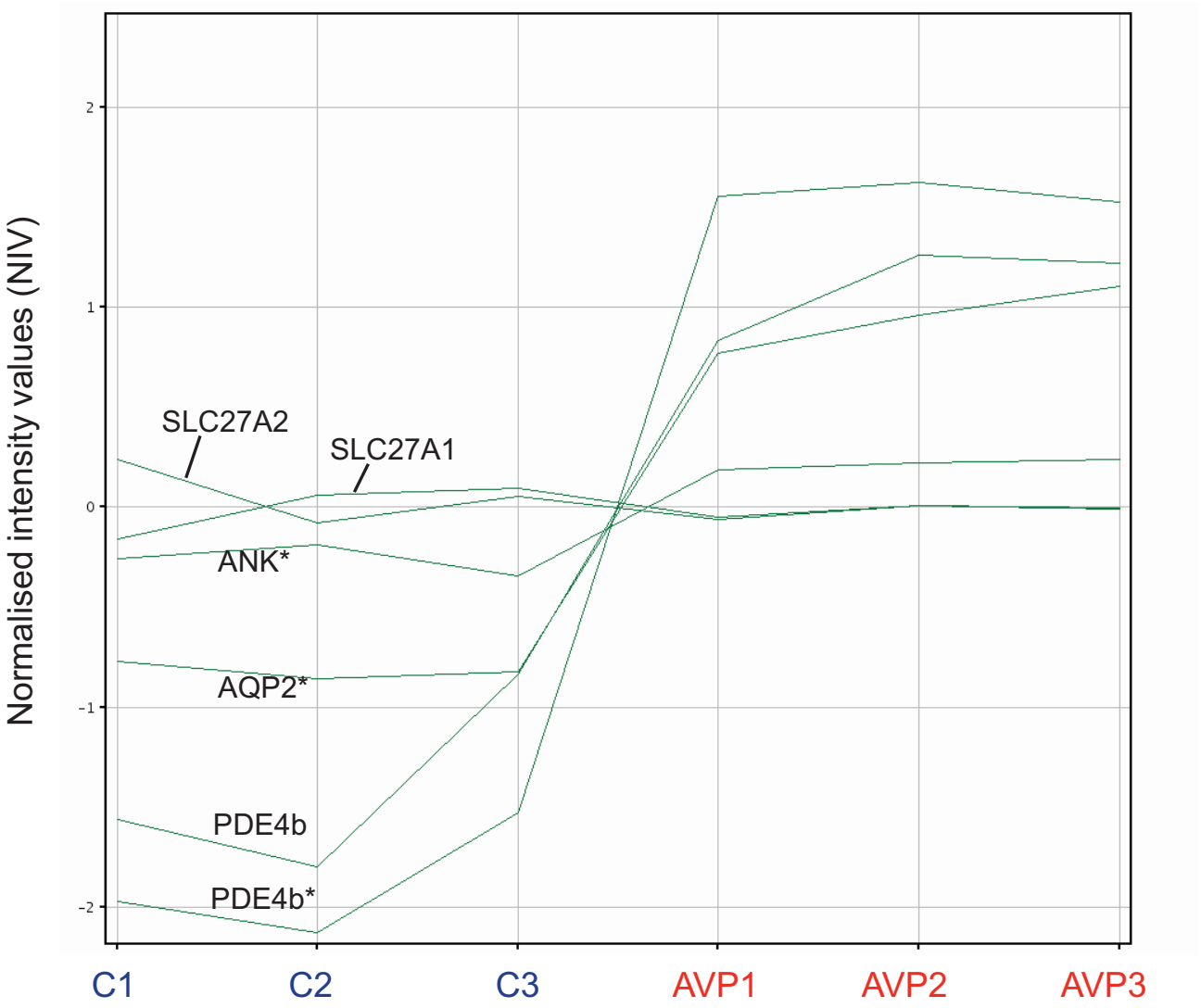

Figure 6.6 Change in expression of five genes with AVP treatment. Each trend line connects a particular probeset plotted at its normalised intensity value (NIV) in each of the six arrays (C1-3: control, AVP:1-3 treated). An NIV of zero indicates the median value of the probeset across all six arrays. Fold changes are given in Table 6.3. Results for both available PDE4b probesets are plotted, but only one of these (*) is significant. * denotes $p<0.05$.

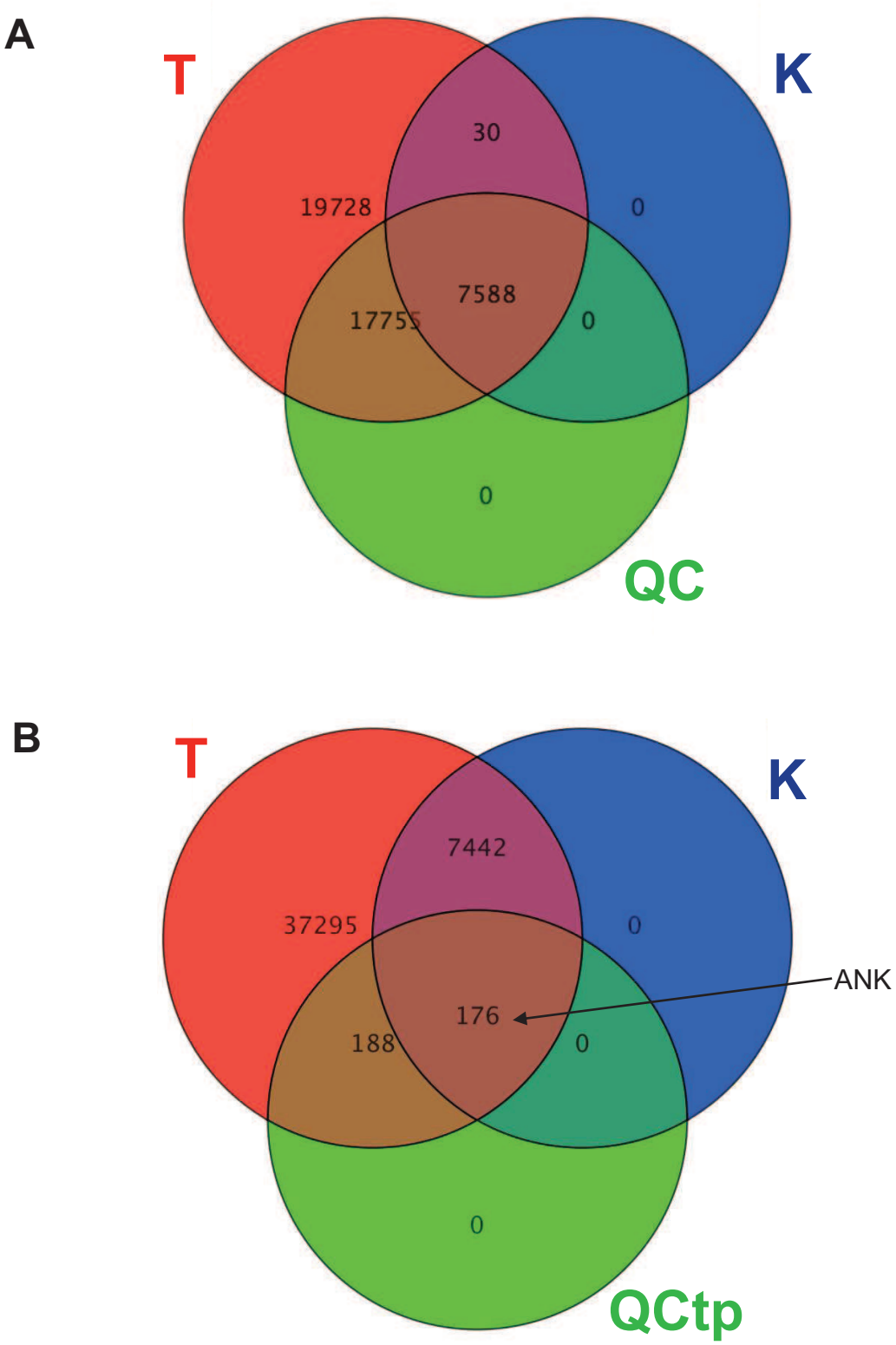

Figure 6.7 Summary of rationalisation of microarray data and overlap with Knepper dataset.

(A) The original 45101 probesets on the microarray (**T**) were reduced to 25343 probesets after normalisation and quality-control of the probeset list (**QC**). There was a high degree of overlap with the Knepper dataset (**K**), with only 30 genes of the 7618 in the Knepper dataset not being included in our QC list.

(B) The QC list was subjected to selection by t-test and fold change >1.18. This gives probesets that are differentially expressed with AVP treatment (**QCtp**). Only about half of these probesets were included in the Knepper list (**K**).

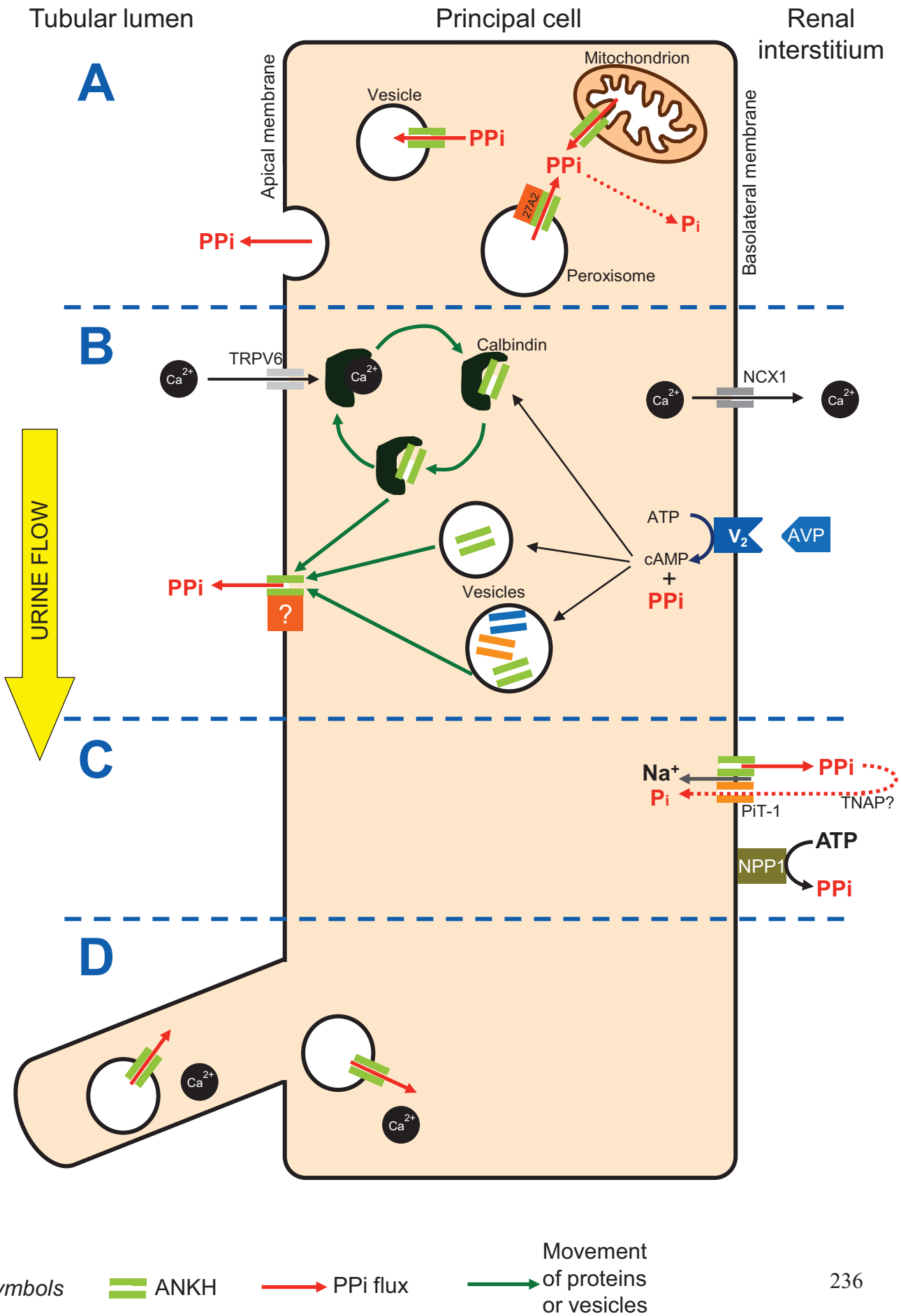
Tubular lumen
Principal cell
Renal interstitium
A
B
C
D
Apical membrane
Basolateral membrane
Mitochondrion
Vesicle
PPi
PPi
Pi
27A2
Peroxisome
TRPV6
Ca2+
Calbindin
NCX1
URINE FLOW
ATP
V2
AVP
cAMP
+
PPi
Vesicles
?
Na+
Pi
PiT-1
TNAP?
NPP1
ATP
Symbols
ANKH
PPi flux
Movement of proteins or vesicles

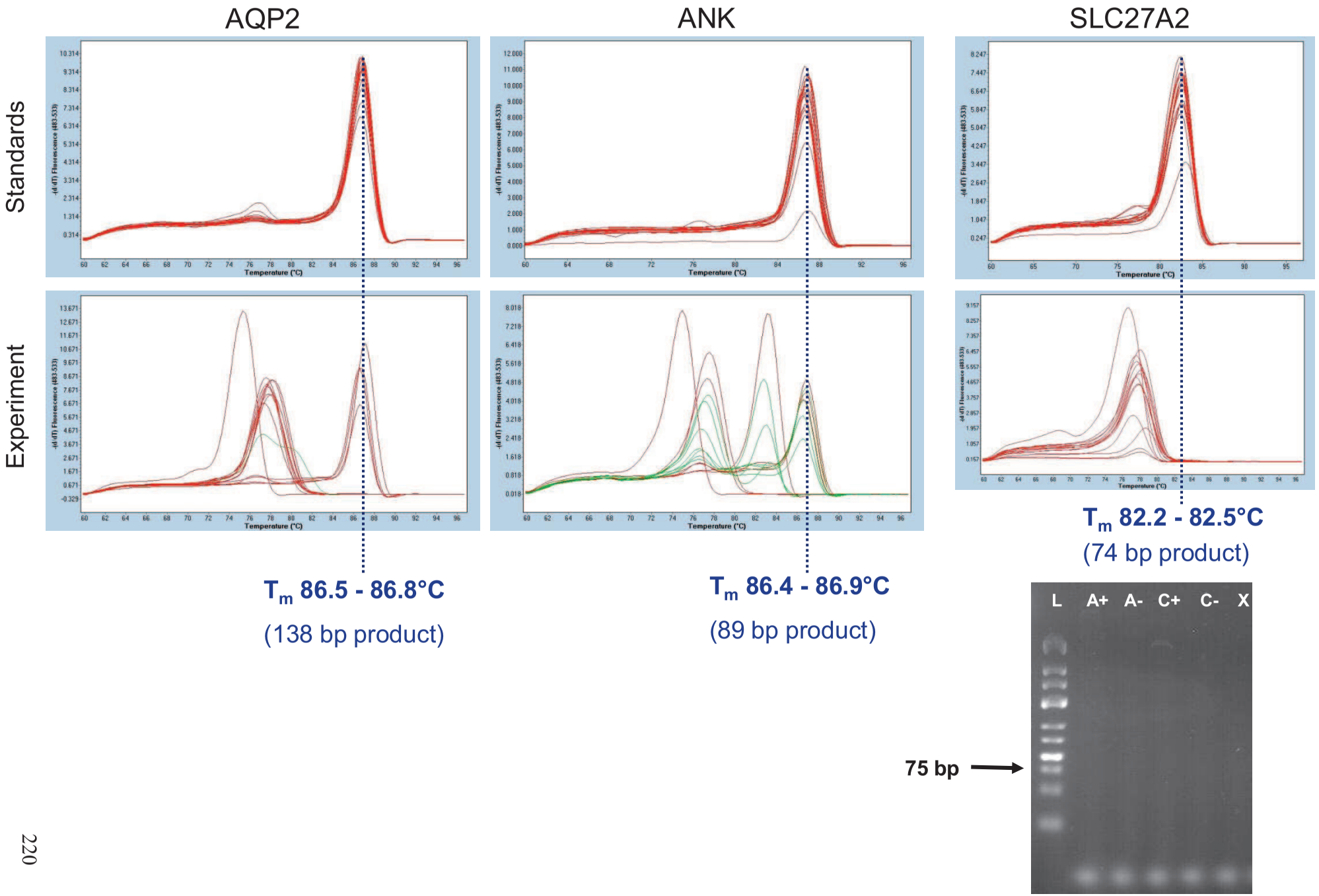
AQP2
ANK
SLC27A2
Standards
Experiment
Temperature (°C)
-(d/dT) Fluorescence (483-533)
T_m 86.5 - 86.8°C
(138 bp product)
T_m 86.4 - 86.9°C
(89 bp product)
T_m 82.2 - 82.5°C
(74 bp product)
L
A+
A-
C+
C-
X
75 bp

PDE4b

Efficiency 2.060

Slope -3.2

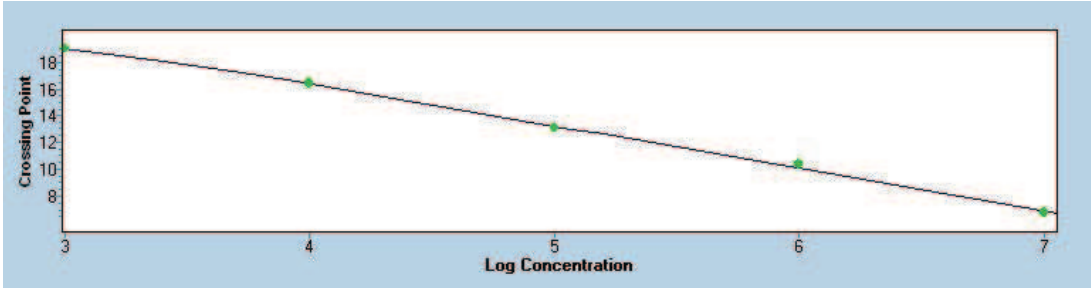

AQP2

Efficiency 1.918

Slope -3.5

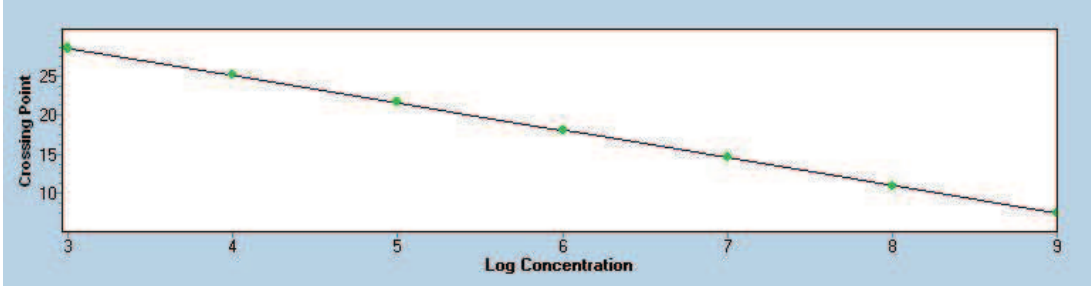

ANK

Efficiency 1.992

Slope -3.3

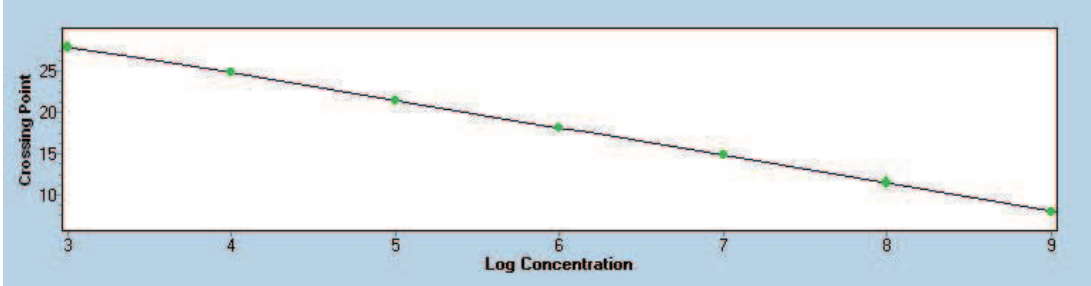

GAPDH

Efficiency 1.967

Slope -3.4

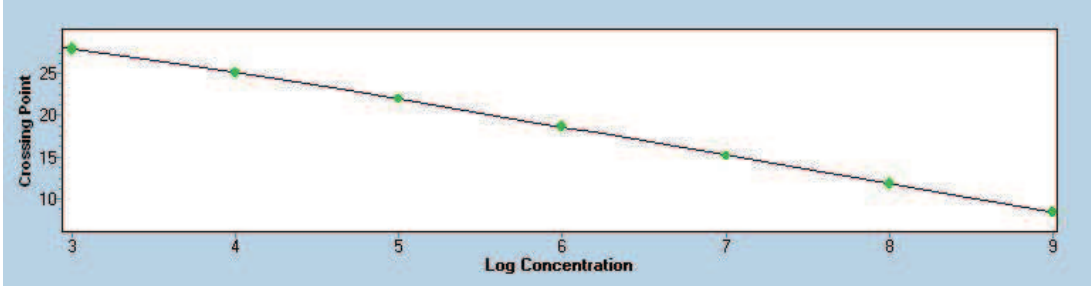

SLC27A1

Efficiency 1.985

Slope -3.3

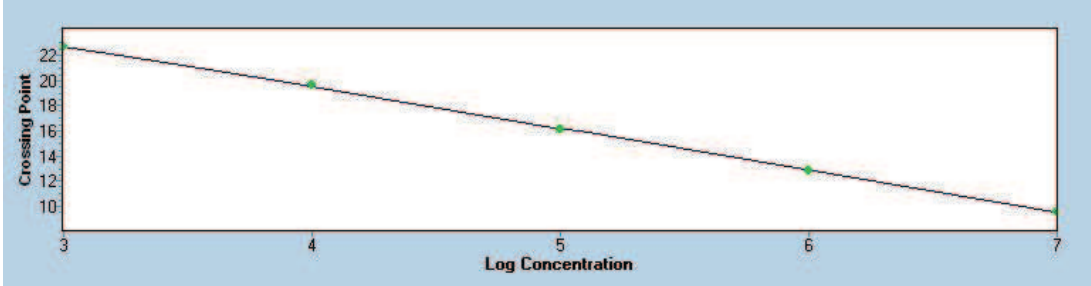

SLC27A2

Efficiency 2.045

Slope -3.2

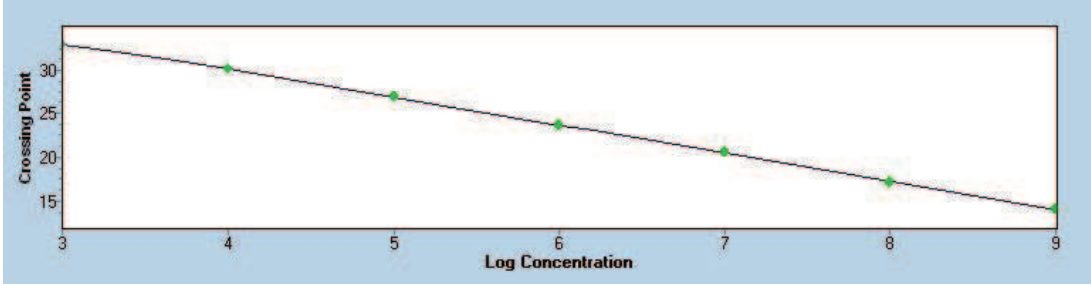

A

ANK standards

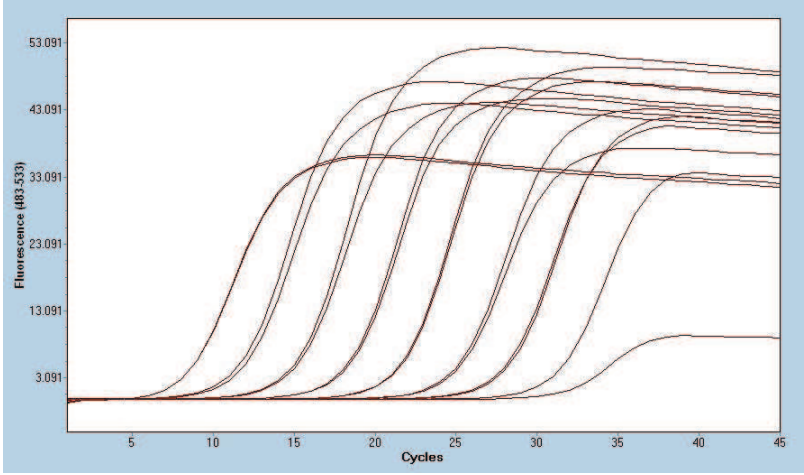

B

ANK

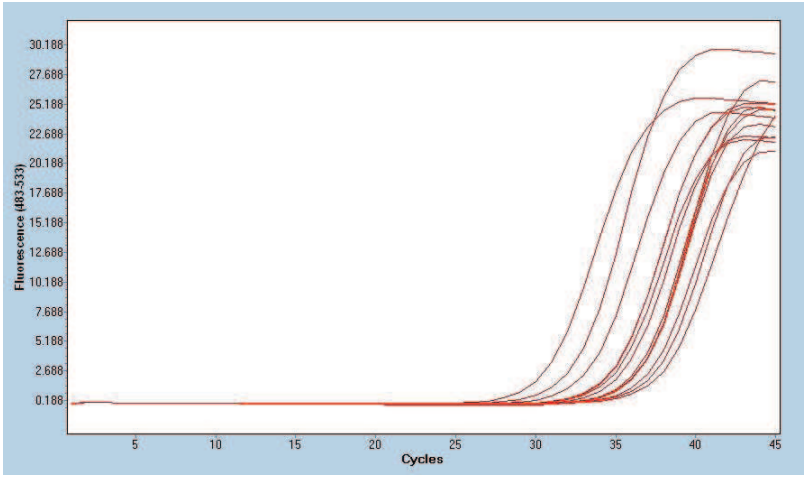

C

AQP2

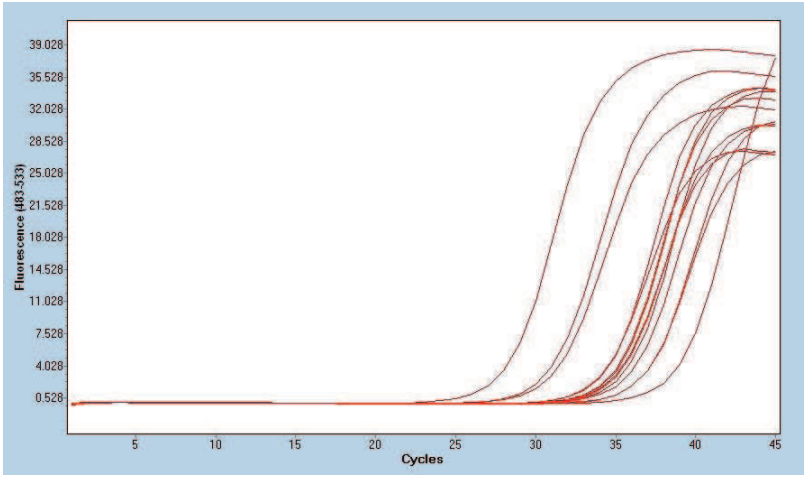

D

GAPDH

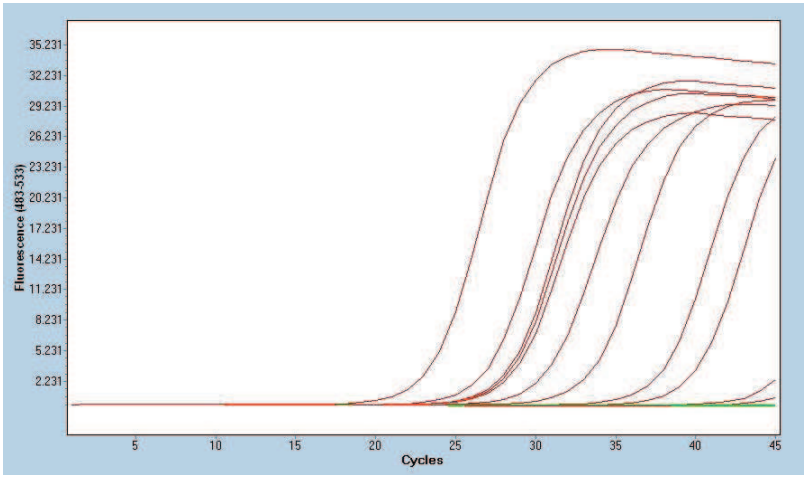

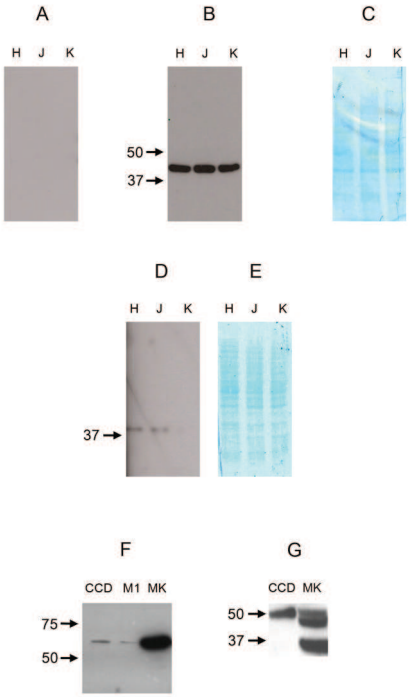
A
H J K
B
H J K
50
37
C
H J K
D
H J K
37
E
H J K
F
CCD M1 MK
75
50
G
CCD MK
50
37

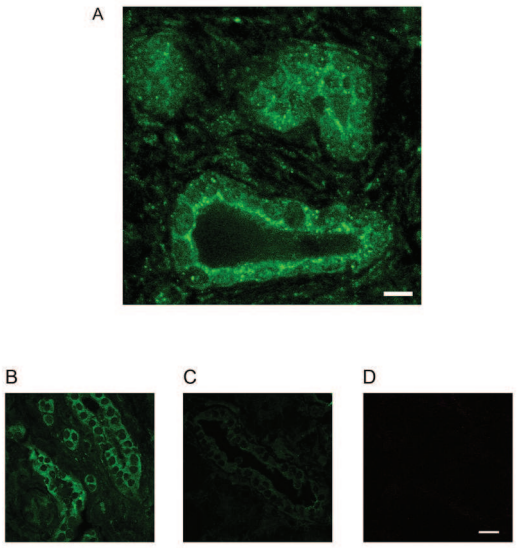

Figure 3.10 ANK immunofluorescence using the Ab3 antibody in human kidney. CLSM images showing immunofluorescence in human renal cortex with anti-C-terminal ANK antibody (Ab3: 1:250). Tubules were identified on morphological grounds. Apical ANK immunofluorescence in demonstrated in tubules viewed cross-sectionally (A: scale bar = 10 mm) and in cortical medullary rays (B). Results are shown for rabbit pre-immune serum (1:250) under the same conditions (C), and for secondary antibody (donkey anti-rabbit FITC: 1:100) alone (D). Scale bars for B-D = 20 μm.

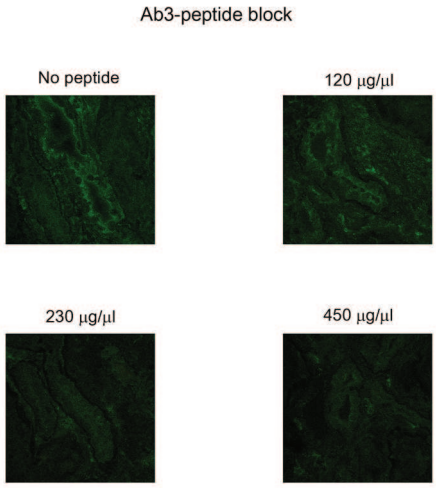

Figure 3.11 Preadsorption of Ab3 antibody by its immunising peptide. CLSM images showing immunofluorescence in human renal cortex with anti-C-terminal ANK antibody (Ab3; 1:250), incubated with the C-terminal immunising peptide (sequence PTEEVTDIVEMREENE; Sigma). Antibody-peptide mixtures were incubated for 1 h at 37°C. Increasing the peptide concentration showed gradually decreasing immunofluorescence due to Ab3.

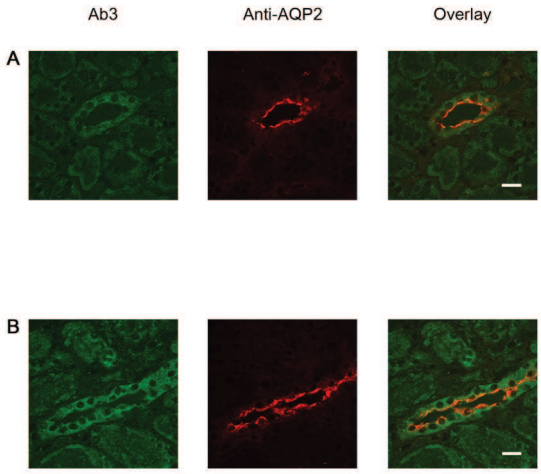

Figure 3.12 Colocalisation of ANK with AQP2 in human kidney. CLSM images showing immunofluorescence in human renal tissue with anti-C-terminal ANK antibody (Ab3; green channel), anti-aquaporin-2 antibody (red channel), and overlay of images. Representative images are shown of (A) medullary collecting duct, and (B) medullary ray (collecting duct) in cortex. Scale bar = 20 µm (applies to all images).

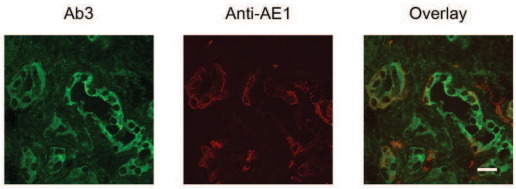

Figure 3.13 Colocalisation of ANK with AE1 in human kidney. CLSM images showing immunofluorescence in human renal cortex with anti-C-terminal ANK antibody (Ab3; green channel), anti-AE1 antibody (from Dr A Toye; red channel), and overlay of images. Scale bar = 20 µm (applies to all images).

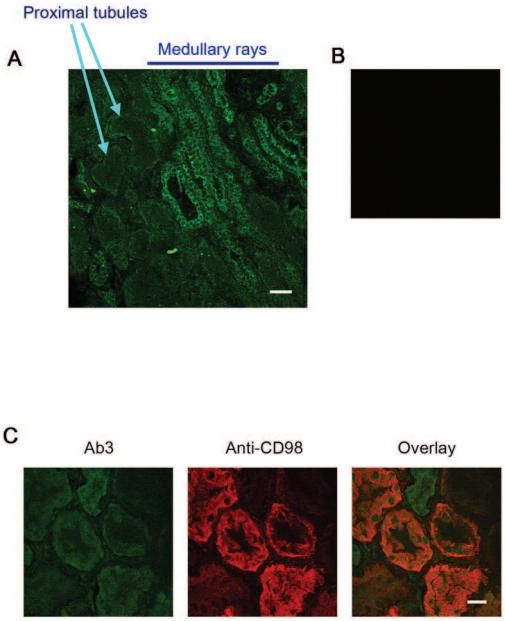
Proximal tubules
Medullary rays
A
B
C
Ab3
Anti-CD98
Overlay

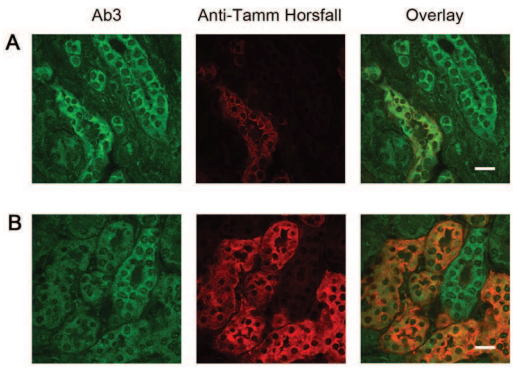

Figure 3.15 ANK is expressed to a limited extent in Loop of Henle/distal convoluted tubule. CLSM images showing immunofluorescence in two sections (A and B) of human renal cortex with anti-C-terminal ANK antibody (Ab3; green channel), anti-Tamm Horsfall antibody (red channel), and overlay of images. Scale bar = 20 µm (applies to all images).

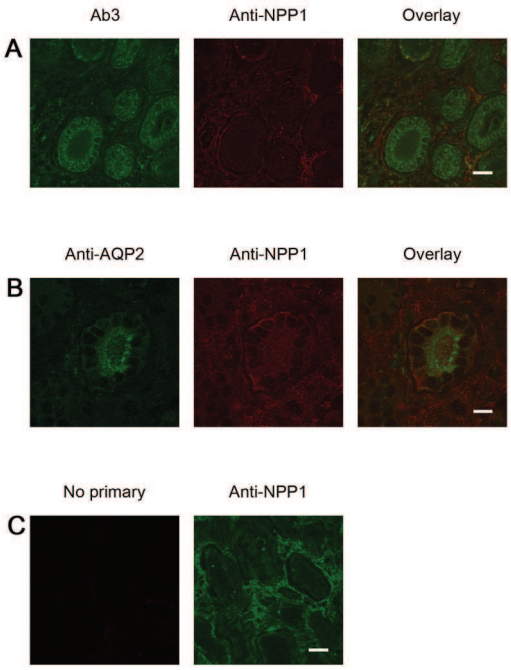
Ab3
Anti-NPP1
Overlay
A
Anti-AQP2
Anti-NPP1
Overlay
B
No primary
Anti-NPP1
C

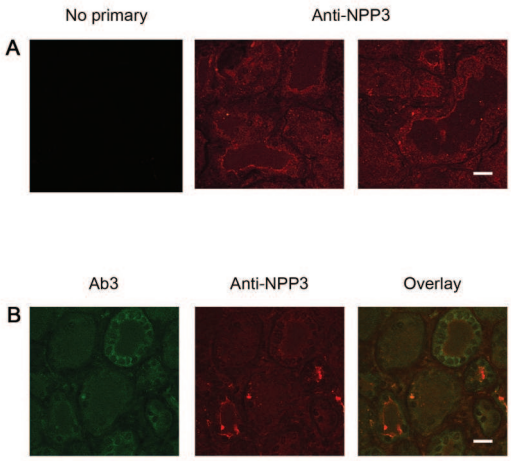

Figure 3.17 Expression of NPP3 in the proximal tubule of human kidney.
CLSM images showing immunofluorescence in human renal cortex. Scale bar = 20μm for all images.
(A) No-primary antibody control, and two images of anti-NPP3 antibody staining alone (red channel).
(B) Anti-C-terminal ANK antibody (Ab3; green channel), anti-NPP3 antibody (red channel), and overlay of images.

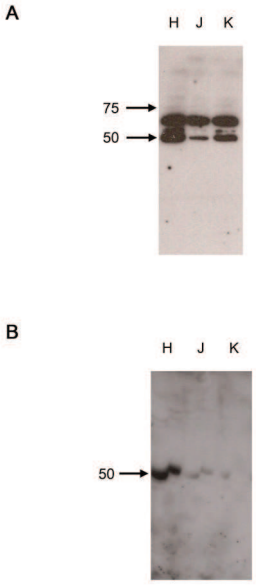
A
H J K
75
50
B
H J K
50

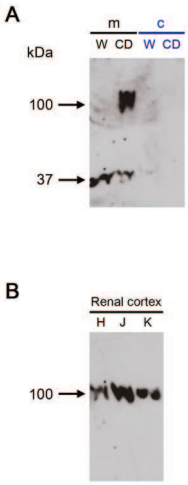
A
m
c
W CD W CD
kDa
100
37
B
Renal cortex
H J K
100

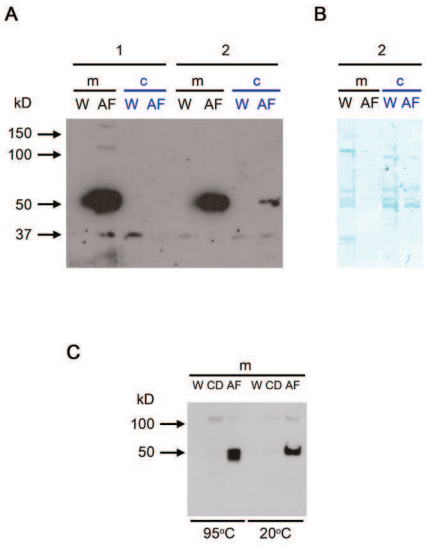
A
1
2
m
c
m
c
kD
W AF W AF W AF W AF
150
100
50
37
B
2
m
c
W AF W AF
C
m
W CD AF W CD AF
kD
100
50
95°C
20°C

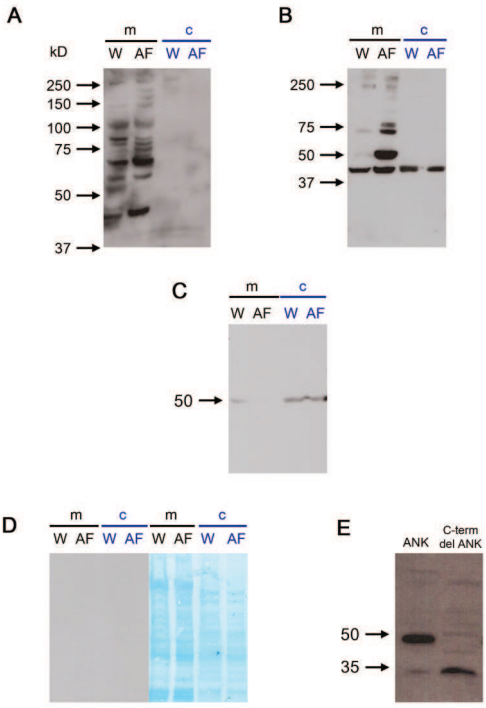
A
kD
m
c
W AF W AF
250
150
100
75
50
37
B
m
c
W AF W AF
250
75
50
37
C
m
c
W AF W AF
50
D
m
c
m
c
W AF W AF W AF W AF
E
ANK
C-term del ANK
50
35

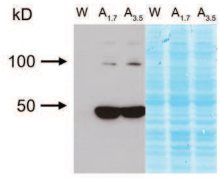

Figure 4.4 Detection of ANKH-pcDNA3.1 expression in oocytes using Ab3 antibody
Western blot analysis of oocytes injected seven days earlier with water (W) or ANKH-pcDNA3.1 cRNA at 1.7 µg/ul ($A_{1.7}$) or 3.5 µg/ul ($A_{3.5}$). Protein lysate was prepared using sucrose/Tris lysis buffer, with centrifugation at 10,000x *g* for 25 mins. After previous unsuccessful attempts, a large amount of protein (200 µg) was loaded with sample buffer containing β-mercaptoethanol at room temperature (as Halestrap protocol), run on a SDS-polyacrylamide gel and transferred to a PVDF membrane before probing with Ab3 at 1:500 overnight at 4°C with anti-rabbit HRP as secondary. The PVDF membrane was stained with copper phthalocyanine for 30 mins, then washed for 30 mins with 12 mM hydrochloric acid (right hand side).

Strongly-staining bands at ~50 kD are seen in the ANKH-injected oocytes with lesser bands at 100 and ~180 kD. No staining is seen in the water-injected lane.

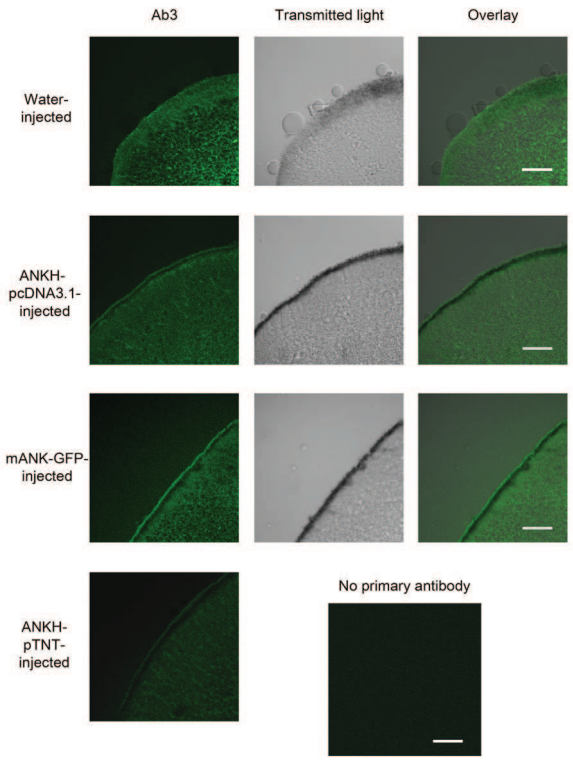
Ab3
Transmitted light
Overlay
Water-injected
ANKH-pcDNA3.1-injected
mANK-GFP-injected
ANKH-pTNT-injected
No primary antibody

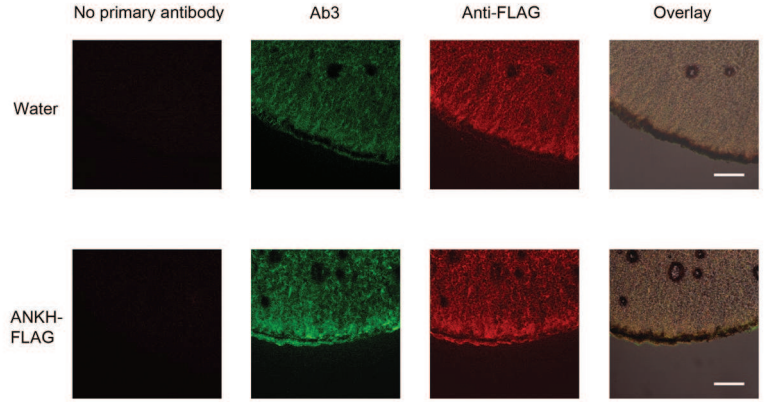
No primary antibody
Ab3
Anti-FLAG
Overlay
Water
ANKH-
FLAG

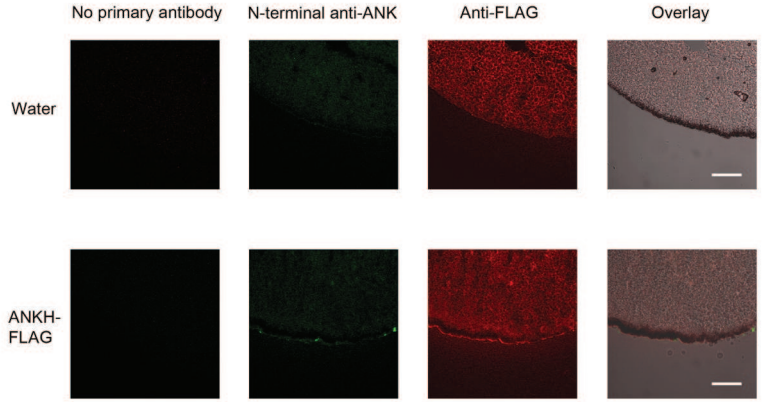
No primary antibody
N-terminal anti-ANK
Anti-FLAG
Overlay
Water
ANKH-
FLAG

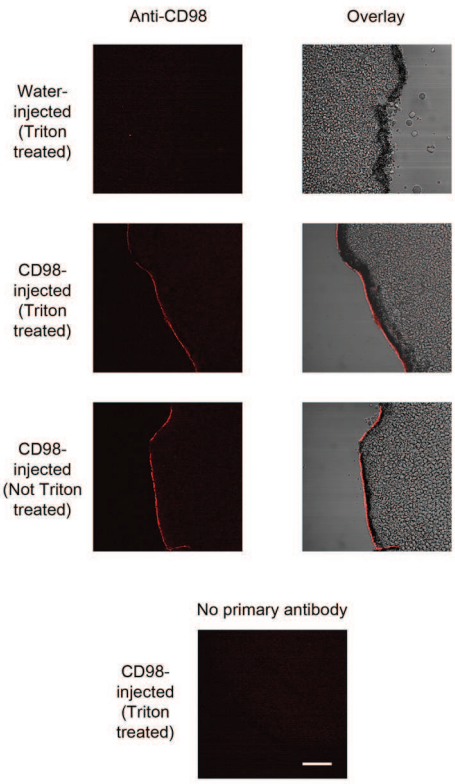
Anti-CD98
Overlay
Water-injected (Triton treated)
CD98-injected (Triton treated)
CD98-injected (Not Triton treated)
No primary antibody
CD98-injected (Triton treated)

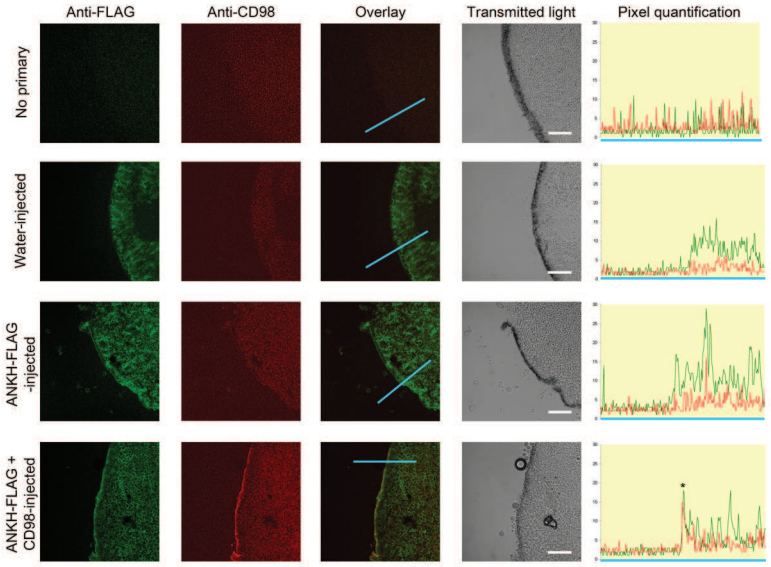
Anti-FLAG
Anti-CD98
Overlay
Transmitted light
Pixel quantification
No primary
Water-injected
ANKH-FLAG -injected
ANKH-FLAG + CD98-injected

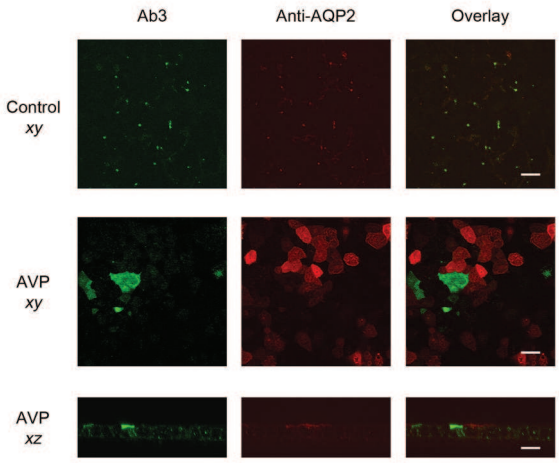
Ab3
Anti-AQP2
Overlay
Control
xy
AVP
xy
AVP
xz

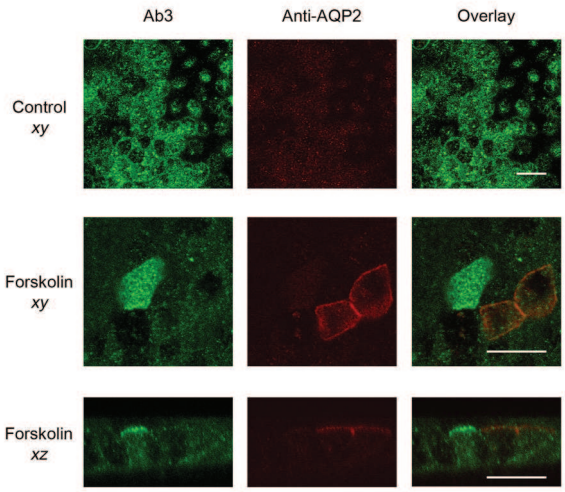
Ab3
Anti-AQP2
Overlay
Control
xy
Forskolin
xy
Forskolin
xz

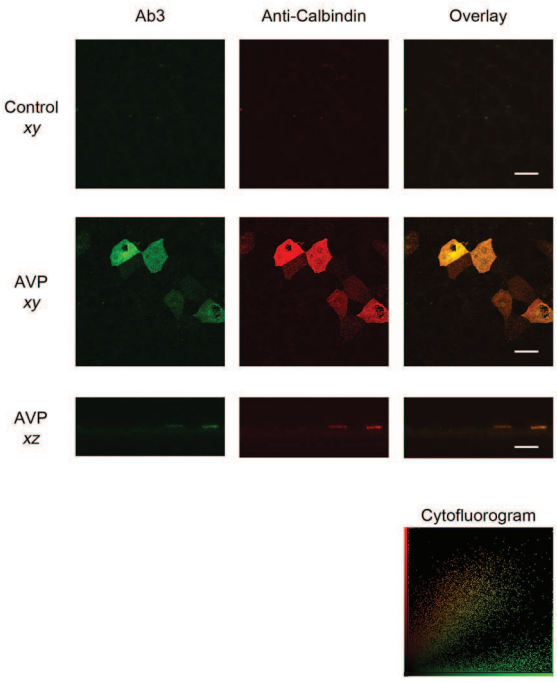
Ab3
Anti-Calbindin
Overlay
Control
xy
AVP
xy
AVP
xz
Cytofluorogram

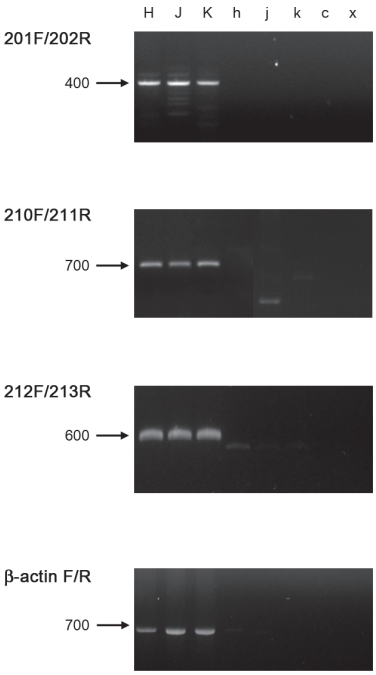
H J K h j k c x
201F/202R
400
210F/211R
700
212F/213R
600
β-actin F/R
700